NASA CR-72244
R-6838-2

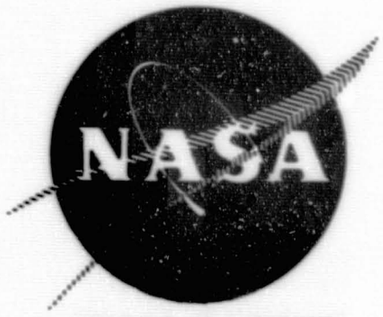

FINAL REPORT

EVALUATION AND DEMONSTRATION OF THE USE OF CRYOGENIC PROPELLANTS (O_2/H_2) FOR REACTION CONTROL SYSTEMS

VOLUME II
EXPERIMENTAL EVALUATIONS AND DEMONSTRATION

by

N. Rodewald, G. Falkenstein, P. Herr
and E. Prono

Prepared for

NATIONAL AERONAUTICS AND SPACE ADMINISTRATION

June 1968

Contract NAS3-7941

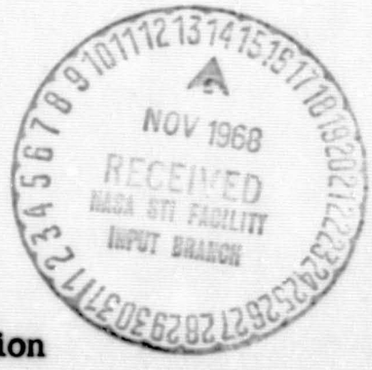

Rocketdyne
A Division of North American Rockwell Corporation
Canoga Park, California

NASA CR-72244
R-6838-2

FINAL REPORT

Volume II

EVALUATION AND DEMONSTRATION OF THE USE OF CRYOGENIC PROPELLANTS (O_2 - H_2) FOR REACTION CONTROL SYSTEMS

Prepared For

NATIONAL AERONAUTICS AND SPACE ADMINISTRATION

Contract NAS3-7941

Technical Management
NASA Lewis Research Center
Cleveland, Ohio
P. N. Herr

Rocketdyne
A Division of North American Rockwell Corporation
Canoga Park, California

EVALUATION AND DEMONSTRATION OF THE USE OF CRYOGENIC PROPELLANTS (O_2-H_2) FOR REACTION CONTROL SYSTEMS

Technically Reviewed and Approved by:

T. A. Coultas
Manager
Propulsion Physics,
Processes, and Applications

Release Approval

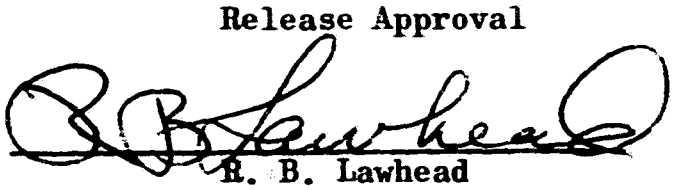

R. B. Lawhead
Manager
Physical and Engineering Sciences

Rocketdyne
A Division of North American Rockwell Corporation
Canoga Park, California

Contract NAS3-7941
National Aeronautics and Space Administration
Lewis Research Center
Cleveland, Ohio

FOREWORD

This report was prepared for the NASA Lewis Research Center, Cleveland, Ohio, by Rocketdyne, a Division of North American Aviation, Inc., Canoga Park, California. The effort described herein was conducted under Contract NAS3-7941.

ACKNOWLEDGEMENTS

The accomplishments described in this report were conducted by the Research Division of Rocketdyne under the program management of R. B. Lawhead and E. V. Zettle. Mr. P. Herr was the NASA Project Manager. The efforts and support of R. Rollins of the NASA Office of Advanced Research and Technology are also acknowledged.

The technical effort was augmented by N. Weber who conducted the thrustor experimental program, F. Hunter and D. Dermody who prepared component designs, and A. Liebman whose computer modeling efforts were invaluable in conducting the conditioner experimental effort.

ABSTRACT

The feasibility of a catalytically ignited spacecraft reaction control system using cryogenic (hydrogen-oxygen) propellants was experimentally demonstrated. The system studied utilized propellant conditioners to prepare the incoming propellants to a temperature and pressure acceptable to the thrustor. A portion of the propellants at a mixture ratio of 1.0 was passed through a catalyst bed. Additional oxygen was injected into the hot fuel-rich gas. Experimental results for the thrustor and conditioner subsystems and a system demonstration are presented. Design criteria for the ultimate development of an operational system are also presented.

CONTENTS

ILLUSTRATIONS

TABLES

SUMMARY

The feasibility of a cryogenic reaction control system for spacecraft applications was experimentally demonstrated. Design criteria for the ultimate development of an operational system were developed. The analysis and conceptual design efforts are reported in Volume I of this report (Ref. 1). Experimental results for thrustor and conditioner subsystems, and the results of a system demonstration test are presented in this volume.

The cryogenic reaction control system studied consisted of a thrustor and a subsystem to condition incoming propellants to a pressure and temperature acceptable to the thrustor. The 20-pound-thrust thrustors operated at a chamber pressure of 10 psia and a mixture ratio (o/f) of 2.5. A portion of the propellant (at a mixture ratio of 1.0) passed through a catalyst bed. Additional oxygen was injected into the resulting 1500 F, fuel-rich gas. The conditioning subsystem used catalytic gas generators to produce hot gas which was recycled and used to increase the temperature of the incoming propellants through a heat exchanger. On-off pressure control was used, although a flight system would probably utilize a more sophisticated proportional type control system.

THRUSTOR SUBSYSTEM

The design and operation of the thrustor, and conditioner gas generators, were based on criteria defined in Volume I of this report (Ref. 1). Additional operational information determined during the course of the program are listed below.

1. The catalyst bed length is determined by the propellant residence time required to ensure reliable ignition. In this program, a time of 0.1 millisecond, calculated using densities based upon preignition temperature and pressure of the propellants, was found satisfactory.

2. A flame arrestor device just upstream of the catalyst bed can prevent flashback as well as accomplish final fine mixing of the propellants. Beds of 1/8-inch-diameter copper shot for the thrustor experiments, and 1/16-inch-diameter steel ball bearings in the gas generator experiments were successfully used.

3. The injector must provide a good gas-gas mixing region to prevent hot spots and high mixture ratio streaks. Further, the gas velocity in the mixing region must be sufficiently high to prevent flashback of the reaction in the catalyst bed to the injector face. Velocities of approximately 30 ft/sec were found satisfactory.

4. Catalyst pellet diameter must be small compared to the reactor diameter to prevent channeling of the gas along the outside periphery of the reactor. A ratio of eight or greater combined with antichanneling turbulator rings was found to be a satisfactory design.

5. Preinjector, manifold, and line volumes should be in the same ratio of the volumetric flowrates of the two propellants. This design constraint minimized mixture ratio variations during the start-up and shut-down transients.

6. Injection of additional oxygen into the fuel-rich catalyst bed gas may be used to increase the overall chamber mixture ratio and specific impulse. This additional propellant must be very uniformly distributed to prevent uneven mixture ratio distribution resulting in low performance and severe heat transfer problems. It was also found that additional oxygen would not react with the fuel-rich bed effluent, unless the resulting mix temperature was above approximately 1260 F.

7. The injector orifice pressure drop should be maximized consistent with system pressure budget. Mixture ratio and total flowrate perturbations are minimized if sonic injection is utilized.

8. To minimize pressure and flowrate oscillations and perturbations, the pressure drop across the injector orifice should be maximized. On the other hand, it was found the pressure response was fastest at minimum injector pressure drops such that the chamber (nozzle) throat became the flow-limiting orifice. To allow higher injector pressure drops, the pressure loss across the catalyst bed should be minimized.

9. The thermal mass of the catalyst bed support structure should be minimized to obtain most rapid thermal response.

10. Performance and heat transfer characteristics were measured under altitude conditions (~100,000 feet) using a lightweight nickel chamber. The thrustor c* performance ranged from 89 to 91 percent after achieving thermal equilibrium. The heat transfer rates were found to be several times larger than expected, probably due to recirculation patterns set up by the downstream oxygen injector. This decrepancy could, however, have been partially due to a radial mixture ratio gradient and/or a poor estimate of the local flame temperature. The heat transfer characteristics appear to be compatible with a refractory chamber and nozzle.

11. Repeatable, reliable catalytic ignition was obtained with a catalyst bed temperature above 360 to 410 R with cryogenic (250 R) propellants at a 10-psia chamber pressure (~2 psia prior to ignition). This constrasts to previous results at higher pressures (~100 psia) where reliable ignition was found at bed temperatures as low as 200 R. This suggests a pressure-temperature interaction on the ignition limit.

12. Two key response parameters were evaluated; pressure (or thrust) and temperature (or specific impulse). Pressure response times on the order of 40 milliseconds were experimentally obtained with a pressure-controlled feed system. Significantly longer response times were obtained with a flowrate controlled system. Specific impulse response time was significantly long. Although response times of less than 1 second have been analytically predicted, experimental results for a cold catalyst bed start condition yielded response times from 2 to 3 seconds.

CONDITIONER SUBSYSTEM

The propellant conditioner is a gas generator-heated liquid heat exchanger which converts liquid propellants to gaseous propellants. This system has the following principal components for each propellant:

1. A hot-tube heat exchanger to supply energy to the incoming liquid
2. An accumulator to store the conditioned gas and attenuate the pressure and temperature fluctuations of the conditioned propellant from the heat exchanger
3. A catalyst gas generator using propellants from the accumulators to provide hot gas to the heat exchanger
4. A control system to control both temperature and pressure in the accumulator

The gas generator designs employed herein utilized applicable thrustor designs. It was found that the use of sonic throats at the gas generator exit minimized the effects of downstream pressure perturbations on gas generator operation. The results of pulse-mode testing indicated that the gas generators should be oversized by approximately 50 percent and operated in a pulsed mode to reduce the likelihood of ice formation at the hot gas exit of the heat exchanger.

A heat exchanger design was desired which resulted in a low pressure drop and a minimum pressure-flowrate oscillation due to boiling (boiling instability). The design utilized in the program was found satisfactory. A helical coil of tubing was placed in an annulus. The hot gas was flowed inside the coiled tubing and the propellant through the annulus. The hot gas heat transfer coefficients were found to be two to three times higher than originally estimated.

Off-on control systems were used for both propellants. This was something less than satisfactory and resulted in large pressure and flow oscillations. This in turn caused mixture ratio and flame temperature variations in the catalyst bed. Accumulators were used to help control the pressure and temperature oscillations.

The heat and material balances accomplished on the conditioner subsystem revealed that approximately 23 percent of the total propellant flow was required to be diverted to the gas generators for conditioning purposes. This could result in a severe penalty on specific impulse. For the design selected for the system demonstration (liquid propellants conditioned to 410 R), this loss may be as high as 130 seconds. Reducing the temperature of the conditioned propellant to 200 R will reduce the loss to less than 75 seconds.

The major objective of achieving automatic and concurrent operation of both propellant systems was successfully achieved. The most difficult step in this task was the establishment of the gas generator feed-back loop, which involved a substantial orificing effort to ensure proper flow control to the gas generators. Freezing of ice in the hydrogen heat exchanger was prevented by changing the exchanger operation from countercurrent to cocurrent.

SYSTEM DEMONSTRATION

The system demonstration was the first of its kind reported in the open literature. Liquid propellants (LOX and LH_2) were "conditioned" to gas at -50 F under flowing conditions and were fed into a small bipropellant thrustor which employed noble-metal catalysts for ignition. This system could deliver a specific impulse of 367 seconds based upon the efficiencies measured in this program. The system losses consisted of a 9-second water removal loss, a 30-second gas generator combustion loss (due to venting excess hydrogen in the hot gas) and a 34-second loss due to combustion inefficiencies in thrustor and gas generator. The integrated system was hydrogen limited because the conditioning system was originally sized to deliver propellants to the thrustor at 260 R. As a result, the hydrogen gas generator was undersized for the required flowrates and remained on throughout thrustor operation. Good correlation was obtained between the expected values and experimental results for the mass and energy balances.

The lightweight thrustor failed (chamber wall burnthrough) during the second test series directed at demonstrating combustion performance. This was due to mixture ratio (2.74 instead of 2.5) and chamber pressure (12.9 psia instead of 10 psia) excursions. Notwithstanding this ocurrence, the demonstration of the cryogenic reaction control system concept was a success.

INTRODUCTION

The purpose of the second phase of this program was to experimentally investigate the feasibility of a cryogenic reaction control system for spacecraft applications, and to generate basic system design data that could be utilized during the ultimate development of an operational system. Accordingly, a 16-month program was conducted to evaluate the potential for a reaction control system utilizing the cryogenic oxygen hydrogen propellent combinations. Analysis and conceptual design were reported in Ref. 1 . Component design and experimental results are presented in this report.

In Ref. 1 , system applications were compiled to identify useful propulsion systems and possible operating constraints. Possible applications were identified as: propellant settling engines, stage recovery power, attitude control, and secondary propulsion for orbital tankers. The most useful range of thrust was found to be from 20 to 100 pounds, and chamber pressure levels were indicated to be either 10 or 100 psia. Existing computer programs were used to calculate the theoretical performance in terms of the thermodynamic state and compositions of the exhaust products, and to obtain estimates of probable compositional freezing during the expansion process. The cryogenic reaction control system was divided into two distinct component subsystems such that the experimental study would be consistent with the very general nature of the program goals. One subsystem was designed to condition the propellants to a given thermodynamic state regardless of the inlet state; the other subsystem consisted of the thrustors. Based on the overall reaction control system application analysis, the low-pressure (10 psia) system was selected for experimental investigation in this program. The selection of such a system concept utilizing main tank propellants was also based on the lack of existing technology at this pressure level for both the conditioner and thrustor.

Analysis of the conditioner operations showed pressure control to be critical in maintaining the thrustor catalyst bed temperature in a range which prevents bed burnout. However, even a small relaxation in the pressure requirement (i.e., increasing maximum thrustor operating pressures by several psia) may markedly alter the criticality of the control problems. The thrustor propellant inlet feed temperature of 200 R was selected as the design point to ensure reliable ignition without oxygen freezing. To prevent freezing, both propellant temperatures should be maintained in excess of 115 R.

Experimental concept evaluations are presented below as two subsystems; the thrustor subsystem and the conditioner subsystem. Evaluation of the thrustor was accomplished by further division into subcomponents associated with thrustor design. Experimental results are described for each subcomponent of the thrustor. The subcomponents were then integrated into a single thrustor subsystem configuration. In a similar manner the conditioner was evaluated by applying the subcomponent technique for both the hydrogen and oxygen propellant sides of the flow system. The subcomponents also were then integrated into a single conditioner subsystem configuration. The subsystems were then assembled together and operating feasibility was demonstrated as a single system unit.

THRUSTOR EXPERIMENTAL EVALUATIONS

The conditioner and the thrustor subsystems were separated for evaluation from both the control and energy transfer standpoints. Thus, the dynamics of each system could be studied without interaction effects. No previous experience was available for thrustor design criteria at the low temperature and pressure combinations selected for evaluation during this program. Therefore, the thrustor was divided into subcomponents for experimental evaluation. These subcomponents were defined in accordance with the areas of expected operational problems within the thrustor. The design operating conditions for the thrustor subsystem were selected from the results described in Ref. 1 , and are as follows:

1. Chamber pressure: 10 psia
2. Mixture Ratio: 2.5:1
3. Thrust: 20 pounds

The low chamber pressure was consistent with the selection of a cryogenic reaction control system which would utilize propellants obtained from the main tankage of a vehicle. The mixture ratio is near optimum from the standpoint of specific impulse based on a predicted frozen-flow expansion of the combustion gases. The thrustor configuration was the conventional cylindrical combustion section with a convergent-divergent nozzle. This choice was based primarily on the fact that existing data were available only for this type of configuration and any change would introduce new variables.

A workhorse thrust chamber assembly was utilized to conduct initial experiments associated with each subcomponent section. The results from these experiments were then employed in the design of a lightweight thrustor which

was fabricated for the purpose of obtaining demonstrated chamber heat transfer and delivered impulse data under simulated environmental altitude conditions of approximately 90,000 feet. The thrustor was tested as a separate subsystem (as described previously) for the altitude performance demonstration and, thus, non-preconditioned gaseous propellants were used. Demonstrated operation feasibility of the integral conditioner and thrustor subsystems as a single unit is described in the System Demonstration Section of this report.

THRUSTOR EXPERIMENTAL APPARATUS AND PROCEDURE

EXPERIMENTAL HARDWARE

The schematic of the thrustor presented in Fig. 1 illustrates the various subcomponent sections, which include the following:

1. The propellant manifold
2. The injector-mixer
3. The catalyst bed reactor
4. The downstream oxygen injector
5. The downstream combustion chamber

The thrustor consisted of a number of identical rings, each with 12 instrumentation ports, connected with two longitudinal bolts. The rings were maintained under compression by two Belleville washer assemblies. These washer stacks also accommodated the thermal growth of the thrustor. Alignment of the rings was accomplished by two tool steel guides extending from the support assembly, which also provided overall longitudinal support for the assembly. The sealing of each individual ring was accomplished through compression supplied by the washer assemblies to the lapped mating surfaces on the individual rings. The longitudinal force exerted on the rings by the washers was 4000 pounds, which was far greater that the axial thrust load. Additional sealing aids used for the compression method were thin copper washers and/or Permatex, the latter being used during all of the downstream injection experiments. The instrumentation ports on the individual rings were contained in two spirals, each spiral containing six ports. These spirals were diametrically opposed

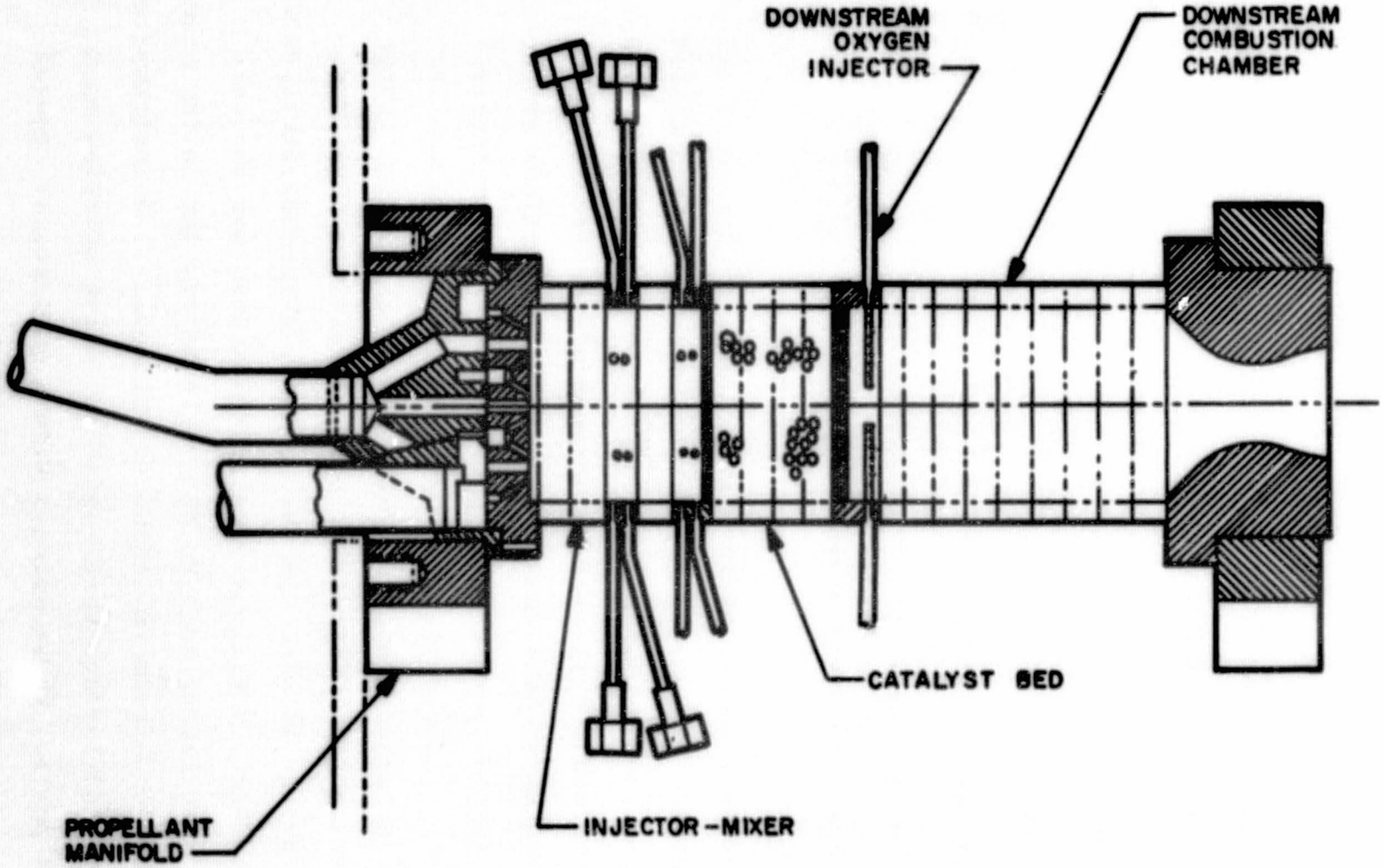

Figure 1. Experimental Thrustor Design. The Spacer Rings Showing the Instrumentation Ports are Typical. The Engine Support Assembly is not Shown for Purpose of Clarity.

so that at any axial location there were two ports, 180 degrees apart, which could be used to measure a pressure and a temperature. An overall view of the workhorse thrustor is shown in Fig. 2 .

The design allowed catalytic beds to be prefabricated as an assembly so that upon completion of an experimental matrix, a new configuration could be readily installed. The individual segment lengths were each 1/2 inch. Therefore, the shortest catalytic bed was 1/2 inch in length.

Also included was an allowance for reducing the diameter of the catalyst bed. This was accomplished by fabricating additional segments with a 2.00-inch ID and with the same outside diameter as the regular segments. An additional section was used between the injector and the entrance to the bed to accomplish a smooth flow transition. The exit section of the bed exhausted directly into the larger diameter chamber. In this manner, it was possible to vary the L/D ratio of the catalyst bed while holding the catalyst mass constant to study the pressure drop parameter. Theoretically, the L/D ratio should have little effect on the thermal response.

The design also provided for flexibility in thrustor length. The maximum obtainable length was governed by the length to which the end plates can be spread (13 inches), and could be increased, if necessary, by providing longer support bars.

Injector-Mixer

The basic function of the injector-mixer is to introduce the propellants to the catalyst bed as a homogeneous mixture. A 4-on-1, fuel on oxidizer, injector configuration with a 60-degree included angle between opposite fuel streams was chosen (Fig. 3). This configuration had been used

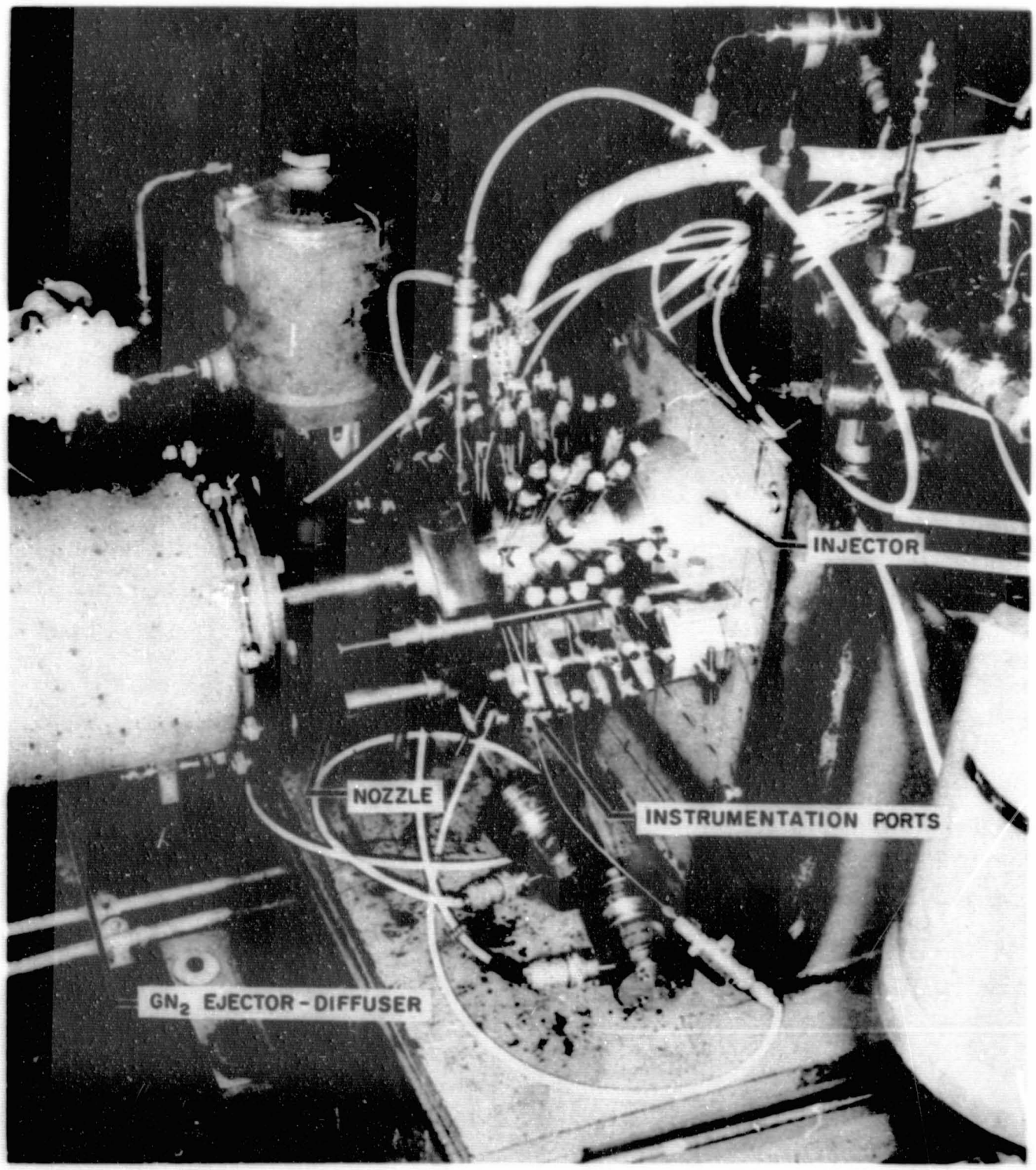

Figure 2. Side View of the Workhorse Thrustor (Showing the Instrumentation Ports in the Chamber)

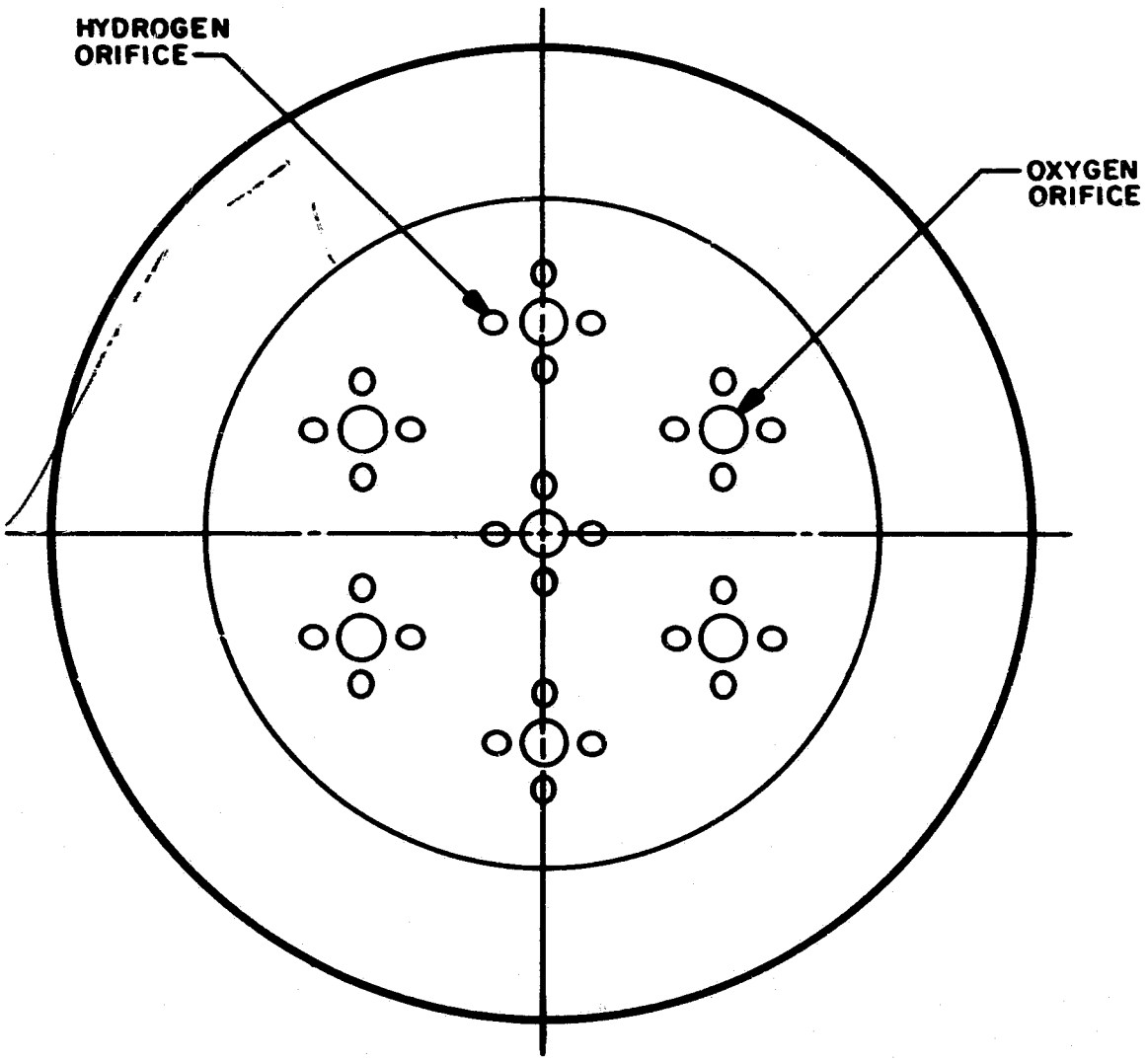

Figure 3. Schematic Representation of the 4-on-1 Injector Face Pattern

successfully during previous hydrogen/oxygen work at Rocketdyne. For orifice sizing, the momentum criteria of Elverum and Morey (Ref. 2) was employed:

$$\left(\frac{\dot{w}_1}{\dot{w}_2}\right) \frac{2}{1} \left(\frac{A_2}{4A_1}\right)^{1.25} = 290 \qquad (1)$$

where

$\dot{w}_1$ = total mass flowrate through all hydrogen orifices

A_1 = area of one hydrogen orifice

$\dot{w}_2$ = total mass flowrate through all oxygen orifices

A_2 = area of one oxygen orifice

Although the preceding equation is based on liquid-liquid system data, it is the most relevant available.

The resulting orifice diameters were:

Fuel, 0.0998 inch

Oxidizer, 0.203 inch

The first two experiments were conducted with a void mixing section length of 2 inches between the injector face and catalyst bed. Insufficient mixing probably occurred, the result being flashback to the injector face. In an effort to eliminate the occurrence of flashback, a high heat capacitance mixing bed was installed. The bed was fabricated from copper pellets 1/16 inch in diameter, was 1/2 inch in length, and was placed just upstream of

the catalyst bed. The bed served two purposes in the prevention of flashback: (1) the heat capacitance of the copper could absorb heat from the gas stream during incipient flashback, thus quenching it, and (2) the velocity of the gases flowing forward through the bed would be increased (for a given volumetric flow), possibly well above the flame front velocity in the gas downstream of the bed. An additional advantage of the copper bed is that it tends to promote mixing of the flowing propellants. The copper shot bed was successful in preventing flashback, and was used during all subsequent experiments. The copper shot capsule was identical to the catalyst bed capsule shown in Fig. 4 .

Catalyst Bed

The design of the catalyst bed was governed by (1) allowable pressure drop, (2) the required mass flow, (3) the degree of reactivity required, and (4) types of catalyst configurations available. In addition, while still meeting the preceding constraints, it was desired to minimize bed weight. Based on the preceding criteria, a 3-inch ID bed employing 1/16-inch MFSA catalyst was selected. Toward the end of the program, 1/8-inch MFSA catalyst also was employed. A variable bed length was included in the design. An example of a catalyst capsule is presented in Fig. 4 .

Bed Supports. Three screens and an end plate were used for support and containment of the catalyst and diffusion beds. At first, light Nichrome (30 mesh, 0.0114-inch-diameter wire) screens were used upstream and downstream of the diffusion bed, and a heavy Nichrome screen (16 mesh, 0.032-inch-diameter wire) was used downstream of the catalyst bed. As an additional downstream support, a 1/4 inch stainless-steel end plate was used (Fig. 5). Problems were encountered as a result of the screens slipping

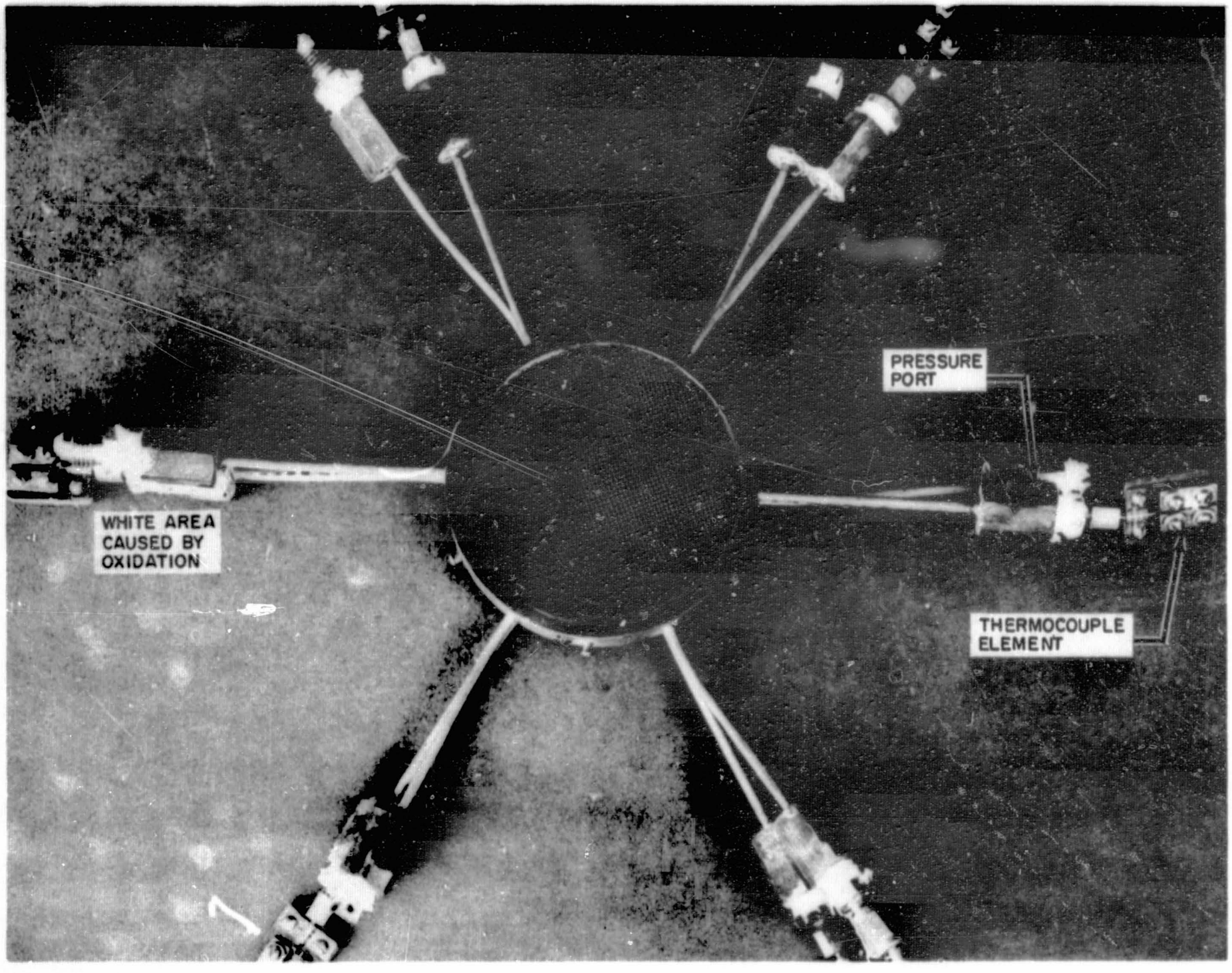

Figure 4. View of the Catalyst Bed Section of the Thrustor From the Downstream Side (as from the throat)

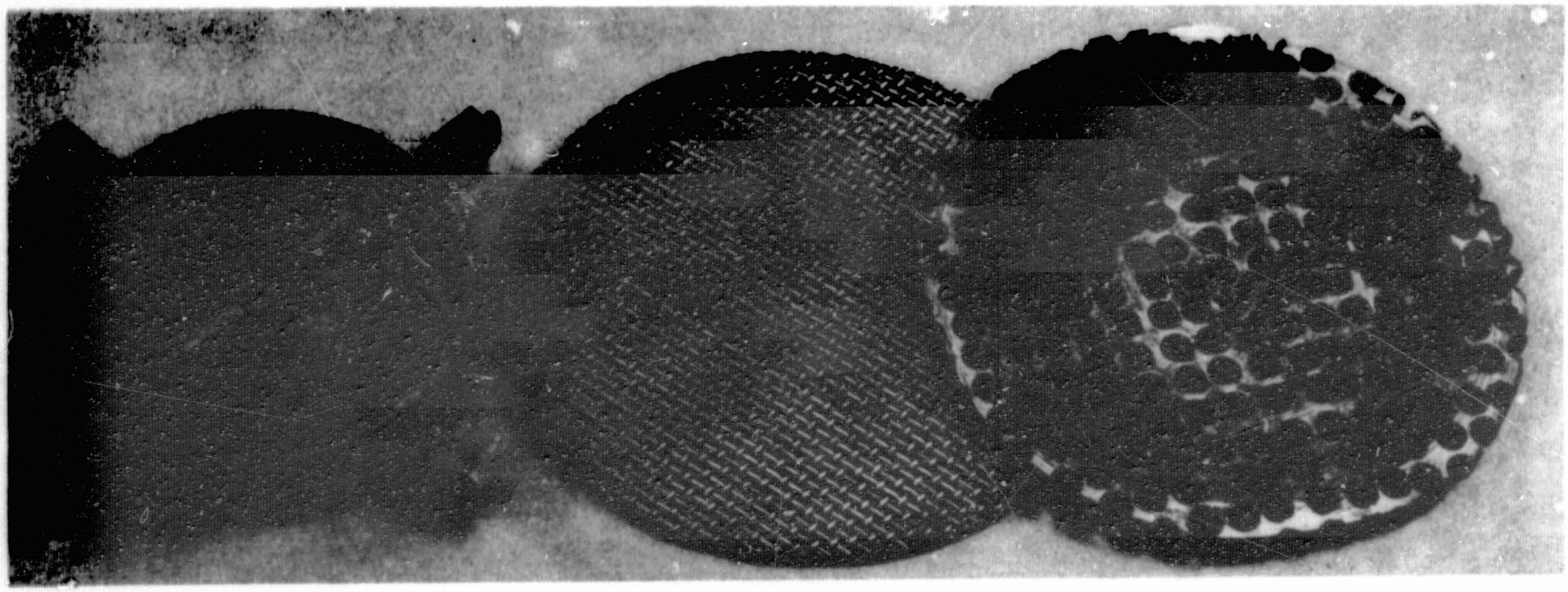

LIGHTWEIGHT RETAINING PLATE USED IN CONJUNCTION WITH THE DOWNSTREAM OXYGEN INJECTOR

SCREEN USED AT THE DOWN-STREAM END OF THE CATALYST BED

RETAINING PLATE USED AT DOWNSTREAM END OF CATALYST BED

Figure 5. The Retaining Plates and Screen Used in the Thrustor Catalyst Bed Section

out of position which allowed catalyst and copper shot to migrate between the segments, and resulted in leaks. This was overcome by spot welding the screens to the dividers with the catalyst or copper shot in place. The screen material used in these instances was a very light tantalum. However, oxidation and embrittlement occurred after a few runs, causing the screens to fail (Fig. 6 shows the catalyst capsule after a hot firing). Light, stainless-steel screen was then used in place of the tantalum. This arrangement worked well for the remainder of the runs.

It was observed, however, that during a run the screens would tend to bow outward allowing the catalyst to redistribute itself leaving a visible gap where channeling quite probably occurred. This was corrected by placing another heavy plate upstream of the diffusion bed.

During the downstream injector evaluation runs, it was observed that the measured temperature downstream of the catalyst bed was considerably lower than that measured in the catalyst bed. This was attributed to the large thermal capacitance of the end plate. Substitution of the large mass end plate with a lighter one eliminated this discrepancy.

Turbulator Rings. An additional design change was made for the performance runs. During the workhorse experiments, there was a strong indication from the mass flowrates that channeling was taking place. Turbulator rings were added within the catalyst bed to curtail this action. The rings were standard snap rings fabricated from stainless steel. They were placed 1/4 inch apart and protruded 1/8-inch into the catalyst bed. The groove positions that accommodate the snap rings are clearly shown in Fig. 7 . One ring is also in place to demonstrate the amount of ring protrusion relative to the catalyst bed.

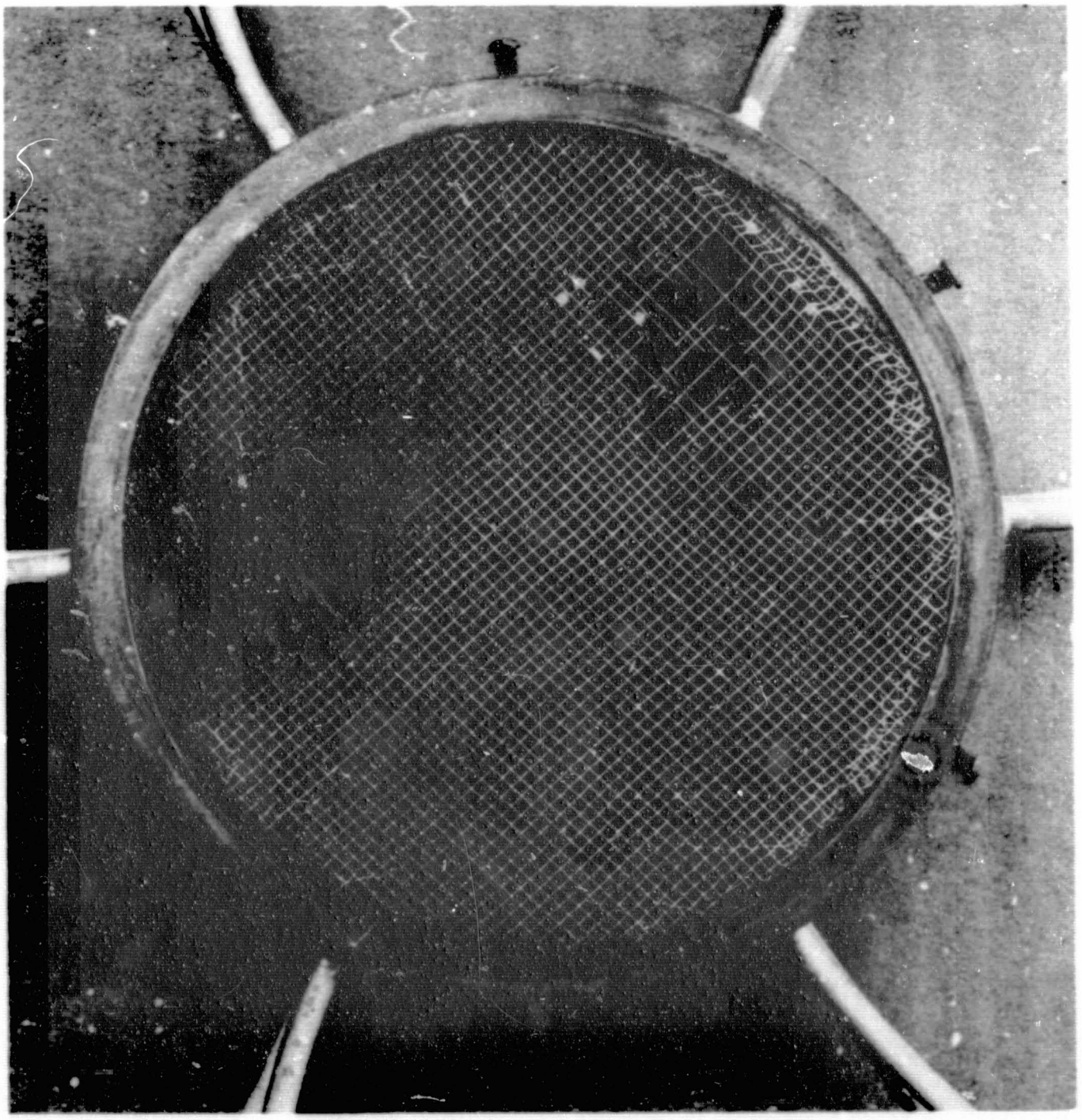

5AA36-8/30/66-S2A

Figure 6. View of Thrustor Catalyst Bed From Downstream (From Throat) Showing Oxidized Tantalum Screen Including Screen Breakdown

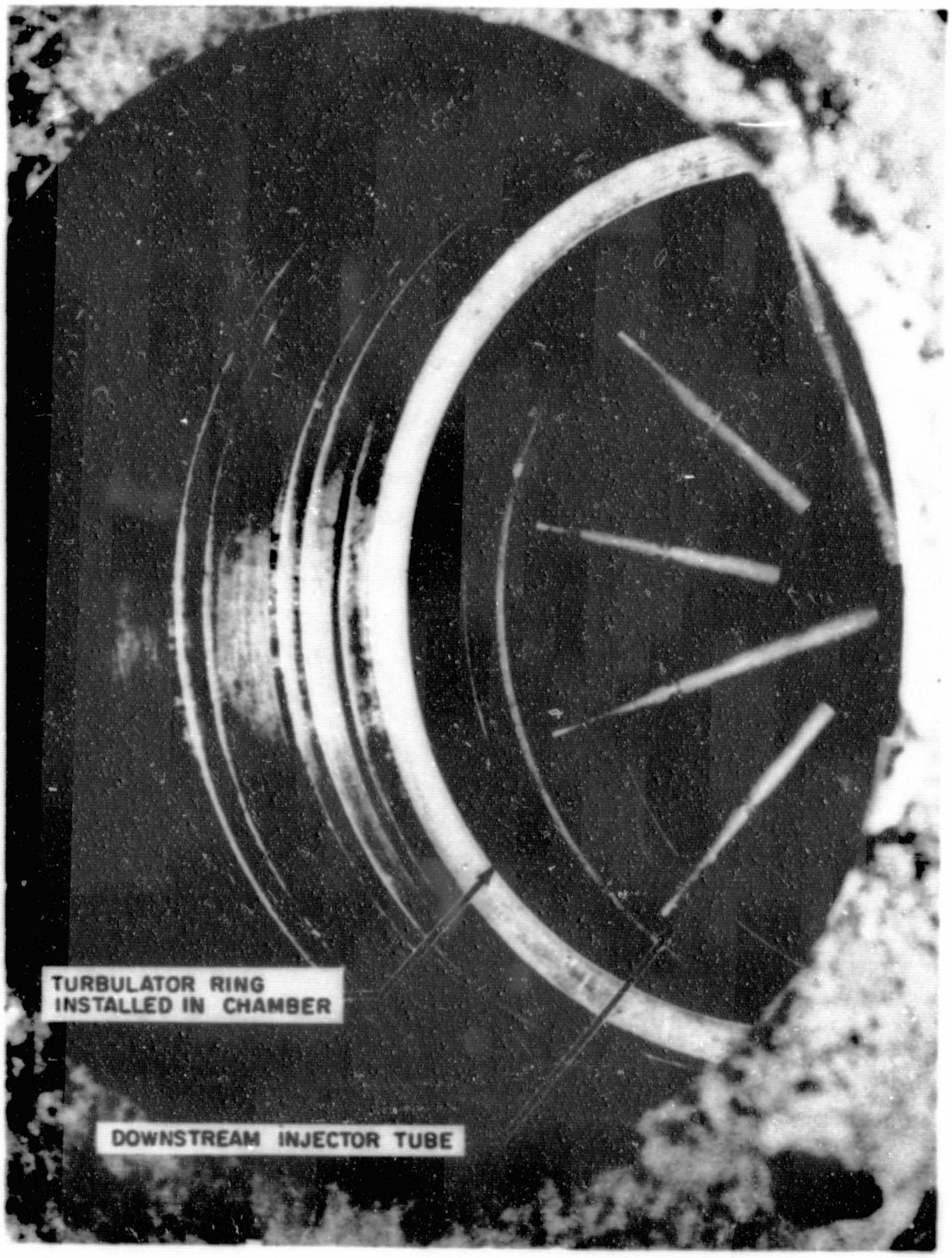

Figure 7. View of Catalyst Bed Chamber (With Catalyst Removed) Showing Installation of a Turbulator Ring

Bed Packing. To ensure random bed packing, the following procedure was used: The lower support screen was installed and the catalyst was poured over it. A very light (1-1/2 ounces) hammer was used to tap the sides of the reactor causing the pellets to settle. More catalyst was then added and the chamber was again tapped. This procedure was followed until the tapping would produce no further pellet movement. At this time, the upper support screen was installed.

Catalyst Activity Measurements

A small-scale laboratory glassware evaluation was conducted to measure the relative catalyst activity. This allowed comparison of activities with catalyst used during previous programs and an indication of activity degradation with use. The evaluations were conducted as described in Ref. 3 .

The results are summarized in Table 1 . The percent conversion as shown in Table is not to be taken as indicative of performance of actual thrustors. These numbers are for this particular test and are for comparative purposes. The conditions of the "standard test" are shown.

Downstream Injector

The downstream injector was designed to provide for homogeneous mixing of the injected oxygen and the effluent stream from the catalyst bed. This was required both from engine performance considerations and to prevent hot spots within the chamber which could result in chamber burnout. Materials of construction that would withstand high temperature oxygen contact were selected.

TABLE 1

RELATIVE CATALYTIC ACTIVITY

Sample	Percent Conversion	
	25 C	-196 C
1/16-Inch MFSA, Unused, Lot Number 118-7-L-130	94.0	70.2
1/16-Inch MFSA, Used During Runs No. 7 Through 11, Lot Number 118-7-L-130	60.6	37.9
1/16-Inch MFSA, Unused, Lot Number C3776	91.8	75.2
1/16-Inch MFSA, Used During Runs No. 5 and 6, Lot Number C3776	89.2	68.4
1/8-Inch MFSA, Lot Number 10008	95.5	59.8
1/8-Inch MFSA, Lot Number C3229	93.0	73.5

Standard Condition::

H_2/O_2 molal ratio	3.1
Carrier gas diluent	nitrogen
Catalyst weight	5 grams
Theoretical yield	0.3969-percent water
Duration of run	10 minutes

For details see Ref. 3.

The design selected is shown in Fig. 8 and 9 . The 12 radial tubes are fabricated from Hastelloy W. There are 72 elements in the downstream injector through which the secondary oxygen flow is introduced. Sawcut injection elements were positioned such that the flow would be evenly proportioned over the chamber cross section. The radial tubes are fed through an annulus which allows for propellant feed from two locations 180 degrees opposed. The peripheral annulus is very large compared to the main diameter of a spoke. This provided for equal pressures to all spokes and, thus, an even flow distribution. The spoke main feed area was 10 times greater than the total spoke outflow area, again helping to ensure an even flow distribution.

Downstream Combustion Chamber

The combustion chamber diameter was set by that selected for the catalytic bed. During the initial experiments, which were only concerned with injector-mixer and catalytic bed investigations, the length of this section was set at 1-1/2 inches. During the later experiments with the downstream injector, the length was increased to 2 inches and then, during the last four experiments, to 2-1/2 inches in an effort to allow for more complete downstream mixing and combustion. Because it was noticed that the thermocouple farthest downstream still indicated the highest temperature, the length of the combustion chamber for the performance engine was increased to 6 inches to allow for even more downstream mixing and combustion.

The downstream injector has smooth surfaces on both sides which joined with the lapped surfaces of the two adjoining segments to form a seal. This seal was aided by using Permatex on the two sealing surfaces. The seal was absolute in that, with 30-psig helium in the chamber, no leakage could be detected using the "soap bubble test."

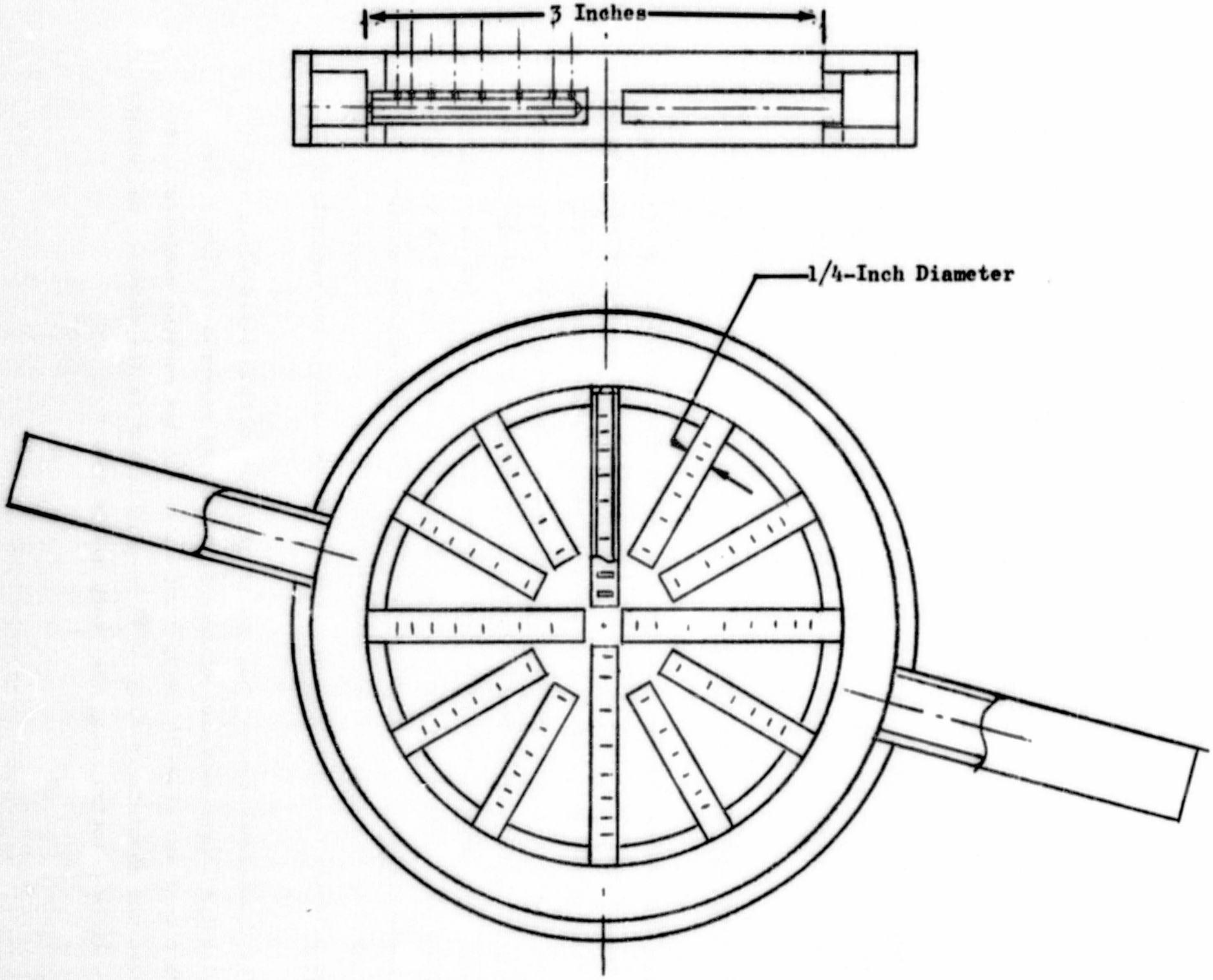

Figure 8. Injector-Downstream Radial Feed-OART Test Engine

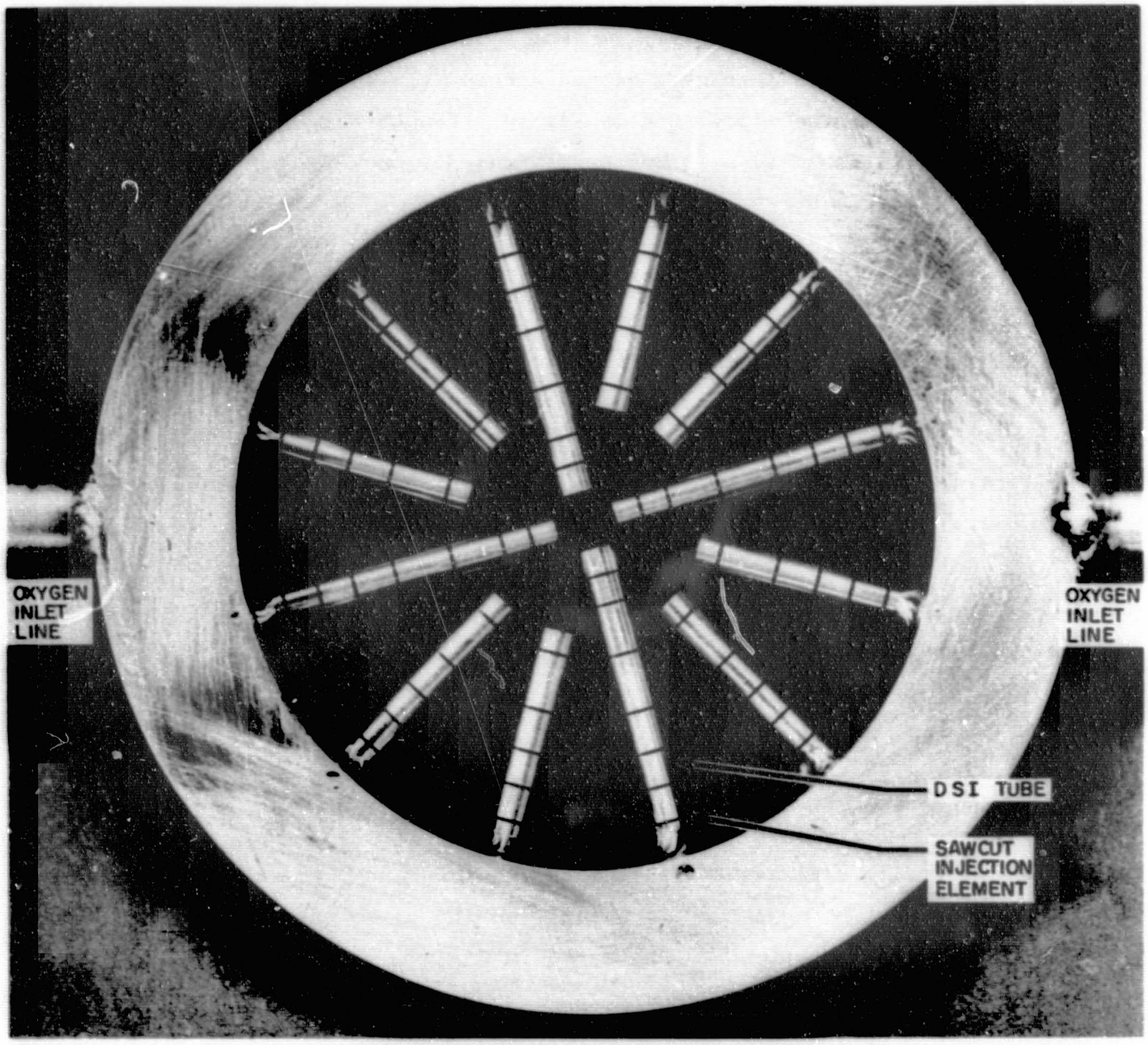

Figure 9. A View of the Downstream Injector (DSI) From the Thrustor Throat Side

Nozzle

The nozzle assembly shown in Fig.10 was fabricated from 300 series stainless steel. The wall thickness at the throat section was 1.4 inches. Provisions for obtaining a pressure measurement downstream of the throat were incorporated in the design. The nozzle contraction ratio was 6:1 and the divergent sections had an expansion ratio of 2.3 and a conical half angle of 17-1/2 degrees.

Workhorse Hardware Details

Thrustor Wall Dimensions. The workhorse hardware was designed for use in experiments where the desired run time would be on the order of 10 to 20 seconds. This duration would allow a steady-state condition to be achieved.

A heat transfer analysis was used to determine run duration limits. This analysis utilized:

1. Heat transfer characteristics as predicted in the analytical portion of this program and reported in Volume I of this report (Ref. 1)
2. Standard transient heating charts for hollow cylinders where the temperature history is a function of the Fourier number, $\alpha\tau/a^2$, and the Biot number, ha/k (Ref. 4)

The wall thicknesses in the chamber and nozzle sections were sized for run durations an order-of-magnitude larger than the desired 10 to 20 seconds. A summary of the dimensions and pertinent parameters for the workhorse thrustor are presented in Table 2 .

Figure 10. A View of the Nozzle Section of the Thrustor From the Upstream (Injector) End

TABLE 2

WORKHORSE THRUSTOR DESIGN DETAILS

Chamber Pressure, psia	10
Thrust (F), pounds	20
Mixture Ratio	2.5:1
Nozzle Expansion Area Ratio (ϵ)	2.3:1
Nozzle Contraction Area Ratio (ϵ_c)	6:1
Reactor Internal Diameter (D_r), inches	3.0
Combustion Chamber Internal Diameter (D_c), inches	3.0
Catalytic Bed Length (L_{ca}), inches	0.5 → 2.0
Diffusion Bed Length (L_{DB}), inches	0.5
Mixing Section Length (L_{MS}), inches	1.5
Combustion Chamber Cylindrical Length (L_{cc}), inches	2 → 2.5
Distance between Catalyst Bed and Downstream Injector (L), inches	0.5
Nozzle Material	Stainless steel
Reactor Material	Stainless steel

NOTE: These dimensions were those during the last thrustor component evaluation experiments.

Instrumentation and Recording Facilities

The recording systems are characterized with a response time of approximately 25 milliseconds which was adequate to monitor the steady-state operation of the conditioner subsystem. The temperatures (~10-millisecond response) was measured by bare-wire thermocouples with the thermocouple type being dictated by the temperature range to be measured. A Rosemont bulb (~100-millisecond response) calibrated to liquid hydrogen temperatures was used to monitor liquid hydrogen flow into the heat exchanger. Pressure measurements (~10-millisecond response) were principally obtained from Tabor or Statham vacuum transduers because the experiments were conducted below atmospheric pressure conditions.

The data were monitored during the experiments on Dynalog circular recorders or Easterline Angus strip recorders. These data were principally used to determine the success or failure of a test in a qualitative manner because of the slow response of the recorders and the difficulty in reducing the data. A Beckman data acquisition unit was used to record the majority of the data. The results from the Beckman unit were reduced on an IBM 7094 computer and presented in graphical form on cathode ray tube plots.

The thrustor design contained provisions for inclusion of extensive instrumentation for pressure and temperature measurements. A schematic showing placement of the instrumentation is presented in Fig. 11. A photograph of an instrumented thrustor is shown in Fig. 2 .

Lightweight Engine Hardware

The design of the hardware for this phase of the experimental effort was substantially different from the workhorse configuration. This was principally caused by the difference of design goals. Here, the emphasis was placed on simplicity, ease of fabrication, and maximization of performance. The valves, manifolds, and injector for the lightweight thrustor were those used in the workhorse studies. The catalytic reactor section was fabricated from a section of stainless-steel tubing. This was welded

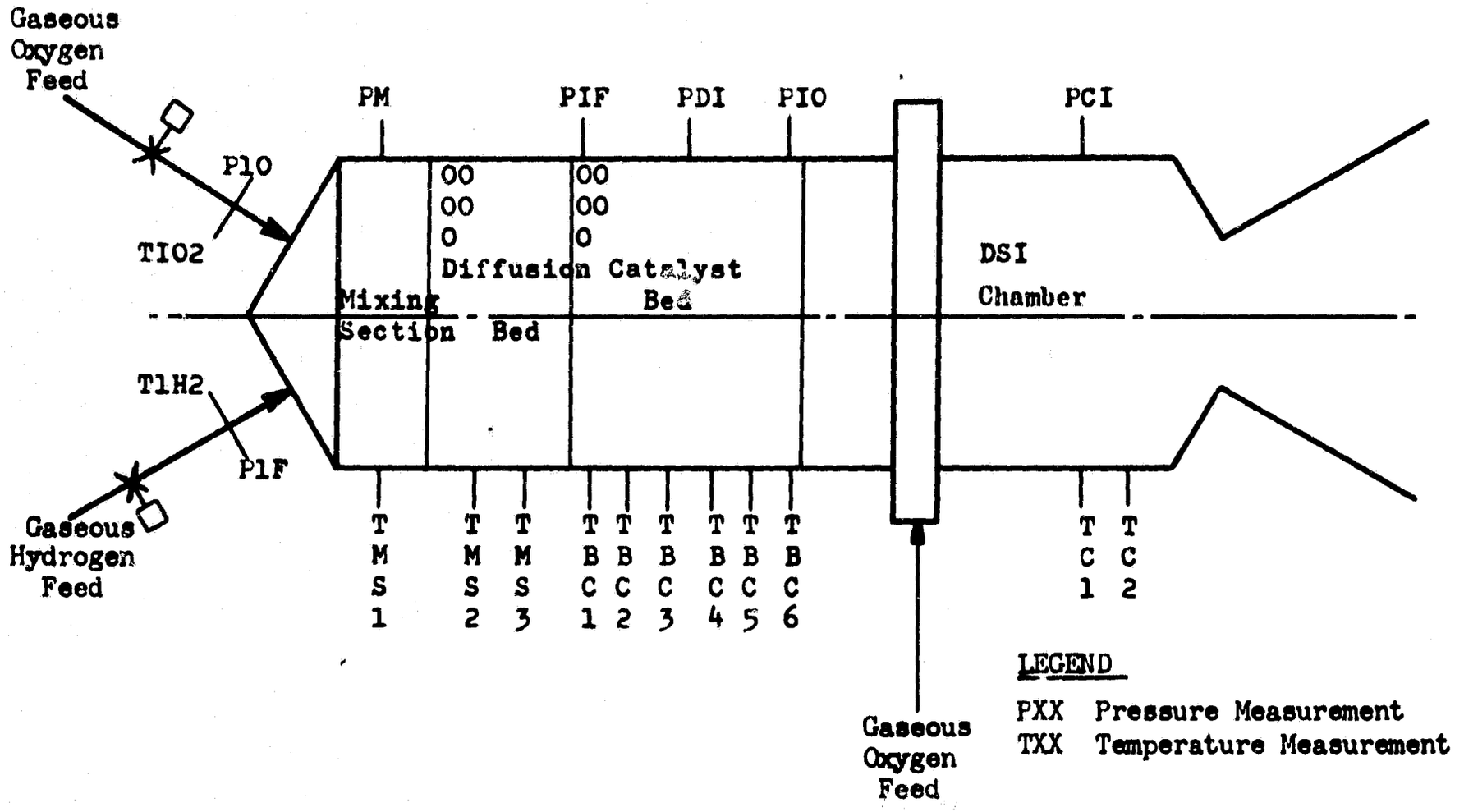

Figure 11. A Schematic Representation of the Workhorse Thrustor With Instrumentation Locations

to the injector-manifold assembly to eliminate sealing problems. The internal diameter of the tube had provisions for nine snap rings. The snap rings provided support for the screens used to separate and/or maintain the catalyst and diffusion beds. Three extra rings were installed in the catalyst bed section as turbulators. These three rings were to prevent channeling of the propellants down the chamber wall, thus promoting higher performance. The thrustor used the lightweight screen support, shown previously in Fig. 5. Additionally, a longer combustion section downstream of the downstream injector was incorporated into the lightweight design.

The upstream section or catalytic reactor was welded to the downstream injector and the downstream section of Type 270 nickel nozzle. The downstream combustion section was designed to provide adequate length for complete downstream combustion to occur and to provide heat transfer data. The choice of nickel was based on the following: (1) good high-temperature strength compared to stainless steel and copper, (2) good thermal conductivity compared to stainless steel, and (3) moderate density, thus providing a lightweight chamber.

The combustion chamber wall thickness was 1/8 inch. To provide some form of thermal isolation to limit the longitudinal and circumferential modes of heat transfer, saw cuts to within 0.020 inch of inside surface, forming 1/2- x 1/2-inch isolation blocks, were made. Eight of these blocks were machined on the external surface of the nozzle, providing eight temperatures to obtain thermal data. The thermocouples were welded to the center of each block, thus providing a good physical contact for accurate temperature measurement.

The nozzle expansion ratio of 5:1 was used to prevent nozzle separation at the simulated altitude.

A summary of the pertinent dimensions and parameters of the lightweight thrustor is presented in Table 3. A schematic of the thrustor is presented in Fig. 12.

Experimental Systems

Workhorse Experiments. The propellant supply system shown in Fig. 13 was designed to provide propellant at temperatures to 200 R at low pressures and at the flowrates consistent with the thrustor operation (~ 0.05 lb/sec). Ambient temperature oxygen and hydrogen were cooled by a liguid nitrogen heat exchanger to the desired temperature. Flowrates were measured using a calibrated venturi meter (hydrogen) and a calibrated metering orifice (oxygen).

A description of the individual components is presented in Table 4. Basically, the facility system consisted of: (1) high-pressure supply for both hydrogen and oxygen, (2) prevalves (not shown) for on-off operation, (3) sensitive pressure regulators (not shown) to give "fine" mixture ratio control, (4) filtering and drying systems to eliminate oil and other minor impurities which might deactivate the catalyst, (5) calibrated venturi or orifice flow measuring devices, (6) shell and tube heat exchangers, and (7) sonic orifices to ensure that thrustor perturbations would not disturb the flow system.

A nitrogen-driven diffuser was used to obtain altitude prior to each test, and to maintain sonic flow at the thrustor throat during each test. The facility is shown in Fig. 14.

Lightweight Experiments. The tests were carried out at Component Test Laboratory 4 (CTL-4), which had altitude simulation capability of above

TABLE 3

LIGHTWEIGHT THRUSTOR DESIGN DETAILS

Chamber Pressure (P_c), psia	10
Thrust (F), pounds	20
Mixture Ratio	2.5:1
Nozzle Expansion Area Ratio (ϵ)	5:1
Nozzle Contraction Ratio (ϵ_c)	6:1
Reactor Internal Diameter (D_r), inches	3.0
Combustion Chamber Internal Diameter (D_c), inches	3.0
Catalytic Bed Length (L_{CB}), inches	1.0
Diffusion Bed Length (L_{DB}), inches	0.5
Mixing Section Length (L_{ms}), inches	1.5
Combustion Chamber Cylindrical Length (L_{cc}), inches	6.0
Distance Between Catalyst Bed and Downstream Injector (L), inches	0.5
Combustion Chamber-Nozzle Material	Type 270 nickel
Reactor Material	Stainless steel

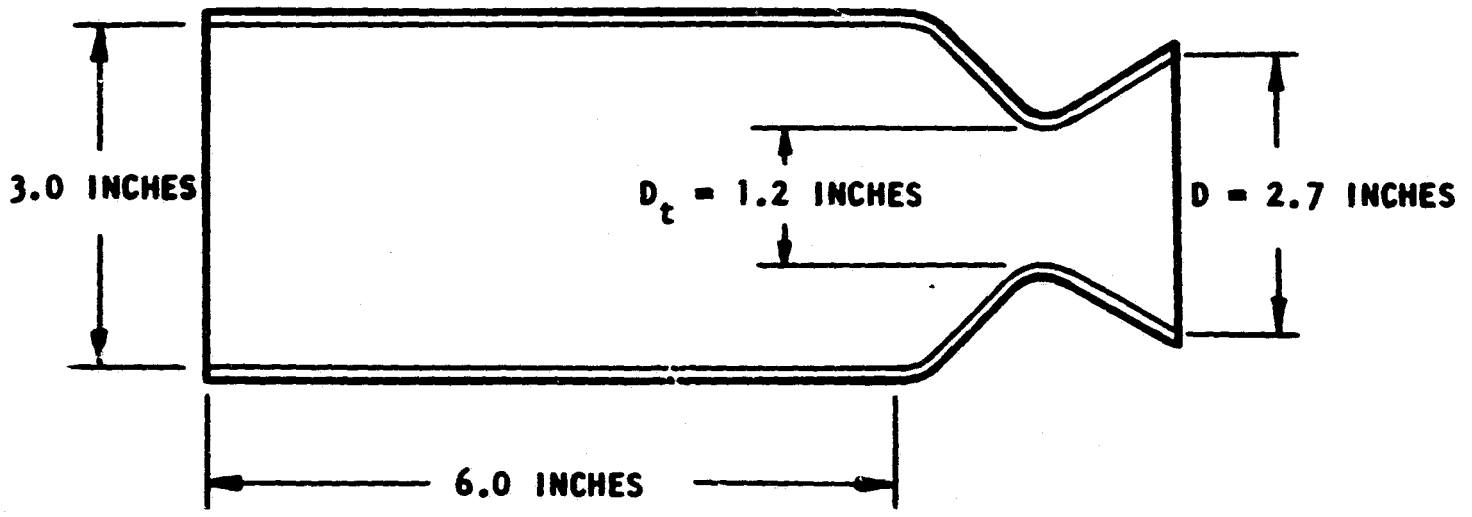

CONTRACTION RATIO 6:1
EXPANSION RATIO 5:1

MATERIAL:
NICKEL, TYPE 270, 1/8 INCH

Figure 12. Lightweight Thrustor

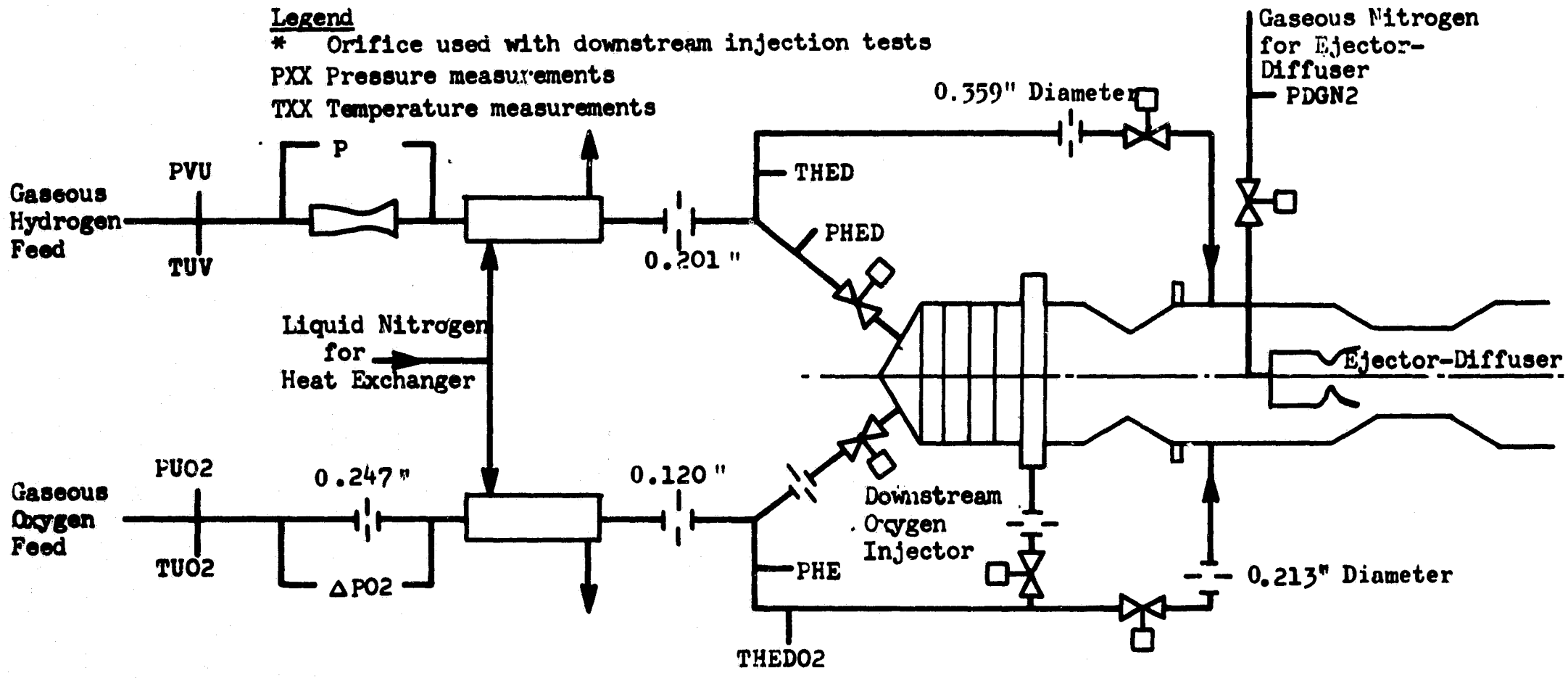

Figure 13. Flow Schematic of the Propellant Systems for Workhorse Thrustor Tests

TABLE 4

DESCRIPTION OF FACILITY COMPONENTS

Component	Supplier	Remarks
Regulators H_2 and O_2	Grove	Pressure loaded from blockhouse H_2: GS 306-04 O_2: WBX 305-N4
Filter	Unknown	10-micron, 6- x 1/2-inch OD
Dryers	In-house Fabrication	Molecular sieve for H_2 system 16- x 2-inch OD Charcoal for H_2 and O_2 systems 15- x 3-inch OD
Heat Exchangers	In-house Fabrication	Four 1/4-inch copper tubes for propellant 1- or 1-1/4-inch outside shell 6-foot long
H_2 Venturi	Flow-Dyne Engineering, Inc. Fort Worth, Texas	P/N: V240600-SA
O_2 Orifice	In-house Fabrication	
Prevalves	Marotta	1/2-inch MV 583

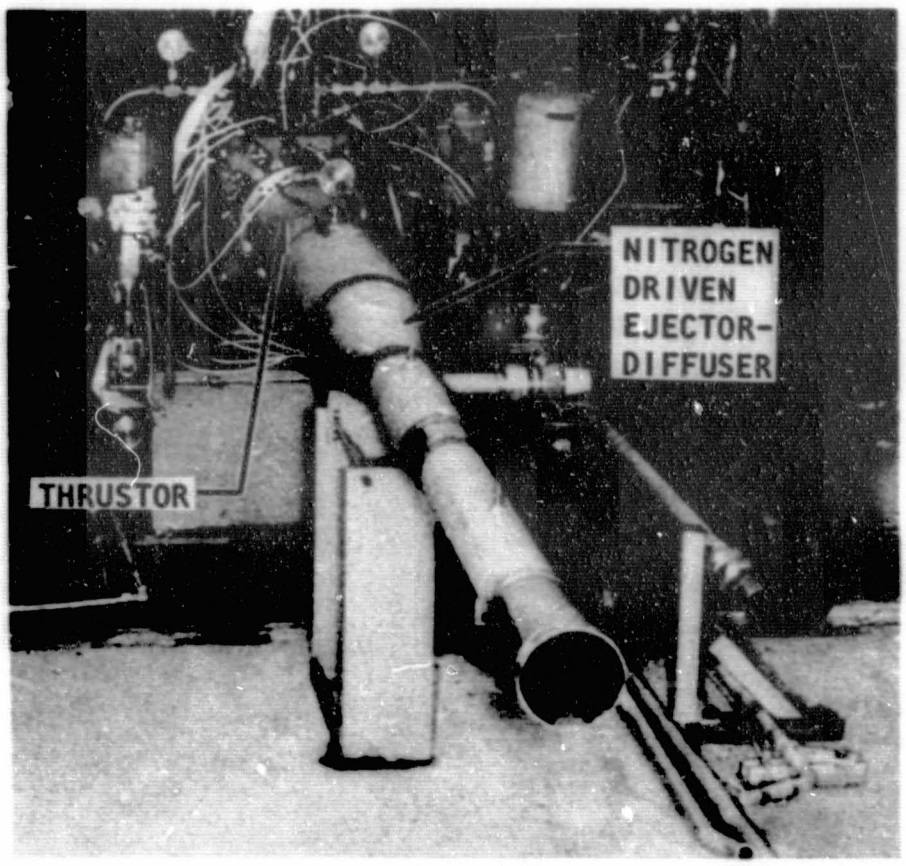

Figure 14. Front View of the Workhorse Thrustor Facility

100,000 feet. The lightweight thrustor system (Fig.15) differed from that employed for the component evaluation experiments in several ways:

1. The feed systems employed were static rather than dynamic in that the system did not require an extended run duration with bleeds to obtain run conditions. This allowed pressurization directly upstream of the valves prior to main valve actuation and, also, eliminated the pneumatic filling or equalization time for the line between the main valve and the bleed valve used in the dynamic system for the component tests.
2. The downstream injector had a separate oxygen source. This decoupled the downstream injector system and allowed independent downstream injector pressurization control which also eliminated an excessive pneumatic fill time for the downstream injector feed system.
3. The heat exchanbers were eliminated since ambient propellants were used.

TEST PROCEDURE

Workhorse Thrustor Experimental Procedure

The test procedure for each test was initiated by starting the nitrogen driver. The system was then primed in a dynamic manner to obtain the requisite flows before operating the thrustor main valves. The hydrogen and oxygen pressures were set at the desired level with the flow diverted through the bleed valves. The liquid nitrogen was then pressurized and fed through the heat exchangers to chill both propellants to the required state. The total run duration was limited by the liquid nitrogen supply which would last approximately 2 minutes.

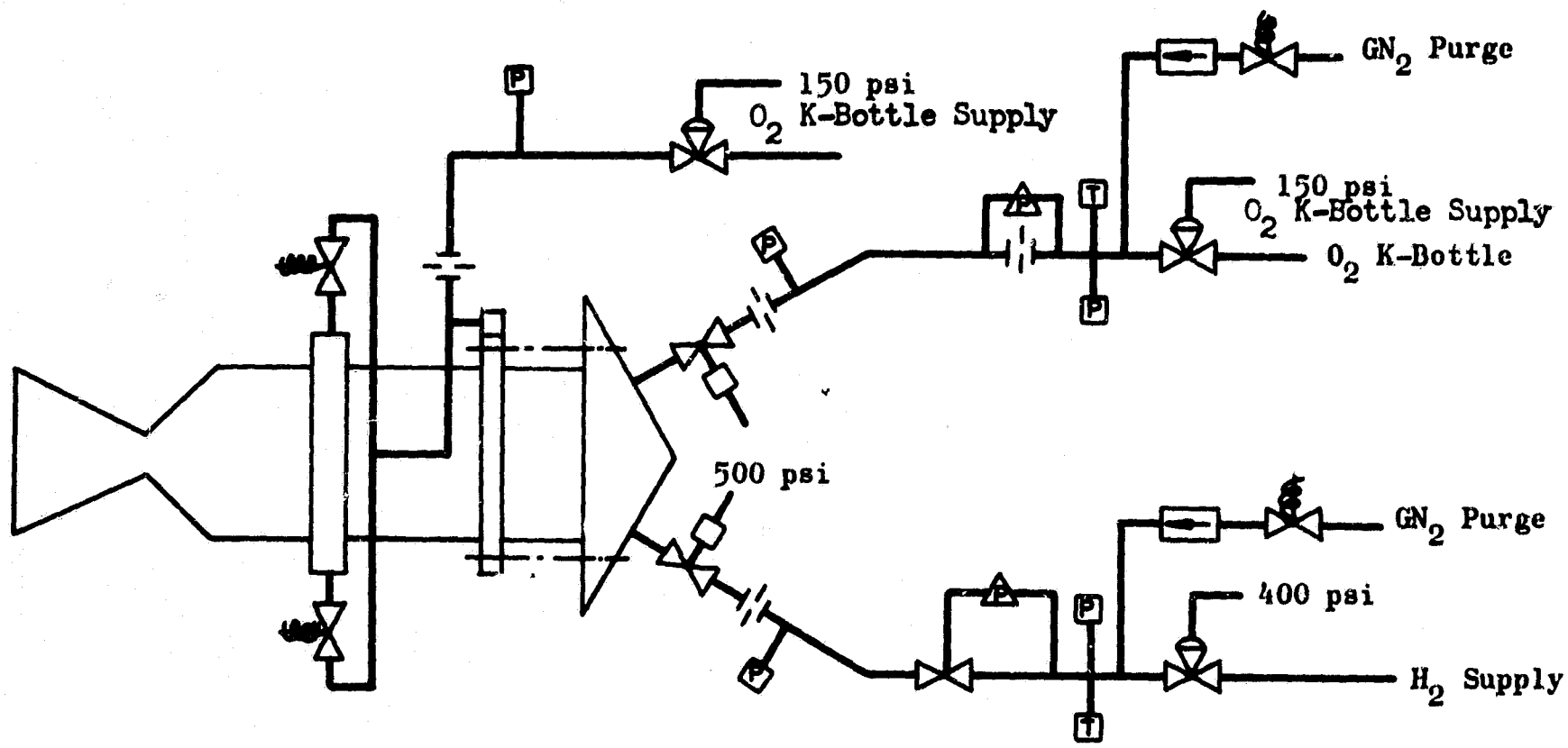

Figure 15. Flow Schematic of the Propellant Systems for Lightweight Thrustor Tests

The flow was diverted to the workhorse thrustor when the propellant temperatures had reached the desired values. Initially, it was necessary to adjust the pressures during the firing to achieve a nominal mixture ratio of 1.0 through the catalyst bed (for a temperature of ~1500 F). During the downstream injection operation, the downstream injector valve was not activated until the thrustor reached steady-state conditions with flow through the catalyst bed. Opening the downstream injector valve generally resulted in a diversion of a portion of the oxygen flow from the catalyst bed. This was corrected by increasing the oxygen pressure until the nominal bed flowrate was achieved. The shutdown procedure was the reverse of that for startup.

Lightweight Thrustor Experimental Procedure

Three valves were operated during a run (two main propellant valves and two downstream injector valves actuated simultaneously, Valve operation was monitored on both a strip recorder and an oscillograph. All runs were accomplished at altitude with the hyperflow operating.

For the initial run, the hydrogen injection pressure was first increased until the desired flowrate was reached, and the oxygen flowrate through the catalyst bed was increased until the desired bed temperature and mass flow were reached. The oxygen flow through the downstream injector was then initiated and increased until the desired flowrate was obtained. The valves were secured in the following sequence: (1) main oxidizer, (2) downstream injector, and (3) main fuel. The regulators were not vented; rather, the regulated settings remained for the duration of the experiments.

The procedure for subsequent experiments was as follows: the propellant flows were initiated by opening the valves as desired, and the run was continued until the objectives were obtained. For the steady-state performance runs, the thrustor was then terminated as before (main oxidizer, downstream injector, and main fuel valves were closed, in that order). The purges were then started to cool the chamber and catalytic bed to ambient temperature.

EXPERIMENTAL RESULTS

THRUSTOR COMPONENT TESTS

The initial objectives of the thrustor experiments were to evaluate components, obtaining general design criteria, and explore possible problem areas. This series of experiments was directed at four principal goals:

1. Obtaining sufficient mixing of the oxygen-hydrogen propellants to prevent severe mixture ratio variations in the catalyst bed
2. Preventing flashback to the injector face
3. Minimizing the necessary catalyst bed length to promote and sustain ignition while minimizing response time and pressure drop
4. Establish a durable downstream injection technique that homogeneously distributes the oxygen in the hot gaseous product of the catalytic reactor.

Components were used which gave adequate service for this purpose, but they were not optimized for either weight or performance. At the conclusions of this series of tests, the results were to be used in designing lightweight hardware for altitude performance heat transfer evaluations. A summary of the component tests is presented in Table 5.

Injector-Mixer Evaluation

The objective of the injector evaluation phase was to obtain sufficient mixing of the propellants to prevent severe local mixture ratio variations in the gases entering the catalyst bed. This was to prevent local burnout of the catalyst bed, obtain efficient reaction of the propellants,

TABLE 5

SUMMARY OF EXPERIMENTAL IGNITION RUNS CONDUCTED ON THE WORKHORSE THRUSTOR FOR COMPONENT TESTS

Run	Run Conditions and Configuration**	Results*
1	GN_2 flow, 1-inch bed	ΔP agreed with predictions
2	1-inch bed, 1/16-inch catalyst ambient propellant and bed	Burned-out bed
3	Lowered O_2 driving pressure; 1-inch bed, 1/16-inch catalyst ambient propellant and bed	Burned-out bed
4	Added 1/2-inch diffusion bed, put plate on H_2 manifold	Good ignition; indicated 0.4-inch bed needed for ignition
5	Catalyst bed length to 1/2-inch, ambient propellant and bed	Ignition
6	Ambient bed, cryogenic propellants	Ignition
7	Ambient temperature bed, chilling propellants	Flameout
8	Ambient temperature bed, chilling propellants	Flameout
9	Ambient bed, cryogenic propellants	Good run
10	Cryogenic bed and propellants	No ignition
11	Ambient bed, cooling propellants	Flameout at ~ -160 F
12	Ambient bed and propellants with downstream injector	No ignition of downstream injector; opened downstream injector at 1200 F and bed temperature dropped to 900 F
13	Repeat but increased O_2 pressure	Smooth ignition
14	Cryogenic propellants and ambient bed with downstream injector	Ignition; increased O_2 pressure
15	Cryogenic propellants and ambient bed with downstream injector	Ignition
16	Cryogenic propellants and bed	No ignition

*Total run time with downstream injector on was 6 minutes; total run time with downstream injector in system was 16 minutes.
**Catalyst was 1/16-inch MFSA (Engelhard) except where otherwise noted.

TABLE 5

(Concluded)

Run	Run Conditions and Configuration**	Results*
17	1/16-inch catalyst, 1-inch bed; change downstream injector orifi s, ambient bed and propellants	Ignition
18	Cryogenic propellants and ambient bed with downstream injector	Ignition
19	Cryogenic bed and propellants	No ignition
20	2-inch bed, 1/16-inch catalyst, cryogenic bed and propellants	No ignition
21	Decreased G_o by half, cryogenic bed and propellants	No ignition
22	1/8-inch catalyst, 2-inch bed, cryogenic bed and propellants with downstream injector	Ignition in bed, after 13 seconds then ignition of downstream injector
23	1/8-inch catalyst, 2-inch bed, cryogenic bed and propellants with downstream injector	Same delay; smooth ignition
24	1/8-inch catalyst, 2-inch bed, cryogenic bed and propellants with downstream injector	Same results
25	Halved the flowrate	Immediate bed ignition
26	1/8-inch catalyst, 1-inch bed, cryogenic propellant bed or ~ -116 F	Ignition after ~3 seconds; no downstream reaction
27	1/8-inch catalyst, 1-inch bed, cryogenic propellant bed or ~ -116 F; bed to -150 F	Ignition delay of 15 seconds; downstream injector started, then temperature dropped
28	LN_2 chilled bed, halved G_o	No ignition

*Total run time with downstream injector on was 6 minutes; total run time with downstream injector in system was 16 minutes.
**Catalyst was 1/16-inch MFSA (Engelhard) except where otherwise noted.

and minimize the danger of flashback of the reaction front to the injector face. The initial injector-mixer configuration used a four-on-one pattern (fuel on oxygen) with six elements as illustrated in Fig. 3. This injector pattern may not be optimum for gas-gas, low-pressure systems, but it had operated well in previous efforts (Ref. 5). The first experiment was of approximately 16 seconds duration and resulted in high temperature damage to the catalyst bed and attendant screens. The mixture ratio was determined to be excessive (~1.5) and in addition, there was evidence of flashback indicating a lack of homogeneity in mixing. This was determined by visual inspection of the hardware in the posttest condition, noting the similarity of burned areas in the bed, and the position of the injector elements. In addition, the mixing section thermocouple measured a high temperature.

Steps taken to correct the situation were: (1) the inclusion of a diffusion bed 3 inches in diameter and 0.5 inch long consisting of copper shot immediately upstream of the catalyst bed, and (2) the addition of a diffusion plate in the hydrogen manifold immediately upstream of the injector to circumvent a hydrogen ramming-starvation effect across the injector manifold, which would result in a nonuniform hydrogen flow from the injector.

After incorporating these changes, further runs indicated that satisfactory mixing was occurring. Hot spots were not evident upon inspection of the hardware following the runs, so the injector-mixer configuration was considered satisfactory. The diffusion bed, a 1/2-inch long segment filled with copper shot, was used for the remaining experiments. The diffusion bed was positioned 1-1/2 inches from the face of the injector. The bed was, in effect, a passive mass consisting of a maze of flow passages that accomplished two functions: (1) promoted additional mixing of the propellants due to the added pressure drop, and (2) increased the velocity of the mixed propellants as a result of the decrease in effective flow area, thus preventing flashback to the injector.

The original tests were conducted with a center post running down the catalyst bed simulating the internal downstream injector concept. After further analysis of this type of injection concept, it was decided to simplify the downstream injector by feeding in the oxygen externally instead of through the bed. This circumvented problems that would be incurred from heat transfer to the oxygen before it was injected downstream. The flow schematic (Fig. 13) depicts the oxygen being externally fed to the thrustor.

Ignition Tests

Catalyst Bed Experiments. After obtaining a satisfactory injector-mixer and preventing flashback to the injector, the minimum catalyst bed length was determined. This was necessary because both the catalyst bed pressure drop and thrustor response time are strongly dependent upon bed length. The initial experiments incorporated cryogenic propellants and an ambient temperature bed to determine the minimum bed length needed to promote and sustain a reaction. The catalyst bed was instrumented as shown in Fig. After the first experiments, the bed was shortened from 1 to 1/2 inch because the reaction was found to occur in the first 1/2 inch.

Temperature and pressure gradients in the thrustor for two distinct time slices during a representative experiment (Run 6 , Table 5) are presented in Fig. 16 and 17 . A well-defined temperature gradient was established through the bed length. The thermocouples were all positioned in the approximate radial center of the bed and, consequently, they were monitoring approximately the same flow stream. The maximum temperature was at TBC 4, which was located 0.2 inch from the beginning of the catalyst bed. The thermocouple in the mixing section had reversed polarity (TMS 1); consequently, the temperature appeared to increase instead of decrease during the run and was deleted from the gradient plot. The thermocouples in the copper shot (TMS 2 and TMS 3) chilled down during the run (to -80 F)

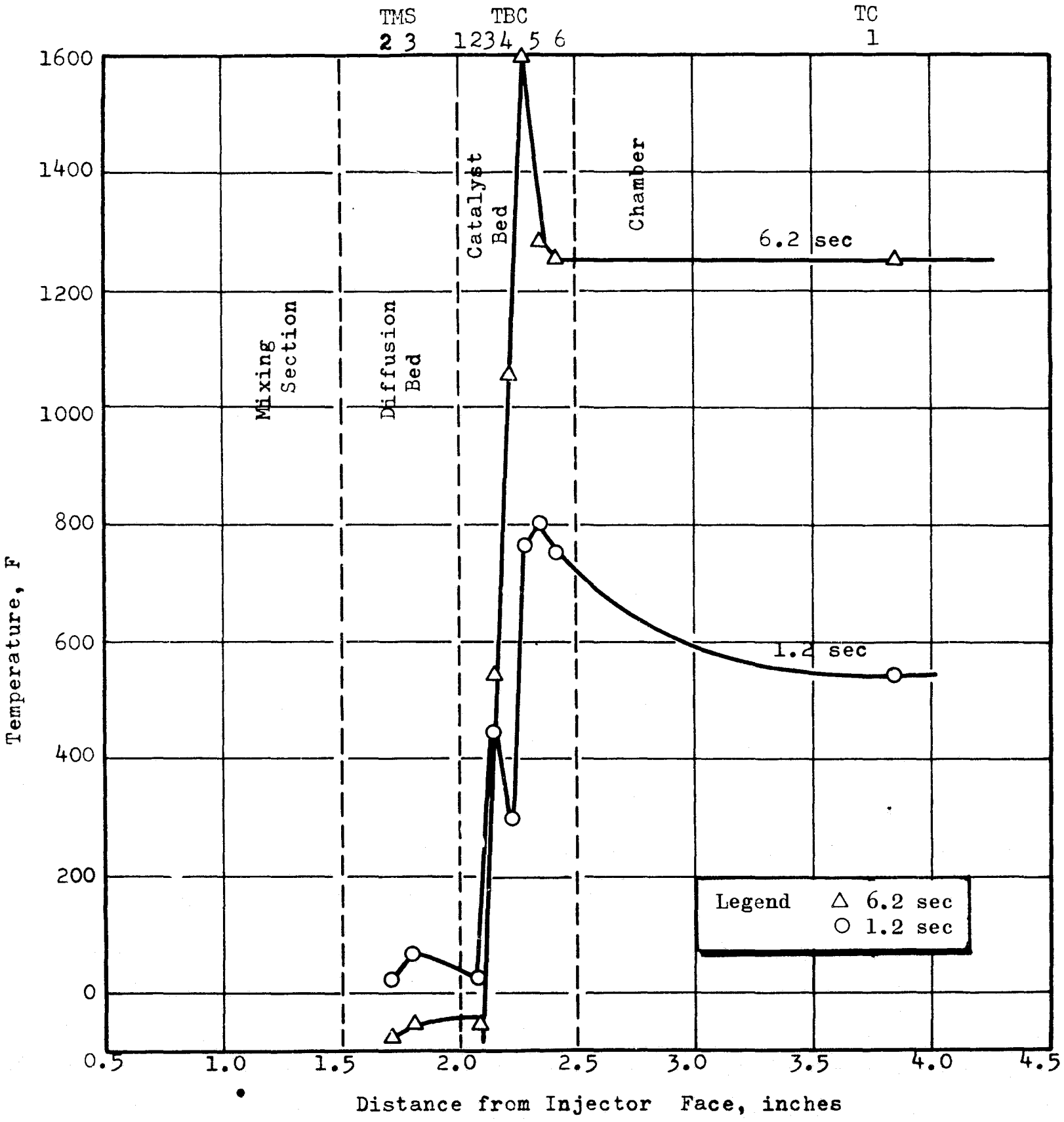

Figure 16. Temperature Gradient in Thrustor as a Function of Distance From the Injector at Two Time Slices During Thrustor Startup

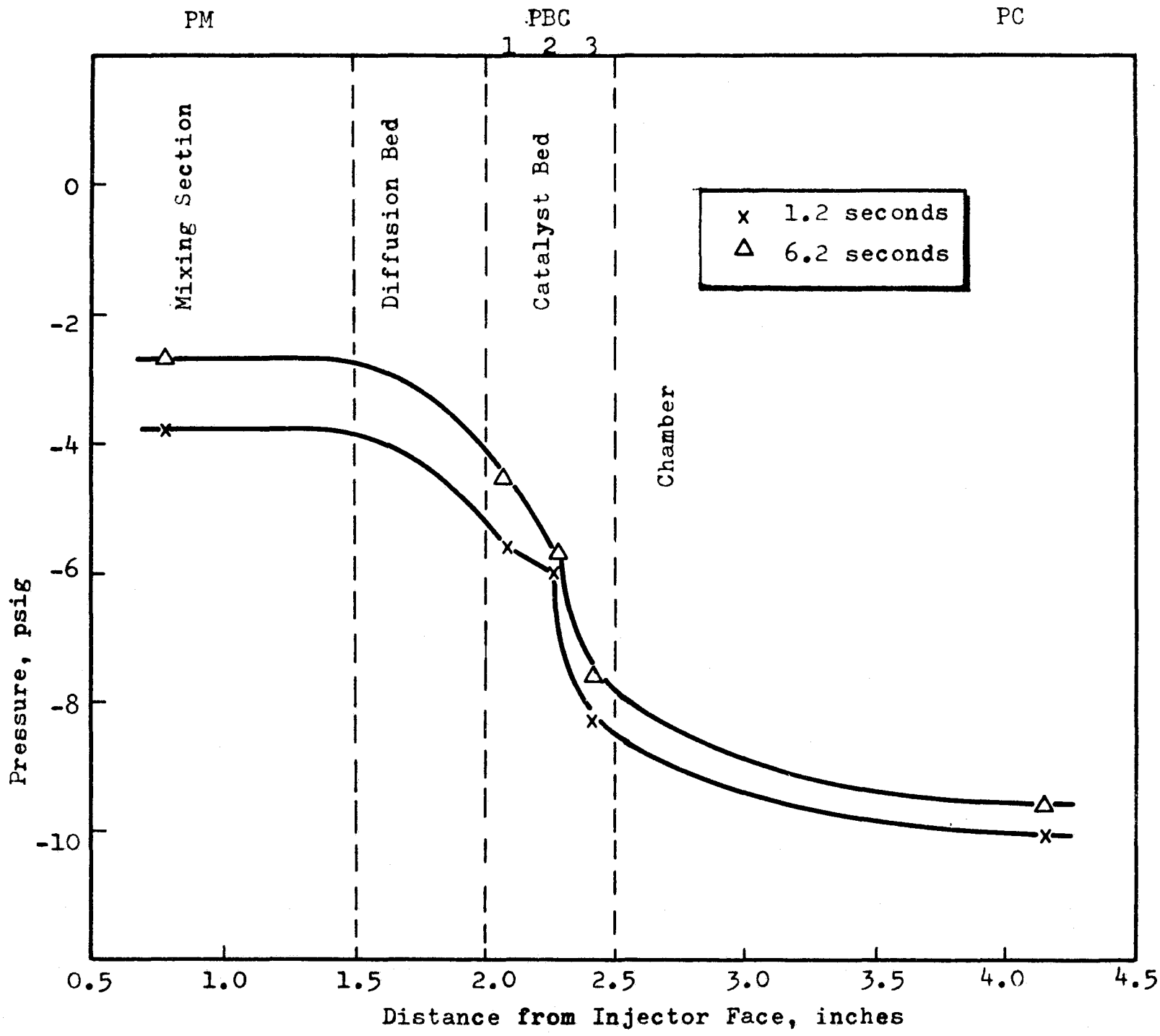

Figure 17. Pressure Gradient in Thrustor as a Function of Distance From the Injector at Two Time Slices During Thrustor Startup

with no indication of the flame front advancing toward the injector. The temperatures in the bed were recorded by thermocouples TBC 1 through TBC 6. After 1.2 seconds, the reaction appeared to near completion at the TBC 5 position in the bed. The remainder of the bed acted as a thermal capacitance. After 6.2 seconds, the temperatures downstream of TVC 4 reached approximately equal values which should have approached 1600 F after an appropriate run duration. The maximum reaction position also moved upstream, as indicated by TBC 4 registering a higher temperature than TBC 5.

The pressure gradient through the thrustor also was well defined. The experimental values are shown in Fig. 17 . The continuous line represents as approximation of the pressure gradient through the thrustor. No loss in pressure should occur in the mixing section because the only impediment to flow is the friction along the thrustor walls. Once the mixed propellants enter the diffusion bed, the pressure decreases. The point of inflection occurs at the PBC 2 station for both time slices because the maximum reaction temperature (TBC 4 or TBC 5) was nearest to this transducer.

Ignition Difficulties at Low Temperature. Previous work at Rocketdyne had demonstrated reliable catalytic ignition of fuel-rich oxygen-hydrogen mixtures at propellant and catalyst bed temperatures below 210 R (Ref. 3). These tests were conducted at chamber pressures substantially higher than 10 psia. One of the objectives of the present study was to determine if the ignition characteristics at these low pressures would be similar to those observed in the previous program. Ignition difficulty occurred at temperatures below 410 R. The ignition temperature results of this and previous programs are summarized in tabular form on the following page.

TABLE 6

SUMMARY OF HYDROGEN/OXYGEN CATALYTIC IGNITION LIMITS

MFSA Catalyst, inch	Bed Temperature, R	Propellant Temperature, R	Preignition Pressure, psia	Ignition
1/16	310	235	3 to 8	No
1/16	410	235	3 to 8	Yes
1/8	360	235	3	Yes
1/8	210	210	46 to 169	Yes

Comparison of the results at high and low preignition pressures indicates a substantial pressure-temperature interaction for a given catalyst. Also, the 1/8-inch MFSA catalyst appears more active than the 1/16-inch MFSA.

It appears that there is a pressure-temperature tradeoff for H_2-O_2 catalytic ignition for a given catalyst. When operation at low initial inlet temperatures is desired, operation above a minimum pressure level is required.

Recently, Shell Development Company (Ref. 6) disclosed that their catalyst, Shell 405, showed a higher activity for catalytic ignition of low-temperature hydrogen-oxygen mixtures than did a catalyst similar to the one used during the present study. Thus, low-pressure ignition at temperatures lower than those obtained with the MFSA catalyst might be possible with the Shell catalyst.

Shell investigators reported catalytic reactivity for 3 volume percent hydrogen, 1 volume percent oxygen, 96 volume percent helium mixtures at a total pressure of 1 atmosphere and at temperatures as low as 140 R for the Shell 405 catalyst. That temperature should not, however, be strictly interpreted as a temperature at which ignition would occur in a thrustor

for a similar mixture at comparable pressures. There are two reasons why 140 R should not be strictly interpreted as an ignition temperature: (1) it has not been precisely determined what properties of the catalyst were measured by Shell's rising temperature reactor technique (for example, when the initial cooling period with the gas feed on was increased from an arbitrary 1 minute to an equally arbitrary 5 minutes, activity was not detected until 221 R), and (2) in a high flowrate system, ignition will only occur when the heat produced by reaction at the reaction sites is greater than the heat loss. The change in boundary conditions would have a significant effect on the temperature limit.

Actual reactor tests of the type conducted during the present study are necessary to establish temperature-pressure-composition ignition limits for the Shell 405 catalyst. At higher pressures, however, with the MFSA catalyst, ignition is known to be possible at initial and inlet temperatures as low as 210 R.

It is emphasized that reliable ignition was obtained with cryogenic propellants under the conditions of an ambient catalyst bed. Although under these conditions with 1/16-inch MFSA catalyst the reaction "flamed out" some time later, this did not occur with the 1/8-inch MFSA catalyst and evidently a stable reaction condition was achieved.

Downstream Injection of Oxygen (DSI)

Because of the restraints placed on the thrustor operation by the catalyst bed (MR $\cong$ 1.0), optimum thrustor performance can only be obtained by introducing additional oxygen downstream of the catalyst bed to raise the mixture ratio to nominally 2.5. A downstream injector technique that homogeneously distributes the oxygen in the hot gaseous products and retains its

integrity was desired. The oxygen was injected from an externally fed manifold that was used as one of the thrustor rings (Fig. 18). Details of the downstream injector design are described in the Hardware Design section. The downstream injector was physically located 1/2-inch downstream of the catalyst bed. The combustion section length between the downstream injector and the start of convergence was 1-1/2 to 2 inches.

The downstream injector tests are outlined in Table 7 . A total run time of approximately 6 minutes was accumulated on the DSI with no loss of physical integrity, as evidenced in Fig. 18 . No attempt was made to optimize the DSI unit, in terms of the uniformity of mixing of oxygen and catalyst bed effluent, beyond the intiial design. Reasonable performance was obtained with the initial design. Once the downstream injection technique was demonstrated to meet the experimental objectives, the experiments were terminated. The experimental procedure was to bring the catalyst bed to steady-state conditions, and then to open the DSI valve. When the DSI valve was opened, a portion of the oxygen flow bypassed the catalyst bed, effecting a reduction in catalyst bed temperature. Therefore, it was necessary to increase the oxygen pressure upstream of the choked orifice until nominal catalyst bed conditions were again met and DSI ignition occurred in the workhorse chamber.

A typical example of the results of a DSI experiment is shown in Fig. 19 . Only the critical parameters, inlet temperature to the catalyst bed-TMS 3, catalyst bed temperatures-TBC 4 and TBC 5, combustion chamber temperatures-TC 1 and TC 2, inlet oxygen pressure, DSI injection pressure, and chamber pressure PC 1 are shown. This run was characterized by (1) an ignition delay of ~10 seconds, because the starting bed temperature was cryogenic; (2) a bed thermal response of ~3 seconds; (3) immediate DSI ignition when the DSI valve was opened; (4) DSI flameout because a portion of the oxygen bypassed the catalyst bed, effecting a reduction in the mixed gas temperature TC; (5) a time period in which the initial conditions in the catalyst

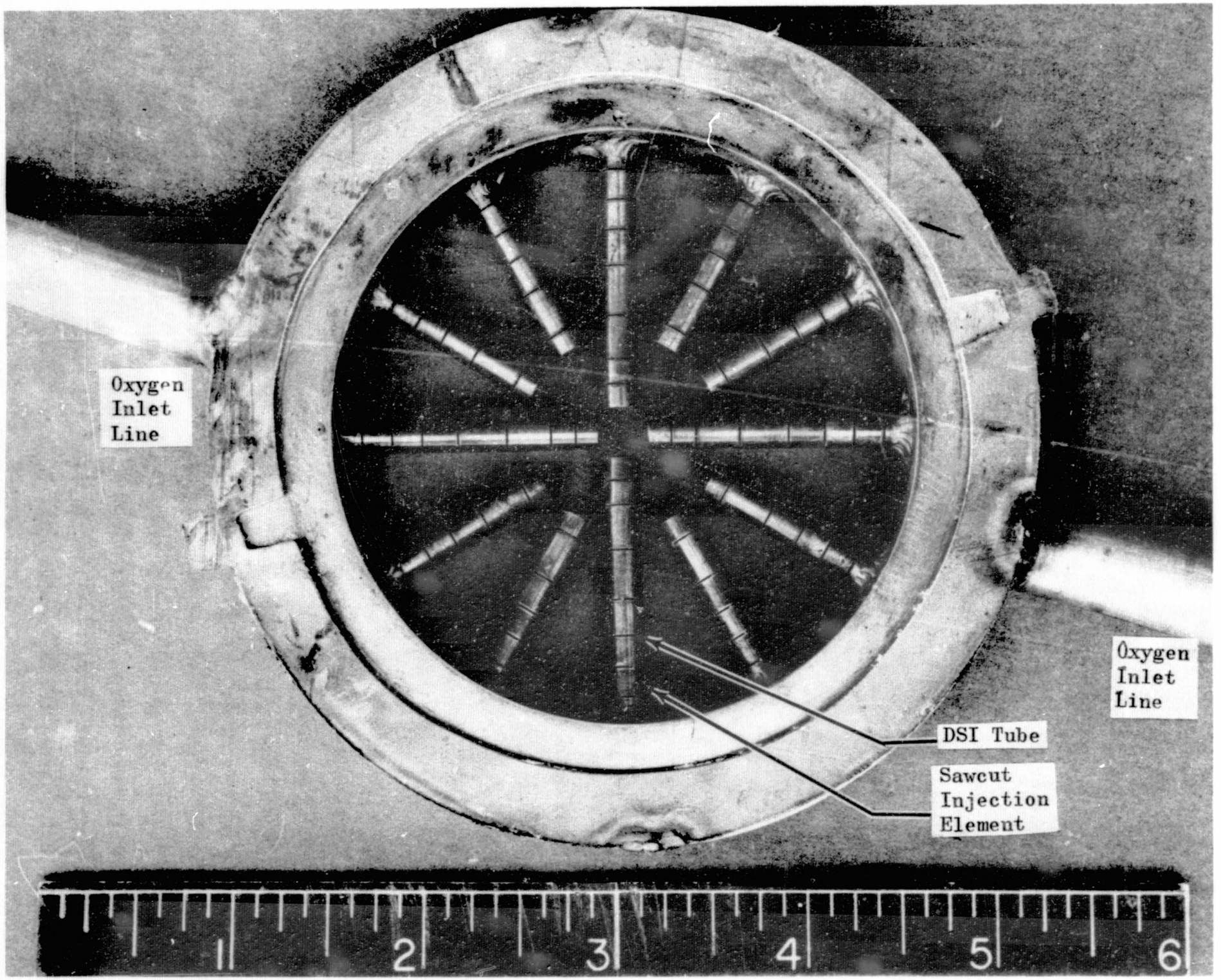

Figure 18. The Downstream Injector (DSI) After the Component Experiments

TABLE 7

SUMMARY OF DOWNSTREAM INJECTION RESULTS

Run	Type*	TBC (Last Nodes), F	Before		After		Response Times, milliseconds			Remarks
			TSC1	TSC2	TSC1	TSC2	Pressure	Temperature TSC2	Temperature TSC1	
18	AB-AP		N_2 purge left on				No ignition			N_2 purge left on; no ignition
19	AB-AP	1360	1560	1540	2570	2450	~3000	~1500	~2,000	Unreliable temperature measurements because PT-PT 10 percent RU thermocouple used (bad channeling)
20	CB-CP	~1410	25	1820	2980	2800	Uneven-2 steps	~4500	~17,500	
23	AB-AP	1335	1175	1200	3540	3330	~2100	~3600	38,000	
24	CB-CP	~1500	80	1280	760	~3300	44	2600	~500	Increasing 0_2 flowrate
28	CB-CP	~1100	32	675	~2250	>4500	88	2800	5,700	
29	CB-CP	1435	1130	1250	1630	3400	55	88	>500	
30	CB-CP	1235	350	1320	1575	2175	<1000	<1000	~17,000	
31	CB-CP	1460	1200	1325	1225	2375	242	253	Declining	Filling and thermal response above threshold temperature
32	CB-CP		N_2 purge left on							
33	CB-CP	1392	675	1550 (1270)	1850	2680	77	99	374	
			Integrated Thrustor-Conditioner							
120	AB-AP		1270	1300	3480	3650	77	100	176	Thermal and filling
	Shutdown		3700	3500	1200	1350	209	231	77	Thermal and emptying

*AB = ambient bed
CB = cryogenic bed
AP = ambient bed
CP = cryogenic bed

FOLDOUT FRAME 1

TEMPERATURE IN DIFFUSION BED
TMS 3
-150° F

TEMPERATURE IN CATALYST BED
TBC 4
~1000° F
-150° F

CATALYST BED TEMPERATURES DROP WHEN DSI FLOW IS INITIATED DUE TO LOWER MIXTURE RATIO IN BED

TEMPERATURE IN CATYLYST BED
TBC 5
~1800° F
IGNITION DELAY
-140° F
THERMAL RESPONSE

TEMPERATURE IN DOWNSTREAM COMBUSTION CHAMBER
TC1
~2100° F

ELAND, OHIO. PRINTED IN U.S.A.

TEMPERATURE IN DOWNSTREAM COMBUSTION CHAMBER
TC 2
THRESHOLD TE
FOR IGNITION

COMBUSTION OF DOWNSTREAM OXYGEN STOPS AS TEMPERATURE OF GAS FROM CATALYST BED DECREASES BELOW CRITICAL VALUE

OXYGEN DRIVING PRESSURE
PHEDO$_2$

OXYGEN DRIVING PRESSURE IS INCREASED TO RAISE TEMPERATURE OF GAS FROM CATALYST BED

OXYGEN MAIN VALVE OPEN

DSI VALVE OPEN

INJECTION PRESSURE IN DOWNSTREAM INJECTOR
PDSI

CHAMBER PRESSURE INCREASE DUE TO DSI IGNITION

PRESSURE IN DOWNSTREAM COMBUSTION CHAMBER
PC1

FOLDOUT FRAME 2

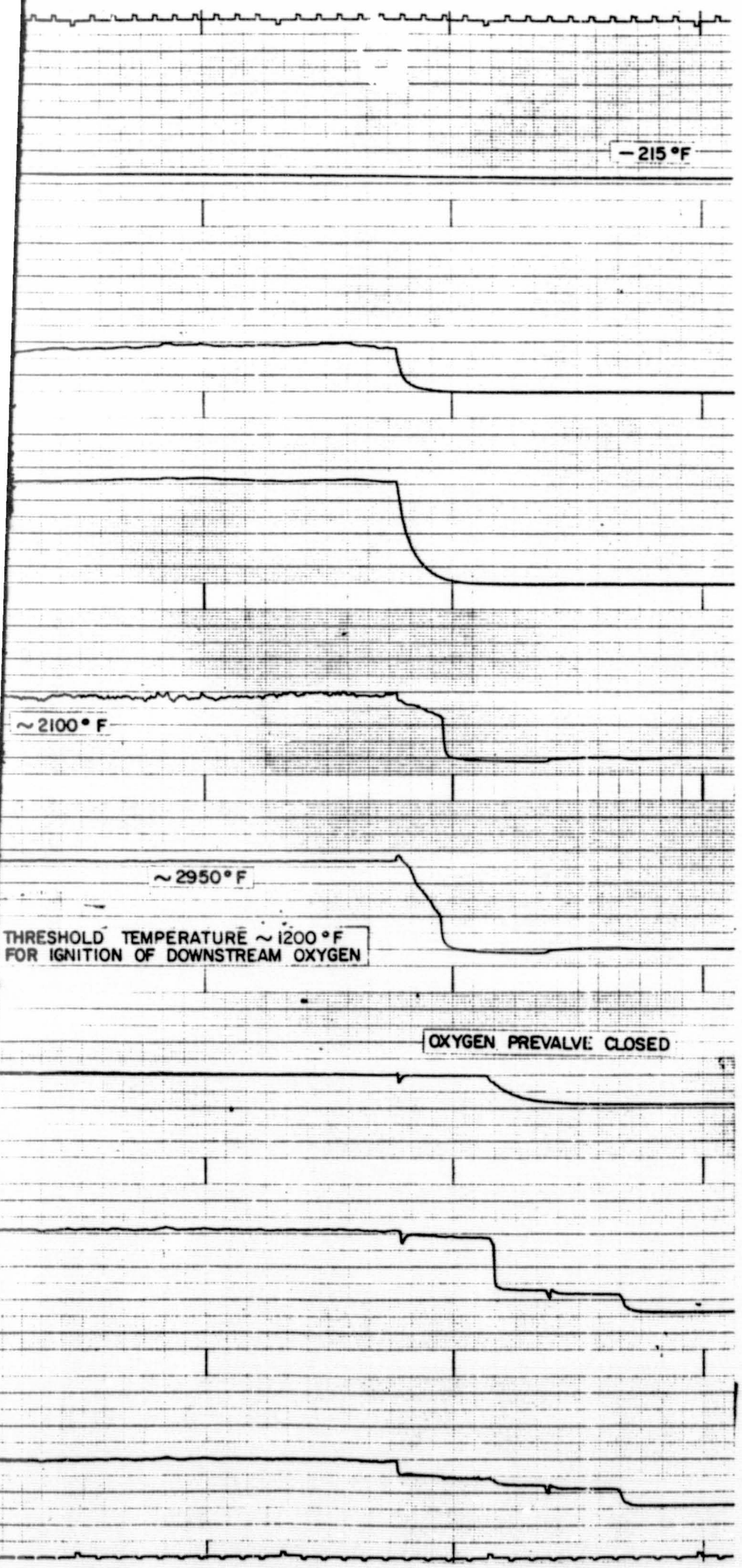

Figure 19. Temperature and Pressure Characteristics for Ignition of Oxygen Injected Downstream of Catalyst Bed in Workhorse Thrust (Run Conditions-Cryogenic Propellants and Prerun Cryogenic Catalyst Bed of 1-Inch of 1/8-Inch Engelhard MFSA Catalyst)

bed were restored by increasing the oxygen flowrate; (6) steady-state DSI ignition; and (7) a prolonged shutdown transient resulting from an oxidizer-rich, three valve sequencing procedure.

As the oxygen flowrate was increased to make up for that portion passing through the DSI valve, the mixed gas temperature gradually increased until the temperature reached a value at which spontaneous combustion occurred. This temperature is the autoignition temperature. The experimental temperature of ignition for the example under consideration was slightly erratic varying from 1270 to 1500 F. Autoignition temperatures from other runs are summarized in Table 7 and if the results of several runs (10, 20, 23, 28, and 31) are discarded for various reasons as noted in the table, the threshold temperature is 1265 ±30 F. If the resulting mixture temperature immediately after opening the DSI valve is above this temperature, combustion will occur as shown in Table 7 for Run No. 31. The thermal and pneumatic responses of the DSI ignition are discussed in the Response and Pulse Mode section of the Thrustor.

Experimental Data Evaluation and Summary

The component tests had the prime objective of determining and demonstrating thrustor components which could then be incorporated into a lightweight thrustor. The latter was to be used in determining thrustor performance and operating characteristics.

A four-on-one injector-mixer with a diffusion bed was found to give sufficient propellant mixing to prevent the occurrence of flashback of the reaction zone to the injector face, and of "hot spots" in the catalyst bed.

A minimum catalyst bed length of 1/2 inch was sufficient to promote and sustain ignition using cryogenic propellants and catalyst bed temperatures greater than 410 R. A catalyst bed temperature limit for reliable catalyst and for the preignition pressures was of interest in this study. Reliable ignition was obtained with cryogenic propellants when catalyst bed temperatures were above this limiting temperature. Previous successful ignition at these and lower temperatures for higher preignition pressures (by an order of magnitude) suggests a temperature-pressure interaction on the ignition limit. A downstream injection technique that homogeneously distributes oxygen in the hot gaseous product was successfully tested, and the physical integrity of the injector was maintained. A long response was observed with the initial downstream injector experiments because of a close coupling between the bed and downstream injector oxygen flow. Decoupling the two feed systems will increase this response, as shown in the conditioner-thrustor integrated system tests.

LIGHTWEIGHT PERFORMANCE THRUSTOR

The major objectives of this phase of the program were to obtain steady-state performance data and engine heat transfer characteristics, as well as to study engine start and tailoff behavior, and engine pulse-mode operation.

A lightweight thrustor was utilized in this effort. The design of this thrustor was based on the results of the component tests. Since extensive optimization was not an objective of the component tests, the resulting lightweight thrustor design is not an optimum design. The downstream combustion chamber and nozzle were fabricated from nickel to allow heat transfer characterization. Based upon heat transfer prediction, it was expected that the chamber could be operated in a steady-state mode for durations of several minutes.

Performance Thrustor Experiments

A series of 10 runs was planned for this phase of the program. It was desired to establish the repeatability of the set point through cycling; the correct flowrate through the catalyst bed would be set, then the oxygen flow would be cycled on and off to see if the same temperature level in the bed were obtained each time. The same type of operation also was specified for the downstream injector. These two operations, in addition to being carried out individually, were then to be carried out simultaneously.

Basic Data. Pertinent data taken during the experiments were chamber pressure, chamber temperature, propellant flows, thrust, catalyst bed temperatures, nozzle external surface temperatures, injector inlet pressures, and facility altitude chamber pressure. With these data, both performance and heat transfer calculations could be carried out. The performance was evaluated from chamber pressure, thrust, and flowrate data, while the heat transfer was evaluated from external surface temperature measurements. Start and tailoff transients were to be evaluated from transient thrust, chamber pressure, and temperature data.

Experiments Accomplished. In the first two runs, the relationship between feed system pressures (corresponding directly to propellant flowrates) and chamber pressure was to be established. The next four runs were designed to provide a steady-state condition for additional performance determinations. Heat transfer and start-tailoff transient information were also to be obtained during these runs. The final four runs were designed to evaluate pulse-mode operation and performance.

The initial run was successful and the goals were accomplished. The run sequence was as follows from the initiation of oxygen flow to the beds.

1. 0 to 92 seconds: catalyst bed flow with MR adjustment
2. 92 to 125 seconds: steady-state catalyst bed flow (MR = 1.35)
3. 125 to 164 seconds: H_2 flow only
4. 165 to 230 seconds: catalyst bed flow with adjustment to MR = 1.0
5. 230 to 251 seconds: adjustment of DSI flow
6. 251 to 275 seconds: steady-state flow at MR = 1.98
7. 275 to 277 seconds: adjustment of DSI flow
8. 277 to 292 seconds: steady-state flow at MR = 2.40
9. 292 to 298 seconds: steady-state catalyst bed flow only

Performance was calculated at four points 2, 4, 6, and 8 in the above run sequence. The results (Table 8) are discussed below.

The second run was started following engine cooldown from the first run. Approximately halfway through the planned duration of this run the chamber failed because of excessively high temperatures on the order of 2400 to 2500 F in the area of the contraction section and throat. The run sequence from initiation of propellant flow to the catalyst bed was as follows:

1. 0 to 23 seconds: steady-state catalyst bed flow at MR = 1.16 to 1.18
2. 23 to 87 seconds: steady-state flow with downstream injector at MR = 2.75
3. 87 seconds: chamber failure

TABLE 8

SUMMARY OF PERFORMANCE RUNS

Run No.	P_c, psia	F_{vac}, lb_f	MR	c^*_{theo}, ft/sec	c^*_{meas}, ft/sec	c^*, percent	$I_{s_{theo}}$, $\frac{lb_f}{lb_m/sec}$	$I_{s_{meas\ vac}}$, $\frac{lb_f}{lb_m/sec}$	I_s	C_f, percent	Was Downstream Injector Operating?
56	7.6	(14.9)	1.35	8100	7360	91	401	(390)	(97.5)	(107)	No
	8.0	(15.1)	1.00	7830	7160	91.5	393	(363)	(92.5)	(101)	No
	11.6	(20.8)	1.98	8320	7485	90.0	406	(363)	(89.4)	(99.4)	Yes
	12.8	(22.6)	2.40	8310	7390	89	407	(350)	(86)	(96.7)	Yes
57	6.3	(11.9)	1.16	7960	6640	83.4	398	(333)	(83.6)	(100)	No
	7.0	(15.2)	1.18	7965	7190	90.4	399	(419)	(105)	(116)	No
	12.3	(24.5)	2.75	8250	7470	90.6	406	(442)	(99)	(109)	Yes

NOTES: 1. The above runs employed 1/8 inch MFSA catalyst, combustion chamber length, 6-inch and 1-inch catalyst bed length

2. Values in parentheses are of questionable accuracy.

Figure 20 shows the thrustor during the high temperature portion of the second run.

A review of the data shows that the chamber conditions at the time of failure were 12.9-psia chamber pressure and 2.74 mixture ratio. The mixture ratio was later found to have increased from that of the previously successful run because of changing tank pressure. Although the chamber pressure was also higher than design, the higher mixture ratio is viewed as the prime cause of failure.

Performance Results

Performance was calculated at four points for the first run and at three points in the second run. The results (Table 8) are discussed below.

The characteristic velocity, c*, was calculated from chamber pressure and mass flow measurements:

$$c^*_{meas.} = \frac{P_c A_t g_c}{\dot{w}_T} \qquad (2)$$

The chamber pressure actually measured was the static pressure; from this measurement a dynamic pressure was calculated and employed in the equation above. The c* as calculated above was then corrected for heat loss to the wall as well as thermal throat expansion in accordance with procedures given in Ref. 7 .

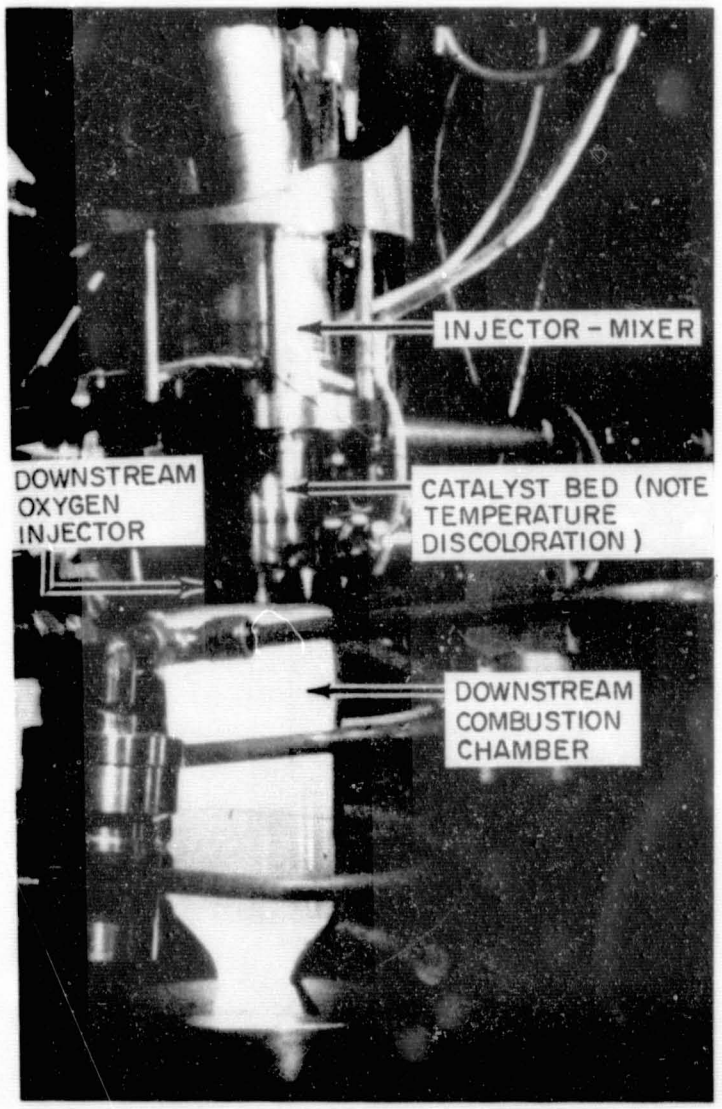

Figure 20. The Lightweight Thrustor Firing Under Altitude Conditions (Altitude of 100,000 Feet)

The vacuum specific impulse was calculated from the measured thrust:

$$I_{sp_{meas,\ vac}} = \frac{F_{meas} + P_a A_e}{\dot{w}_T} \qquad (3)$$

The c* and I_s efficiencies (η_{c*} and η_{I_s}) were calculated as the ratio of actual to theoretical values. The thrust coefficient is defined by:

$$C_f = \frac{I_s g_c}{c^*} \qquad (4)$$

The thrust coefficient efficiency was calculated as:

$$\eta_{C_f} = \frac{C_{f_{meas}}}{C_{g_{theo}}} = \left(\frac{I_s}{c^*}\right)_{meas} \left(\frac{c^*}{I_s}\right)_{theory} = \eta_{I_s}/\eta_{c*} \qquad (5)$$

The performance data evaluated from the experimental data and the pertinent parameters are given in Table 8.

The calculated values of η_{C_f} shown in Table 8 are unrealistic. This was probably caused by a propellant line stiffening interaction with the thrust measurements. The zero point for the load cell was observed to change as the injection pressures were changed. Therefore, the pressure data were used to characterize performance.

The c* efficiencies are seen to vary from 83 to 91.5 percent with all but one of points in a range of 89 to 91.5 percent. The 83-percent point was obtained at the initiation of a run and prior to the achievement of a steady-state thermal condition. This is a reasonable performance in view of the nonoptimized nature of the hardware.

The effect of mixture ratio on c* efficiency is shown in Fig. 21. The differences in efficiency between the values at mixture ratios of approximately 1.1 and those at mixture ratios of from 2.0 to 2.8 are quite small, if not insignificant. Also, the two groups of data reflect the performance characteristics of two mixing devices, the injector-mixer upstream of the bed and the downstream injector unit.

Experimental c* efficiencies for the workhorse thrustor were about 15 percent lower than for the lightweight hardware. There were two basic differences in the hardware configurations: (1) turbulators were added in the catalyst bed to curtail channeling of propellant down the wall of the chamber, and (2) the length of the combustion chamber downstream of the downstream injector was increased from 2.0 to 6.0 inches, allowing a longer residence time for reaction to take place. Although their combined effect was assessable from the data, there is no way of separating the effects attributable to each change.

It appeared from analysis of the workhorse data that the size of the catalyst pellets did not have any effect on engine performance. Since the lower bed pressure drop is obtained with the 1/8-inch pellets, they were used in this phase of the program.

Heat Transfer Results

During the initial two runs heat flux measurements were made by the transient wall temperature technique. Heat transfer coefficients were determined for the thrustor from these measurements. External surface temperatures were measured at eight locations. Thermal isolation blocks were cut to minimize longitudinal heat conduction. Chromel-alumel thermocouples were welded to each isolation block at its midpoint.

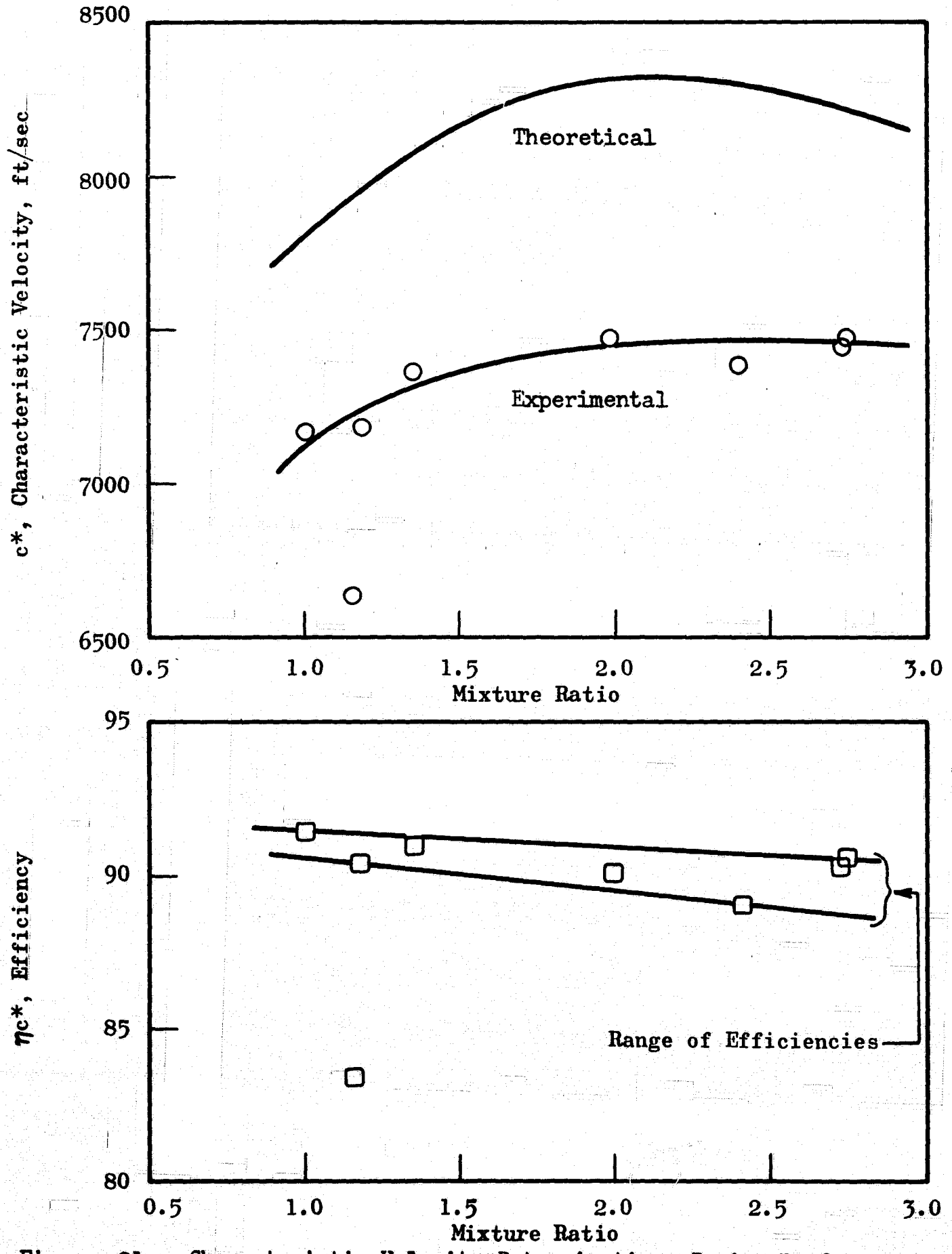

Figure 21. Characteristic Velocity Determinations During Performance Evaluation With the Lightweight Thrustor

The rate of temperature increase for a block of constant cross section is related to the net energy transfer rate as:

$$q = A\rho LC_p \frac{dT_B}{dt} \tag{6}$$

where

A = area of block

ρ = density

C_p = specific heat capacity

T_B = block temperature

t = time

L = block thickness

Assuming (1) small radiation effects within the chamber, (2) one-dimensional heat flow, (3) high thermal conductivity of the block material (block is essentially uniform temperature), and (4) heat transfer from the block to the surroundings takes place by radiation only,

then

$$q = h_f A (T_g - T_B) - \sigma \epsilon A(T_B^4 - T_a^4) \tag{7}$$

where

T_g = chamber gas temperature

h_f = film heat transfer coefficient

T_a = ambient temperature

σ = Stefan-Boltzmann radiation constant

ϵ = emmisivity of surface

For a given time increment, the net heat transfer rate, q, to a block was determined from Eq. 6 . Substituting that value of q together with the average values of the block temperature, chamber gas temperature, and ambient temperature into Eq. 7 , the local chamber film heat transfer coefficient was determined.

The chamber gas temperature T_g, was set equal to $\eta_{c*}^2 T_c$ where T_c was a theoretically calculated combustion temperature and η_{c*} was an experimentally determined value of c^*_{act}/c^*_{theor}. It should be noted that for low values of the temperature differences $(T_g - T_B)$, the calculated h_f was strongly dependent on the value of η_{c*} and thus the experimentally determined c^*_{meas}. At temperature differentials of 700 R, a 1-percent error in the evaluation of the c^*_{meas} would produce a 12-percent error in h_g. With larger temperature differentials, the sensitivity of the h_g determination to the η_{c*} value is diminished.

Figure 22 presents curves of local heat flux at various axial positions along the thrustor for three time increments during each of the two runs. The local heat flux values were normalized to a chamber pressure of 10 psia by multiplying by the term $(10/P_c)^{0.8}$ as suggested by the theoretical equation of Bartz (Ref. 8). This implicitly assumes a turbulent boundary layer.

Figure 23 presents curves of the film heat transfer coefficient normalized to 10 psia at various axial positions along the thrustor for the same three time increments during the two runs. Analytical estimates of the heat transfer coefficients were made based on a developing turbulent boundary layer and on Reynold's analogy with the Prandtl number and viscosity assumed constant. The analytical prediction for a chamber pressure of 10 psia and a mixture ratio of 2.5 is also shown in Fig. 23. The agreement is poor. In the chamber portion of the engine the coefficients are

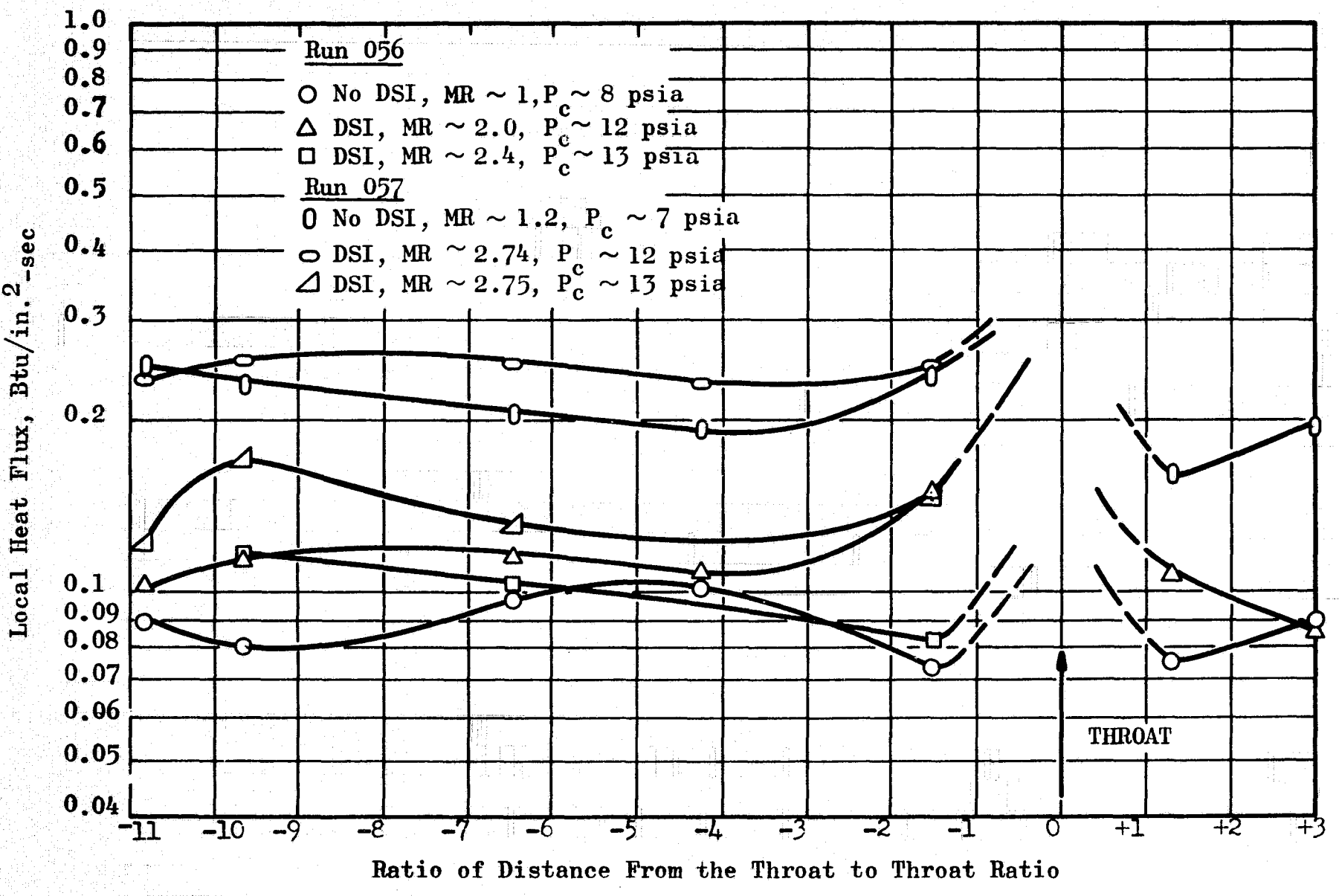

Figure 22. Local Heat Flux Characteristics for the Lightweight Thrustor

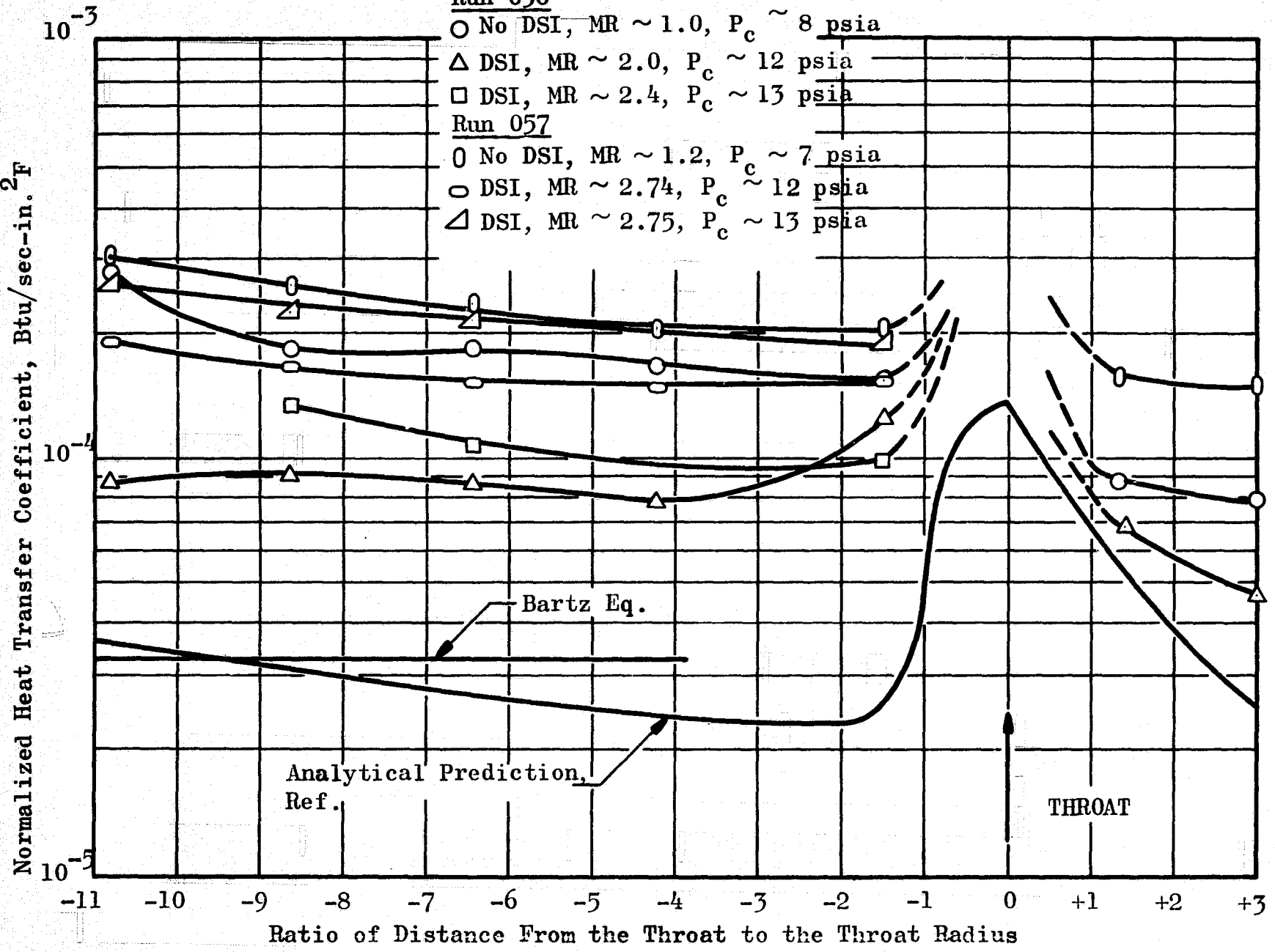

Figure 23. Heat Transfer Coefficient Distribution for the Lightweight Thrustor

from two to five times greater than predicted. Also shown is an analytical prediction from the Bartz equation. That, too, agrees poorly with the present data while agreeing quite well with the more detailed analytical predictions.

The elevated chamber heat transfer coefficients are partially the result of the chamber gas recirculation discussed in a later section of this report. Recirculation wakes form downstream of the downstream injector spokes. This reduces the available flow area and increases the gas velocity along the chamber walls and increases the heat transfer coefficient.

The difference between the experimental values and the analytical prediction could be partly attributed to a poor estimate of ΔT. This could have occurred because of a radial mixture ratio gradient produced by the downstream injector and/or error in estimation of the temperature factor, η_{c*}^2. For example, consider that the mixing is not homogeneous and that an oxygen-rich zone exists close to the wall. The temperature in that zone would be higher, the resultant driving temperature difference would also be higher, and thus, for the measured heat flux the film coefficient would be lower. However, even if the oxygen-rich zone was at the maximum theoretical flame temperature for hydrogen-oxygen, it could still not account for all of the deviation between experiment and theory.

Summary of Performance and Heat Transfer Evaluation

Although the planned series of runs was not completed because of a chamber failure during the second run, several of the objectives were achieved. The thrustor c* performance was found to be between 89 to 91 percent after thermal equilibrium was obtained. The heat transfer coefficients were found to be several times larger than expected, so that a refractory metal is necessary for a radiation-cooled chamber and nozzle operating at

maximum efficiency. The performance achieved is considered satisfactory because no effort has been made to optimize the method of injecting the additional oxygen downstream of the catalyst bed. Increased combustion performance and/or shorter downstream combustion chamber lengths should result from such an optimization.

ANALYSIS OF THRUSTOR RESULTS

EXPERIMENTAL DATA EVALUATION

Thrustor Response Analysis

The determination of thrustor response and pulse-mode operating characteristics was a goal in the subject program. Two response parameters are of interest, thrust and specific impulse. The first measures output, the second measures efficiency. These two response parameters are, in turn, related to chamber pressure (thrust) and chamber stagnation temperature (specific impulse). The thrust (or pressure) response is of greatest interest in most cases. However, degradation of specific impulse because of extended thermal response periods will have an adverse effect on the attractiveness of a given system. Therefore, maximum response is a prime objective.

Applicable Experimental Results. Experimental results from three sources were used in the evaluation: the lightweight engine tests, gas generator experiments performed in conjunction with the conditioner effort, and the workhorse thrustor tests. The lightweight engine experiments were directed at obtaining combustion performance and thrust response characteristics under altitude conditions. A series of 10 test runs was planned, with pulse-mode operation runs scheduled near the end of this series. An engine failure during the second test run terminated the experiments before the pulse-mode characteristics could be determined. In the initial 2 of 10 planned test runs, only slow response instrumentation recording was utilized, so that the measurement of the transient characteristics was not detailed. Fortunately, the lack of these data from the lightweight thrustor experiments did not preclude a response and pulse-mode analysis based on the results of the workhorse thrustor and the gas generator experiments.

The major portion of the response data was obtained with gas generator reactors (for the conditioning system), these being equivalent to an in-line thrustor operating at a mixture ratio of ~1.0. The gas generators were checked out as separate components, and then immediately connected with their respective heat exchangers and operated as an integral part of the conditioner subsystem for the remaining conditioner tests. During the course of these tests, the gas generators were frequently pulsed (both manually and automatically by the temperature controller) and transient response data were obtained. These data are significant from the analogy with an in-line catalytic thrustor and are presented here for a direct comparison with the thrustor response.

Most of the experimental workhorse thrustor effort was devoted to (1) determining a viable internal configuration, (2) measuring the lower temperature limit for reliable catalytic ignition, and (3) developing a DSI technique. Because of the difficulty encountered in low-pressure, low-temperature catalytic ignition, additional experimental effort was diverted to this area from the pulse-mode and response studies with the workhorse hardware. Thus, only several long-duration (~10 seconds) pulses were made with the workhorse hardware. Neither the experimental equipment or procedure was optimized with respect to rapid response.

Comparison of Thrustor and Gas Generator Designs. The actual gas generator design, which is discussed in detail later, was based primarily on the optimum internal configuration found in the first thrustor studies. The pertinent similarities and differences were:

1. Nominal mass loading: G_o thrustor = 0.0041 lb/in.^{2}-sec
   G_o large gas generator = 0.0058 lb/in.^{2}-sec
   G_o small gas generator = 0.0052 lb/in.^{2}-sec

2. a. Identical catalyst bed lengths of 1/2 inch of 1/16-inch MFSA
   b. A thrustor diffusion bed length of 1/2 inch of copper shot vs 1/2 inch of 1/16-inch stainless-steel ball bearings for each gas generator.

3. Approximate internal volumes, $in.^3$

	Preinjector Volumes		Mix Section Volume	Combustion Chamber Volume
	O_2	H_2		
Thrustor	9.8	12.3	10.5	15.8
Large Gas Generator	0.38	6.0	2.2	0.48
Small Gas Generator	0.36	5.8	0.82	0.22

4. The gas generator throats were sized to give sonic flow at a nominal pressure of 10 psia and a temperature of 1500 F (mixture ratio of 1.0), whereas the thrustor throat was sized for a nominal 10 psia at 3500 F (mixture ratio of 2.5).

Because of the similarities in mass loading and the length of catalyst beds for the thrustors and gas generators, similarity in thermal response should occur. Obviously, less similarity or scaling exists among the various internal volumes and throat areas; thus, only qualitative agreement among pneumatic responses can be expected.

After the checkout phase of the gas generator testing was completed, the heat exchanger coil was coupled to its respective gas generator. Comparison of thermal and pneumatic responses before and after coil hookup showed the gas generator responses to be independent of the downstream heat exchanger, undoubtedly the result of the sonic nozzles in the gas generators.

A minimum amount of instrumentation (chamber pressure and temperature, inlet pressures, and electrical signals to the valve) was installed on the gas generators, so that only chamber pressure and temperature response can be compared with that of the thrustor.

Comparison of Feed Systems. Three different feed systems were employed with the gas generators. The first feed system, was a dynamic feed system similar to the thrustor system without the upstream sonic orifices. This system was used for the initial checkout of the gas generators. Later, the vents were plugged and the gas generator oxidizer and fuel valves were opened simultaneously. In the final series of integrated testing, the feeds to the gas generators were taken from the accumulators.

Three different feed systems also were employed in the thrustor studies. The feed system for the workhorse thrustor tests utilized heat exchangers for cooling the propellants and choked orifices in the heat exchanger exit and bleed lines so that the propellants could be vented until the desired thrustor inlet temperature was reached under dynamic conditions. A static, ambient feed system was employed in the lightweight thrustor tests. In the final thrustor-conditioner system tests, the thrustor was connected to the accumulators.

Transient Response Characteristics

Temperature and Pressure Response. Typical responses for both gas generators and the thrustor are compared in Fig. 24 and 25. The large gas generator responses also are shown in Fig. 26 and 27, with an expanded time scale. The feed system utilized in obtaining the two gas generator transients was that of a direct accumulator feed. The oscillating nature of

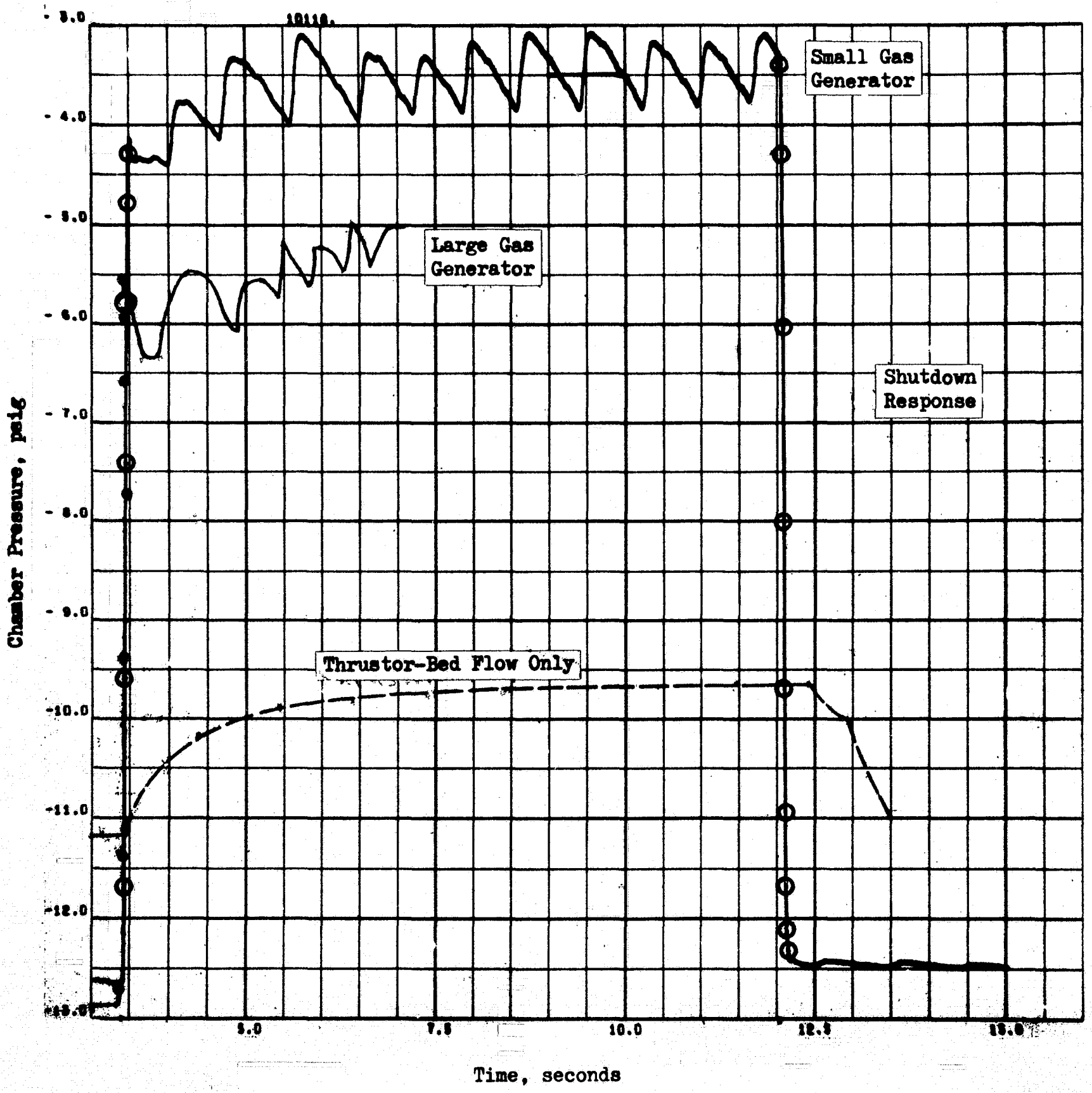

Figure 24. Comparison of Chamber Pressure Response Characteristics (for the Large Gas Generator, Small Gas Generator, and Thrustor)

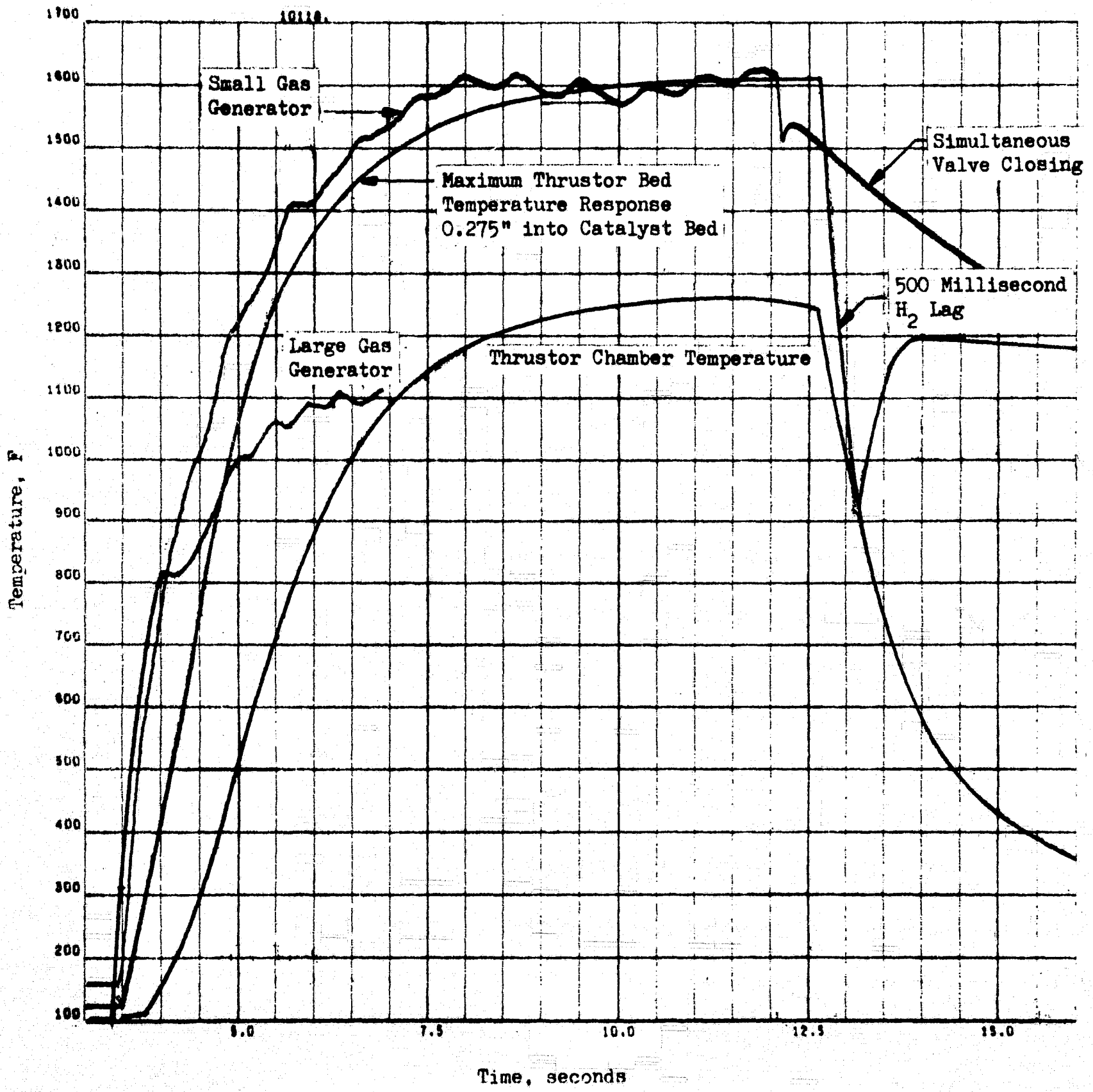

Figure 25. Comparison of Temperature Response Characteristics (for the Large Gas Generator, Small Gas Generator, and Thrustor)

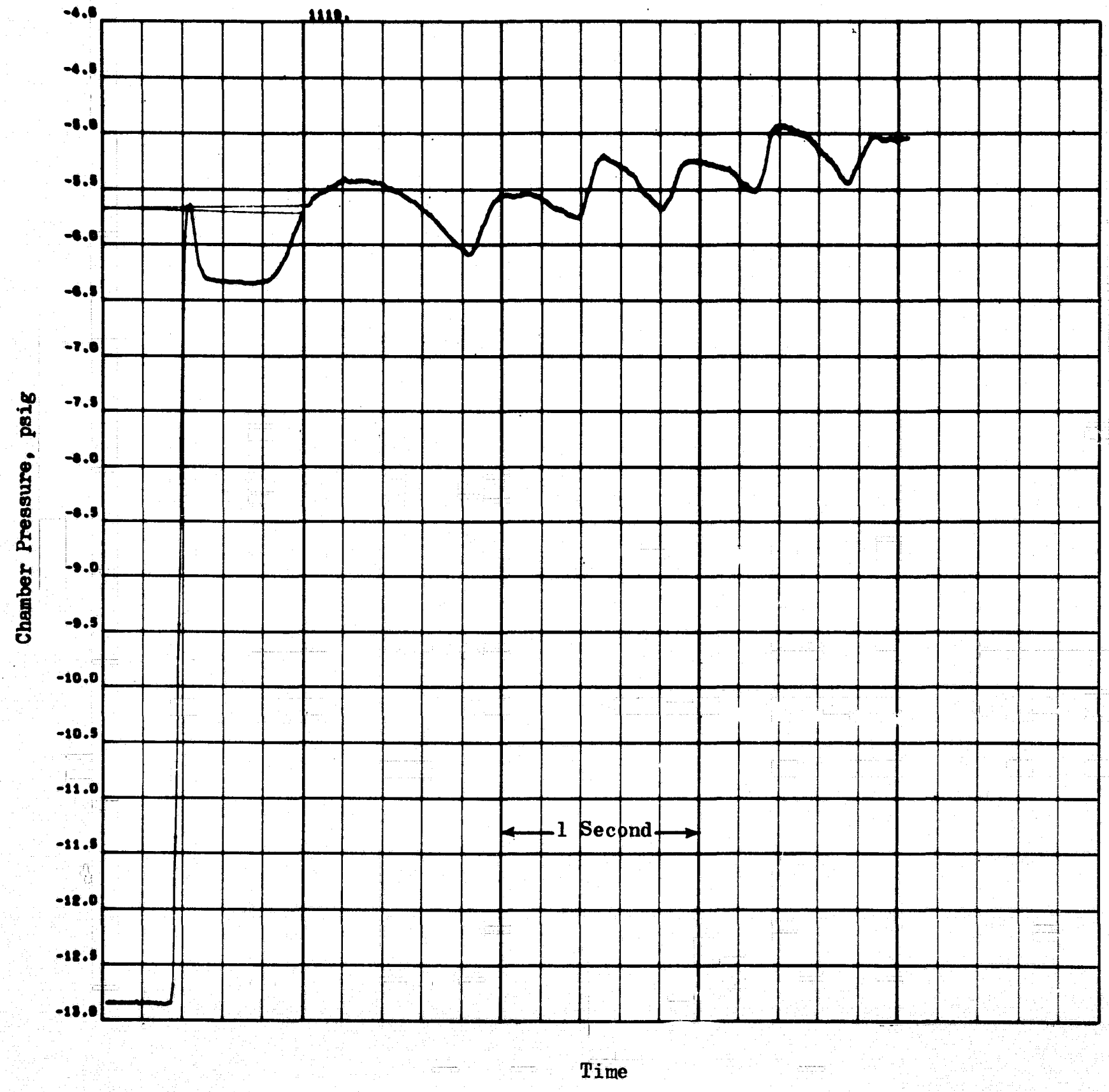

Figure 26. Chamber Pressure Response-Large Gas Generator Startup From Ambient Temperature

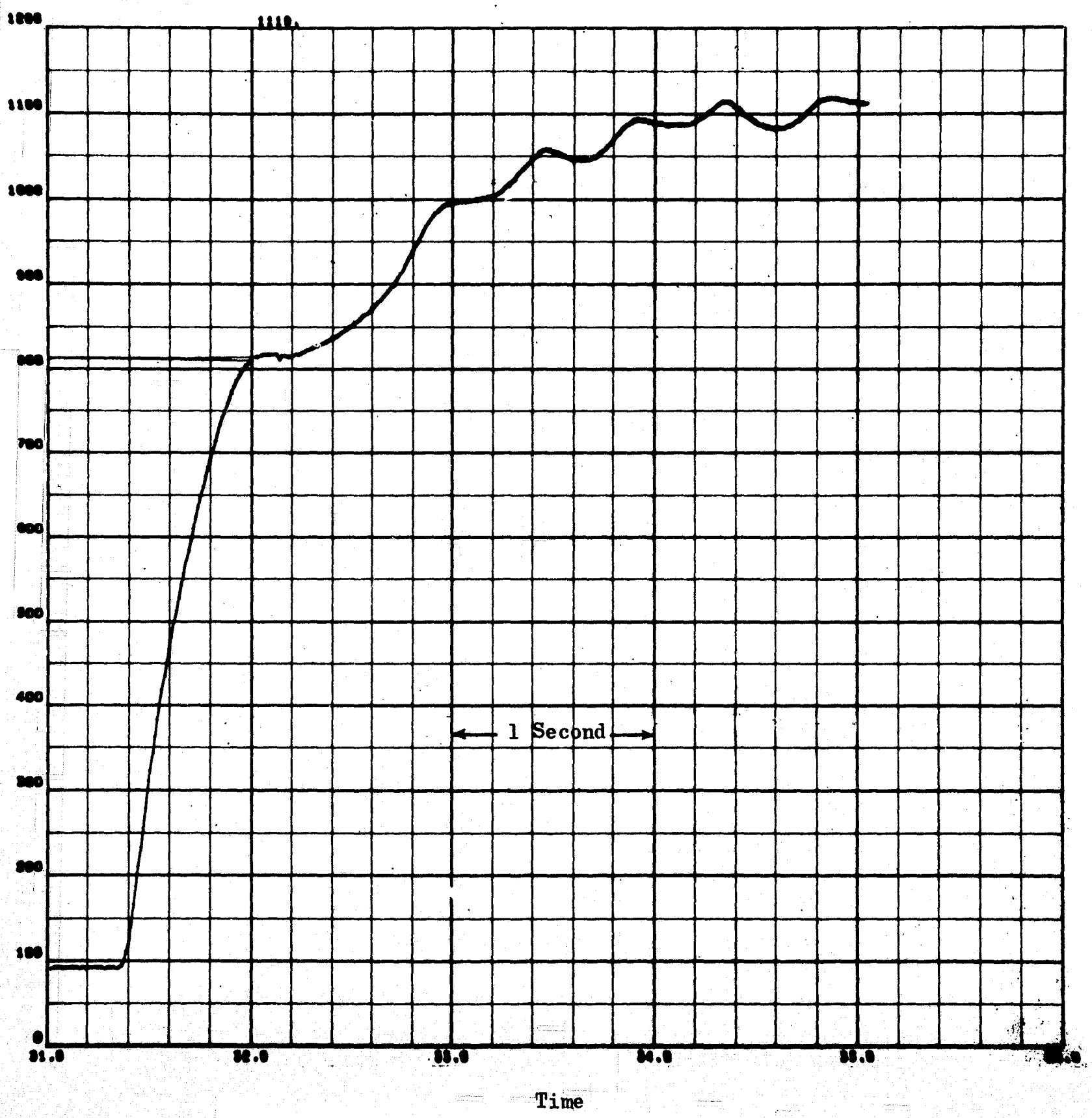

Figure 27. Chamber Gas Temperature Response-Large Gas Generator Startup From Ambient Temperature

the accumulator pressures, which produced the uneven response curves, is illustrated in Fig. 28 and 29. The propellant valves were opened and closed simultaneously. The thrustor response is for the workhorse thrustor with a dynamic feed system. Typical inlet pressures to the thrustor are shown in Fig. 30. Valve operation was programmed for a 3-millisecond H_2 lead and a 500-millisecond H_2 lag on shutdown with a total oxidizer on-time of 8.693 seconds.

The results show conclusively that, with a starting bed temperature of 100 to 170 F, thermal responses near 3 seconds can be expected. The chamber response of the thrustor was much slower than the maximum thermal response because of the large mass (approximately 100 grams) associated with the retaining plate and an additional length of catalyst (0.5 - 0.275 = 0.225 inch) past the optimum.

The actual response times are significantly slow compared to those predicted (approximately 750 milliseconds), based on the assumption of complete 0_2 reaction during startup. At the end of 750 milliseconds, the actual chamber temperature is between 700 and 900 F instead of the predicted 1500 F. A decrease in bed starting temperature was found to have an adverse effect on response, with response times of 5 to 10 seconds for bed starting temperatures of -100 F. The most reasonable explanation for such phenomena is that an appreciable fraction of the propellant flows through the bed without reacting during the transient start period of operation. As the temperature of the bed increases to 1500 F, a greater fraction is reacted. It is suspected that this bypassing phenomenon is also pressure dependent; however, this has not been clearly shown.

The thrustor thermal response for thermocouples placed axially in the catalyst bed was not always internally consistent for each run nor was it consistent from run to run. The former is illustrated in Fig. 31 in which

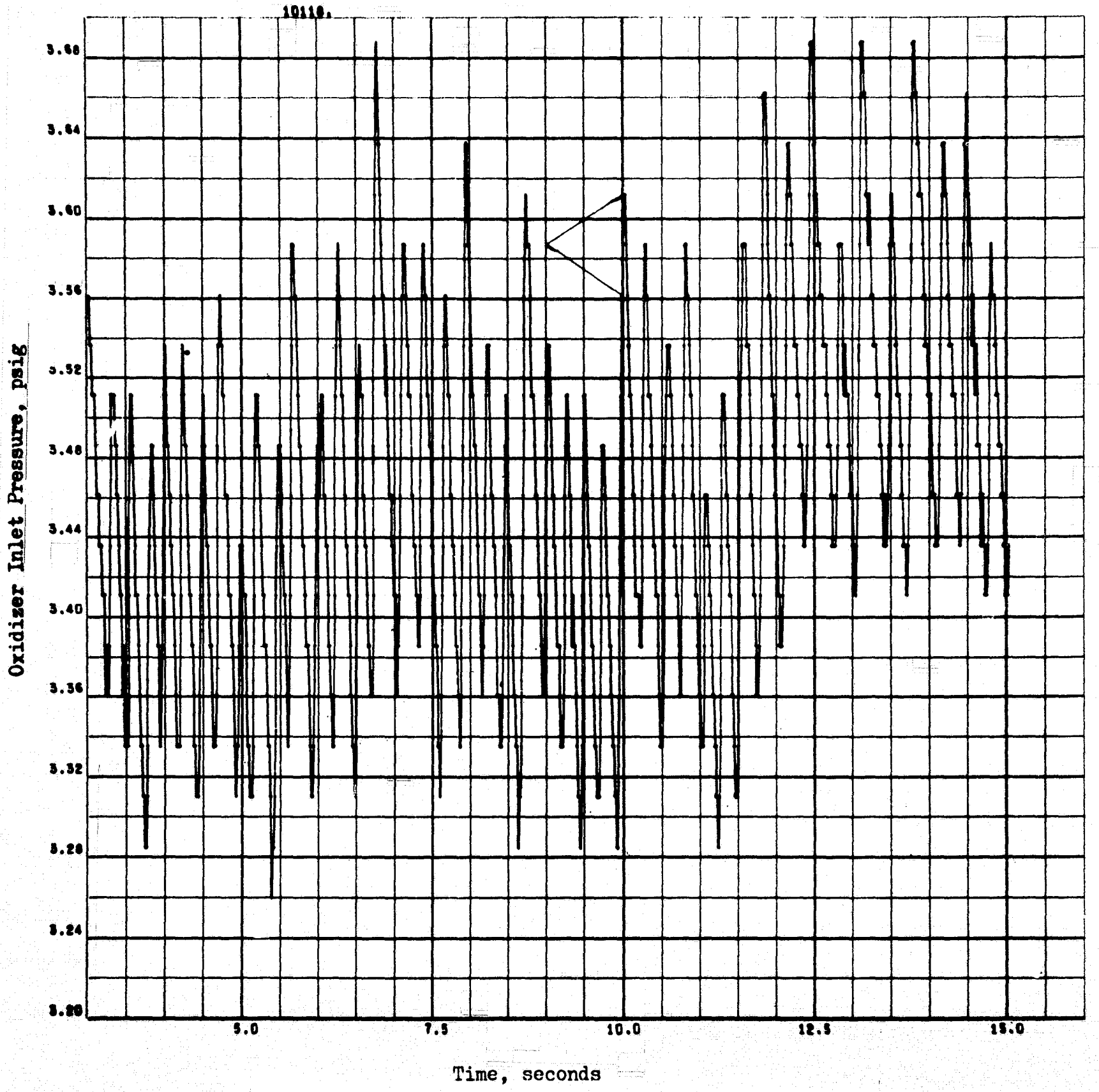

Figure 28. Oxidizer Inlet Pressure History Illustrating Pressure Oscillations-Small Gas Generator Startup

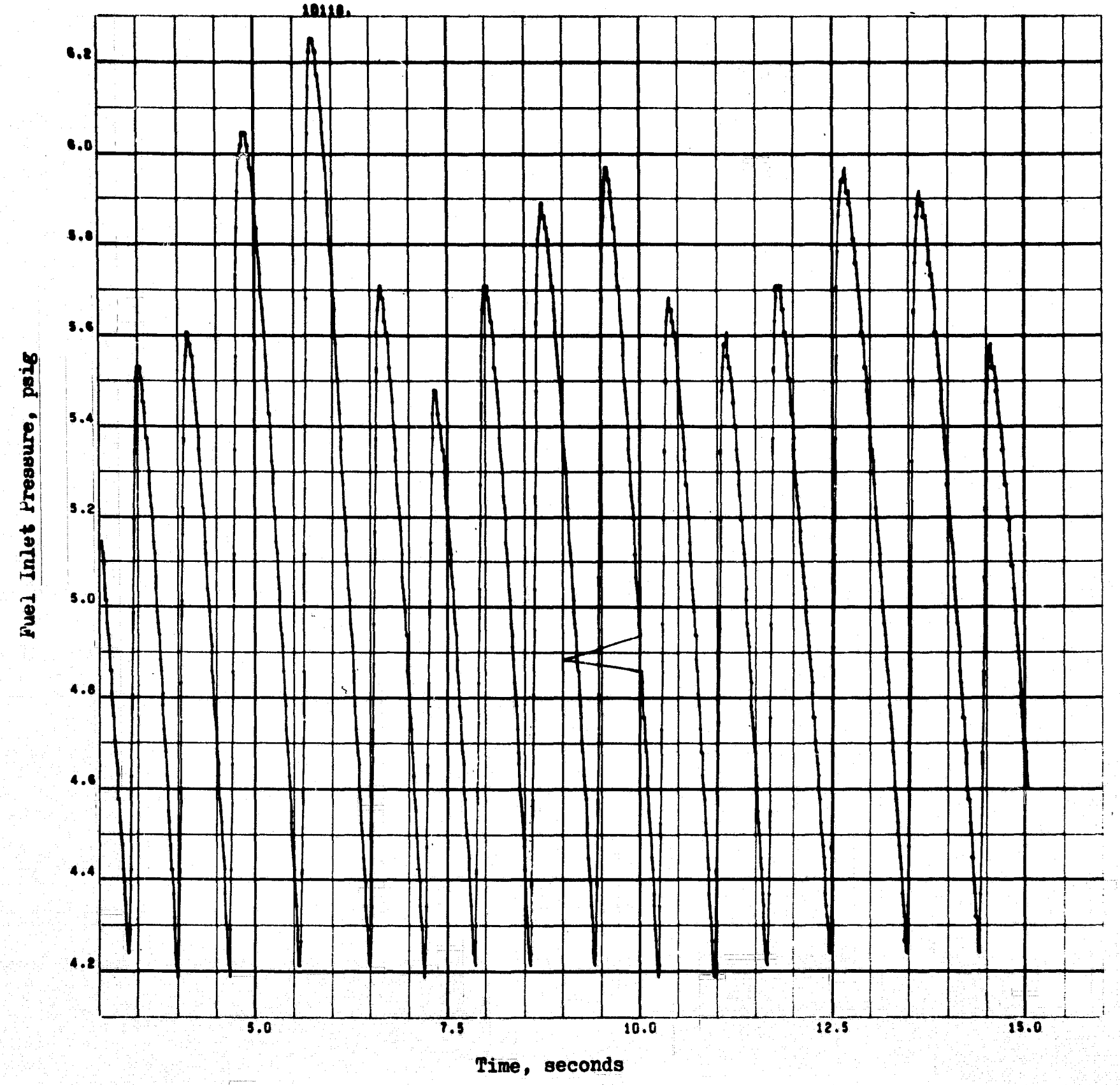

Figure 29. Fuel Inlet Pressure History Illustrating Pressure Oscillations-Small Gas Generator Startup

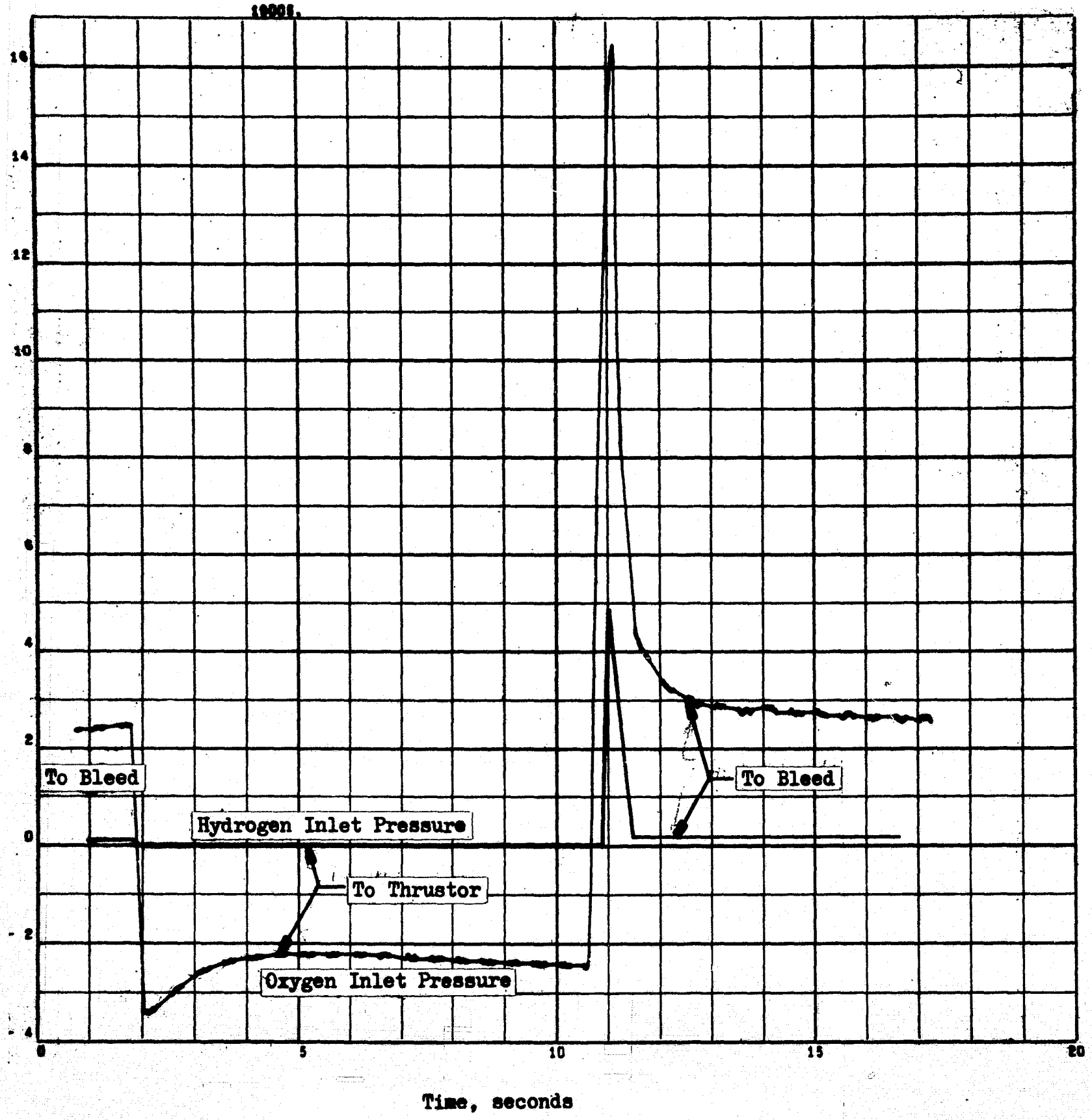

Figure 30. Typical Propellant Inlet Pressure History-
Thrustor With Dynamic Flow System

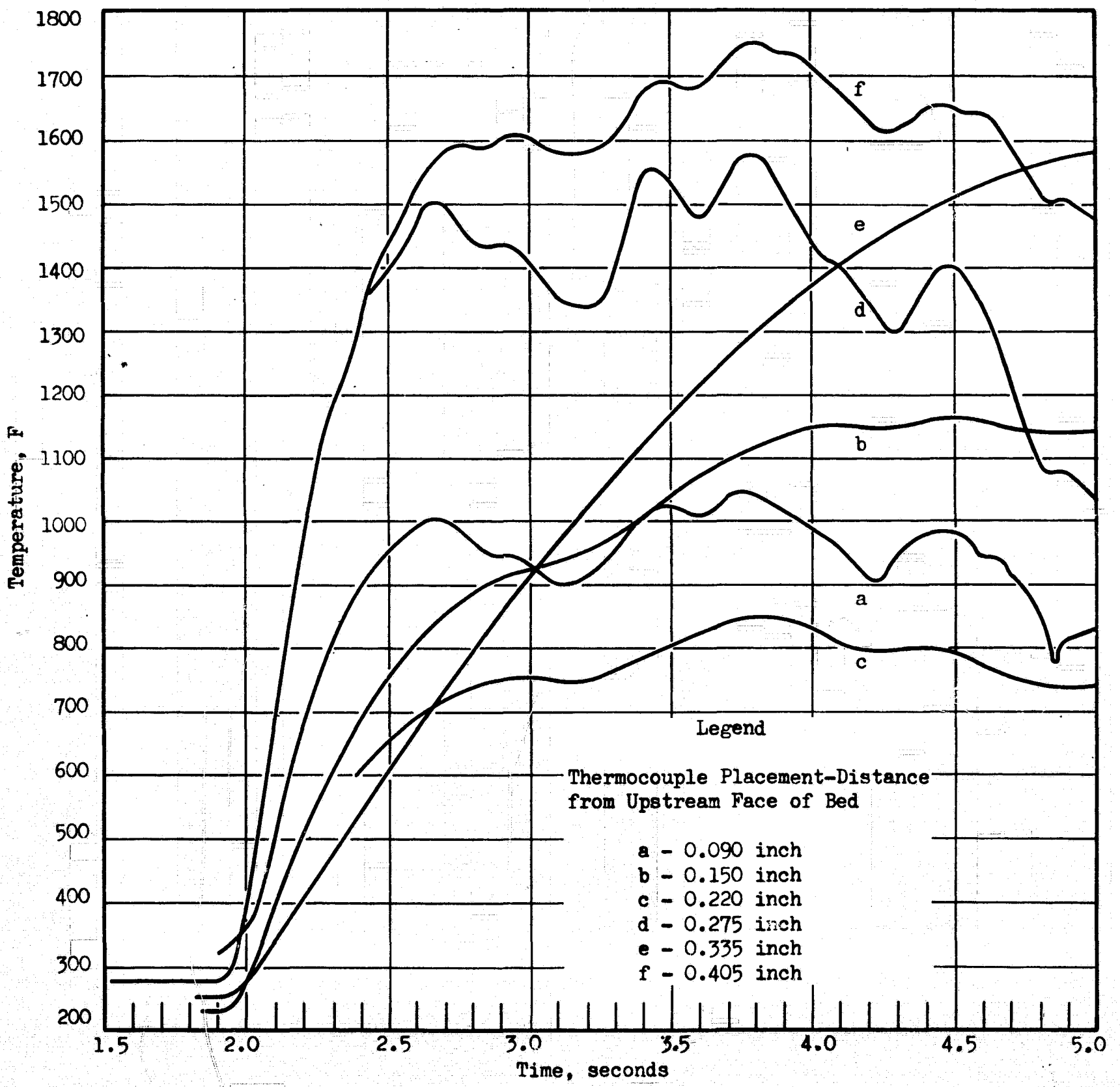

Figure 31. Comparison of Catalyst Bed Temperature Response for Various Longitudinal Locations in a Thrustor Catalyst Bed

three of the bed thermocouple response times were observed to be near 700 milliseconds, while the other 3 ranged from 2 to 3 seconds. This was undoubtedly caused by gas channeling.

Pressure responses associated with the temperature responses of Fig. 31 are given in Fig. 32. The large differences in the final pressure obtained with the gas generators, compared to the thrustor, occurred because of the configurational differences between the in-line gas generators and the downstream injector thrustor. However, the most significant difference is the initial pressure response during the chamber temperature transient to steady state. The gas generator pressure response appears to be almost independent of its associated thermal response, whereas the thrustor temperature and pressure responses are coupled.

The more rapid gas generator response results from different feed system and design characteristics. A major design factor is the ratio of the injector orifice area to the throat area. The thrustor was designed for operation at 10 psia using downstream injection of oxygen, whereas the gas generators were operated at 10 psia using only flow through the catalyst bed. As a result, the gas generator throat areas were smaller relative to the injector-mixer orifice areas than for the thrustor and the gas generator throats acted more as a choking orifice. Also, the gas generator combustion volume was significantly smaller than the thrustor volume (normalized for flowrate differences), thus decreasing the fill time.

The thrustor feed system with upstream sonic orifices also contributed to the coupling effect by restricting the startup flow and, thus, making the pressure buildup dependent on the temperature response. In the absence of the sonic orifices, the flow into the thrustor would be highest during startup and, therefore, tend to increase startup chamber pressure. In this case, the chamber pressure would be primarily dependent on the driving pressures.

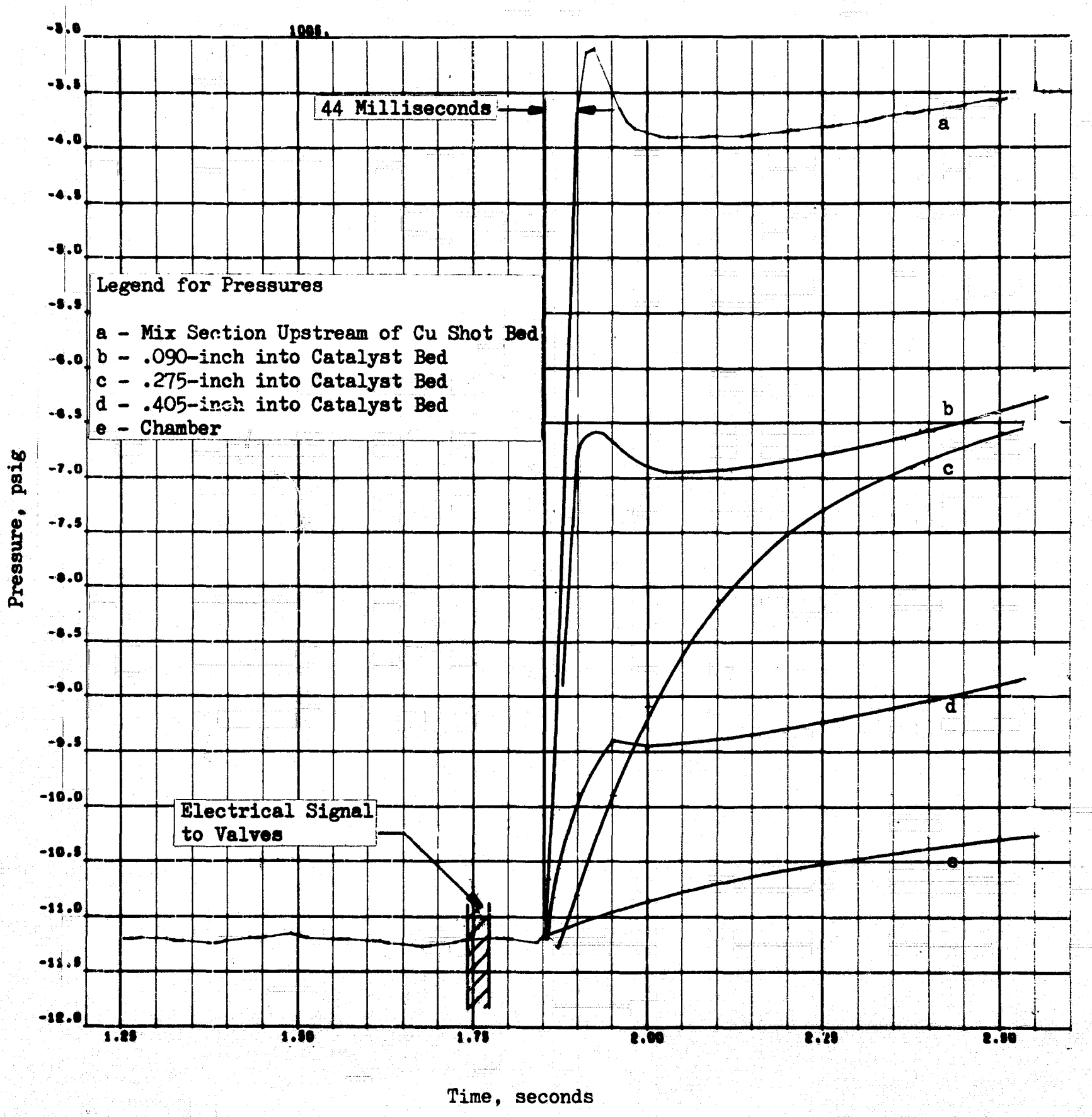

Figure 32. Thrustor Pressures Startup Responses Using a Dynamic Feed System

The large mass of the retaining plate downstream of the catalyst contributed indirectly to the slow pressure response by causing a chamber temperature lag and, hence, an increased flow from the throat.

An enlargement of the startup and shutdown transient pressure responses for the workhorse thrustor run presented earlier is shown in Fig. 33 and 34. The startup pressure response ranges from ~44 milliseconds in the mix section to several seconds in the chamber. The mix section response on shutdown is approximately 80 milliseconds, while the chamber pressure response was much slower, i.e., 250 to 300 milliseconds. This long "tail" is caused by the large amount of gas which, on shutdown, must bleed out of the large preinjector volumes through the mix section and catalyst bed. The transient thermal response on shutdown was shown earlier in Fig. 25 in which the cooling effect of a 500-millisecond H_2 lag, and a subsequent oxidizer-rich spike can be noted. The latter was caused by an incorrect ratio of preinjector volumes for the two propellants. (See transient mixture ratio discussion in the Thrustor Modeling section in Volume I of this report.)

Shown in Fig. 35 is the chamber pressure trace associated with the best thermal responses obtained, Run 15. The associated thermal responses are shown in Fig. 36. In this case, the chamber pressure is relatively decoupled from the chamber temperature response and is an order of magnitude faster than the response shown in Fig. 34 for Run 5. Based on a comparison of the engine parameters for these two runs, several factors could be partially responsible for the response differences:

1. The starting bed temperatures in Run 15 were 110 to 210 F hotter than that of Run 5.
2. The flowrate and MR for Run 15 were, respectively, 20 percent and 5 to 10 percent higher than that for Run 5.

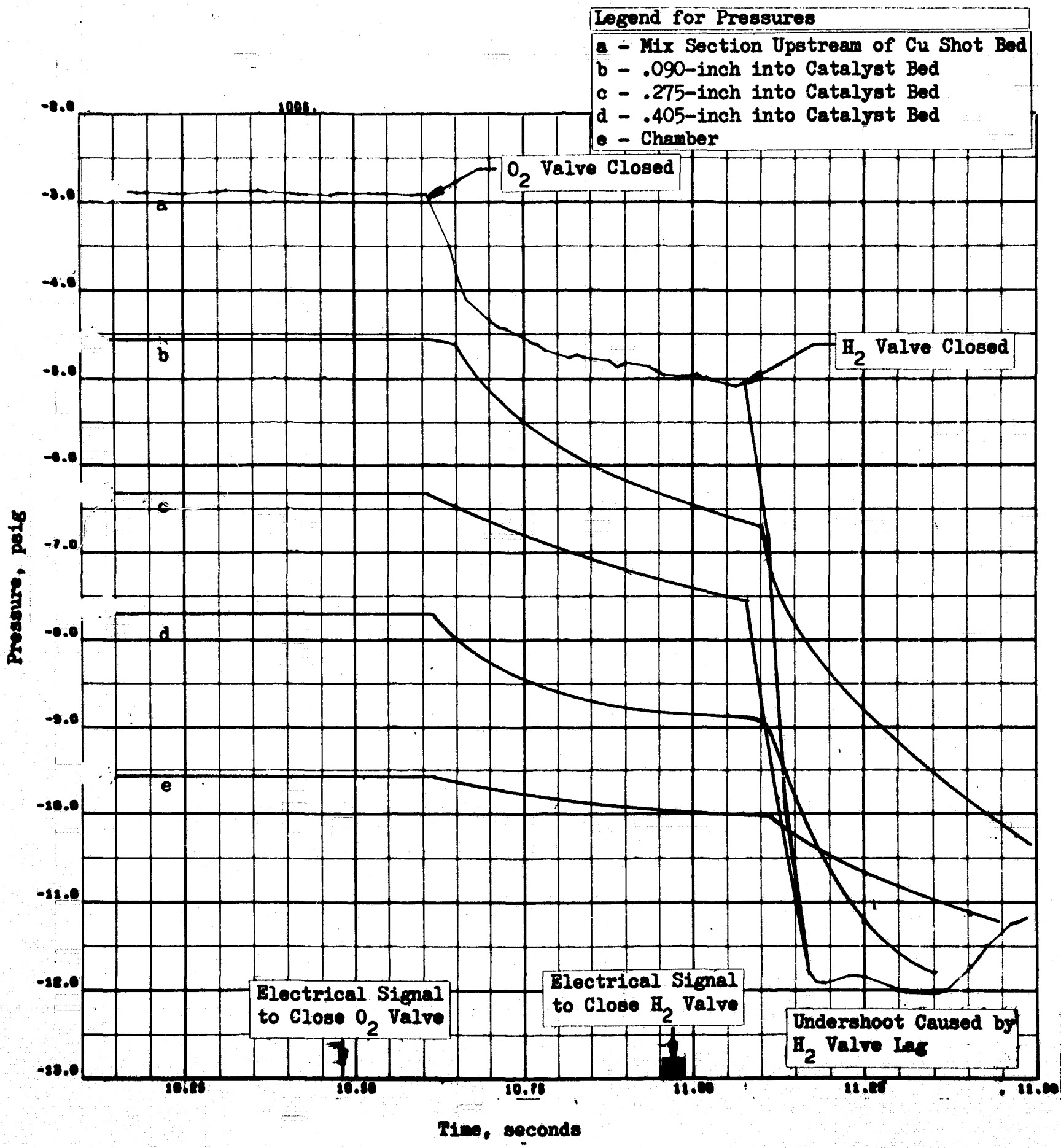

Figure 33. Thrustor Pressure Shutdown Responses Using a Dynamic Feed System

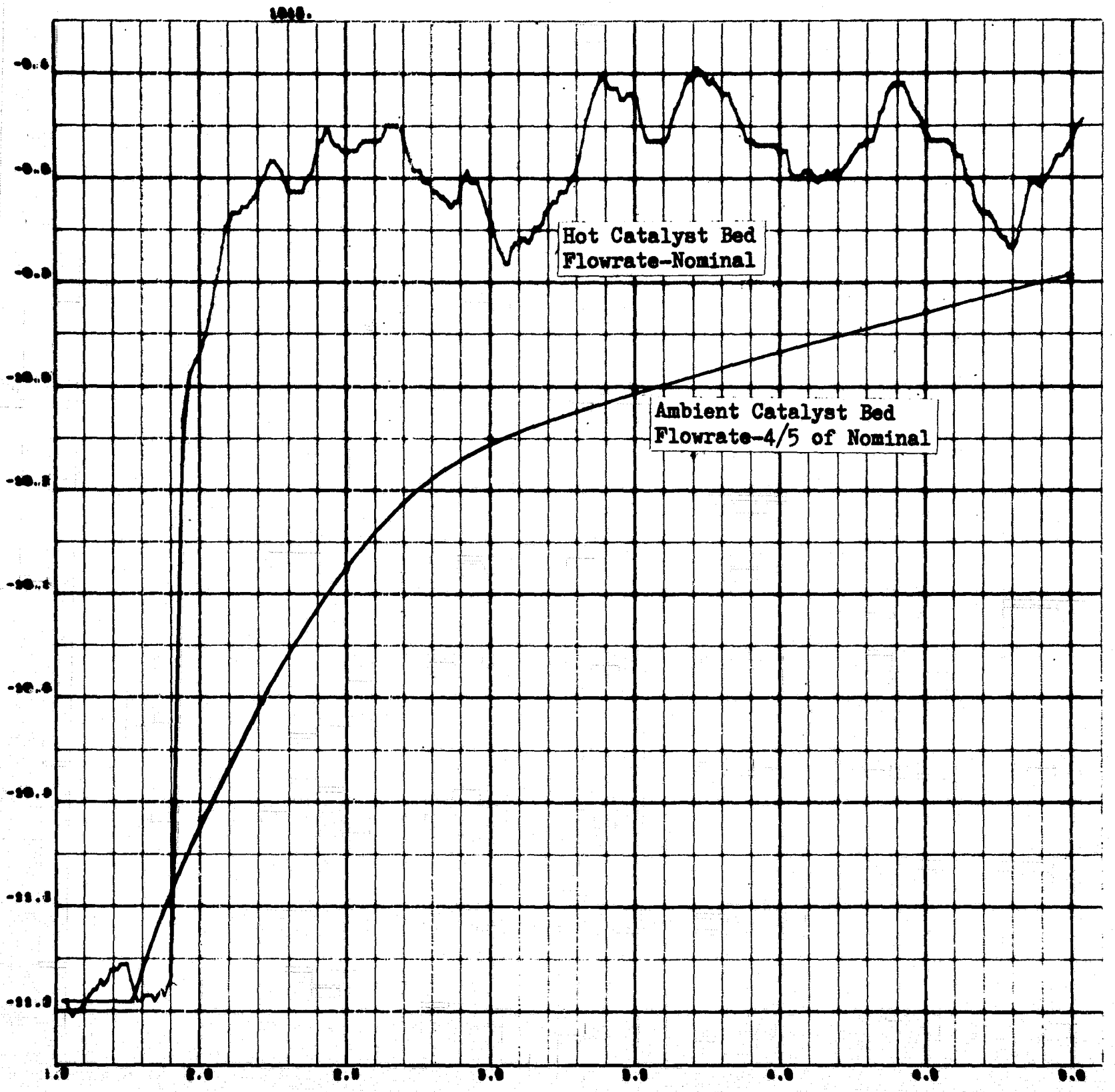

Figure 34. Thrustor Chamber Pressure Response (for Two Initial Bed Conditions and Two Flowrates)

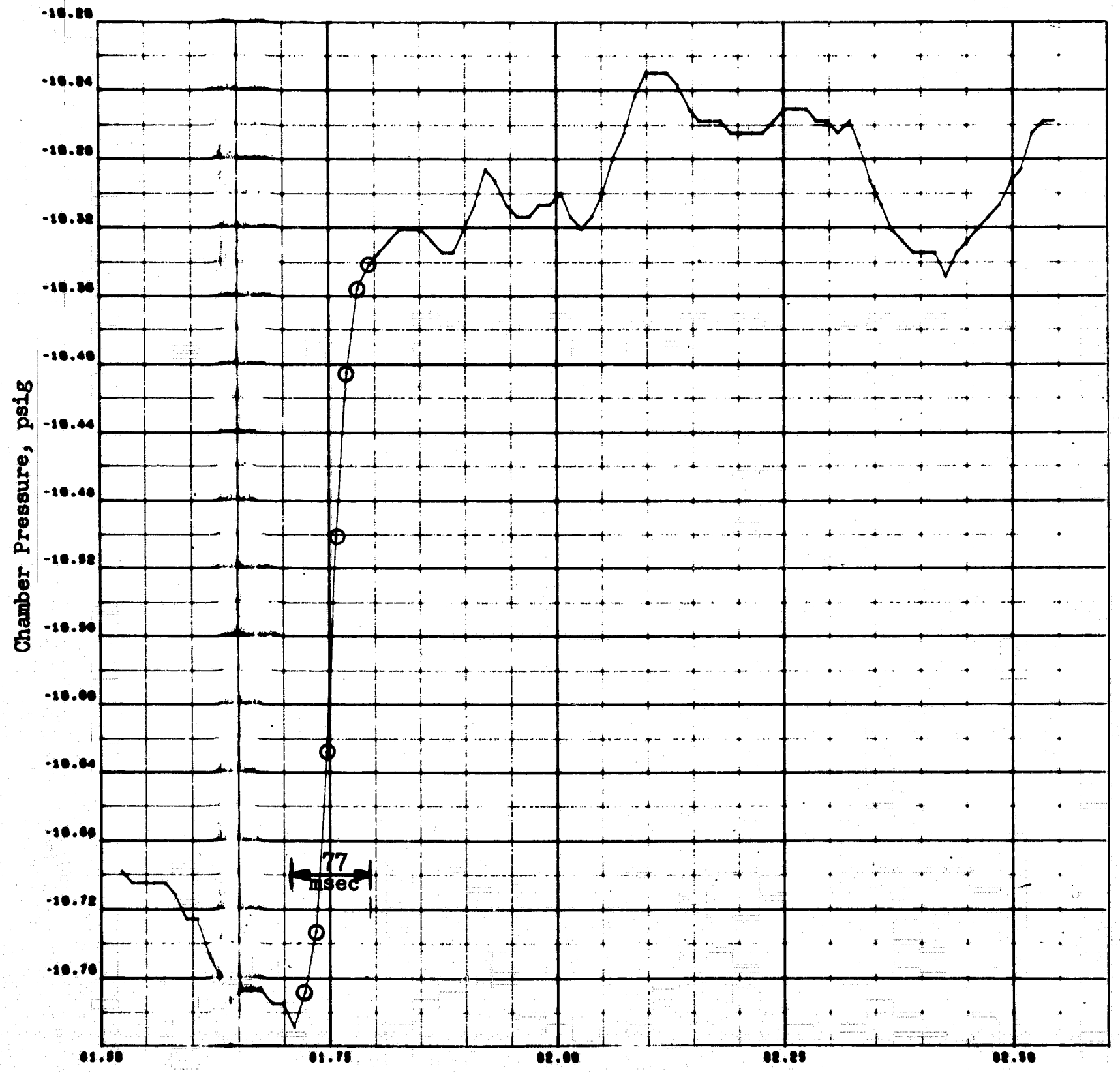

Figure 35. Ignition Response Characteristics for Downstream Injection of Oxygen, Chamber Pressure

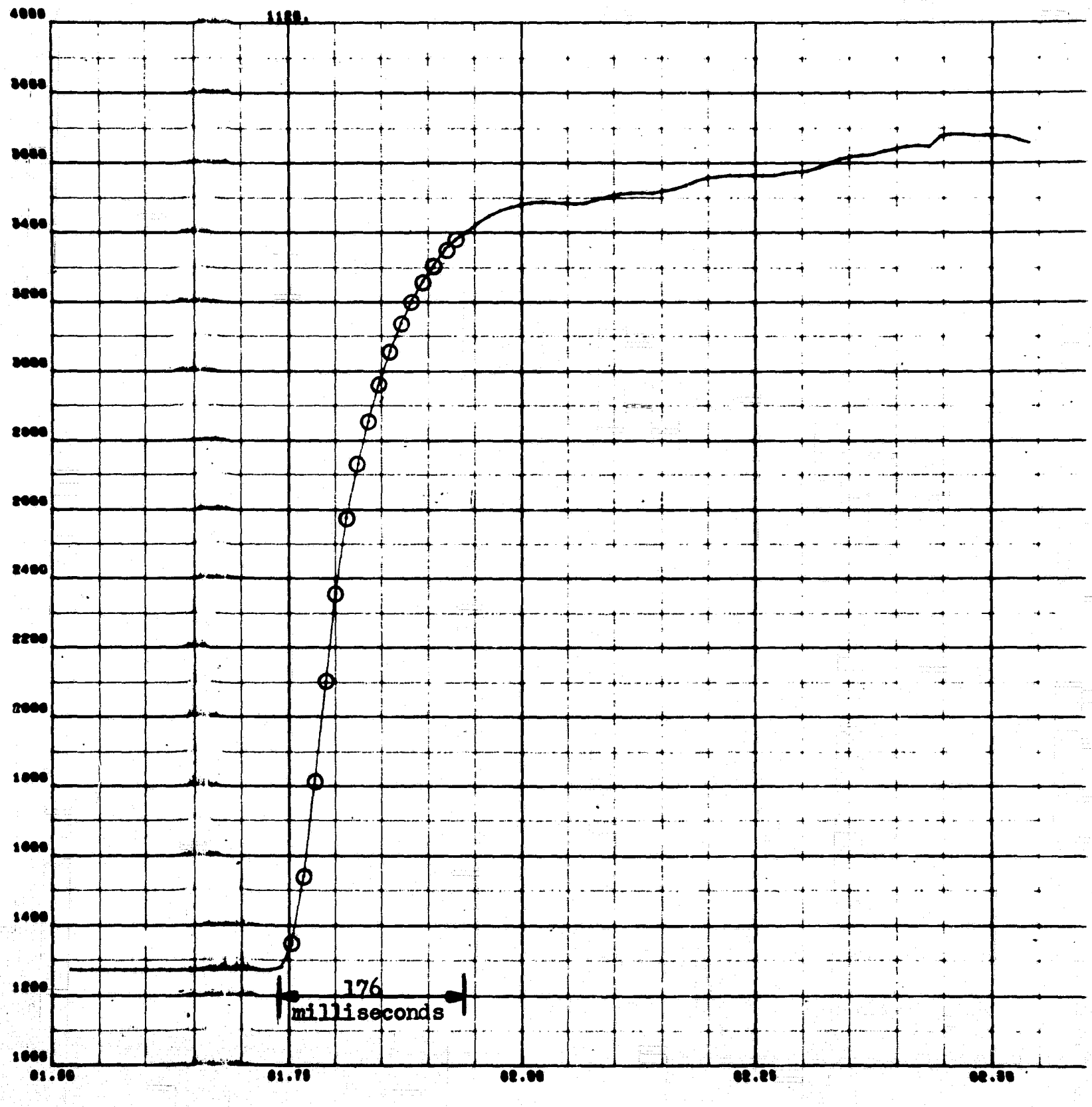

Figure 36. Ignition Response Characteristics for Downstream Injection of Oxygen, First Chamber Temperature

3. The mass of the retaining plate and screen downstream of the catalyst bed was reduced from 107 to 70 grams by using a more porous and thinner retaining plate.

DSI Temperature and Pressure Response. Measurement of the temperature and pressure response of downstream combustion was an important part of this work. The exact cause of the difference between pneumatic and thermal response is now known, but thermcouple location is suspected to be an important parameter in view of gas channeling. Since the 0_2 is flowing through the thrustor at the time of ignition, the responses do not include any filling delays associated with the DSI device. The responses of all the runs are summarized in Table 7. The pneumatic response for runs 24, 28, 29, and 33 were approximately in the same time range (40 to 90 milliseconds) although there appears to be no association between the pneumatic and thermal responses. Obviously, the thermocouples were not in the location where burning initially started.

A description of the integrated thrustor-conditioner tests and an example of a long-duration DSI pulse are given in the System Demonstration section of this report. In these tests the flowrates were approximately 1/5 nominal. With the complete cryogenic reaction control system, it was possible to cycle the DSI valve without disturbing the flow to the catalyst bed. Examples of the chamber pressure, and the two stagnation temperature responses during startup and shutdown, are presented in Fig. 37 through 40. The startup chamber responses are on the order of 100 milliseconds, much of which can be attributed to the filling time for the volume between the DSI valve and the injection slot in the spokes. The shutdown response appears to be about twice as long as the startup response. This is probably caused by the decay of oxygen from the filling volume.

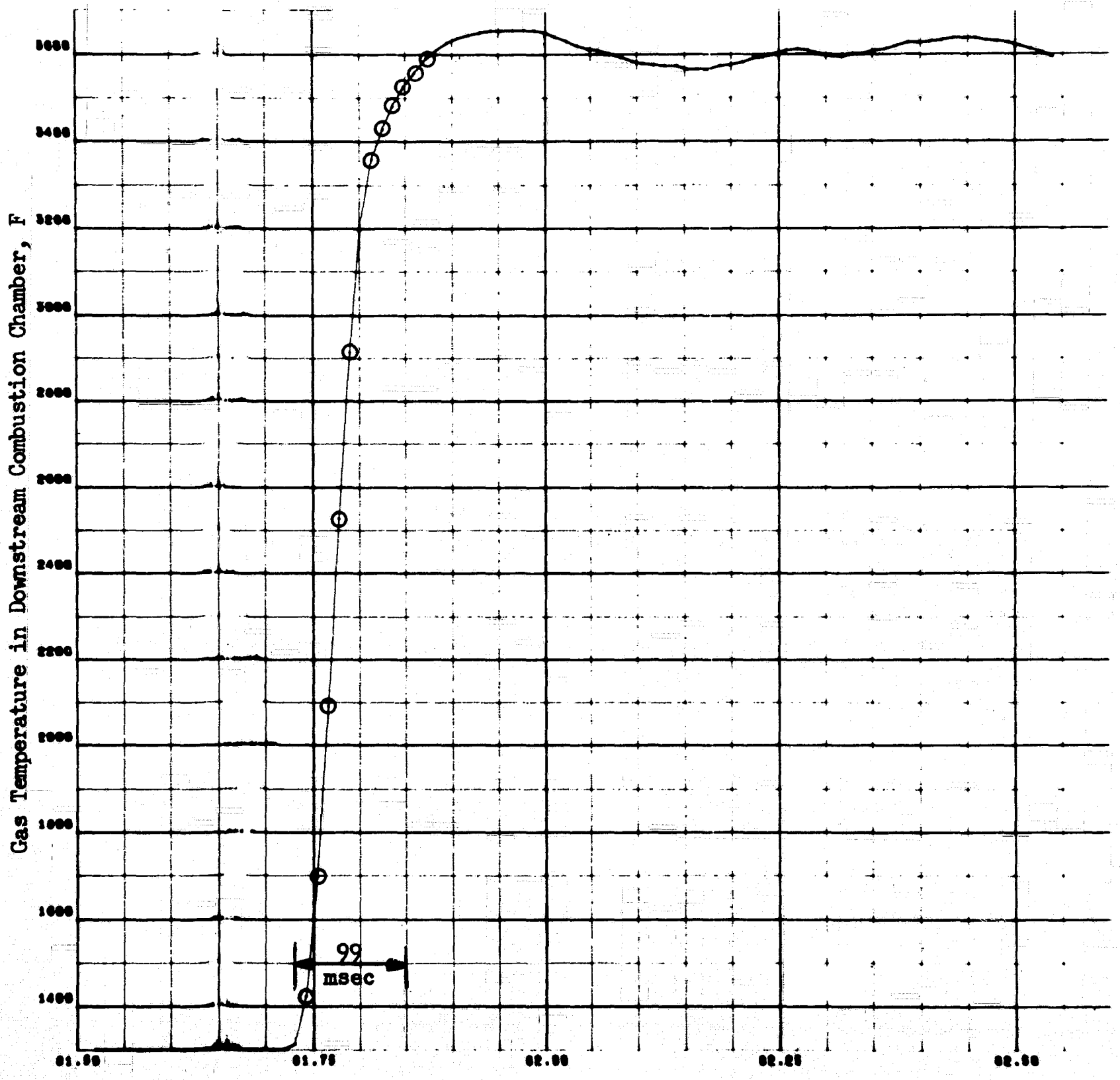

Figure 37. Ignition Response Characteristics for Downstream Injection of Oxygen, Second Chamber Temperature

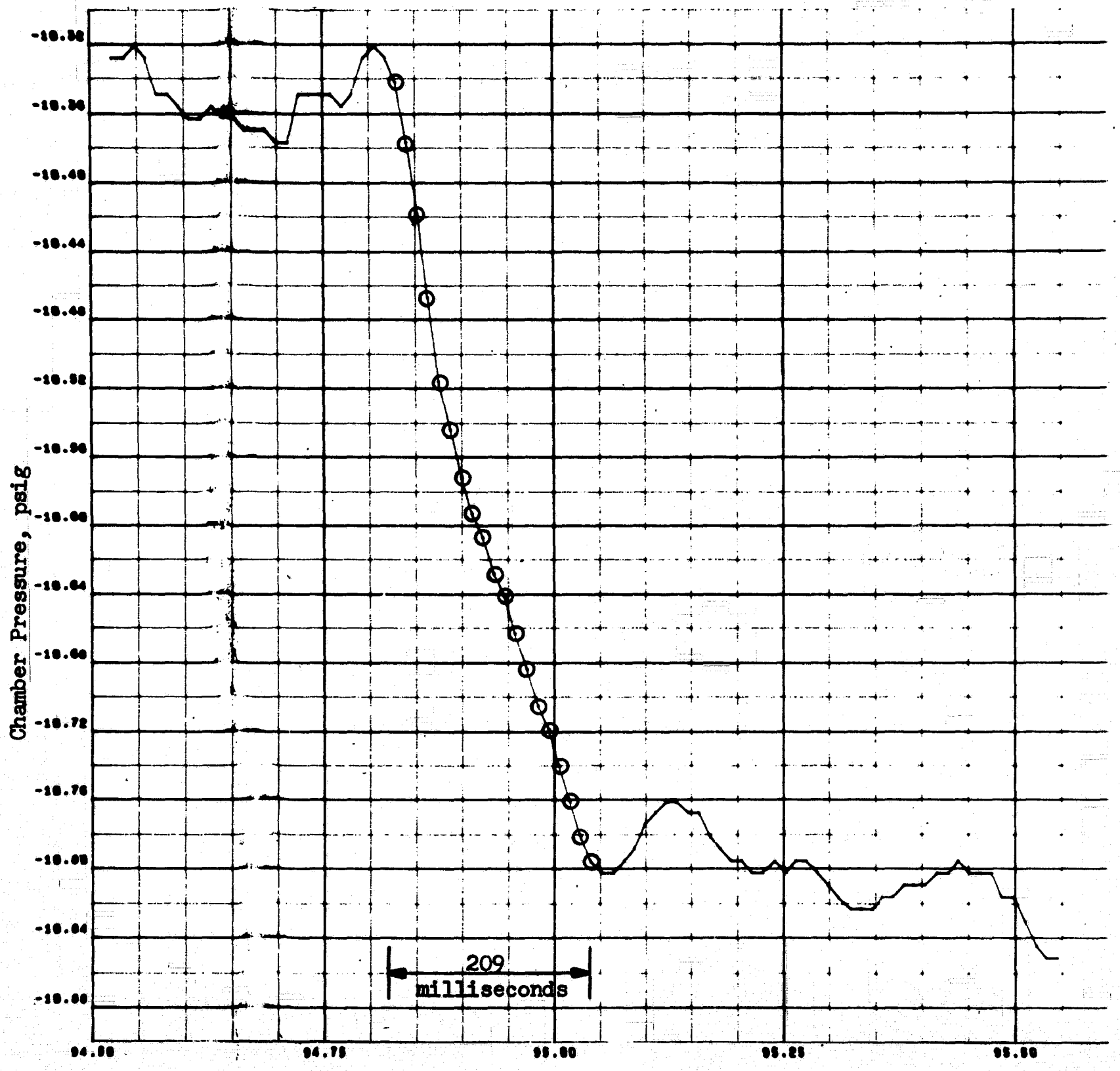

Figure 38. Shutdown Response Characteristics for Downstream Injection of Oxygen, Chamber Pressure

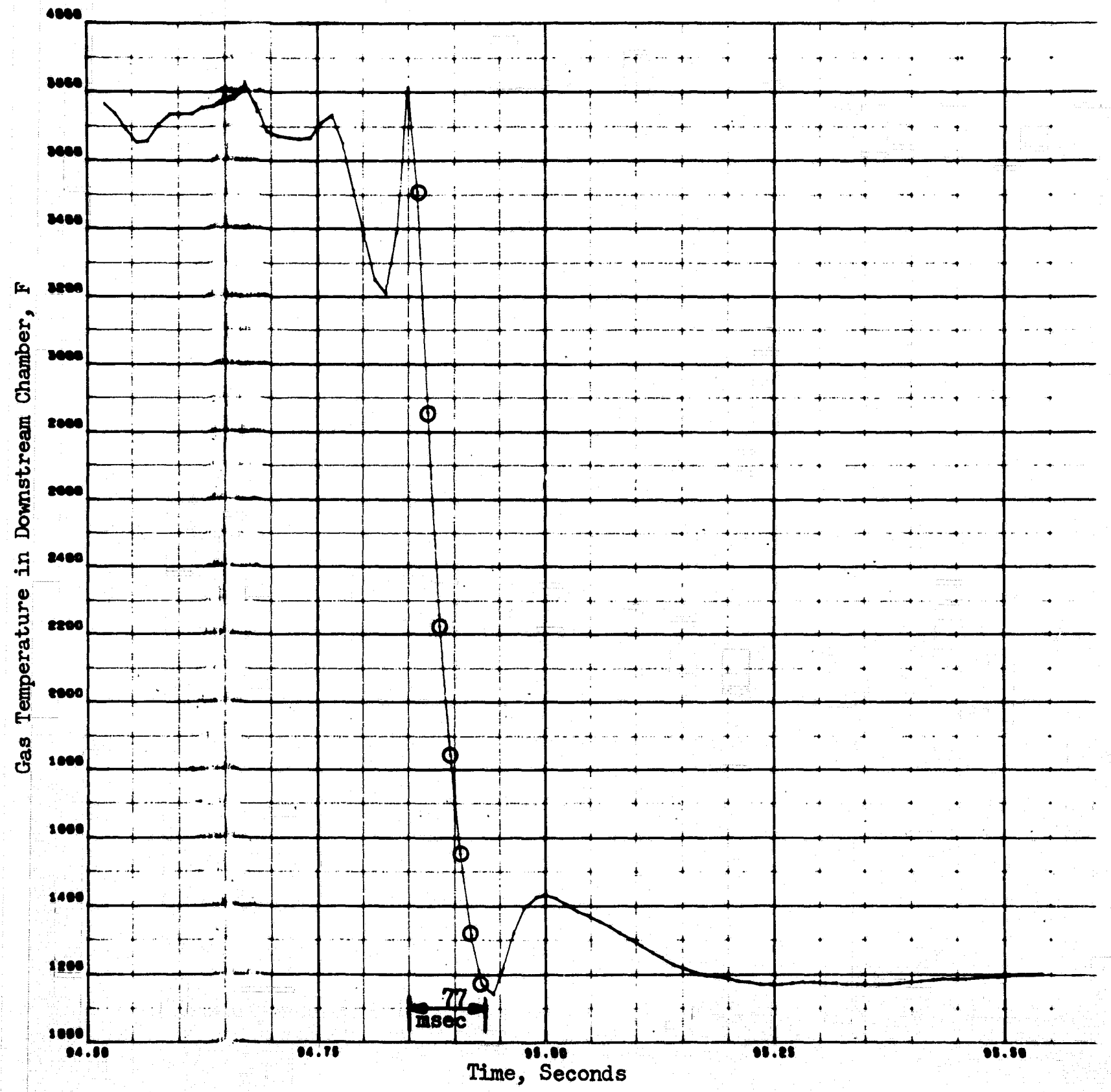

Figure 39. Shutdown Response Characteristics for Downstream Injection of Oxygen, First Chamber Temperature

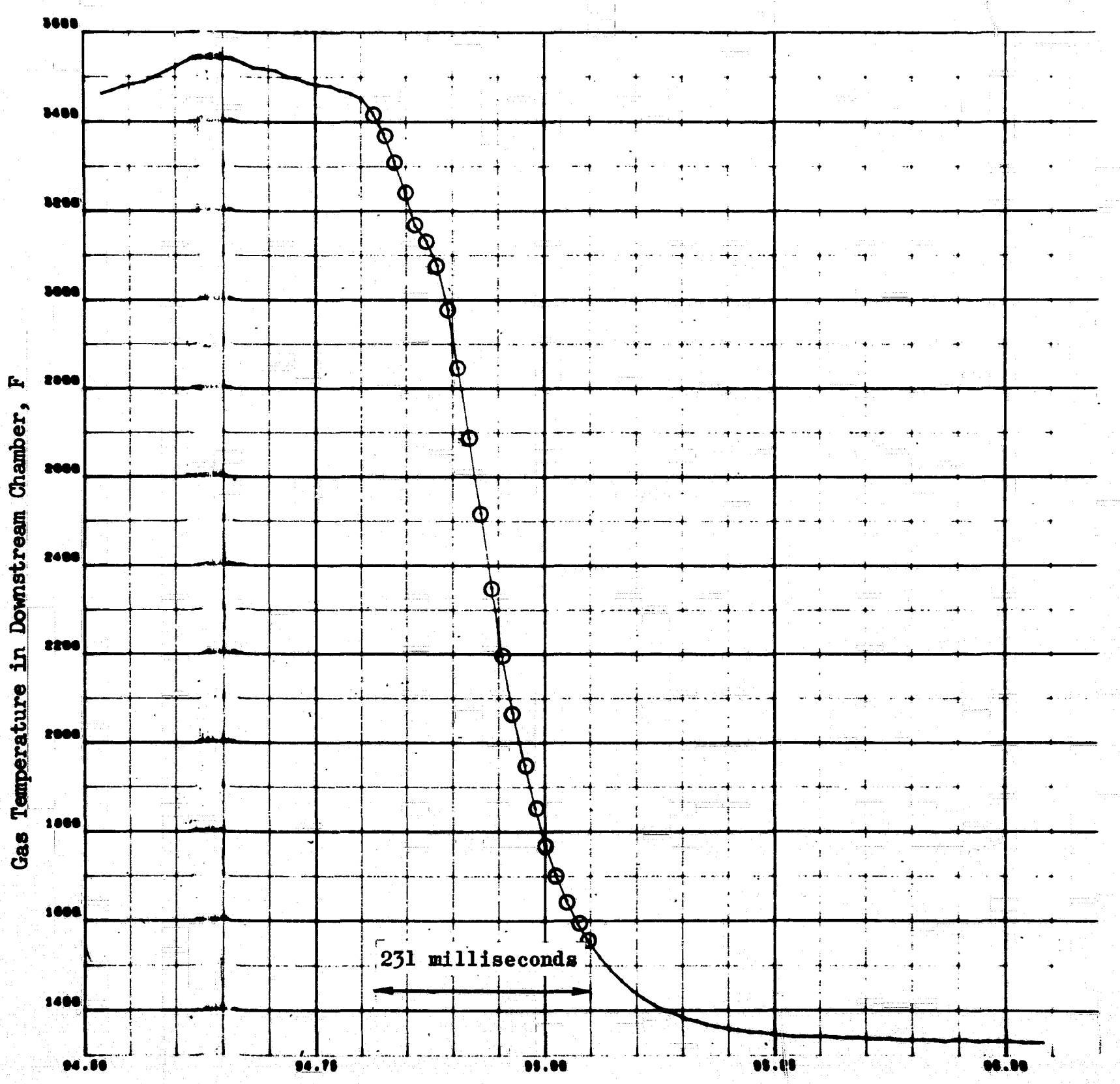

Figure 40. Shutdown Response Characteristics for Downstream Injection of Oxygen, Second Chamber Temperature

It is interesting to note that the initial threshold temperature was 1270 to 1300 F for the successful ignition, which corroborates the workhorse experiments.

Thrust and Specific Impulse Response. Thrust response is, in most cases, the most significant response characteristic. This response characteristic is closely related to that of pressure:

$$F = P_c A_t C_F \qquad (8)$$

where

F = thrust

P_c = chamber pressure

A_t = area of the throat

C_F = thrust coefficient

Small changes in the value of the thrust coefficient will be closely coupled to the temperature response. However, the only first-order effect on thrust is that of chamber pressure. Therefore, it is of significance that pressure response times as small as 40 milliseconds were measured. Similarly, the shutdown responses were of the same magnitude. Thus, pulses that essentially reach full thrust and are approximately 100 milliseconds in duration are seen to be feasible. Additional design refinements to reduce free volumes have the possibility of reducing the minimum pulse width further.

The specific impulse response characteristics during transient operation in a vacuum environment is dependent on the combustion efficiency characteristics and on the characteristics of heat transfer to the catalyst bed, the structure supporting the bed, and the remaining engine hardware. Incomplete reaction of the propellants during the initial portions of the ignition transient was thought the most likely cause of the excessively long thermal response transients from a cold bed, as discussed above. The specific impulse response is related to the temperature response by:

$$I_{sp} = K\sqrt{T/M}$$

Specific impulse response times are characteristically quite long. The importance of specific impulse response and the actual characteristics will vary with the application. In particular, an operational mode resulting in a continuously hot catalyst bed will eliminate the specific impulse response problem.

The thrust and specific impulse response characteristics are, in general, related only by the interrelationship between the temperature and pressure responses. The latter relationship is quite dependent on the engine and feed system designs, as discussed above.

Lightweight thrustor experiments were planned to determine experimentally the thrust and specific impulse response characteristics. However, hardware failure in the initial lightweight thrustor hardware experiments, as discussed in an earlier section of this report, prevented the accomplishment of the response and pulse-mode experiments.

Pulse-Mode Operation

The results of pulsing the small gas generator with a hot catalyst bed controlled by the automatic temperature controller are shown in Fig. 41 through 45. These results were obtained in the initial system testing, where the feed system was of the static type. Overall, the gas generator was cycled on and off three times during a 1-second period, with the valve open times ranging from 100 to 200 milliseconds. The individual pulses are characterized by a startup transient of 60 to 70 milliseconds and a shutdown transient of 120 to 130 milliseconds.

The chamber and throat temperatures are shown in Fig. 42 and 43. The oscillation in temperature can be attributed to transient MR variations (fuel-rich on startup and oxidizer-rich on shutdown) and to the oscillating inlet pressures. The difference of ~150 F between the chamber and throat temperatures can probably be attributed to gas channeling and incomplete combustion.

An example of 540-millisecond, hot-bed pulse with the large gas generator is given in Fig. 46 through 49. This example was taken from the final conditioner tests, where the gas generator was being fed from the accumulators. The startup and shutdown transients are nearly identical to those observed for the small gas generator. Also, the effect of the out-of-phase accumulator oscillation on chamber pressure and temperature should be noted.

Discussion of Downstream Injection of Oxygen

A simplified schematic of the nominal heat and material balance processes occurring in the thrustor is shown in Fig. 50 . The hydrogen and oxygen are first mixed to an equilibrium temperature, then reacted in the catalyst

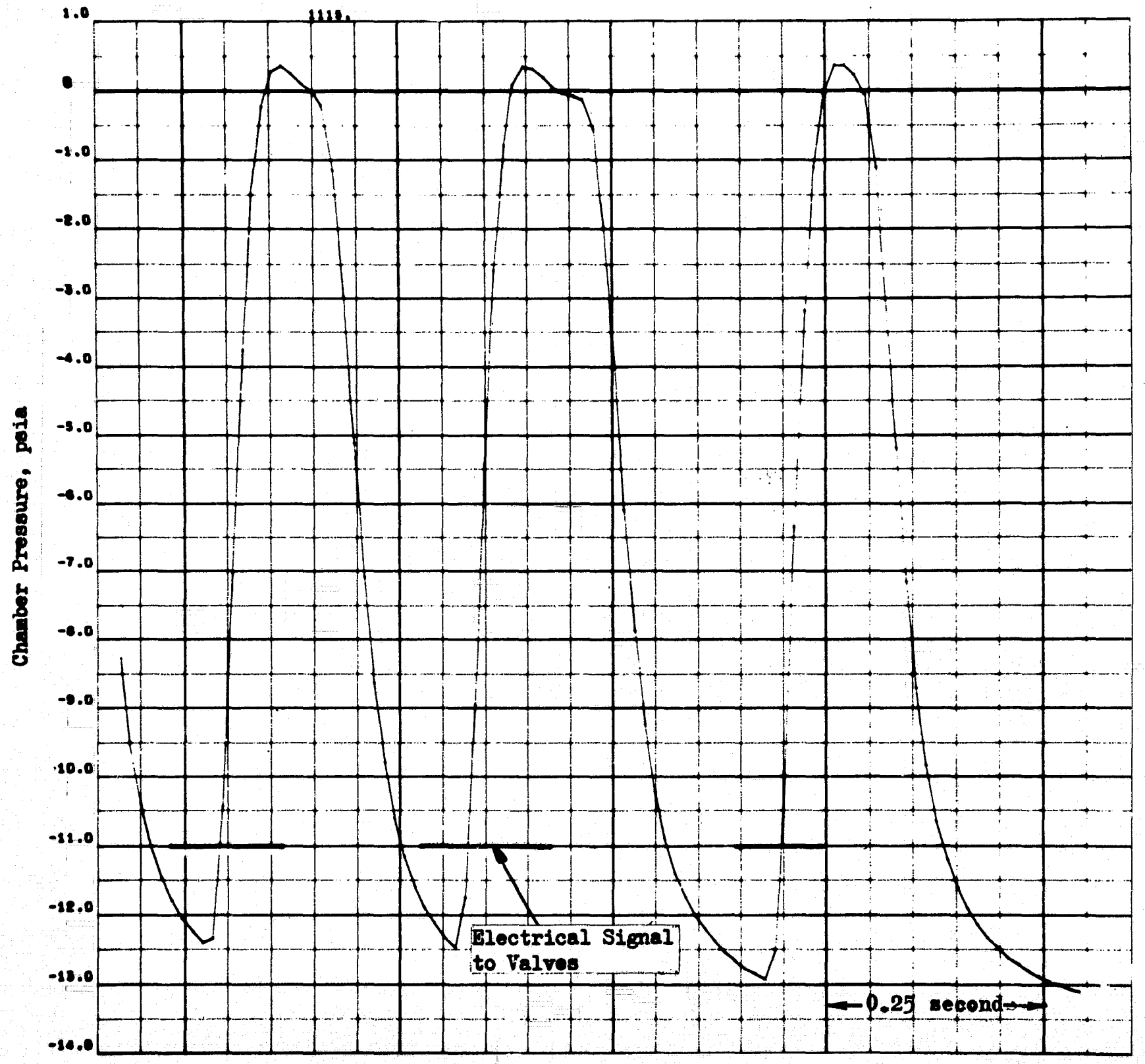

Figure 41. Chamber Pressure Response-Small Gas Generator Pulsing With Pressure Controlled (Static) Feed System

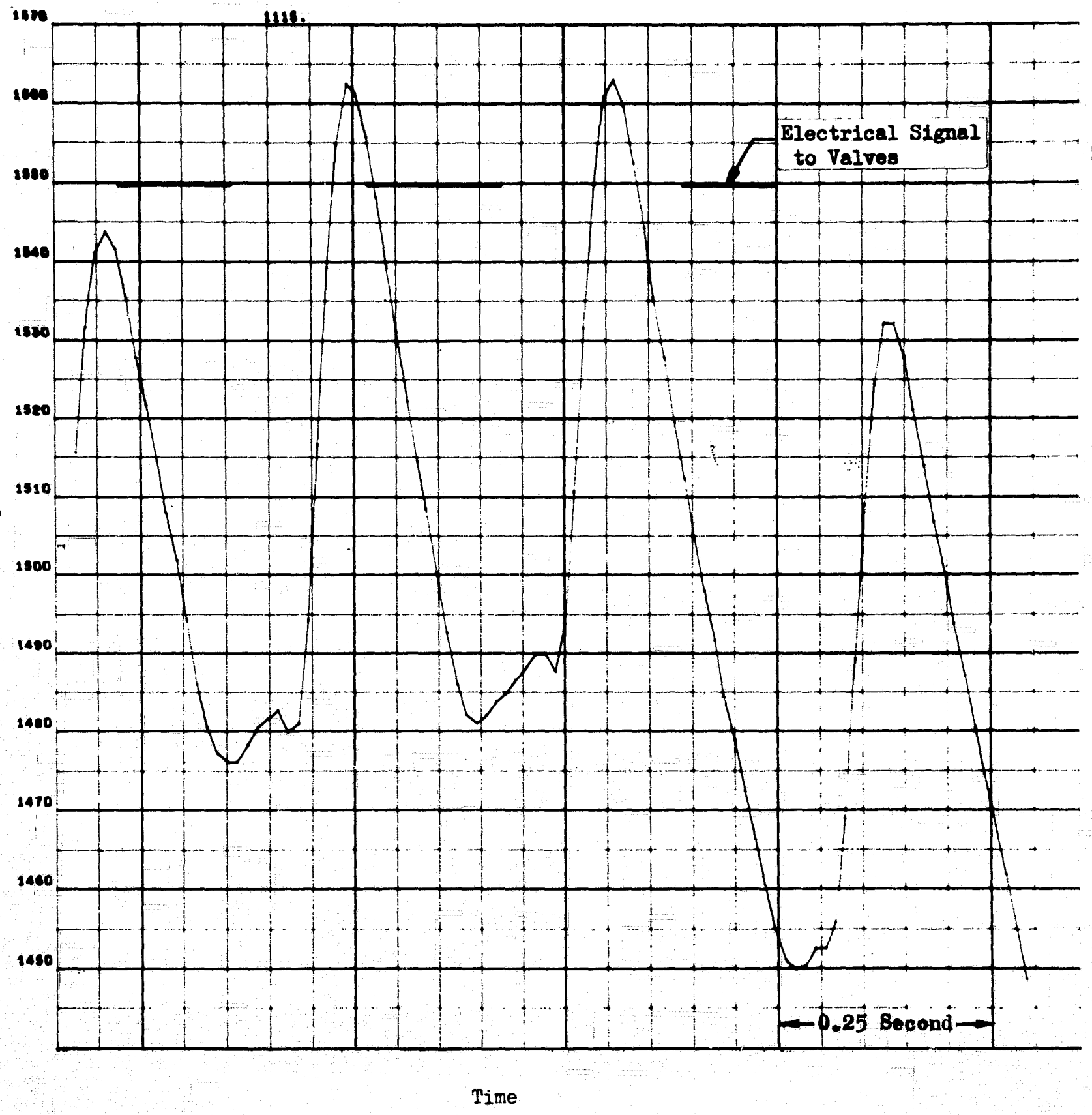

Figure 42. Chamber Temperature Response of Combustion Gas-Small Gas Generator Pulsing With a Pressure Controlled (Static) Feed System

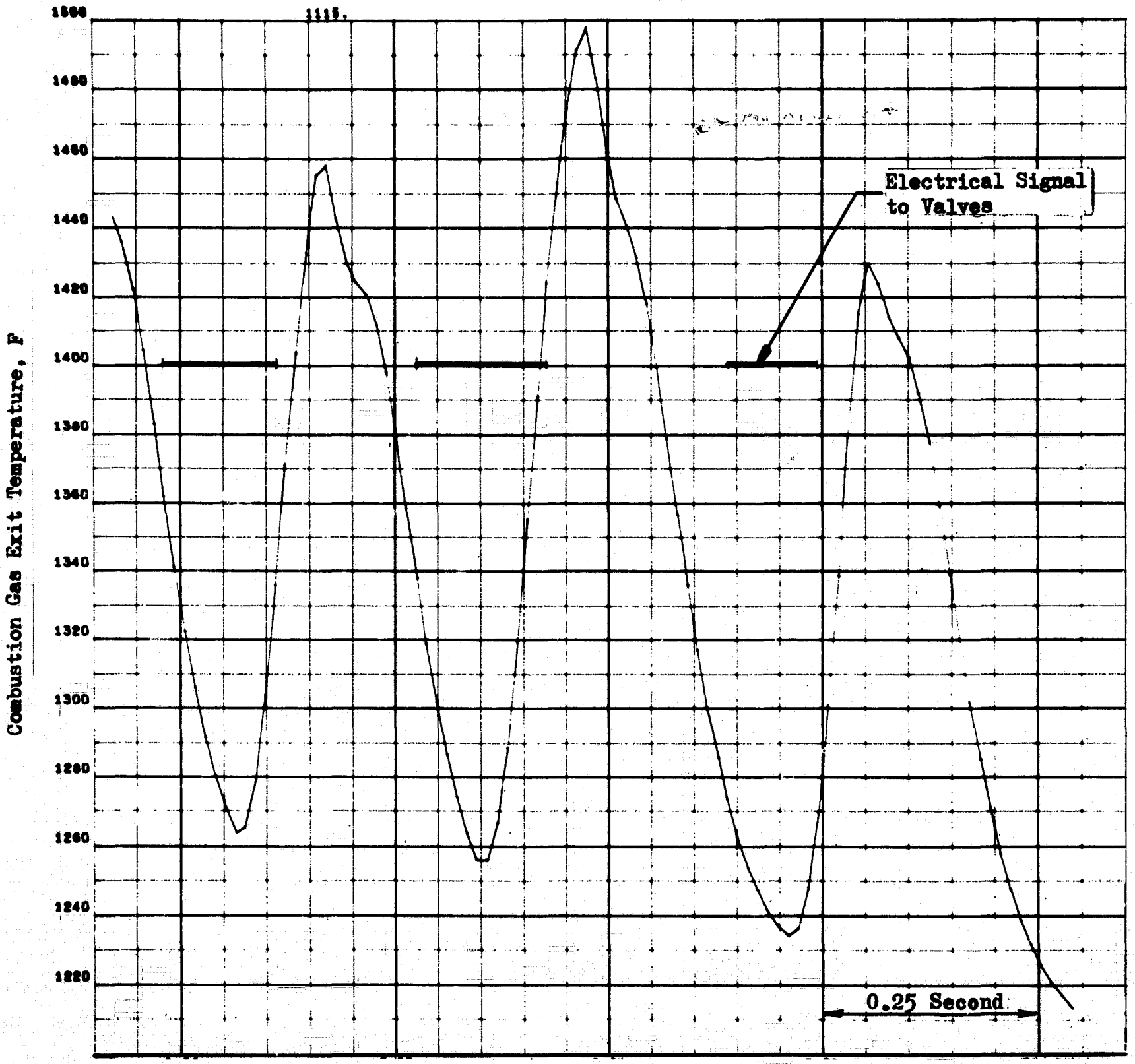

Figure 43. Nozzle Temperature Response of Combustion Gas-Small Gas Generator Pulsing With a Pressure Controlled (Static) Feed System

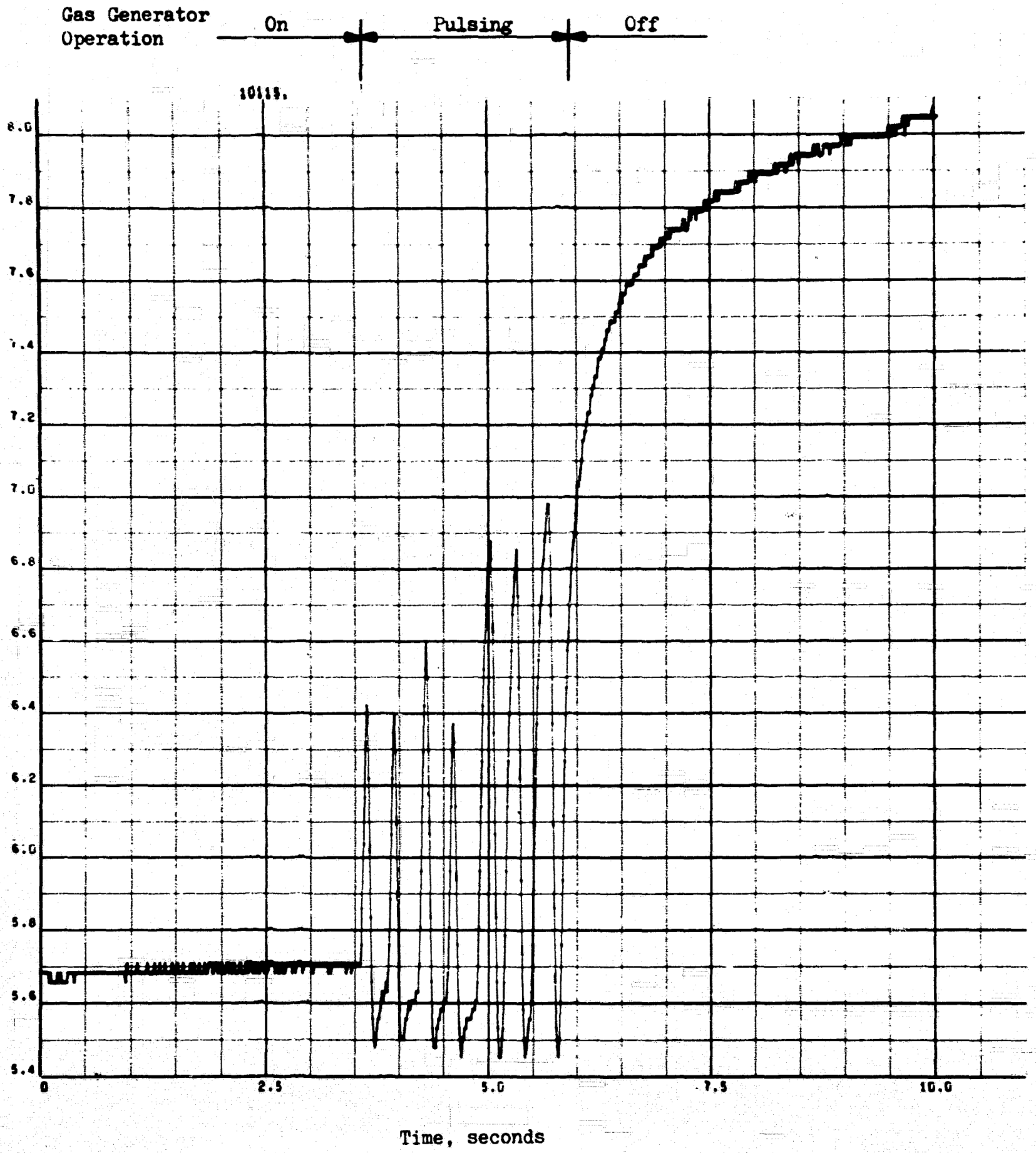

Figure 44. Fuel Inlet Pressure History-Small Gas Generator Pulsing With a Pressure Controlled (Static) Feed System

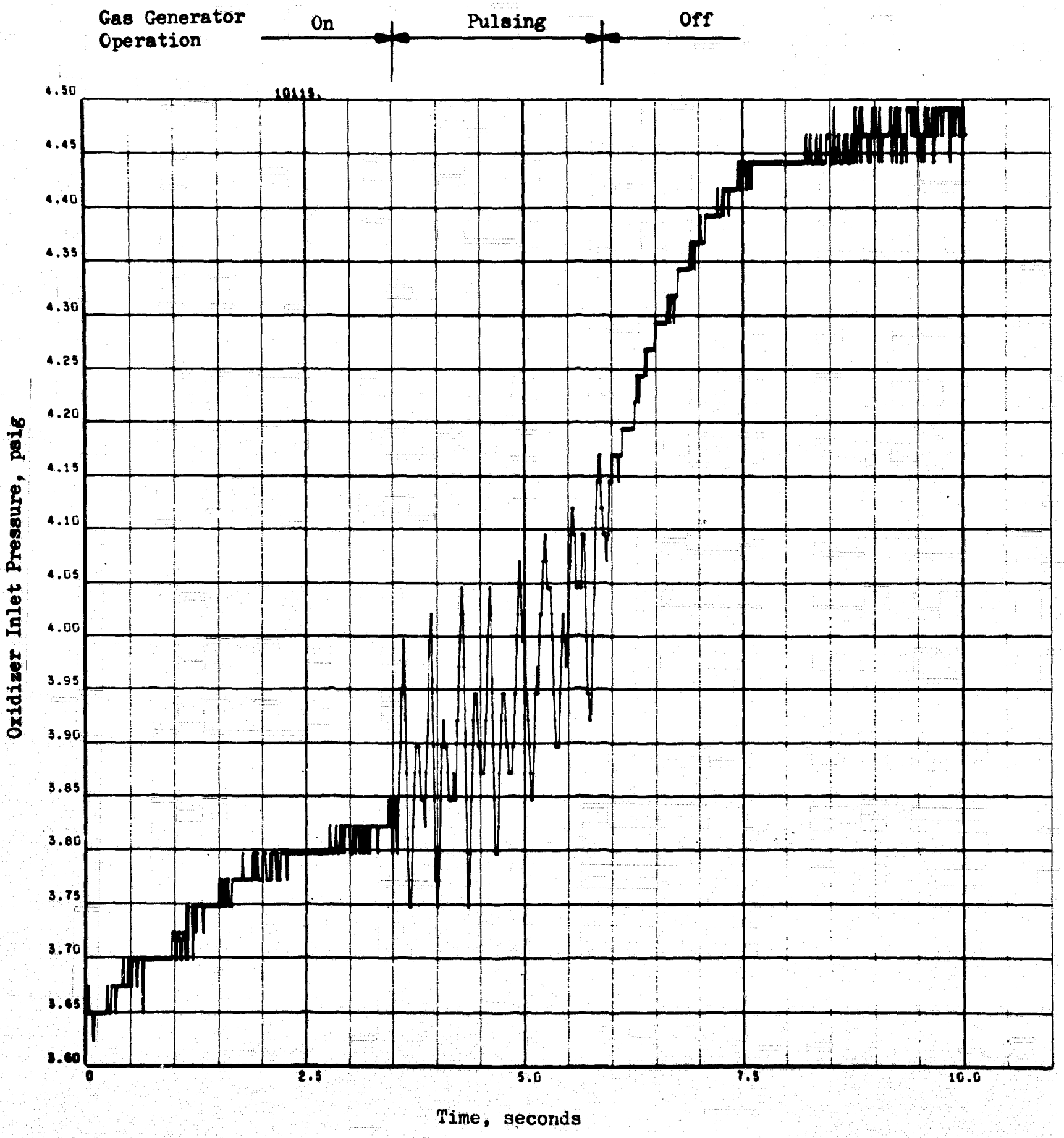

Figure 45. Oxidizer Inlet Pressure History-Small Gas Generator With a Pressure Controlled (Static) Feed System

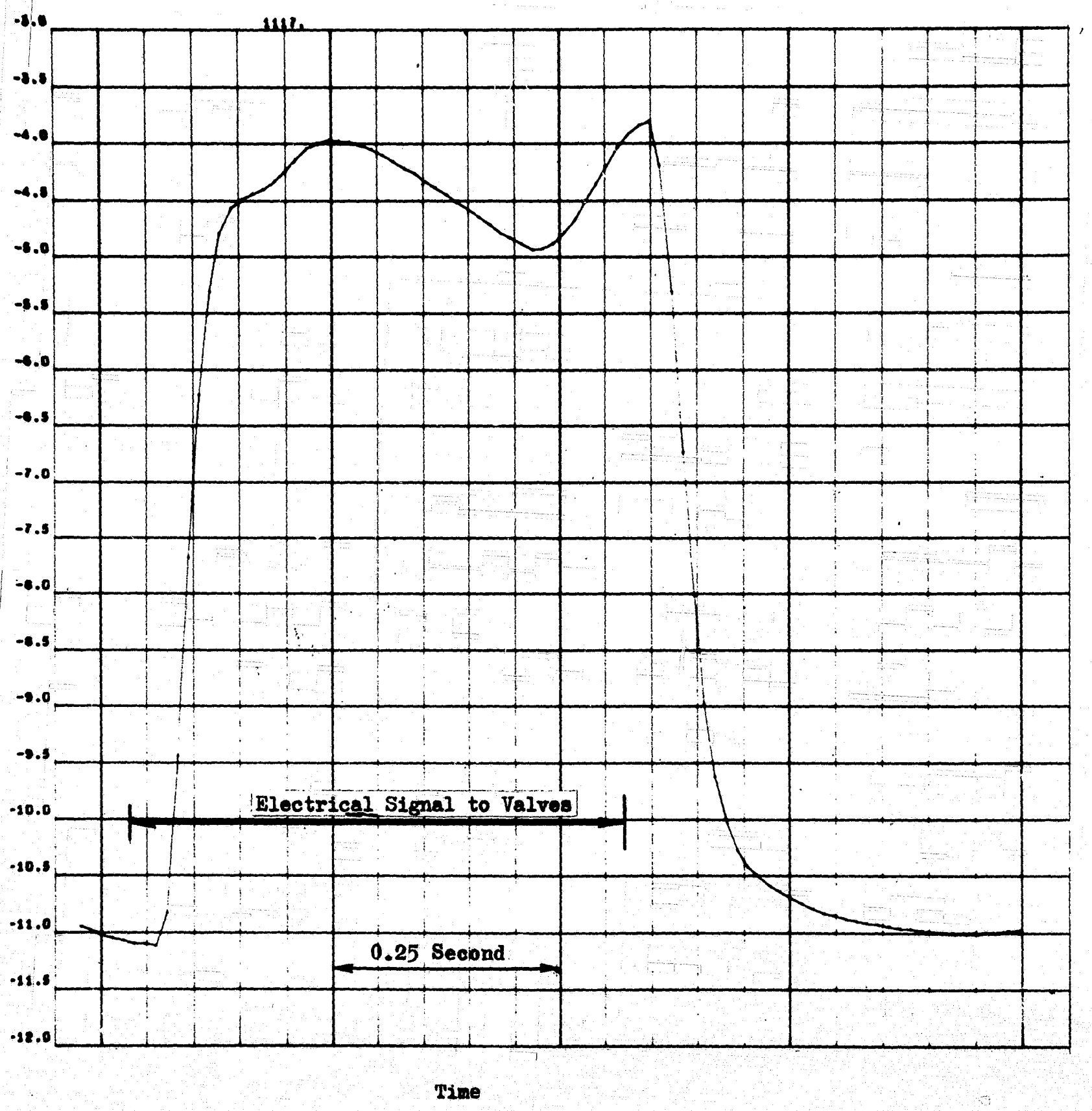

Figure 46. Chamber Pressure Response-Large Gas Generator Pulse

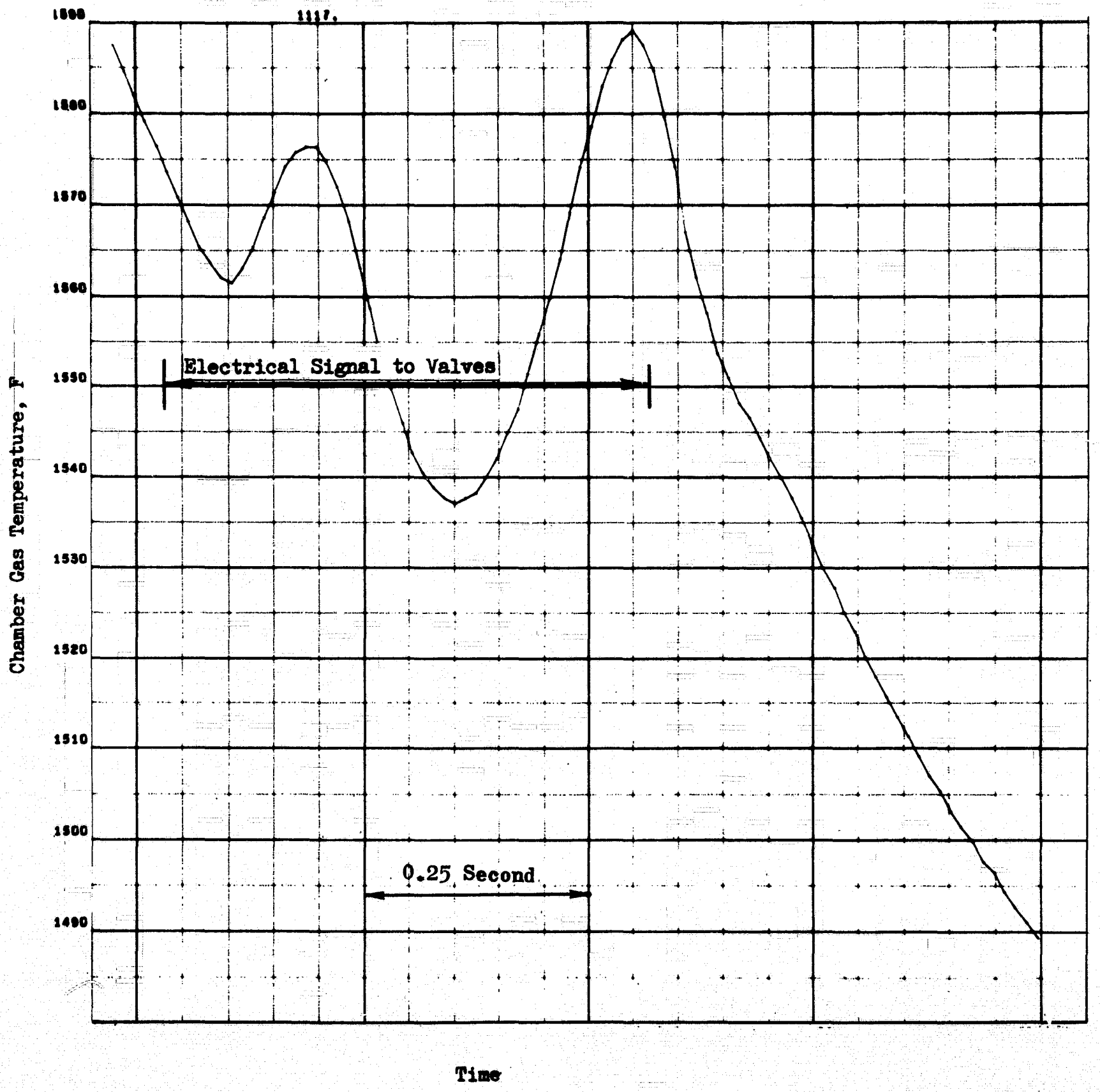

Figure 47. Temperature Response of Combustion Chamber Gas-Large Gas Generator Pulse

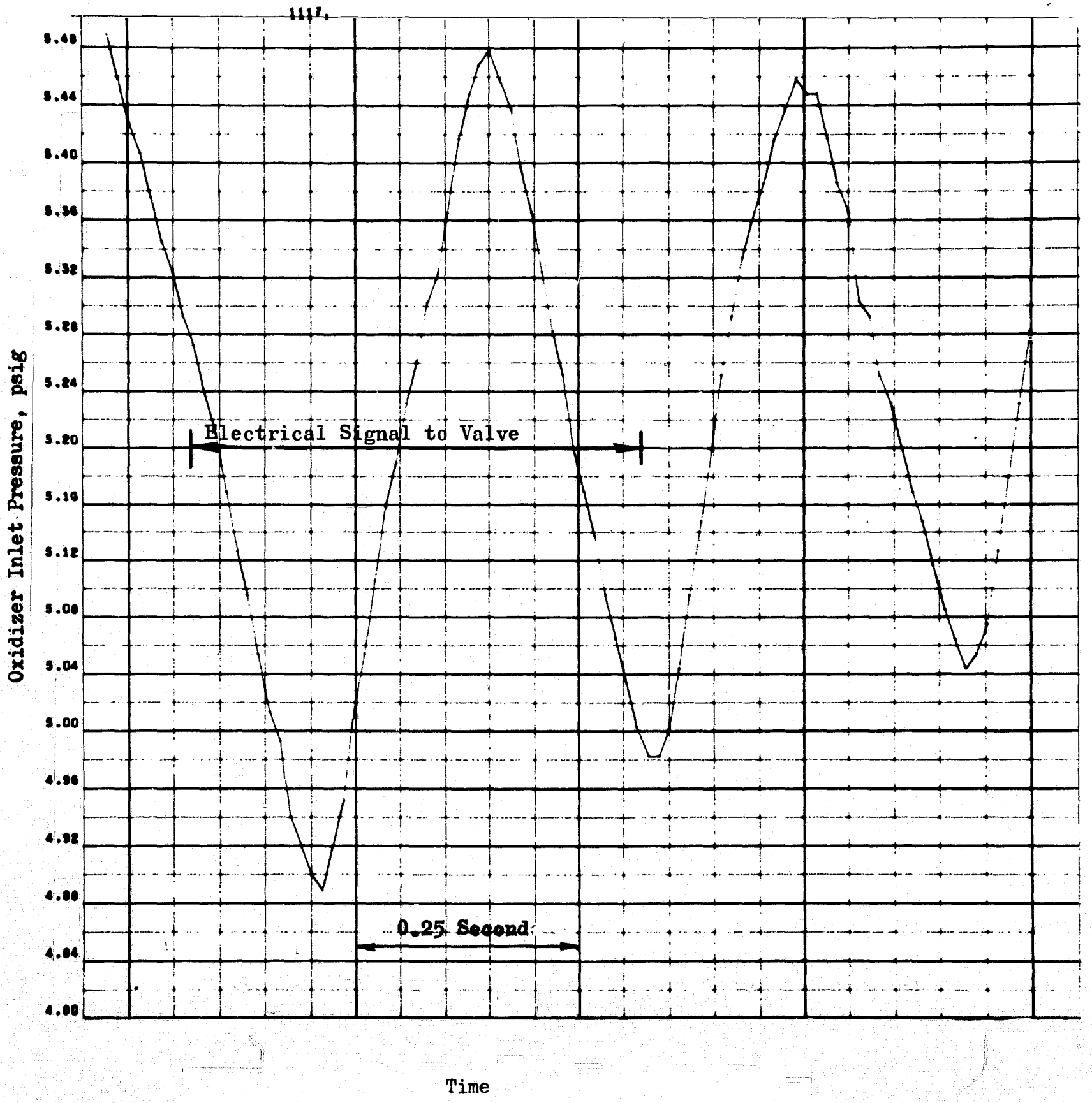

Figure 48. Oxidizer Inlet Pressure History-Large Gas Generator Pulse

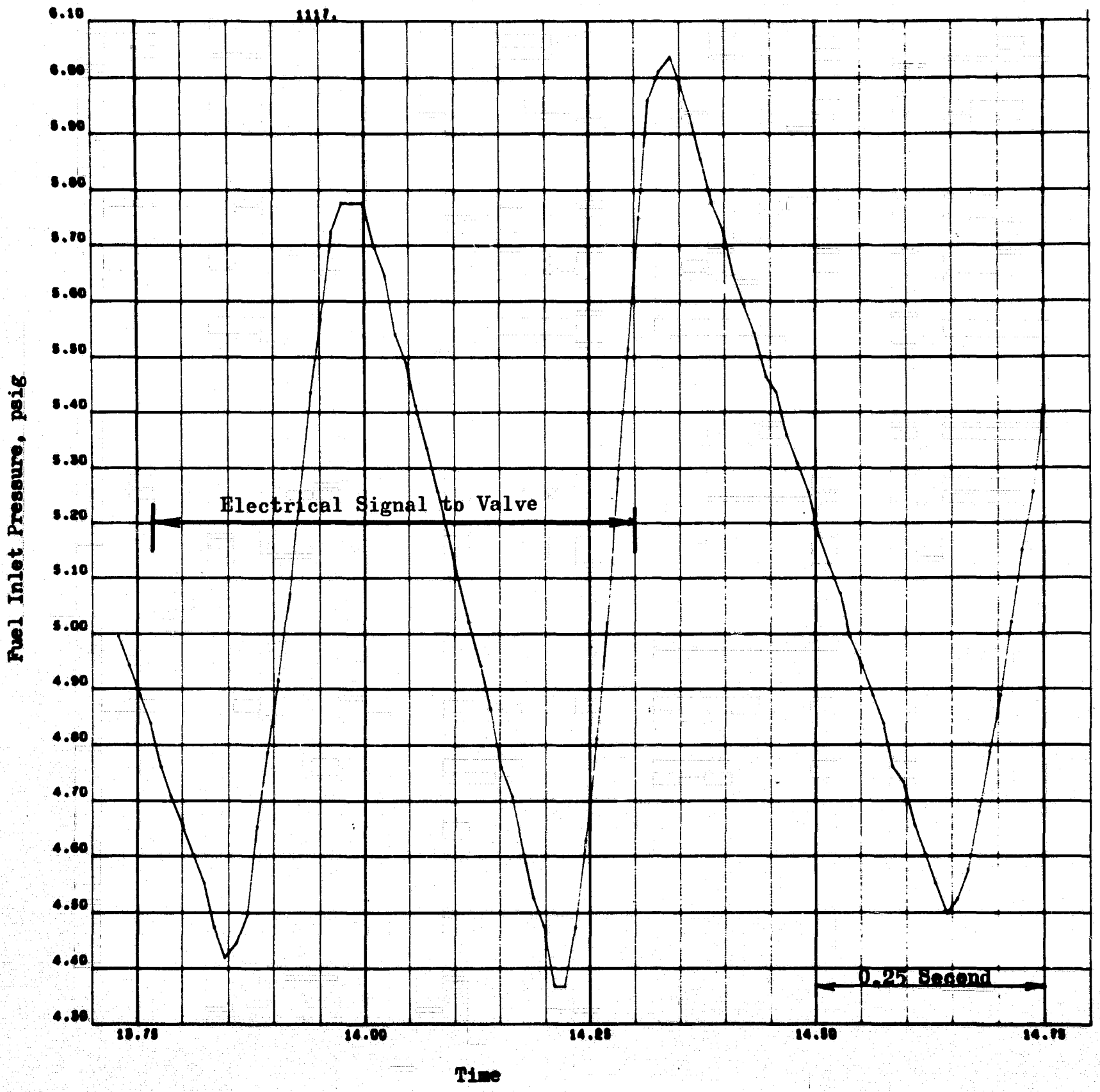

Figure 49. Fuel Inlet Pressure History-Large Gas Generator Pulse

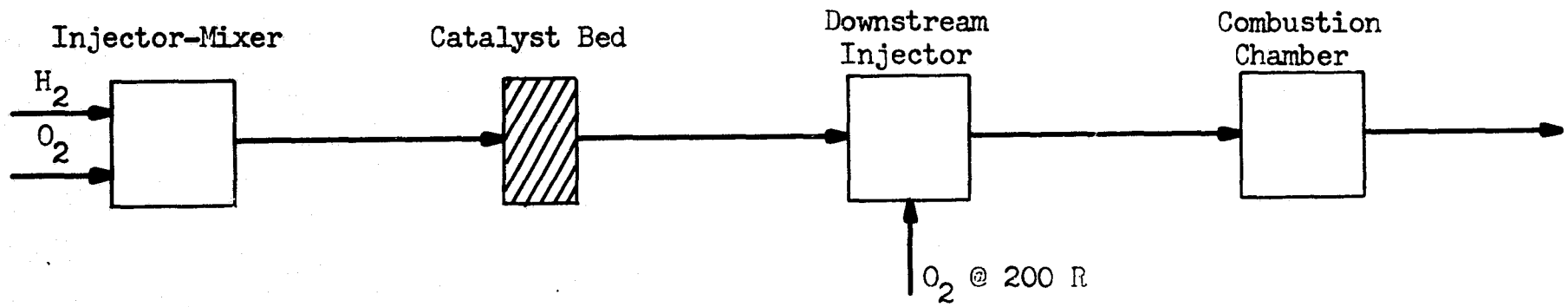

Gas Mixture Ratio	1.0		2.5	
Gas Temperature	200 R	1500 R	1350 R	3560 R

Gas Composition	O_2	H_2	H_2O	O_2	H_2	H_2O	O_2	H_2	H_2O	O_2	H_2	H_2O
Weight percent	50	50	-	-	43.8	56.2	42.9	25.0	32.1	-	19.6	80.4
Mole percent	94.2	5.8	-	-	87.5	12.5	8.6	80.0	11.4	-	68.7	31.3

Figure 50. Summary of Nominal Heat and Material Balances for Thrustor Operation

bed producing water and heat and, finally, additional cryogenic oxygen is injected into the hot-gas stream. Before the oxygen can react, several criteria must be met:

1. The oxygen must mix with the hot gas.
2. The gas mixture composition must be within the flammability limits of the hydrogen-oxygen-water system at ~1300 F and 10 psia.
3. The resulting mixture temperature must be above the dynamic autoignition temperature of ~1260 F.
4. The stream velocity must be less than or equal to the turbulent flame speed of the mixed gas at ~1300 F and 10 psia. Otherwise, the flame may be forced out of the combustion chamber.

Gas Mixing. The downstream oxygen injection method was previously shown and discussed, and it was explained how the method of injection ensured even distribution of oxygen. Uneven distribution can conceivably cause part of the mixture to pass from the engine without combusting, while local hot spots exist in other parts of the chamber.

Flammability Limits. In previous work (Ref. 3), the hydrogen-oxygen ambient, fuel-rich flammability limit was extrapolated to near 1200 F, where it was shown that mixtures of 2 to 3 percent (MR ~0.3 to 0.4) oxygen are marginally flammable. The addition of water vapor to hydrogen-air mixture has been studied experimentally at 300 F and pressures of 15 to 115 psia by Zabetakis (Ref. 9). His results show that the addition of water causes the fuel-rich concentration limits to decrease 1 volume percent hydrogen for every 1 volume percent water added. Thus, the

addition of 11 volume percent water contained in the hot gases from the catalyst bed may reduce the fuel-rich flammability limit to 86 volume percent hydrogen, 11 volume percent water, and 3 volume percent oxygen. Fortunately, the nominal design mixture 80.0 volume percent hydrogen, 11.43 percent water, and 8.57 percent oxygen is within the projected flammability range. However, it might be concluded that there is a minimum oxygen flowrate if ignition of the oxygen injected downstream is to occur.

Autoignition Temperature. The relationship between the amount and temperature of hot gas to be mixed with a given amount of additional oxygen so that a spontaneously combustible mixture occurs can be stated by a heat balance:

$$\dot{W}_{H_2} C_{pH_2} T_{H_2} + \dot{W}_{O_2} C_{pO_2} T_{O_2} = \left[(\dot{W}_{O_2} + \dot{W}_{H_2}) C_p T)\right]_{\substack{\text{mixed} \\ \text{gases}}} \quad (10)$$

If $T)_{\text{mixed gases}}$ is equal to or greater than the autoignition temperature of 1260 F, combustion will occur. For the nominal design conditions shown in Fig. 50, the temperature of the mixed gases after injection of cold oxygen can be calculated to be ~150 F lower than the temperature from the catalyst bed, but ~90 F above the threshold temperature. Therefore, combustion will occur. With an increase in the DSI oxygen flowrate by ~33.3 percent to a MR of 3.0, the temperature of the mixed gases would decrease to the threshold temperature, 1260 F, and ignition might not occur.

Because of the nearness of the hot-gas outlet temperature to autoignition temperature, a slight amount of gas channeling and subsequent uneven temperature distributions from the catalyst bed can cause similar uneven

temperature distribution about the autoignition temperature and, consequently, erratic DSI combustion. This point is further illustrated in Table 7 by comparing TC1 with TC2 before and after ignition. For the cryogenic runs which were characterized by ignition delays and slow thermal response and subsequent gas channeling, temperature differences on the order of 1500 F were sometimes observed. However, the temperature profiles were much smoother for the AB-AP runs, 19 and 23. Low performance also may be a byproduct of this undesirable phenomenon.

The measured autoignition temperature of 1260 F is considerably above those reported in the literature for other systems containing hydrogen-oxygen. For example, Zabetakis (Ref. 9) experimentally found the minimum static autoignition temperatures for intermediate compositions of hydrogen-air-water to vary from 977 to 1075 F as the water content was increased from 10 to 30 volume percent. He also measured minimum spontaneous ignition temperatures of hydrogen-water vapor mixtures flowing in a pipe into unheated air at atmospheric pressure. The dynamic temperature of the flowing stream varied linearly from 1260 to 1370 F for a 0 to 60 percent water vapor variation. These results are qualitatively similar to those observed in this study but it should be pointed out that an exact comparison is impossible because of the inert diluent nitrogen in Zabetakis' work and the difference in the concentration ranges, intermediate vs fuel rich, for this study.

Turbulent Flame Speed Criteria. Turbulent flame speed data for the conditions under interest, i.e., 1300 F and 10 psia for fuel-rich mixtures containing water, are nonexistent. The ambient, stoichiometric, turbulent flame speed for hydrogen-oxygen is on the order of 30 ft/sec, and it is known that increases in propellant temperature cause increases in turbulent

flame velocity. However, it is unlikely that the turbulent flame speed increases to the range of 500 to 800 ft/sec, the range of the free stream velocity before or after DSI ignition. How, then, does the stable flame front exist? To answer this question, one must consider the DSI and how it affects the flow pattern. Because the DSI spokes are cylindrical in shape and are placed perpendicular to the flow, one can expect a region of stagnation and back-circulation on the downstream side of the spokes, as shown schematically below:

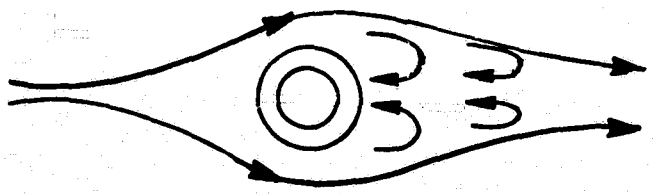

Oxygen is injected, sonically, into the region of backflow and stagnation where it mixes with the recirculating gases and reacts. The recirculating zone serves to increase residence time and thus overcome flame speed limitations. An excellent discussion of flame holders and bluff body combustion with photographs is presented by Lewis and von Elbe (Ref. 10).

Summary of DSI Analysis. The DSI analysis shows that there are some rather severe restrictions that should be considered in the design of a DSI combustor. Because of the lack of quantitative flammability limits, autoignition temperatures, and turbulent flame speed for the concentration, pressure, and temperature ranges of interest, the design of DSI device involves much guesswork.

There are other implications of this analysis, e.g., how severe will the effect of the minimum hot-gas temperature restriction, ~1410 F, be on the pressure and temperature control circuit of the conditioner system? How will the addition of a small amount of helium diluent affect the combustion? Would it be better to inject a flammable hydrogen-oxygen mixture into the hot-gas stream, thus eliminating the mixing and cooling steps with injection of only oxygen?

Catalyst Bed Pressure Drop Analysis

A number of pressure and temperature measurements were obtained in the engine to better understand how pressure drop changes with time, and to develop an expression for this relationship. Figure 51 shows how pressure drop varies between different stations in the bed as a function of time for the run discussed previously (pages 53 through 65). The stations were located in the following manner:

PM-PIF	The mixing section to first part of the catalyst bed; this includes the passive diffusion bed plus retaining screens
PIF-PDI	Approximate first third of catalyst bed

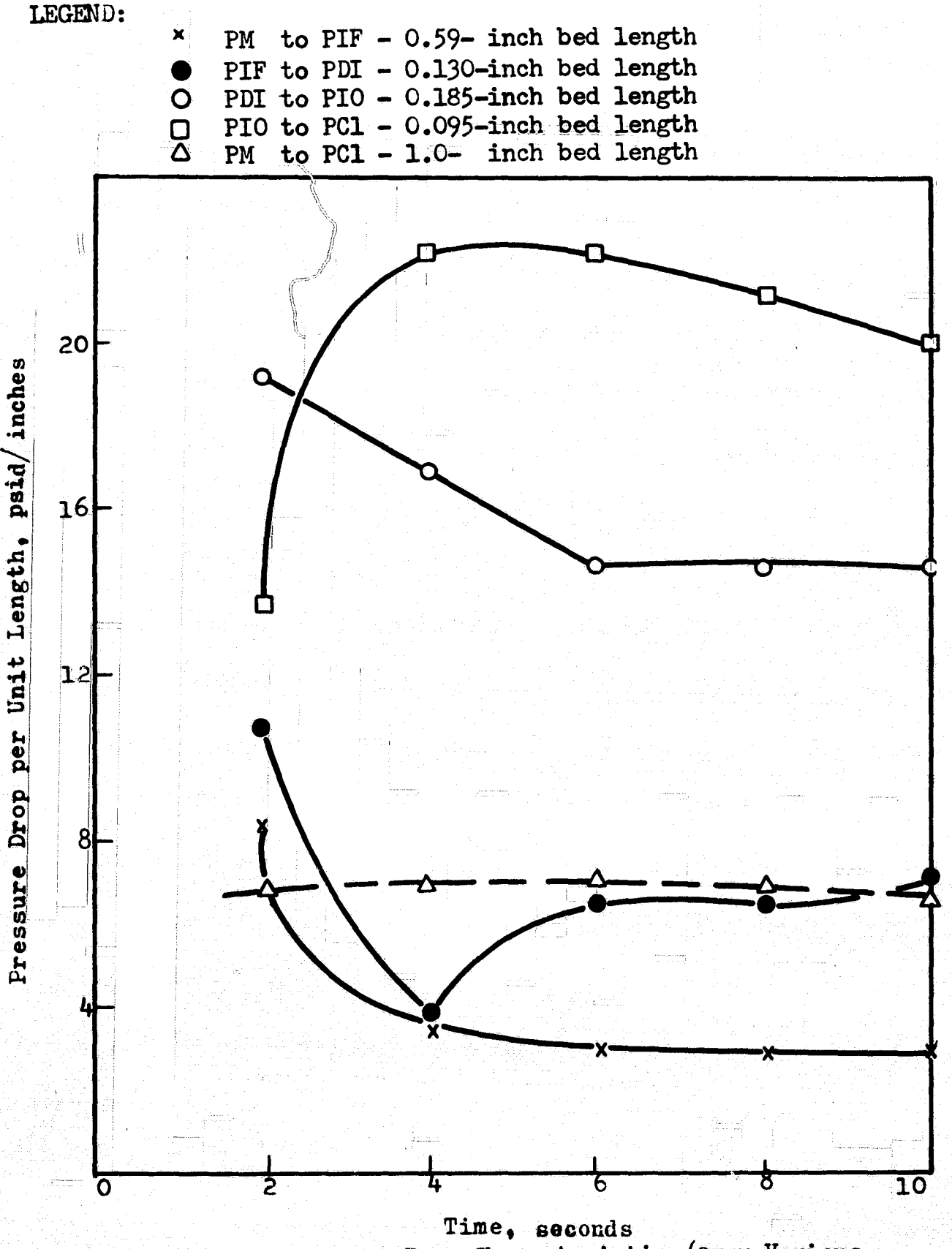

Figure 51. Packed Bed Pressure Drop Characteristics (Over Various Portions of the Catalyst and Diffusion Beds)

PDI-PID Second third of catalyst bed

PID-PCI Last third of bed plus retaining screen

PM-PCI Entire pressure drop from injector face to chamber

The superficial flowrate (G_o) was 0.00318 ±0.00007 lb/sec or essentially a constant value. From the "orifice" equation (Eq. 11) for a constant G_o,

$$\Delta P = \frac{K_2}{\rho} = K_3 \frac{T}{P(MW)} \qquad (11)$$

assuming the molecular weight will remain essentially constant and the pressure drop should be proportional to the ratio of temperature to pressure at the particular location.

The first section of the engine (PM-PIF) shows a decreasing ΔP with time as the temperature in the passive mass (diffusion bed) decreases. The first third of the catalyst bed (PIF-PDI) initially cools as the pressure rises. Both effects result in a decreasing ΔP; however, an increasing temperature begins to have a more significant effect after 4 seconds as shown by the increase in ΔP. The pressure drop (PDI-PID) over the middle third of the catalyst bed has the same characteristics although the ΔP assumes a constant level at 6 seconds. The pressure drop over the last third of the bed (PID-PCI) indicates that temperature is the controlling factor. This was expected because the point of complete reaction was established in this section of the bed.

The pressure drop through the entire engine remains relatively constant during the run which shows that increasing temperatures in the bed locally influence the flow characteristics but not in an overall manner. The constant pressure drop would not exist over the time span associated with a short duration pulse (~50 milliseconds) because pneumatic filling and discharging would occupy an appreciable fraction of the pulse.

Data prediction and correlation were attempted by two methods: the Ergun Equation and a graphical method found in unit operations by Brown (Ref. 11). The Ergun equation for pressure drop in a packed bed is given by the following equation:

$$\frac{D_p \, g\rho \, \Delta P}{G_o^{\,2} L} \left(\frac{\epsilon^3}{1-\epsilon}\right) = \frac{150\,(1-\epsilon)}{D_p \, G_o/\mu} + 1.75 \qquad (12)$$

If one drops the first right-hand term, i.e., the friction contribution, the following equation results:

$$\frac{\dot{w}}{\epsilon A_o} = \sqrt{2g\rho \, \Delta P} \left[\frac{D_p}{L} \; \frac{1}{3.5} \; \left(\frac{\epsilon}{1-\epsilon}\right)\right]^{1/2} \qquad (13)$$

where

ϵA_o = an effective orifice area across the bed

L/D_p = number of orifices per flow path

$\frac{1}{3.5} \frac{\epsilon}{(1-\epsilon)}$ = specific density of orifices

This simplified equation is quite similar to the standard orifice equation

$$G_o^2 = K_1 \, g \rho \Delta P \qquad (14)$$

Hand calculations predicting pressure drops for both cold and reacted flow conditions are given in Table 9. The relative sizes of the frictional and orifice contributions to the pressure drop also are presented. Pressure drops also were calculated by a graphical method (Ref. 11). In the hot part of the catalyst bed, pressure drops on the order of 20 to 25 psi/in. were measured. This range is somewhat lower than that predicted range of 34 to 38 psi/in. shown in Table 9. Note that the agreement is much better at the low-temperature end. It should be pointed out that the calculated results are extremely sensitive to the value of ϵ selected. This value was taken from a correlation presented in Ref. 11.

In addition, the Ergun equation was written in the differential form and programmed on the computer using the Midas technique (Ref. 12). An additional parameter fraction of reacted propellants, α, was defined accordingly:

$$\alpha \text{ (fraction of reacted propellants)} = A \tanh [B \, (x-C) \,] + D$$

where

A, B, C, and D are selected to approach experimental data and x is the length of catalyst bed; then:

T, MW, and μ = f (α)

An example of the computer output is given in Fig. 52 and 53 for $\epsilon = 0.45$. This value of ϵ was the value which made the measured pressure drop for the H_2 cold-flow test fit the calculated pressure drop from the Ergun equation. The predicted pressure drop for 1 inch of 1/16-inch catalyst was 6.5 psi.

TABLE 9

SUMMARY OF PRESSURE DROP CALCULATIONS FROM ERGUN EQUATION AND GRAPHICAL METHOD OF BROWN

(ϵ= 0.31; D= 3 in.; $\dot{w}_{full\ flow}$ = 0.05 lb/sec; $\dot{w}_{DSI}$ = 0.0286 lb/sec)

Condition	Temperature, R	Pressure, psi	Ergun Equation			Brown Method
			Size of Term, inches		Δ P/L psia/in.	Δ P/L psia/in.
			Functional	Orifice		
Full Flow	200	10	0.0661	1.75	5.32	4.84
Full Flow	4050	10	0.676	1.75	124.8	152.
Downstream Injection	2000	10	0.548	1.75	33.9	38.4
Downstream Injection	200	10	0.108	1.75	2.81	2.75

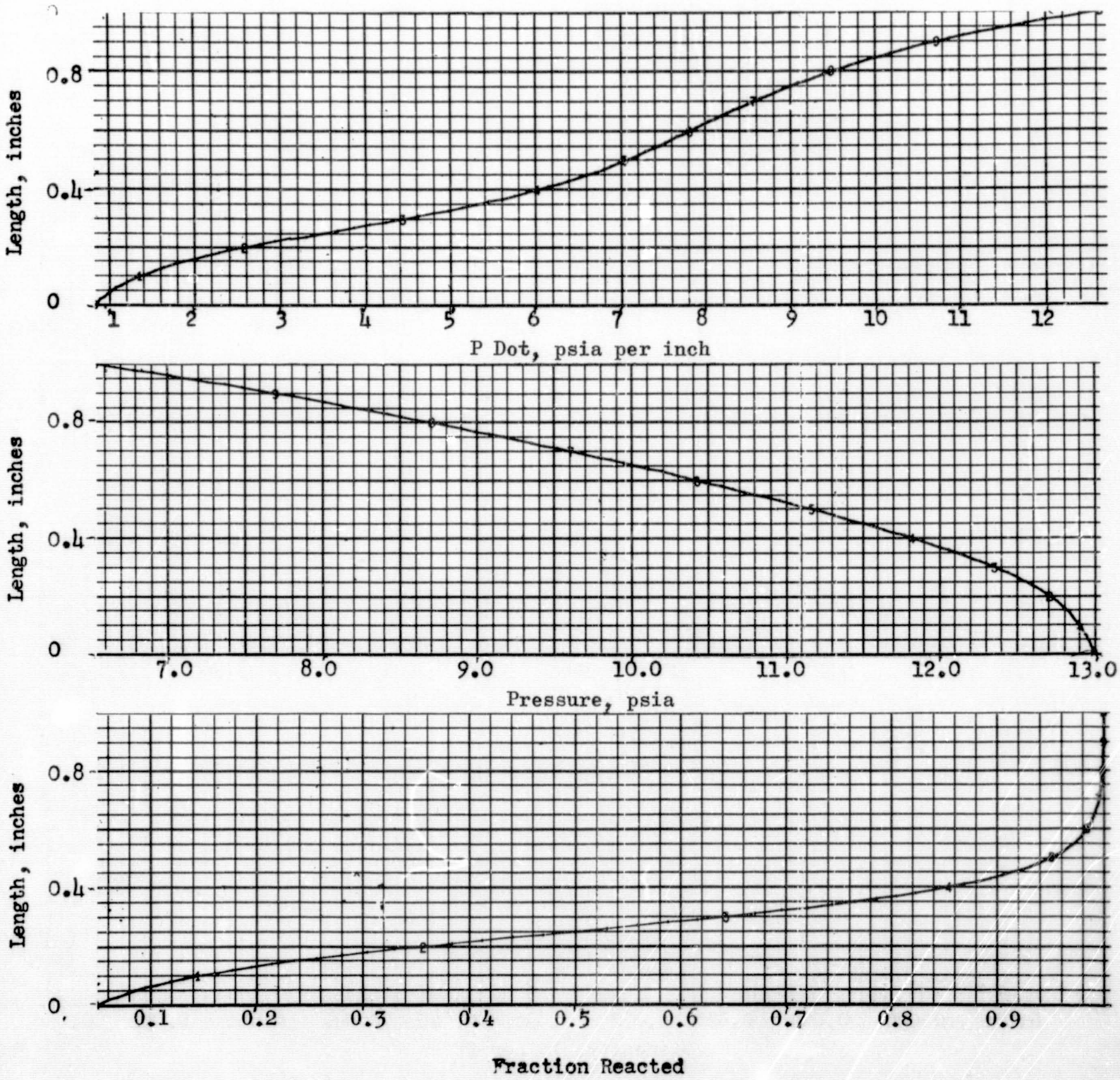

Figure 52. Midas Program Output Describing Pressure Drops (From the Ergun Equation)

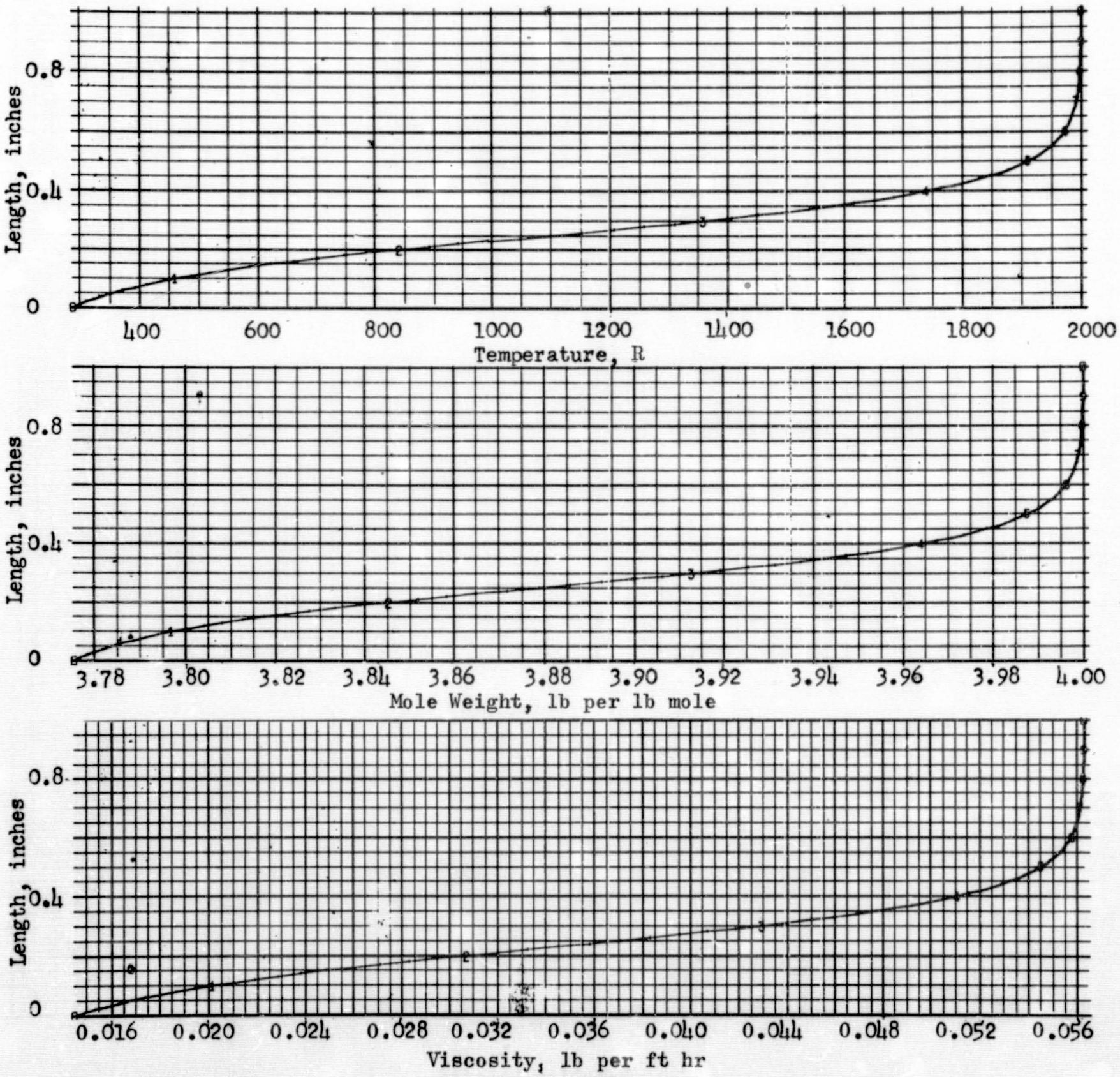

Figure 53. Midas Program Output Describing Temperature and Viscosity Gradients (Using the Ergan Equation)

Later, this model was run also for cases of ϵ = 0.5, 0.45, 0.40, 0.35, and 0.30, and compared with hot-fire data. It was concluded that the value of ϵ that closely corresponded to experimental pressure drop data was from 0.45 to 0.50. To determine the exact value of ϵ more efficiently, the Ergun equation can be rearranged in a form more amenable to experimental data, e.g.,

$$\epsilon = 1 + \frac{\Delta P_{bed}\, P_{av}}{\left[1.75 \frac{G_o^2\, R}{D_p\, g} \int \frac{T}{mw}\, dx\right] \frac{1}{\epsilon^3} + \left[\frac{150\, G_o\, R}{D_p^2\, g} \int \frac{\mu T}{MW}\, dx\right] \frac{1-\epsilon}{\epsilon^3}} \qquad (15)$$

Because ΔP_{bed}, P_{av} are known and T = f (x), MW = f(T), and μ = f(T). The equation can be reduced to a polynominal of ϵ. Iteration is then required to give the correct value of ϵ.

Recently, Fan (Ref. 13) compared a variety of methods for predicting packed-bed pressure drop with selected experimental data and concluded that the most universally superior method was the previously cited one found in Brown. He concluded that if these calculated pressure drops are multiplied by a factor of 1.2, the method will predict results within an error range of -34 percent to +33 percent, with a standard deviation of 15 percent. The corresponding error range for the Ergun equation is =67 to +46 percent, with a 40 percent standard deviation. Fan also points out that several investigators have found that the constants 150 and 1.75 in the Ergun equation vary depending on the shape of the particle.

The results of this study seem to confirm the wide disagreement between calculated and measured pressure drops that Fan reports, although the results of the Ergun equation are in slightly better agreement with those measured than the results of the graphical method.

Fan's work also shows that the constants in the Ergun equation should be fitted to the experimental data rather than finding the value of ϵ which correlates the data. The latter was done in this study.

In summary, both the Ergun equation and the effective orifice equation (Eq. 11 and 12) gave fair approximation to the bed pressure drop measured in the thrustor. A void fraction of $\epsilon \sim 0.45$ was needed to correlate the model results with experimental data. The superficial orifice equation was used on the thrustor computer model, thus neglecting the friction loss which was shown to be less than 30 percent of the orifice term.

COMPARISON OF COMPUTER SIMULATION TO EXPERIMENTAL RESULTS

Shown in Fig. 54 through 56 are the predicted pneumatic and thermal responses for a DSI thrustor having a 0.525-inch catalyst bed. A thermal response of 700 milliseconds was predicted, as compared to measured thermal response times of 2 to 3 seconds. The most plausible explanation for the large difference in observed vs predicted thermal responses is that a portion of the oxygen passes through the catalyst bed without reacting during the transient period, as discussed above.

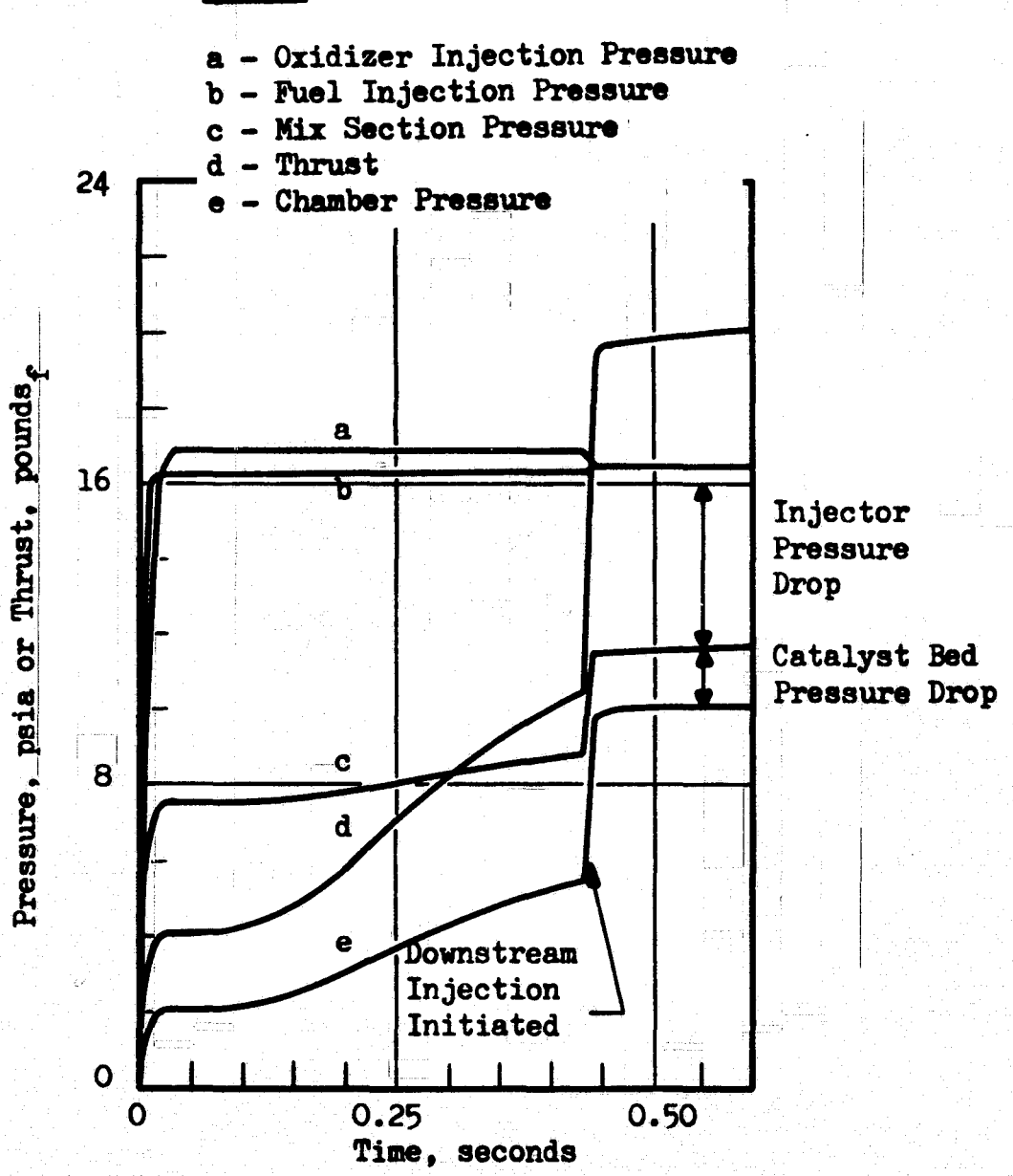

Figure 54. Predicted Response of a Thrustor With Downstream Injection of Oxygen and a 0.525-Inch Catalyst Bed. Pneumatic and Thrust Response

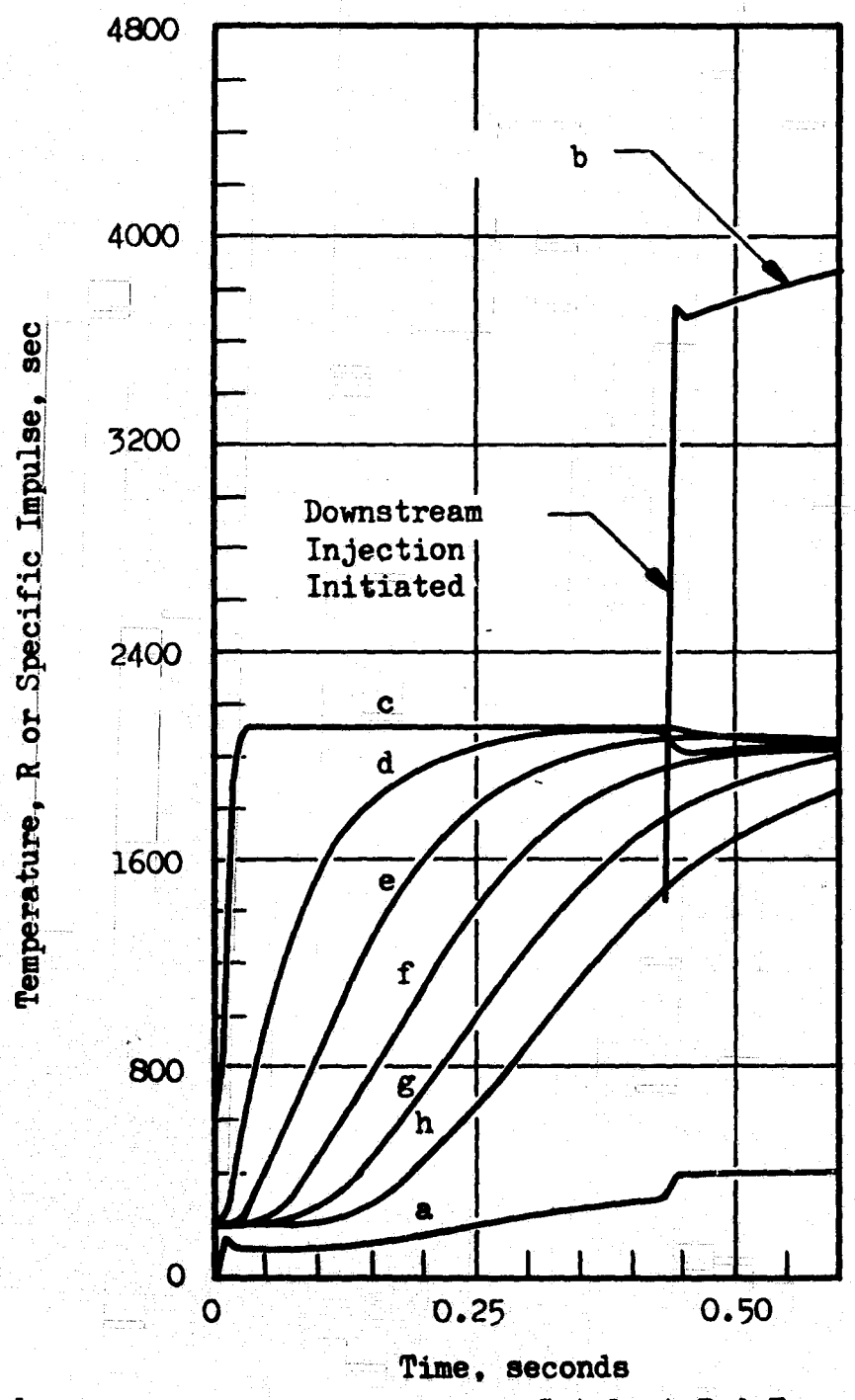

Legend:

a - Specific Impulse
b - Combustion Chamber Temperature
c - Theoretical Temperature of Gas Fed to Catalyst Bed

Catalyst Bed Temperatures-Distance from Upstream Face of the Bed

d - 0.105 inches
e - 0.210 inches
f - 0.315 inches
g - 0.420 inches
h - 0.525 inches

Figure 55. Predicted Response of a Thrustor With Downstream Injection of Oxygen and a 0.525-Inch Catalyst Bed. Temperature and Specific Impulse Response

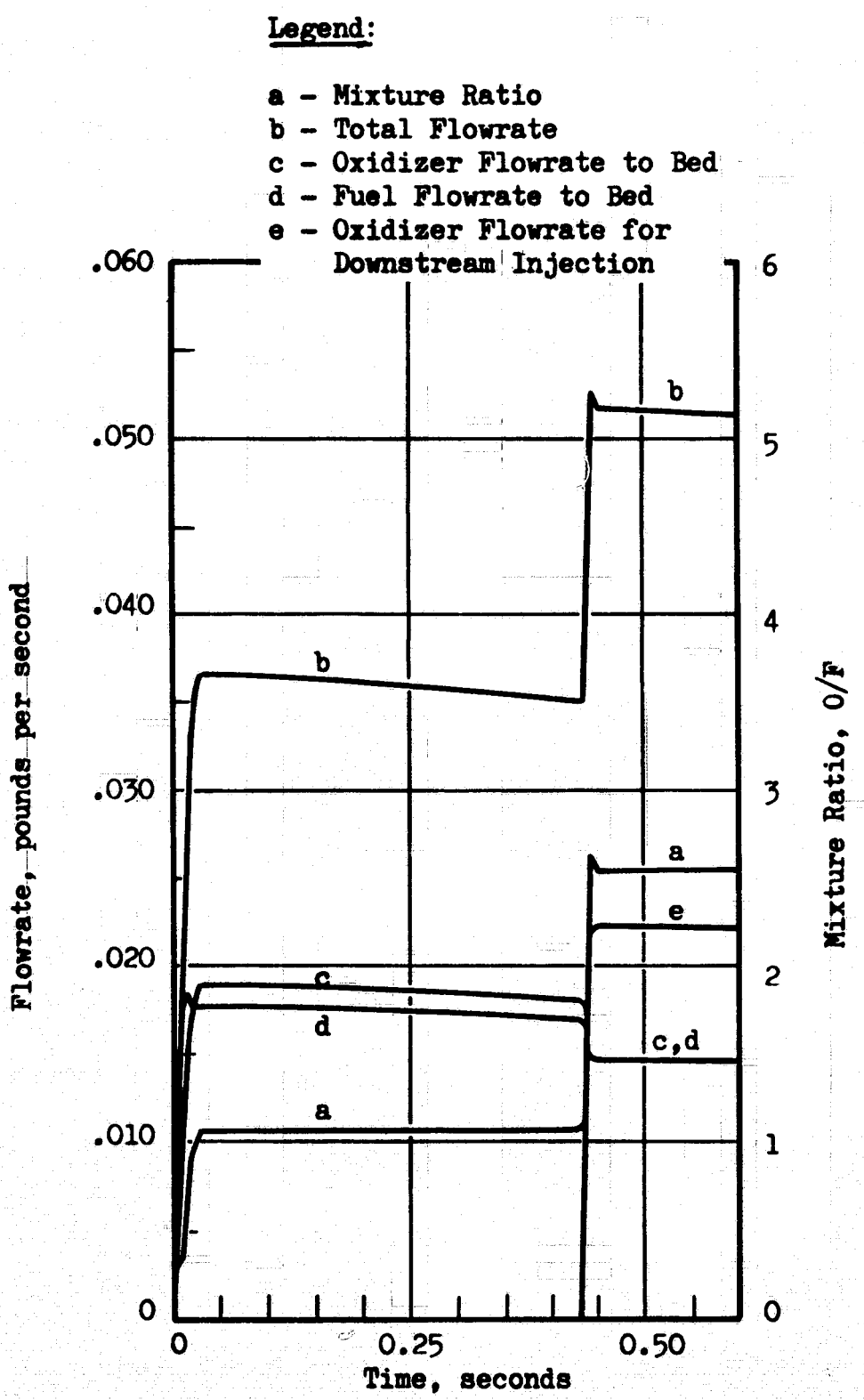

Figure 56. Predicted Response of a Thrustor With Downstream Injection of Oxygen and a 0.525-Inch Catalyst Bed, Flowrate and Mixture Ratio Response

An example of the predicted pneumatic response of an in-line thrustor is given in Fig. 57 through 59 for an internal geometry of 1/2 inch of void mix section (3.5 cubic inches), 1/2 inch of copper shot, 2/3 inch of catalyst bed, and 2 inches of combustion chamber and the nominal full flowrate of 0.05 lb/sec. The workable thrustor parameters correspond to those initially selected except for the void mix section which was 10.6 cubic inches (1-1/2 inch long) and the flowrate which was a nominal 0.0286 lb/sec with downstream injection of oxygen. Thus, the predicted 20- to 30-millisecond mix pressure responses were 2 to 3 times faster than the observed response with the gas generators or thrustor. This illustrates how important it is to minimize thrustor volumes if optimum performance is to be obtained.

THRUSTOR RESPONSE-SUMMARY AND FUTURE CONSIDERATIONS

Summary of Response Characteristics

Two responses are of prime interest for the design and evaluation of small thrustor systems, those of thrust and specific impulse. The former characterizes system output, the latter measures system efficiency. The relative importance of the two can be defined only with respect to a given application. However, thrust response, which by inference from pressure response data is fairly rapid, is expected to be most important.

The specific impulse response is directly related to the response of the combustion gas temperature. Although response times of less than 1 second are predicted on the basis of heat transfer characteristics in the catalyst bed, the experimental response times were, in general, found to be on the order of 2 to 3 seconds for a cold catalyst bed start. Subsequent restarts with a hot catalyst bed would not have an appreciable

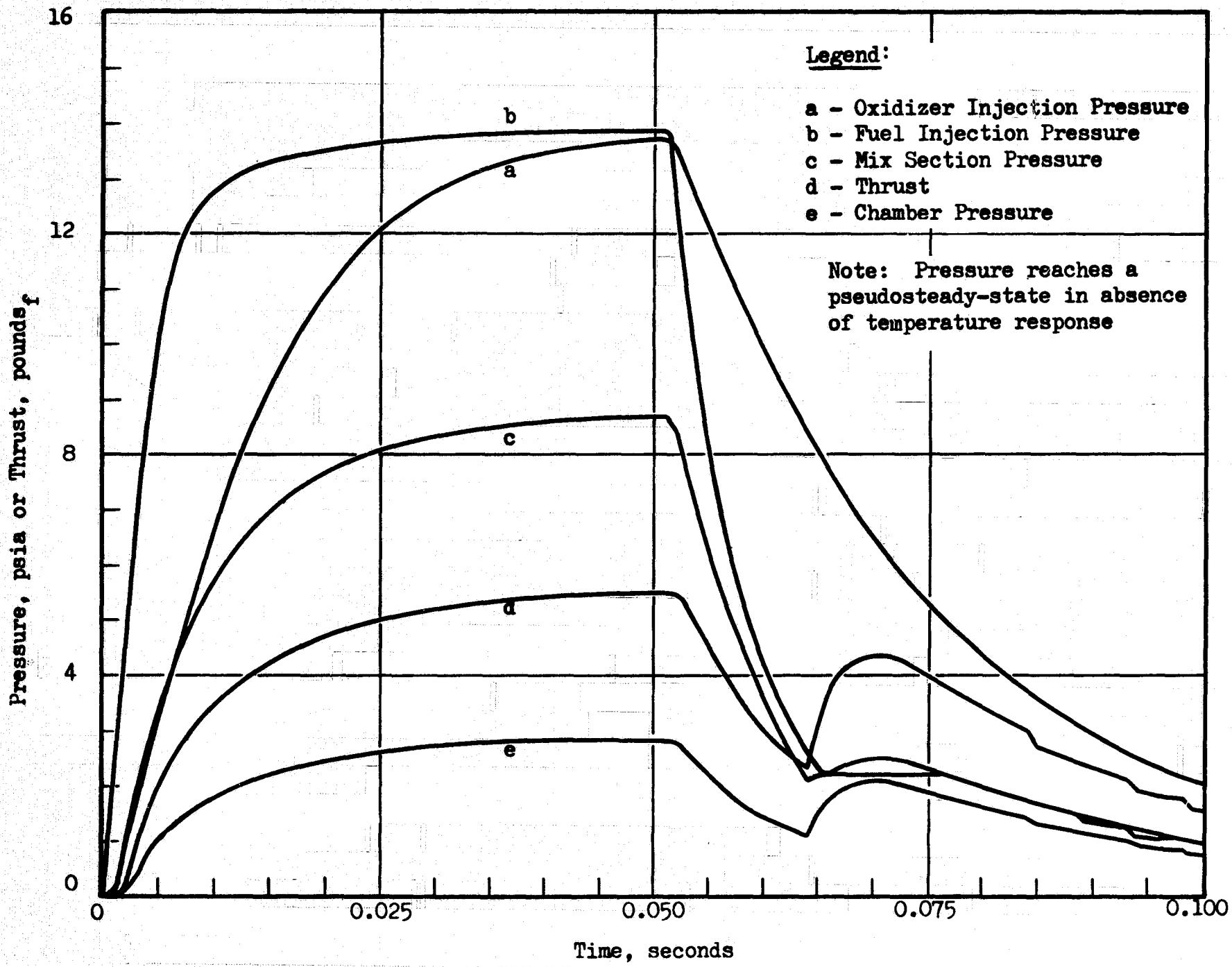

Figure 57. Predicted Response of a Thrustor With an In-Line Catalyst Bed of 0.667-Inch Length, Pressure and Thrust Response

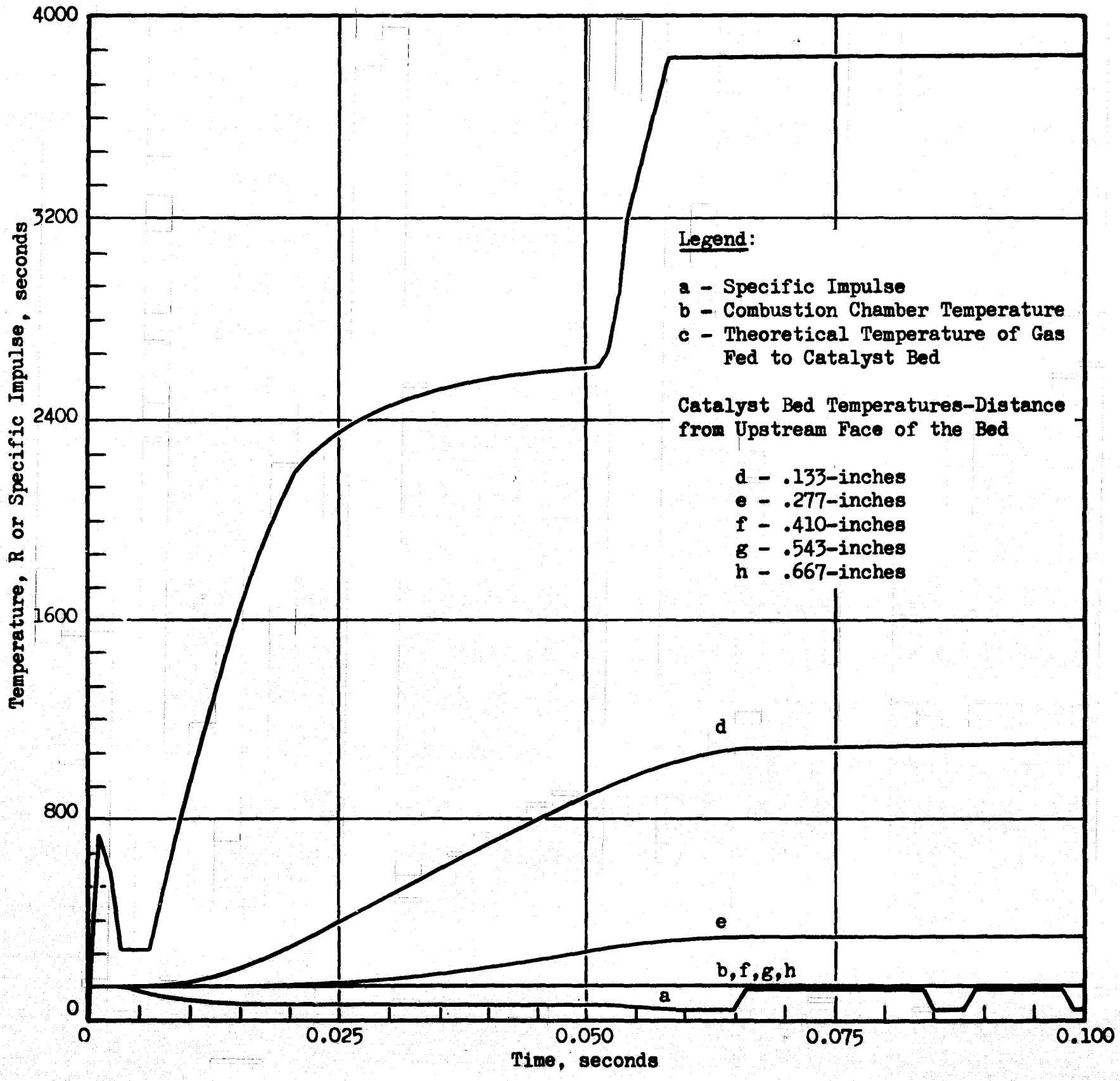

Figure 58. Predicted Response of a Thrustor With an In-Line Catalyst Bed of 0.667-Inch Length, Temperature and Specific Impulse Response

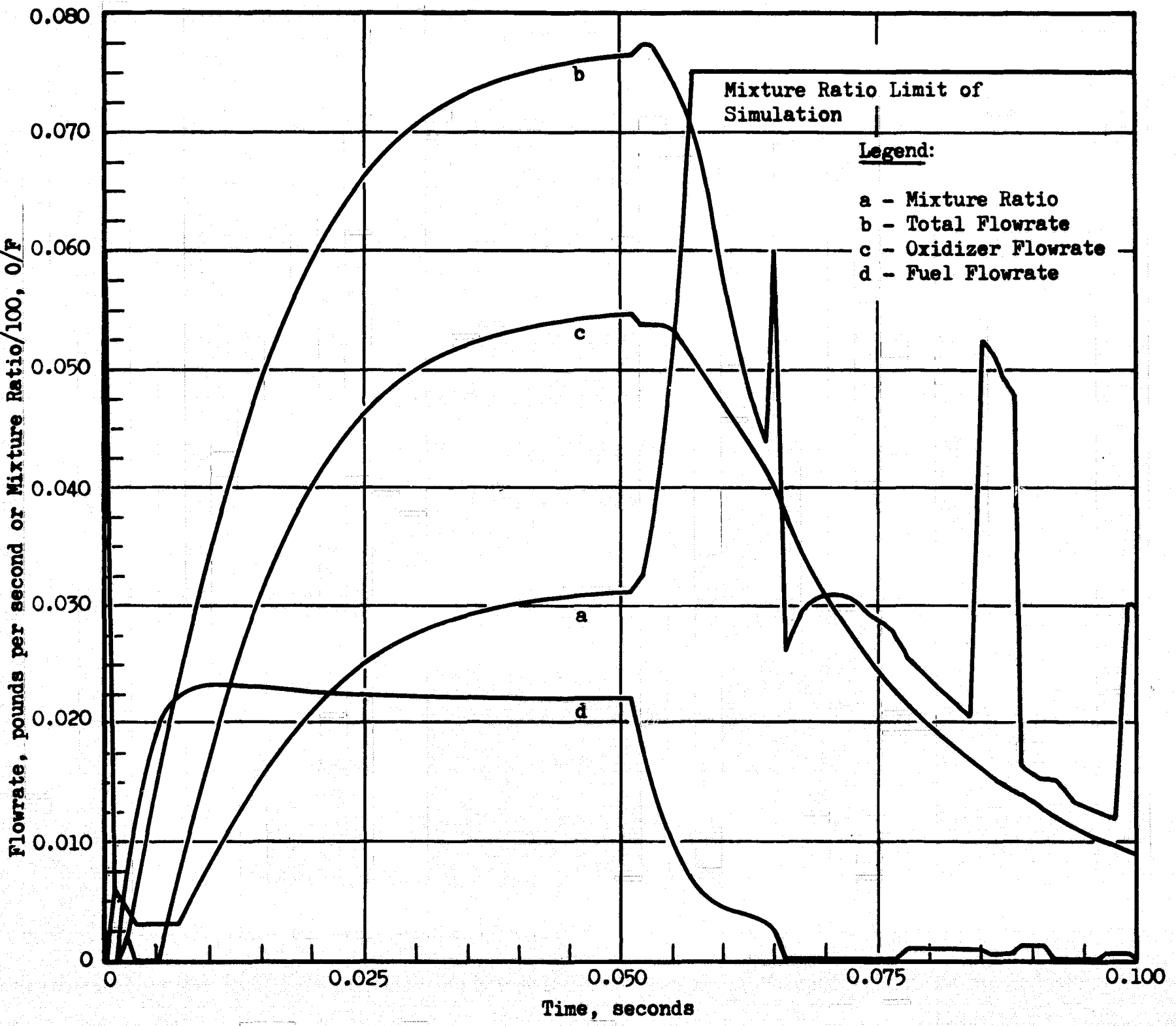

Figure 59. Predicted Response of a Thrustor With an In-Line Catalyst Bed of 0.667-Inch Length, Flowrate and Mixture Ratio Response

temperature response time. Typical temperature responses for an in-line catalytic thrustor, both experimental and analytical, are shown in Fig. 60 Minimization of the temperature response time should be an important goal for future effort. Two physical processes must be considered in such a minimization; reaction efficiency during the transient should be at a maximum, and the ratio of the engine thermal mass to that of the combustion gases should be minimized. Experimental results obtained with the 1/16-inch MFSA catalyst indicate that both factors were affecting thermal response.

Since specific impulse is proportional to the square root of the combustion gas temperature (neglecting second-order effects of gas properties and condensation phenomena), a specific impulse response can be determined from the data of Fig. 60 . A steady-state delivered specific impulse efficiency of 92 percent is assumed. The time required to reach 90 percent of the steady impulse efficiency is seen to be ~2 seconds for cold chamber.

The thrust response is most directly related to that of pressure. Two extreme pressure response characteristics are possible. The propellant flowrates can be limited by the injection devices to a value near the steady-state flowrates. In this case, the pressure response will follow t the temperature response so that sonic flow relationships are followed at the thrustor throat:

$$\dot{w} = KP/\sqrt{T} \qquad (16)$$

where $\dot{w}$, the propellant flowrate, remains constant. The pressure, or thrust, will then follow the specific impulse, or $\sqrt{T}$, during the transient startup.

A faster response is obtained with a lower injector pressure drop and the thrustor throat acts as the flow limiting device. In this case, the pressure in the thrustor will approach the steady-state value. This is

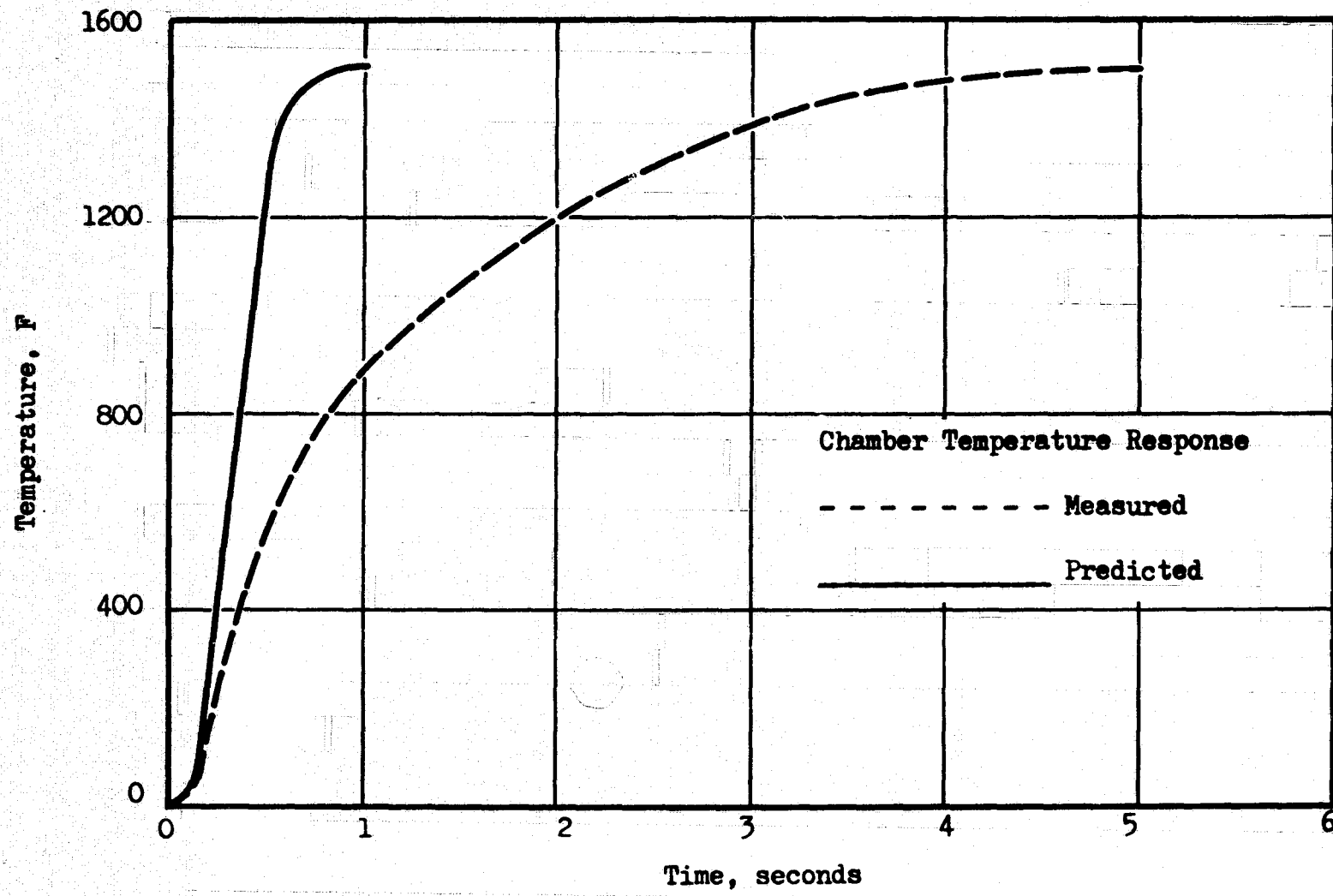

Figure 60. Comparison of Predicted and Measured Chamber Temperature Response for an In-Line Thrustor With a 1/2-Inch Catalyst Bed (Cold Start)

achieved by high initial flowrate. The flowrate will then decrease as the combustion gas temperature increases:

$$\dot{w} = K/\sqrt{T} \tag{17}$$

The pressure response in this case is governed by pneumatic filling considerations. Experimentally, response times on the order of 40 milliseconds have been obtained with an in-line bed configuration. By minimizing free volumes between the propellant valves and the thrustor throat, these times can be further reduced.

The parameters which directly affect the pressure response characteristics also determine other thrustor operating characteristics. For example, some degree of flow control is required upstream of the throat to maintain ratio control. However, such orifice devices also limit total flowrate during the startup period and tend to lengthen the response time. Also, a combustion volume is required to obtain combustion of the downstream oxygen. This volume increases the pneumatic fill time and, thus, increases the pressure response time. As the above indicates, a detailed tradeoff must be made and tested experimentally before a minimum response-time thrustor configuration can be defined.

Proposed Design Criteria

The transient results show the requirement for a correct flow system if optimum response is to be obtained. Such a system would be of the static type (without bleeds and sonic or flow-limiting orifices) which allows for varying flowrates to the thrustor, but maintains a constant pressure head at the injector. This system is comparable to the overall RCS system design utilized in this program.

Four thrustor design factors are discussed below for consideration in future efforts for maximizing thrustor response. First, the preinjector volumes should be minimized and matched in the ratio of the volumetric filling rates, so that simultaneous valve operation gives a constant nominal mixture ratio during the transient operation. Likewise, all volumes should be sized for an absolute viable minimum to maximize the startup and bleed-down response. These steps will maximize the pressure, or thrust, response. Second, it is readily seen from a simplified equation:

$$\text{rate of change in temperature of catalyst bed} = \frac{\text{(rate of heat input to catalyst)}}{\text{(thermal mass of catalyst)}}$$

$$\frac{dT}{d\theta} = \frac{(\dot{m}\,\Delta H)_{gas}}{(M\,C_p)_{catalyst}} \qquad (18)$$

describing the thermal response of a catalyst bed when complete combustion to a temperature, T_o, occurs at the front phase of the bed, that the response $dT/d\theta$ can be increased by increasing the factors in the numerator or by decreasing the factors in the denominator, e.g., the thermal mass of the catalyst might be reduced by using a gauze or spaghetti type (hollow) of catalyst. Raising the initial combustion temperature also will increase $dT/d\theta$. Since T_o is a function of mixture ratio, the method would vary the mixture ratio during startup. A very simple method is shown below:

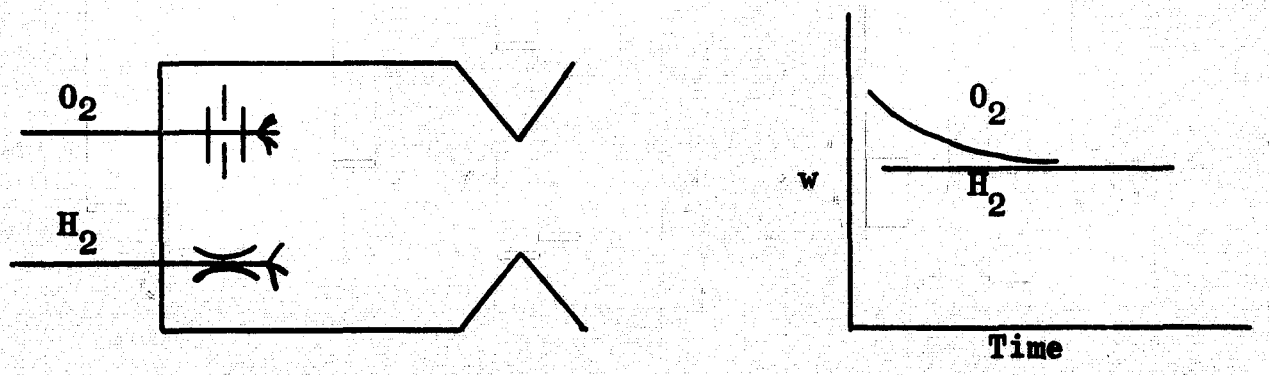

where the H_2 is fed to the mix section through a sonic venturi, thus making its flowrate independent of downstream pressure, and the oxygen is fed through an orifice. For cold-bed startup, the oxygen flowrate is initially above nominal and then decays. During hot-bed pulsing, the pressure response is on the order of several milliseconds and, thus, the transient MR should remain near nominal. By making the throat of the H_2 venturi the "valve seat", the size of the valve could be reduced from a subsonic diameter of 1-inch size to near 0.3 inch, thus reducing the mechanical opening times.

The weight of the catalyst bed screens and retainer plates, and DSI spokes downstream of the catalyst bed must be minimized. This is special consideration for larger thrust engines up to 100 pounds thrust. Heavy retaining plates weighing approximately 100 grams were used in the present program to support the catalyst bed to prevent bed settling and subsequent bed channeling. Since the weight of these plates was nearly twice the weight of the catalyst, the chamber responses were about twice the best catalyst response. Obviously, a change in thrustor design is necessary to eliminate this mass of metal if optimum response is to be realized. A previously suggested flow scheme might be reconsidered, e.g.:

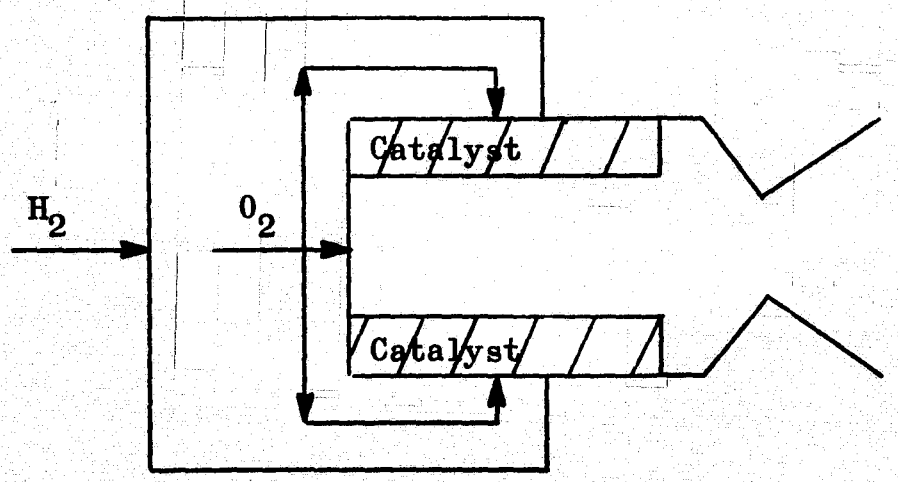

Advantages of this design would be (1) no DSI spokes are needed, (2) the flow area (and, hence, pressure drop and residence time) available to feed the catalyst can be increased markedly without increasing the thrustor ID, (3) the walls of the thrustor would be film cooled, thus improving vehicle packing, and (4) most of the thrustor length would be utilized for combustion, thus shortening the thrustor by perhaps 4 to 6 inches and minimizing the shutdown tails. Disadvantages would be (1) complexity of radial injection, and (2) possibility of local MR variation which could melt the catalyst and/or cause low performance.

Finally, the use of an in-line configuration should be considered for high-response applications. The minimum fill volume characteristic of such a configuration would lead to the most rapid pressure and thrust response.

PROPELLANT CONDITIONER EXPERIMENTAL EVALUATIONS

Propellant conditioning was determined to be necessary by Phase I analysis to guarantee a sufficiently high hydrogen temperature to ensure reliable catalytic ignition and to determine temperature and pressure bands for reliable flowrate control. The conditioner subsystem has the function of accepting the propellants from the tankage and delivering propellants to the thrustor within given temperature and pressure bands. This function, in general, involves the transfer of energy to the propellant and the control of pressure.

Several energy transfer concepts were evaluated during the initial portions of this program. Two primary requirements were established as a result of the general system operating goals: (1) a high power level (as indicated in Fig. 61) for steady-state operation, and (2) a capability to supply propellant to the thrustor on a rapid-response basis. It was determined that the use of hydrogen-oxygen reaction energy was the most promising as an energy source.

Two transfer methods were evaluated in more detail: (1) the use of a heat exchanger to transfer the energy between a hot generator gas and the propellant, and (2) direct mixing of the reacted gas with the propellant. The former method was selected for further evaluation because of its minimum weight and volume and a minimum of technical uncertainties. To provide rapid-response operation for a long-duration mission, the heat exchanger should be maintained at, or near, operating temperature and a surge volume (accumulator) should be included in the system. A schematic of the selected system is presented in Fig. 62 .

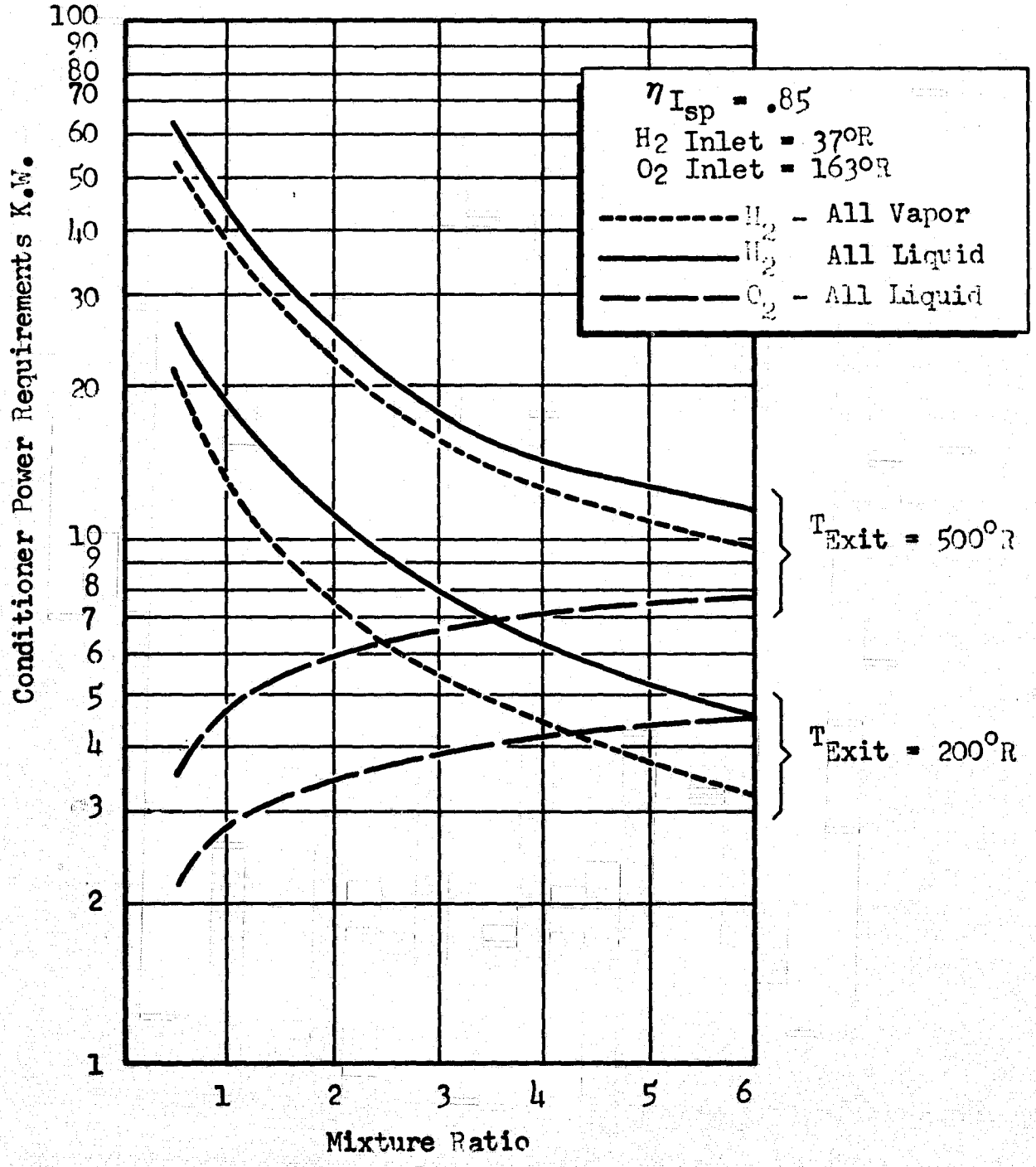

Figure 61. Conditioner Power Requirements for Steady Propellant Flow

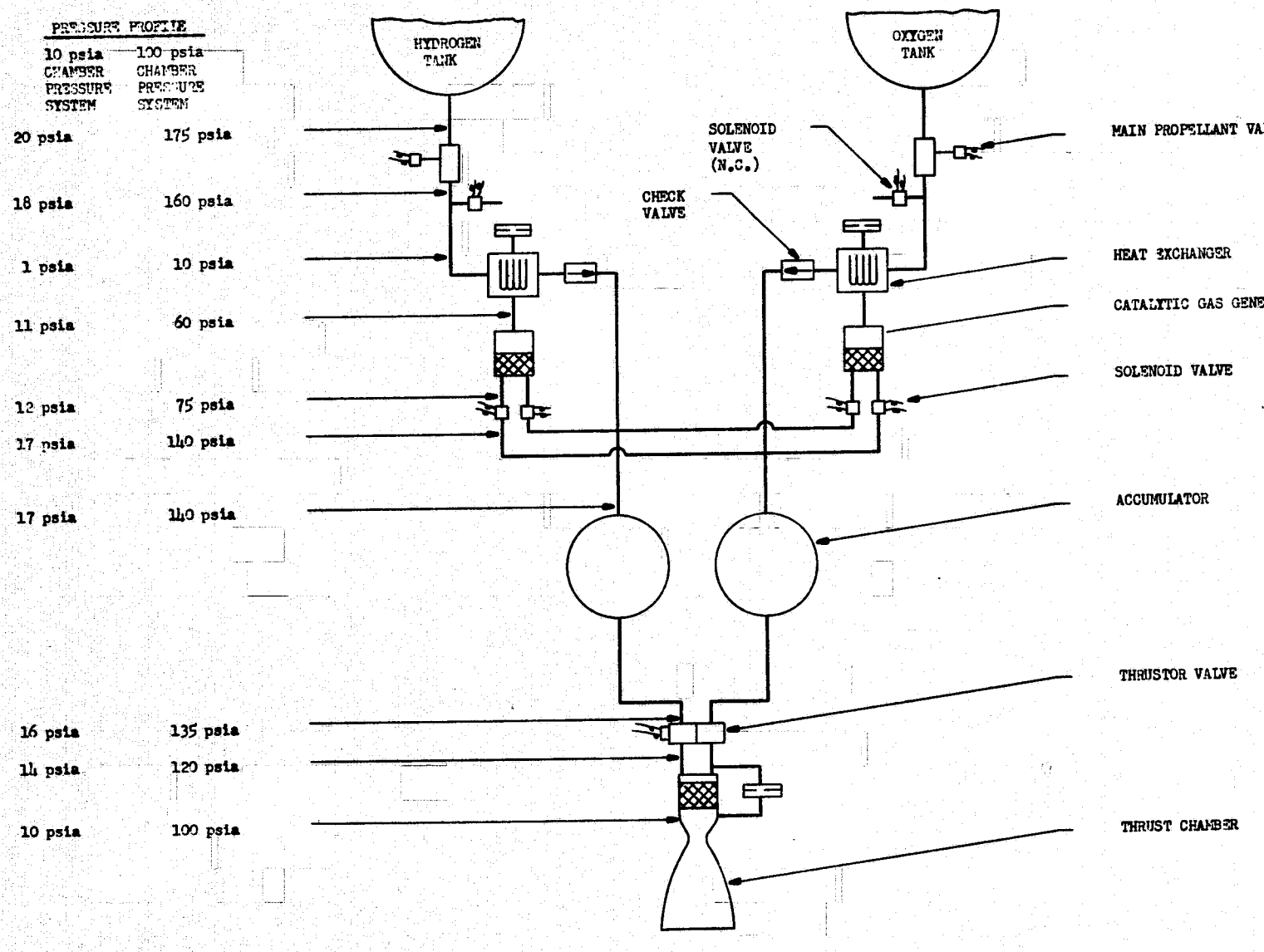

Figure 62. Schematic Representation of a Hot-Tube Heat Exchanger Propellant Conditioner Unit

During the thrustor experimental effort, it was determined that catalytic ignition with Engelhard MFSA catalyst would not occur at the 200 R and 10-psia nominal temperature and chamber pressure conditions. These difficulties are discussed in another section of this report. To accomplish the goals of the conditioner effort, the conditioned propellant temperature goal was raised to 410 R.

The principal goals of the propellant conditioner experimental program were to define problem areas and demonstrate the feasibility of an integrated conditioner-thrustor system. Therefore, when problem areas were encountered, feasible, but not necessarily optimum, solutions were adopted in the interests of accomplishing the feasibility demonstration goal.

The conditioning system has parallel hydrogen and oxygen sides, each having the following principal components:

1. A hot-tube heat exchanger to supply energy to the incoming fluid
2. An accumulator to store the conditioned gas and damp the pressure and temperature fluctuations of the conditioned fluid from the heat exchanger
3. A catalytic gas generator that taps off from the accumulators and provdes the heating fluid for the heat exchanger
4. A closed-loop feedback control system for both temperature and pressure in the accumulator to meet the thrustor feed requirements

During the experimental program, each component was tested separately and then integrated into the final conditioner system.

The conditioner design and experimental tasks are discussed in the following section:

1. Experimental Apparatus and Procedure
2. Discussion of Component Experimental Results
3. Discussion of Conditioner Subsystem Results

EXPERIMENTAL APPARATUS AND PROCEDURE

CONDITIONER COMPONENT DESIGN

Prior to initiation of the experimental effort, it was necessary to evaluate several conditioner concepts. The basic operating requirements for each component were as defined by the material and energy balances observed in Volume I of this report. The Volume I considerations included the effect of operating requirements on system performance. The overall conditioner design effort discussed below included the design of the individual components and an investigation of three control concepts.

Gas Generator Designs

The actual sizing of the gas generators depends upon optimization with respect to the following factors:

1. Mixing volume velocities sufficiently high to prevent flashback
2. Catalyst bed length sufficiently long for ignition. Information feedback from the thrustor studies was used to optimize the internal gas generator design, although it was recognized that optimum performance was not as important as reliability.
3. Low catalyst bed pressure drop consistent with total pressure head
4. Efficient reaction by satisfying the relationship $(D_{reactor} - D_{pellets}) \geq 8$ to prevent gas channeling to the outside of the reactor. It was concluded that the installation of deflection rings would be a practical solution to this problem. Overloading the reactor will cause the reaction to be pushed out of the bed and result in incomplete combustion.

5. The maximum steady-state flowrates to the individual gas generators as shown in Table 10. Later experimental pulse-mode testing has shown that the gas generators should be oversized from steady-state conditions by approximately 50 percent and operated in a pulsed mode to eliminate ice formation.

6. Past experience (Ref. 3) has also shown the 4-on-1 injector to be superior for mixing. The thruster perturbation studies indicated that a maximum injector face pressure drop was the most desirable for minimizing catalyst bed temperature fluctuation.

7. Setting the preinjector volume ratio at the ratio of the filling rates (16:1 for a mixture ratio of 1.0), to eliminate the possibility of transient mixture ratio variations. It was not difficult to satisfy this volume ratio restriction because the injector designs minimize the oxygen volume and maximize the hydrogen volume.

8. Sizing the throat areas for sonic flow, thus minimizing the effect of downstream perturbations on gas generator behavior.

Using these criteria, two gas generators (Fig. 63 and 64) were designed. The pertinent design parameters are presented in Table 10. The gas generator for the hydrogen conditioner subsystem (large gas generator) is also shown in Fig. 65 with several mix sections and catalyst bed capsules.

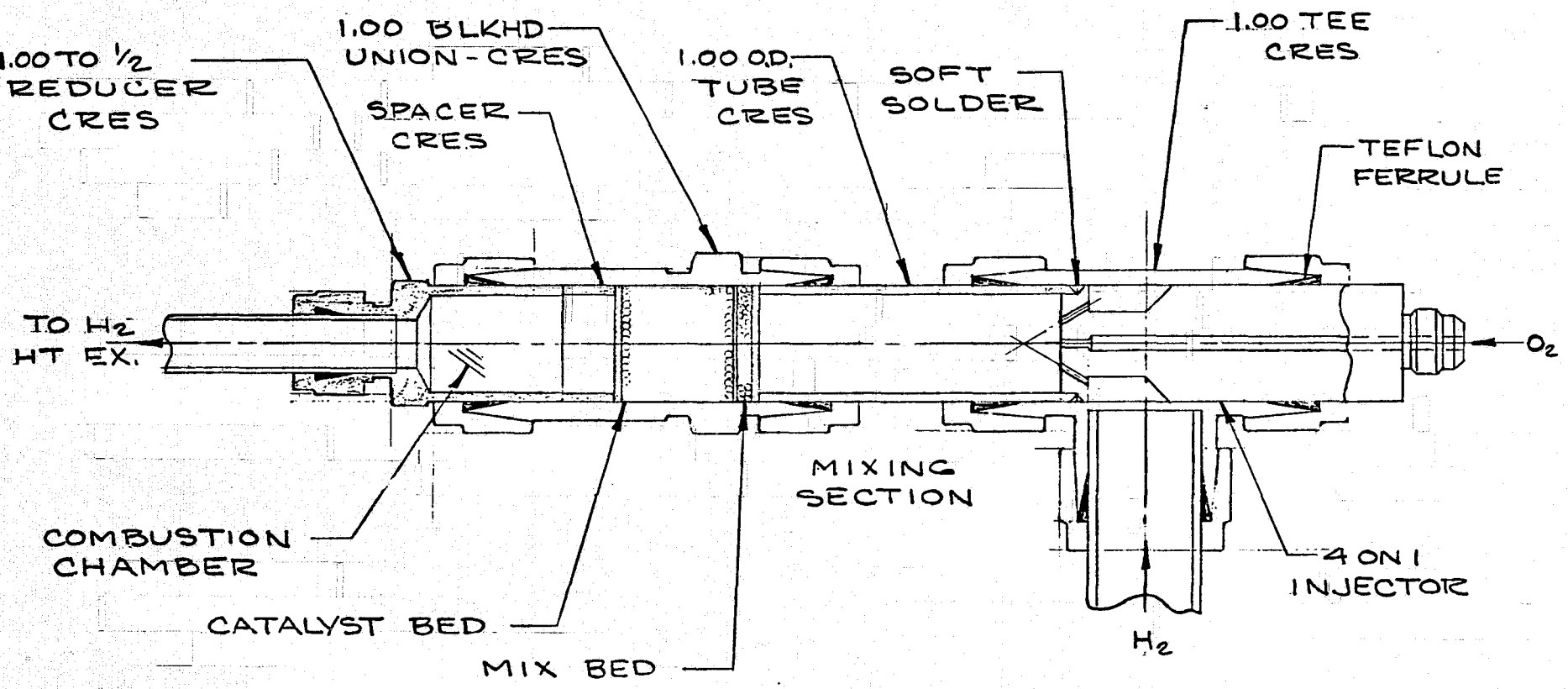

Figure 63. Full-Scale Schematic of the Hydrogen Heat Exchanger Gas Generator

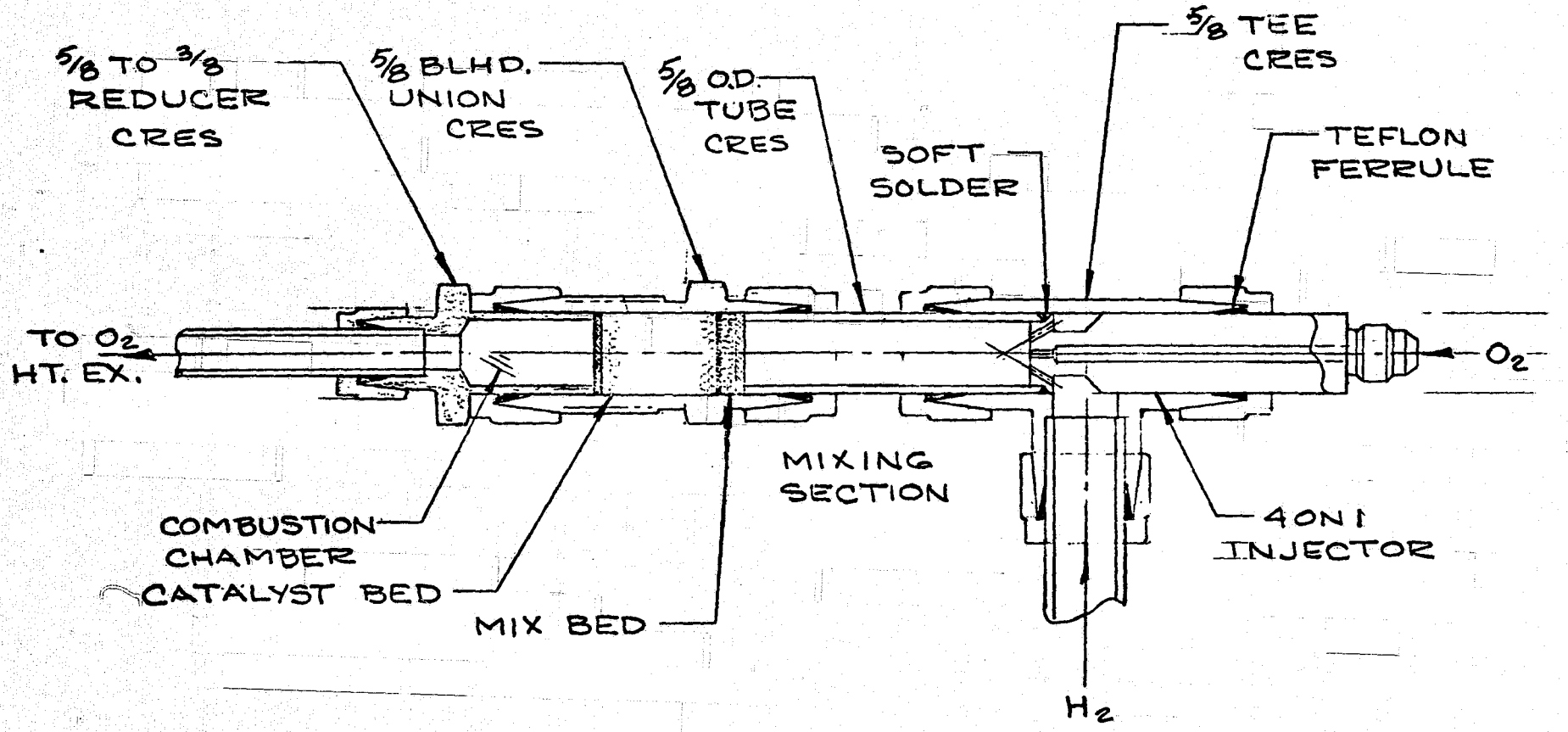

Figure 64. Full-Scale Schematic of the Oxygen Heat Exchanger Gas Generator

TABLE 10

GAS GENERATOR PARAMETERS

Parameter	Hydrogen Gas Generator	Oxygen Gas Generator
Diameter, inches	1.0	0.625
Weight Flowrate, lb/sec		
Oxygen	0.00229	0.0008
Hydrogen	0.00229	0.0008
Superficial Mass Velocity, lb/sec-sq in.	0.00584	0.00521
Velocity, ft/sec (Mixer)	36.8	33.0
Pressure Drop, psi		
Valve	0.5	0.5
Injector Face	2.5	2.5
Mixer Section	0.5*	0.5*
Catalyst Bed	3.5	3.5
Areas, sq in.**		
Injector Orifices		
Hydrogen	0.02494	0.00871
Oxygen	0.00626	0.00219
Throat (Mixture Ratio = 1.0)	0.10335	0.03611

*1/2 inch of 1/8-inch beads

**C_D A where C_D = 0.73

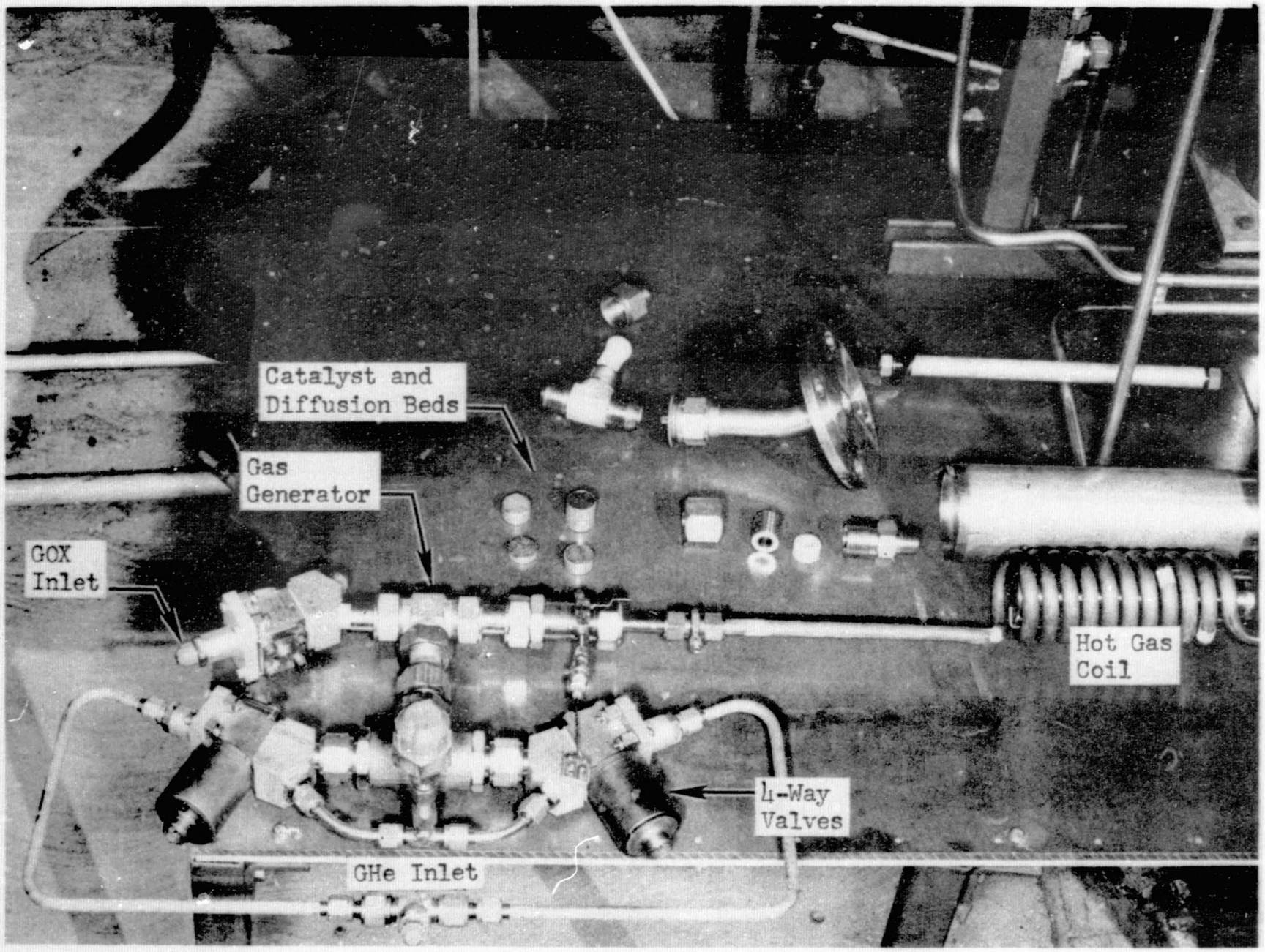

Figure 65. Gas Generator and Heat Exchanger Coil for the Hydrogen Conditioning Subsystem

Heat Exchanger Designs

From a concept comparison, it was determined that the hot tube exchanger was the most promising; (Ref. 1) thus, it was selected for a detailed design and experimental effort. Particular design goals were:

1. Low propellant pressure drop
2. Fast thermal response
3. Minimization of heat leak
4. Simplicity of construction

Several types of heat exchangers were evaluated to determine the type best suited for the conditioner application. The favored design consisted of a helical tube inserted into an annular shell with the hot gas flowing in the tube while the cryogenic propellant flowed through the shell. The experimental design which is constructed from as many standard items as possible, to facilitate quick assembly and modification, is illustrated in Fig. 66 .

A flight design using the same geometry is illustrated in Fig. 67 . The essential difference is that the gas generator is installed internally in the flight design while it is connected externally for the experimental design to facilitate expected modifications. Installation of the gas generator inside the heat exchanger ensures a minimum heat leak to the surrounding environment during the coast mode phase, and it also utilizes the void center volume of the experimental heat exchanger. This design was not experimentally evaluated however.

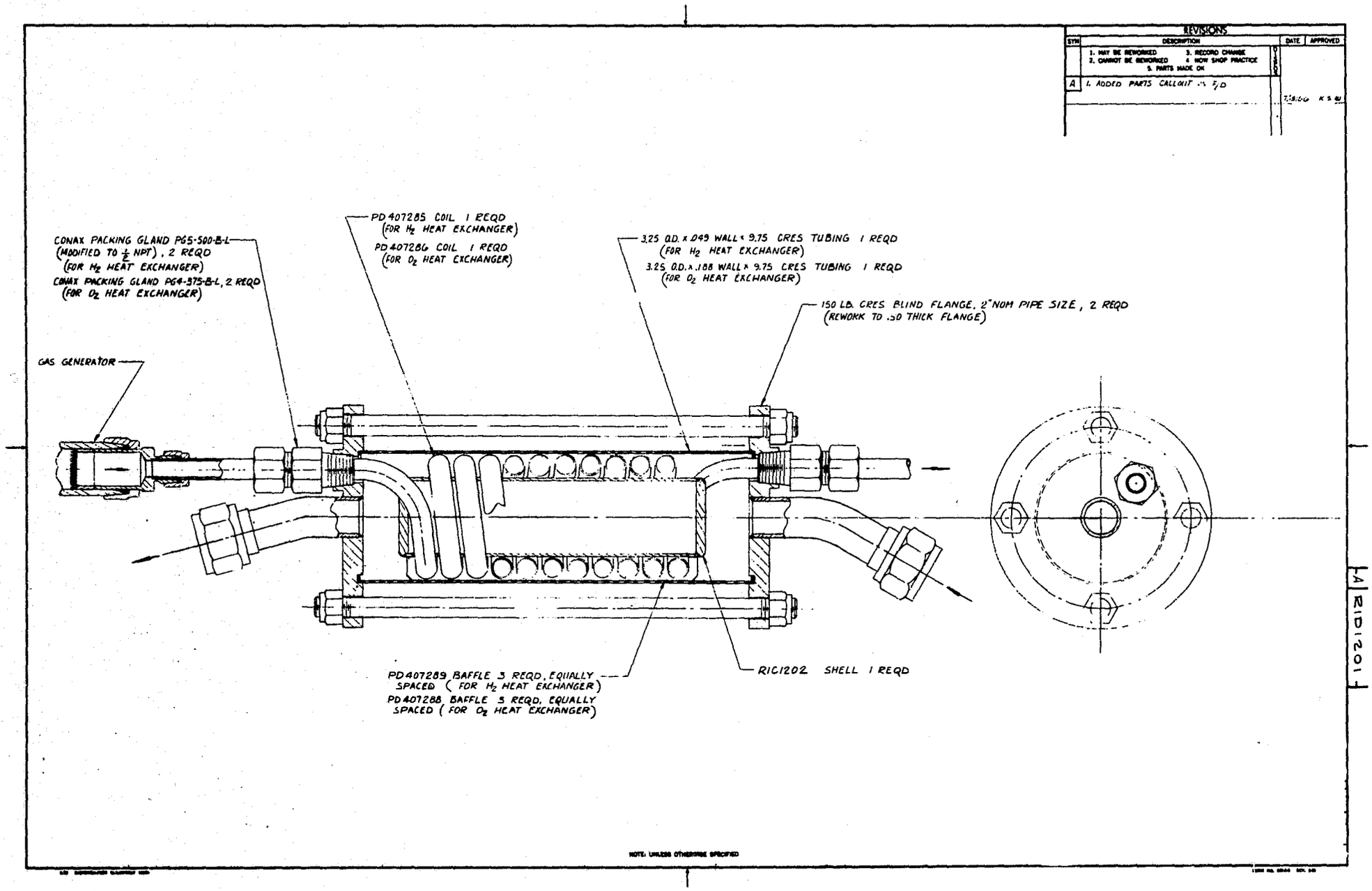

Figure 66. Assembly Schematic for the Hydrogen and Oxygen Heat Exchangers

FOLDOUT FRAME 1

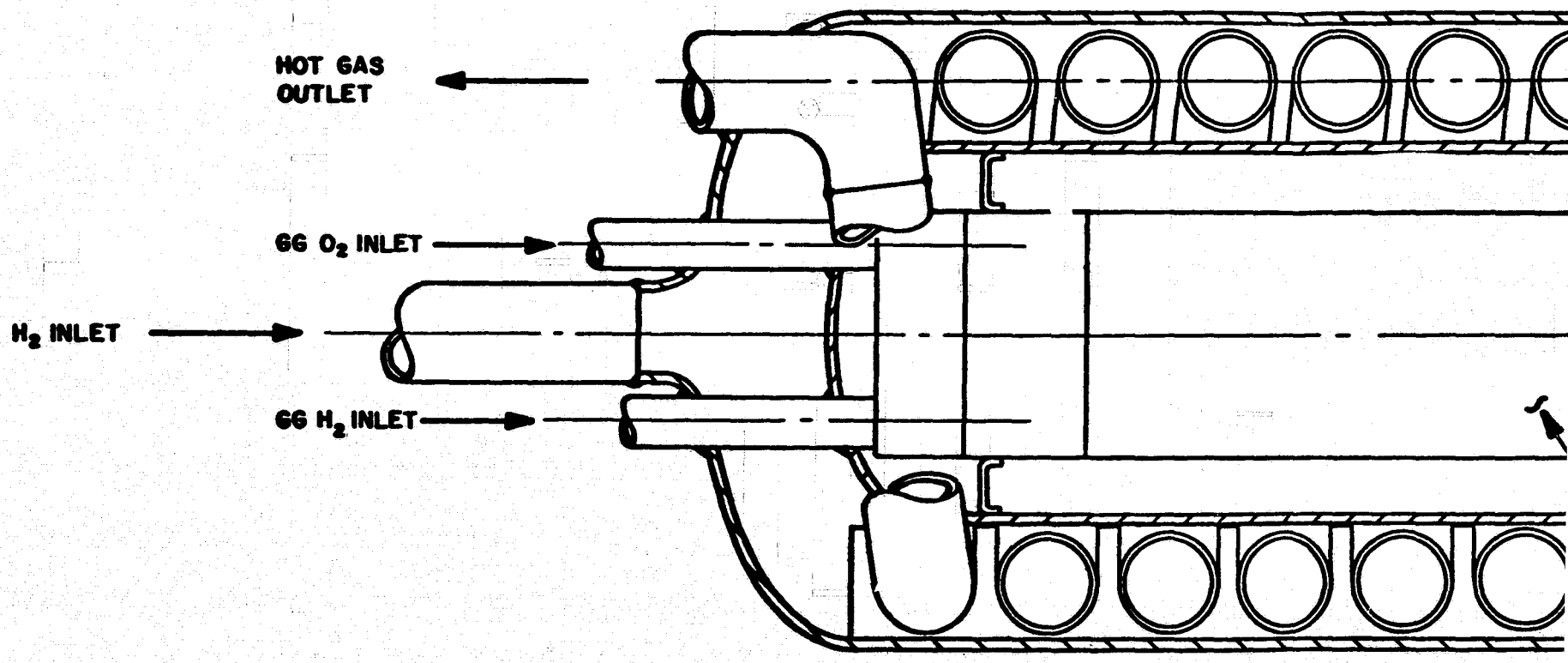

BASIC SPIRAL TUBE DESIGN

FOLDOUT FRAME 2

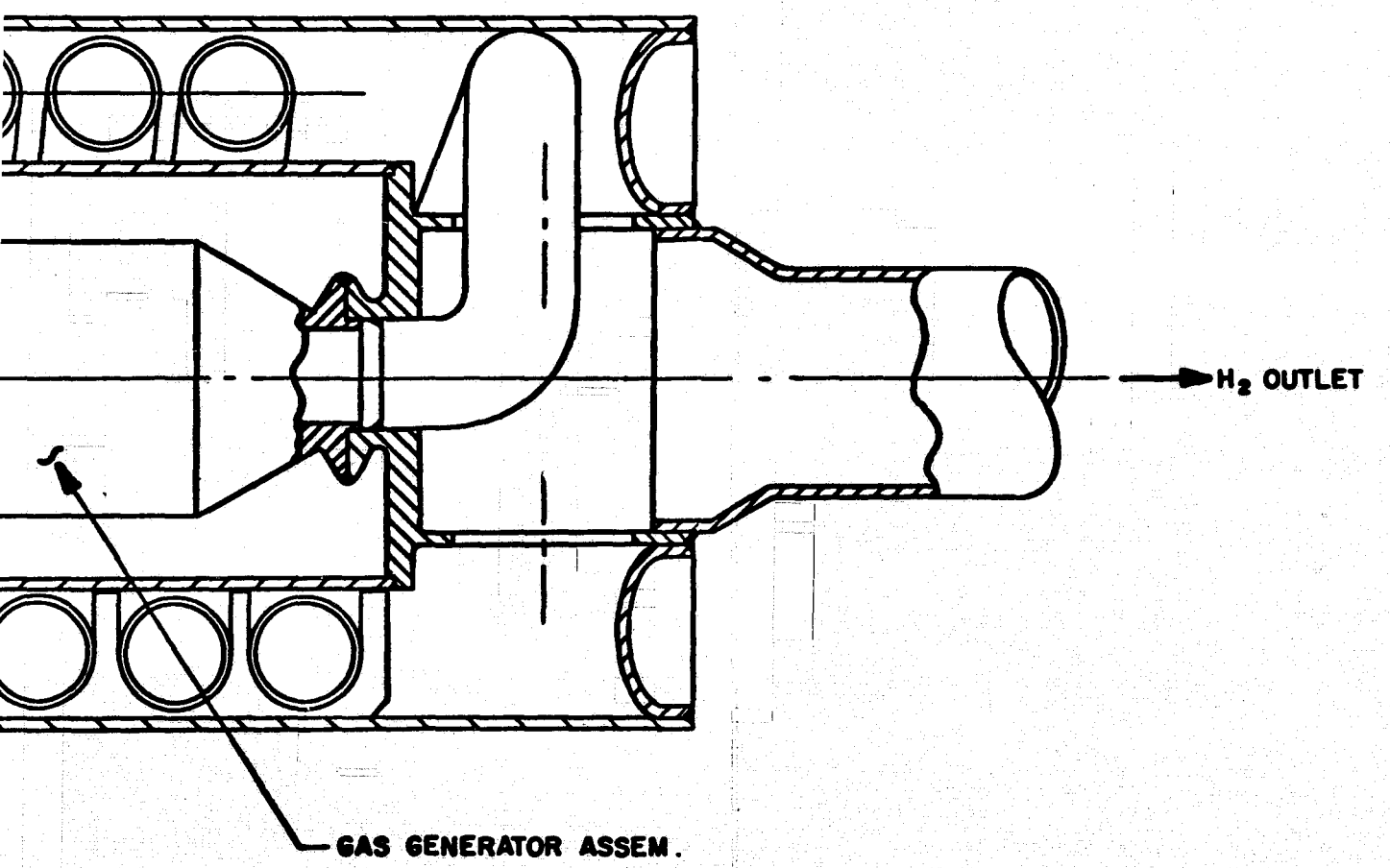

SIGN

Figure 67. Conceptual Flight Design of the Gas Generator and Heat Exchanger for the Hydrogen Conditioner

Hydrogen Heat Exchanger Design. The theoretically calculated values of heat transfer coefficient and pressure drops for six alternate cases are summarized in Tables 11 and 12. The resulting heat transfer calculations for the 2500 R combustion gas indicated that 70 inches of tubing were required to condition the hydrogen to 410 R.

The original experimental hydrogen heat exchanger employed a 0.5-inch OD spiral tube carrying the 2500 R hydrogen-oxygen combustion products (mixture ratio of 1.33) from the catalytically operated gas generator (Case I in Tables 11 through 12). Because of the uncertainty in estimating the experimental heat transfer coefficients, which were expected to be on the order of 20 percent, the tube length was increased by 25 percent to 87.5 inches. Case II gives the final nominal design condition for a single-stage 2000 R combustor-heat exchanger.

The increase in heat transfer area required for the final nominal case of 2000 R feed gas was slightly less than the 25 percent overdesign so that original design was not changed.

The hot-gas tube was fabricated of Type 321 stainless steel and was inserted in an annulus through which the propellant was fed. The annulus had dimensions of: 2.0-inch ID, 3.25-inch OD, and approximately 7-inch length (excluding manifolds). The annulus was also fabricated of 321 series stainless steel. The disassembled hydrogen heat exchanger is illustrated in Fig. 68.

Calculated steady-state temperature profiles through the heat exchanger are presented in Fig. 69. The tube wall temperature was calculated from:

$$h_g(T_g - T_w) = h_l(T_w - T_g) \qquad (19)$$

TABLE 11

DETAILS FOR STEADY-STATE OPERATION OF PROPOSED DESIGN OF OXYGEN HEAT EXCHANGER

Hot Side

Case No.*	Propellant Flowrate $\dot{w}_o$, lb/sec	Propellant Flowrate $\dot{w}_f$, lb/sec	MR	T_c, R	T_{outlet} R	ID, inch	ΔP psi	h_g, Btu/hr-ft^2-F	Area in.^{2}	L, inches
I	0.000778	0.000585	1.33	2500	672	0.335	8.0	59.2	124	105
II	0.00080	0.00080	1.00	2000	672	0.354	8.0	59.2	144	122.2
III	0.0000596	0.0000596	1.00	2000	672	—	—	—	—	—
IV	0.00132	0.00156	0.85	2000	672	—	—	—	145.44	—
V	0.00055	0.00066	0.85	2000	672	—	—	—	61.8 (6.35 coils)	—
VI	0.00049	0.00056	0.88	2000	672	—	—	—	43.3 (5.5 coils)	—

Cold Side

Case No.*	$\dot{w}_o$, lb/sec	T_i, R	T_o, R	q, Btu/second	ΔP psi	h_ℓ, Btu/hr-ft^2-F	h_g, Btu/hr-ft^2-F	U_ℓ	U_g
I	0.03852	163	200	3.85	1.0	18.1	72.7	13.1	32.6
II	0.03879	163	200	3.86	1.0	18.1	72.7	13.9	32.6
III	0.03722	163	500	0.2905	—	—	—	—	—
IV	0.04518	163	500	7.48	—	—	—	25.0	—
V	0.01918	163	500	3.17	—	—	—	25.0	—
VI	0.01901	163	400	2.73	—	—	—	25.0	—

$\dot{w}_o$ = oxidizer weight flowrate
$\dot{w}_f$ = fuel weight flowrate
MR = mixture ratio
T_c = combustion temperature
T_{outlet} = temperature at heat exchanger outlet
ID = inside diameter
ΔP = differential pressure
h_g = heat transfer coefficient (gas)
h_ℓ = heat transfer coefficient (liquid)
L = length
T_i = inlet oxidizer temperature
T_o = heat exchanger outlet oxidizer temperature
q = heat exchanger heat load
U_ℓ = overall heat transfer coefficient (liquid)
U_g = overall heat transfer coefficient (gas)

* Refer to Table 11 for definition of cases

TABLE 12

PROPOSED STEADY-STATE DESIGN OF FLIGHTWEIGHT HYDROGEN HEAT EXCHANGER

Hot Side

Case No.*	Propellant Flowrate $\dot{w}_o$, lb/sec	Propellant Flowrate $\dot{w}_f$, lb/sec	MR	T_c, R	T_{outlet}, R	ID, inch	ΔP, psi	h_g, Btu/hr-ft^2-F	Area	L, inches
I	0.002044	0.001536	1.33	2500	672	0.46	8.0	71.4	110.0 sq in.	70.0
II	0.00229	0.00229	1.0	2000	672	0.50	8.0	71.4	136.0 sq in.	86.6
III	0.00146	0.00146	1.0	2000	672	-	-	-	-	-
IV	0.00816	0.00961	0.85	2000	672	-	-	-	2.25 sq ft	-
V	0.00351	0.00424	0.85	2000	672	-	-	-	0.989 sq ft	-
VI	0.00264	0.00301	0.88	2000	672	-	-	-	0.71 (7.5 coils)	-

Cold Side

Case No.*	$\dot{w}_f$, lb/sec	T_i, R	T_o, R	q, Btu/seconds	ΔP, psi	h_ℓ, Btu/hr-ft^2-F	h_g, Btu/hr-ft^2-F	U_ℓ	U_g
I	0.01642	37	200	10.13	1	39.2	275	25.4	56.7
II	0.01739	37	200	11.2	1	39.2	275	25.4	56.7
III	0.01582	37	200	7.12	-	-	-	-	-
IV	0.02517	37	500	46.1	-	-	-	70.0 Overall Assumed	-
V	0.01119	37	500	20.3	-	-	-	70.0 Overall Assumed	-
VI	0.00992	37	400	14.55	-	-	-	70.0 Overall Assumed	-

* See Table 11

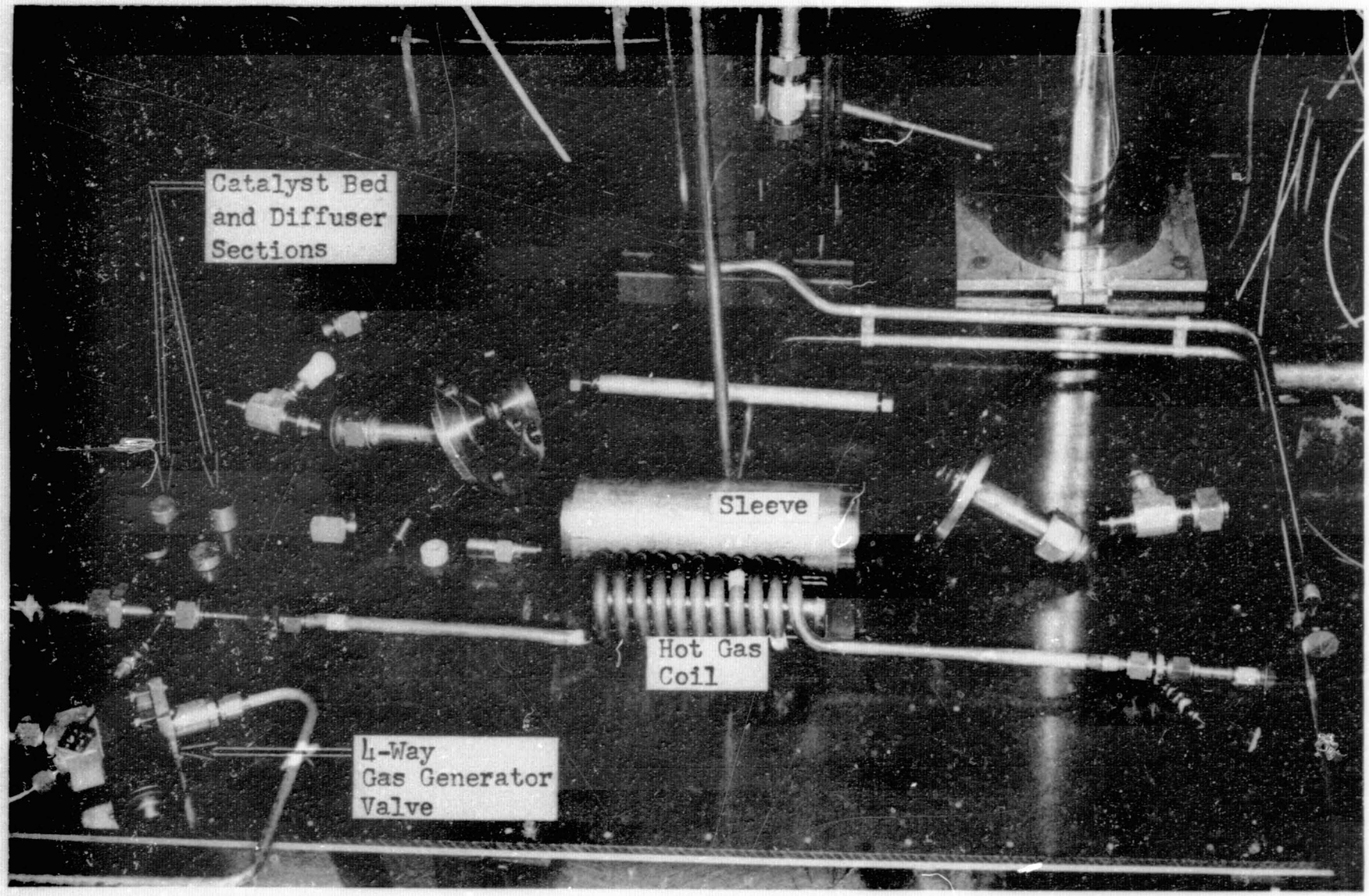

Figure 68. The Disassembled Heat Exchanger and Gas Generator for the Hydrogen Conditioning Subsystem

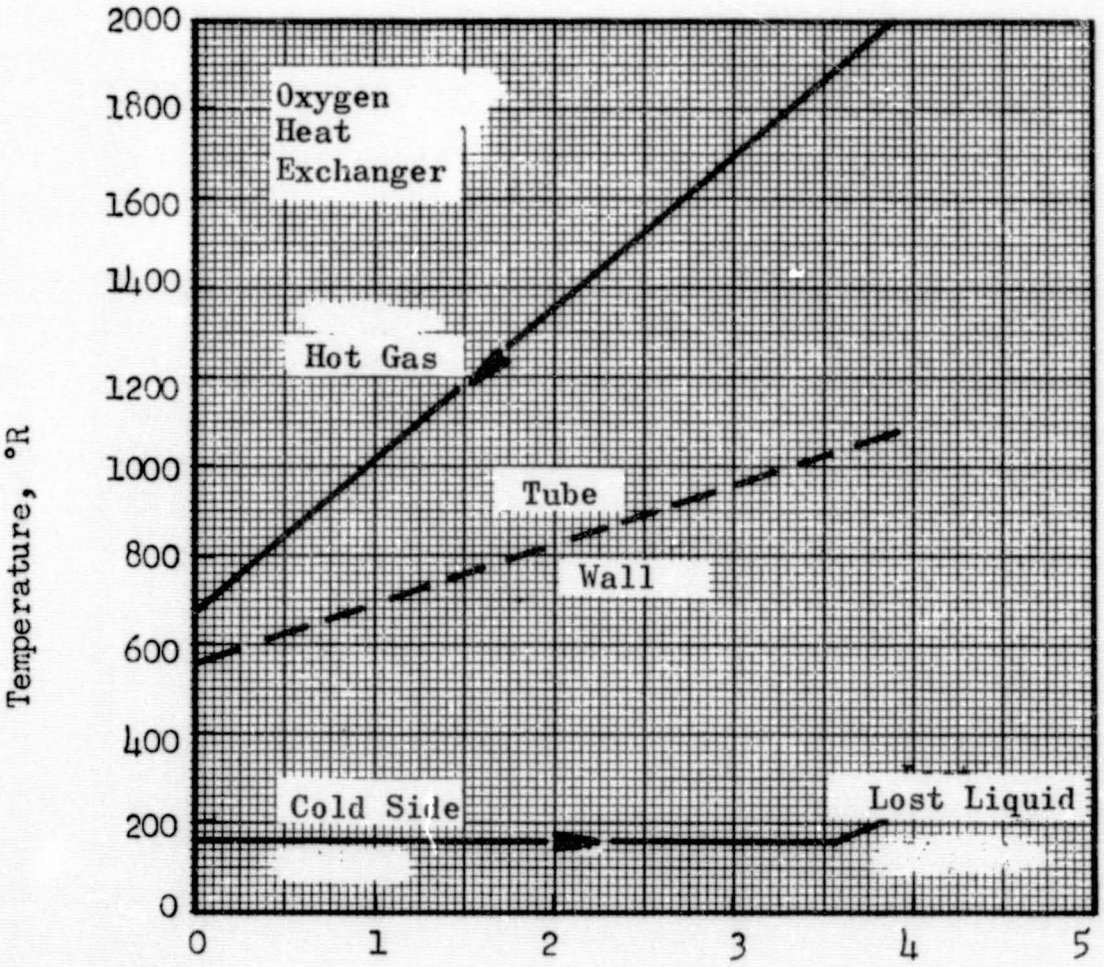

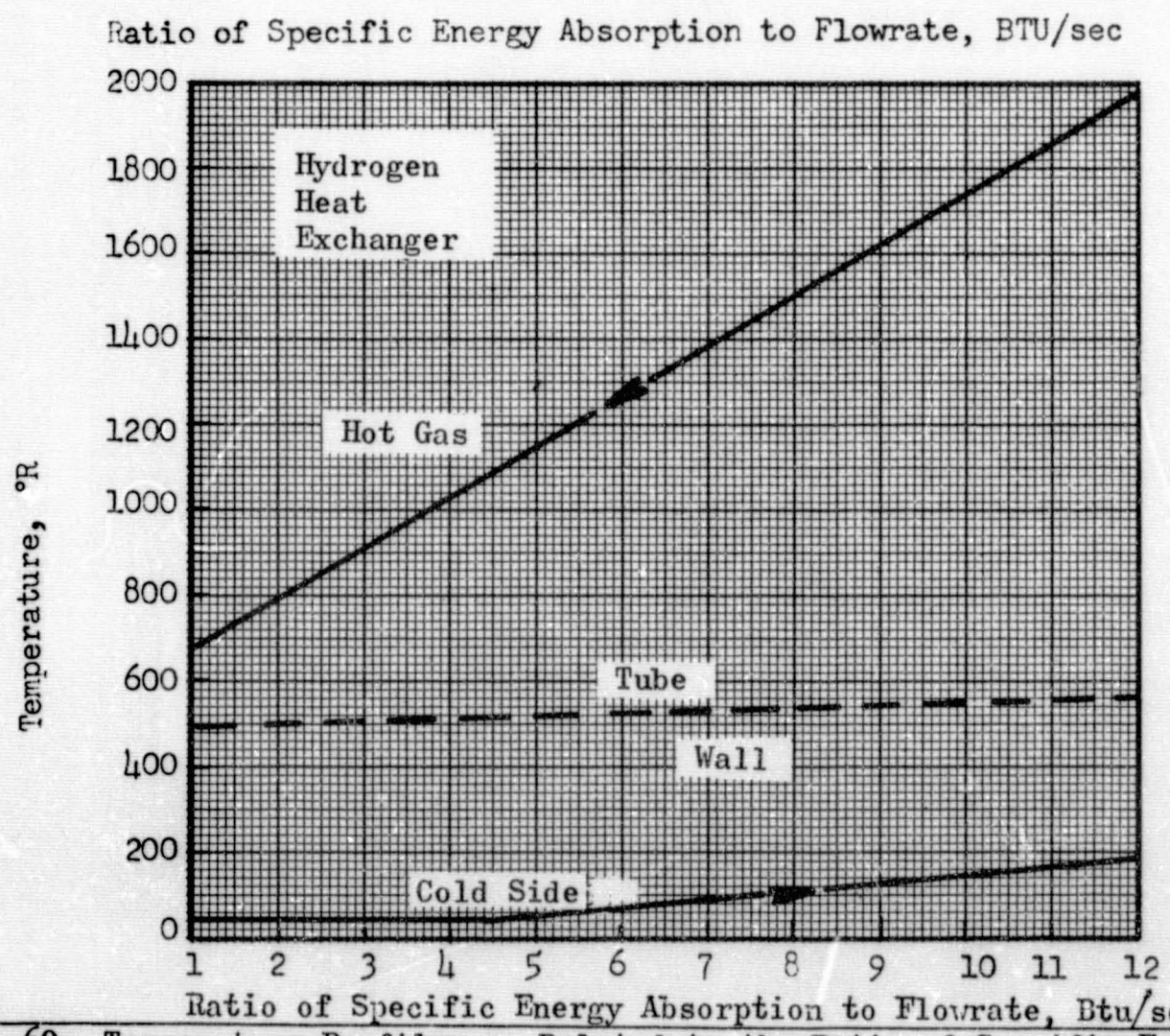

Figure 69. Temperature Profiles as Related to the Ratio of Specific Energy Absorption to Propellant Flowrate-(Cumulative Heat Absorption Rate--for the Hydrogen and Oxygen Heat Exchangers)

A study of the available literature was made to determine the probability of flow instability in the conditioner heat exchangers caused by boiling and two-phase flow. Although relatively little was known regarding the onset of exchanger instability, the use of an upstream orifice was expected to alleviate this undesirable condition. The magnitude of the orifice pressure drop was not known precisely, but several preliminary correlations were obtained. The relatively large pressure drop across the upstream main propellant valve was greater than the total propellant heat exchanger acceleration loss which ensured stable flow.

Oxygen Heat Exchanger Design. A literature search revealed little data for heat transfer correlations with boiling oxygen. Therefore, the equations used for boiling hydrogen were adopted to the oxygen flow conditions to estimate the necessary film coefficients. Consequently, the hot-gas film coefficient was calculated for a 3/8-inch tube using Eq. 19. A heat transfer tube length was calculated and increased by 25 percent to ensure adequate heat transfer area. This was also sufficient heat transfer area for Case II where the inlet hot-gas temperature was reduced to 2000 R.

The LOX tube wall temperature was calculated as explained previously. Figure 69 shows that there is considerable difference between the oxygen and hydrogen heat exchangers. First, the hydrogen tube wall temperature was considerably lower than for oxygen because of the much higher heat transfer coefficient for the hydrogen. Secondly, more than 90 percent of the oxygen heat exchanger area was required for the vaporization of oxygen, whereas only 30 percent was required for the hydrogen heat exchanger.

The experimental exchanger design is shown in Fig. 66 , and utilizes as much of the hydrogen exchanger designs as possible in an effort to minimize manufacturing costs. The heat transfer area can be varied in the same manner as in the hydrogen exchanger by shortening the hot-gas tube. Pressure drop calculations based on this configuration are compatible with the propellant conditioner pressure profile.

Accumulator Design

The accumulator is used to decouple the thrustor from the conditioner system. To accomplish this, the accumulator must be of sufficient size to alleviate pressure perturbations caused by valve delays (for an on-off pressure control system) and by flow instabilities in the heat exchanger. The former is quite amenable to analysis and was used as the sizing criterion. The latter type of pressure perturbation, and an accompanying temperature perturbation, was not amenable to an a priori solution. There was considerable uncertainty as to the approach in mathematically modeling the heat exchanger under dynamic, and possibly surging, operation. However, subsequent testing showed the combination of accumulator size and control system design controlled perturbations caused by the heat exchanger flow instability.

The accumulator volume sizing criteria developed in Volume I is presented in Fig. 70. The final size of the accumulator selected for experimental evaluation depends primarily on the weight flowrate and the response of the control circuit. Because the response of the propellant valves was rather slow, it was necessary to select relatively large accumulators

(700 cu in. for liquid oxygen and 4000 cu in. for hydrogen). Because a good portion of the system weight and volume was represented by the accumulator, an important part of this experiment was to minimize the accumulator size.

Control System Design

A control system is needed for the conditioner to guarantee that the propellants are fed to the thrustor at a predetermined thermodynamic state. The basic conditioning system can be schematically represented as three components: (1) a heat exchanger, (2) a hot-gas generator, and (3) an accumulator to store the conditioned fluid.

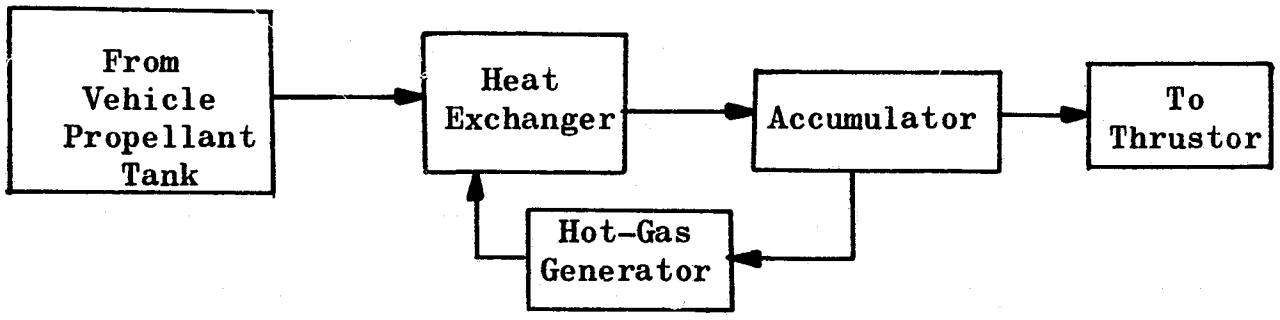

The orginial control scheme that was considered employed three separate control systems. The principal control loops were as follows:

1. Hot-tube temperature control in the heat exchanger. This loop controls both the hydrogen and oxygen flow to the gas generator during the coast modes of the vechicle. The tubes are kept hot to circumvent the relatively long time (~2 to 5 seconds) needed to obtain steady-state conditions. An automatic reset capability of the reference temperature is included to allow for

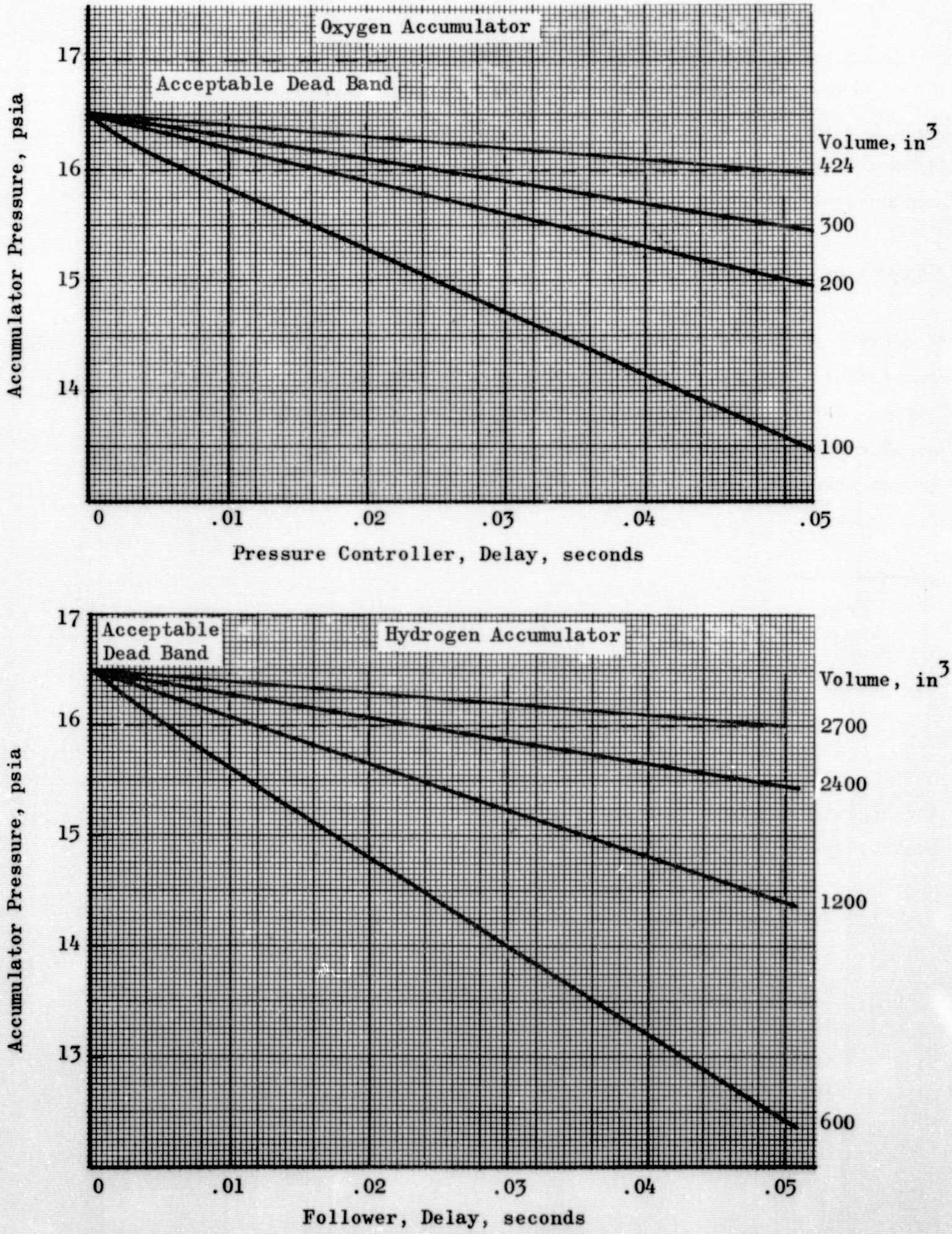

Figure 70. Accumulator Sizing Chart Based on Valve Response

variations in the inlet condition of the propellant as it flows from the main tanks. The reference point is determined prior to closing the main thrustor valve and is maintained through the coast period.

2. Accumulator temperature control. When the hot-tube temperature control is nullified (during thrustor operation), the accumulator temperature controls the flow of hydrogen and oxygen to the gas generator.

3. Accumulator pressure control. The accumulator pressure control causes the tank valve to open at a specified low pressure and close at the nominal accumulator pressure. If the accumulator pressure exceeds the nominal value, the backup pressure relief valve opens to relieve the overpressure.

The control system used during the experimental effort employed a combination of these variations. The tests were directed toward obtaining steady-state thrustor flow and a demonstration of pulse capability. These requirements eliminated the need for a hot-tube temperature control because no extended coast mode was necessary to achieve the program objectives. The accumulator temperature control was used to operate the gas generator. The circuit was arranged such that both the fuel and oxygen valves of the gas generator would operate simultaneously.

The pressure control concept was used for both the fuel and oxygen side with a slight modification to the initial design. Instead of providing a pressure relief valve to vent the overpressure in the accumulator, the

ullage tank valve was set to open when both the bleed and thrustor main valves were closed (no major demand placed on the system). This would allow the entire system to stabilize at the ullage tank pressure. The principal reason for deviations from the initial concept was that a suitable pressure relief valve could not be obtained as a stock item for the test phase.

The semiconductor pressure- and temperature-sensing elements are shown in Fig. 71. The temperature control switch was placed in the outlet tube of the accumulator. This was to increase the response of the switch, which was principally controlled by convective heat transfer to the sensing element mass. The placement of the pressure switch was not as critical because the pressure in the accumulator remained essentially uniform.

Alternative Control Schemes. A number of alternative control schemes were considered. These are discussed in detail in Volume I of this report. A bellows arrangement to obtain equalized pressures between the oxygen and hydrogen accumulators was among the alternatives considered. Consideration of the bellows led to the conclusion that cycle life failure would be the principal problem, although one manufacturer, Belfab Corporation, reported a 30,000-cycle life. This is greater than would be expected from past experience. Further, an excessive lead-time requirement precluded the use of a custom-built bellows for the reported program.

Another promising concept is the use of a follower valve in one side of the accumulator. Such a device would slave the regulated pressure to that existing in the other accumulator and, thus, control the key parameter, that of the difference in accumulator pressures. The result

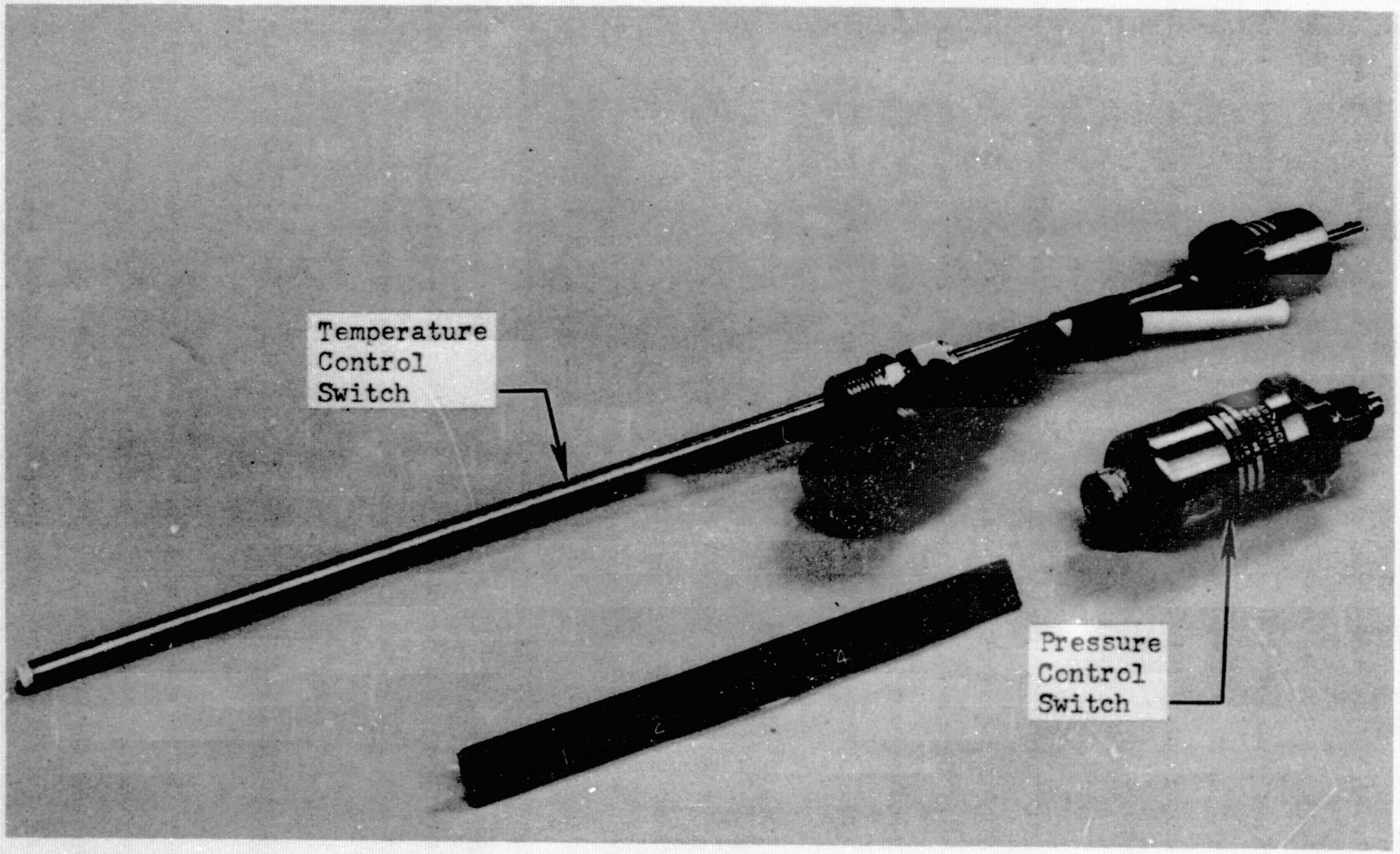

Figure 71. The Temperature and Pressure Semiconductor for Switch Devices(Used for Accumulator Pressure and Temperature Control)

of such a system is that the accumulator pressures may vary, but will vary closely in phase so that thrustor mixture ratio remains under control and the variation in accumulator driving pressure is then limited by the thrust level tolerance of ±10 percent. This latter requirement imposes a less stringent limit on accumulator pressure variation, thus allowing for smaller accumulator volumes and/or slower overall response of the pressure control loop.

The oxygen conditioner was selected for use with the follower valve because of the higher ratio of liquid or vapor density of oxygen as compared with hydrogen. It was believed that an additional benefit would be the metering of the liquid oxygen into the conditioner system. Testing of the component was planned; however, a leakage problem was incurred with the valve.

Control Components. The definition of specific control components was necessary following the selection of the basic conditioner concept. The chief requirements for these components, i.e., valves and regulators were: (1) low pressure operation with a small pressure loss, (2) rapid response (50 milliseconds or less), and (3) compatibility with liquid hydrogen and liquid oxygen environments. Approximately 20 vendors in addition to Rocketdyne in-house groups were contacted. The detailed results of these contacts are discussed in Appendix A. In summary, suitable off-the-shelf items were not available and modification of existing hardware was necessary.

Propellant Supply Systems

The propellants fed to the conditioner system were supplied by a 40-gallon liquid hydrogen dewar vessel and a 108-gallon liquid oxygen dewar vessel (Fig. 72). During the initial experiments, the liquid oxygen dewar vessel was half filled to allow the remaining ullage volume to act as a capacitance and attenuate decays in the driving pressure. Later, separate pressurizing systems that could be controlled during the experiments were installed on the dewar vessels. This eliminated the need for an ullage volume.

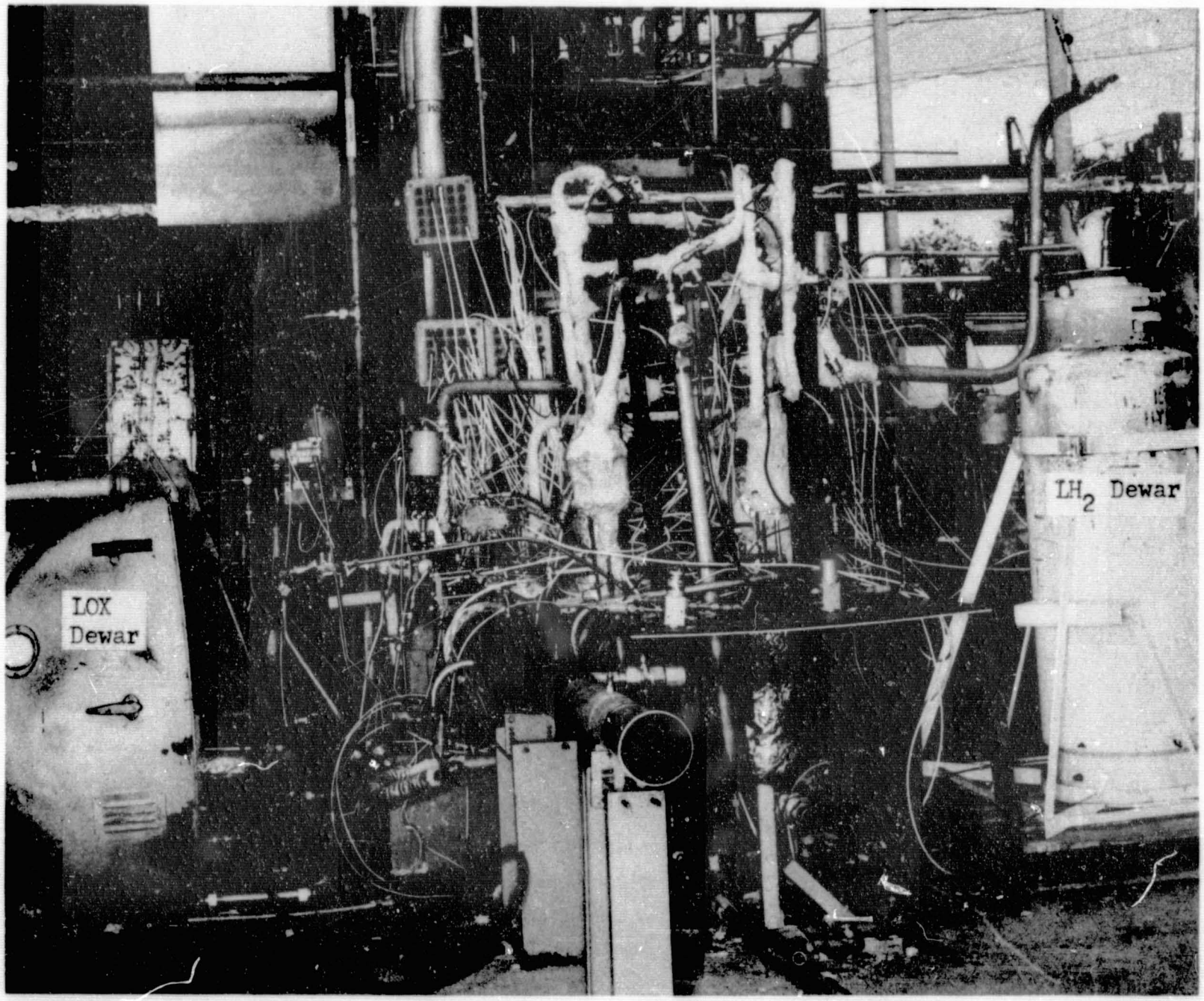

Figure 72. The Test Stand Used for the Conditioner Evaluation(With the Cryogenic Propellant Supply Dewar Vessels)

PROPELLANT CONDITIONER COMPONENT TESTS

The initial experimental effort was directed at characterizing the conditioner components. Included in these tests were checkout of the system valves for response and pressure drop characteristics, checkout of the gas generators for operating and response characteristics, and a coupling of the heat exchanger coils with the gas generators to evaluate operation and determine response.

CONDITIONER COMPONENT TESTS

Valve Characteristics

Six solenoid-operated valves (either main or pilot valves) were used in the entire conditioner system. It was necessary to obtain the characteristic response times for both opening and closing, and the times necessary to saturate the electrical coil before poppet movements. These response times were used in defining the necessary deadbands for the control system and matching propellant entry to the gas generators.

The pressure drop flow characteristics for each valve were necessary because of the low-pressure valve inventory available. The valves were the best that could be obtained from existing hardware, but did not necessarily meet the optimum requirements.

The required valves are divided into four principal categories:

1. Gas generator main valves
2. Accumulator pressure-relief valves
3. Fast-response on-off valves
4. Rapid-response valves simulating the thrustor main valves

The simulated thrustor main valves were those used during the workhorse thrustor program for system balance. The on-off valves were rapid-response pneumatic valves. The remaining valves were flightweight hardware.

Gas Generator Valve Operating Characteristics

The gas generator valves were four-way, solenoid-operated valves obtained from the Rocketdyne Liquid Rocket Division. It was important that the total energizing and de-energizing times were known so the valves for each generator could be operated in a pulse mode. This was necessary to obtain short bursts of hot gas from the gas generators. Consequently, the valve response times had to be accurately known so that the gas generator injection volumes could be correctly sized or the appropriate electrical delay could be used to ensure that the mixture ratio did not become oxidizer rich in the catalyst bed during startup and shutdown.

In addition to the response times, a minimum pressure drop was necessary because of the low pressure inventory available. The equivalent orifice and discharge coefficient for the four-way, solenoid valves were as follows:

Equivalent orifice	0.14-inch diameter
Discharge coefficient (C_D)	0.6

Using these values, a pressure drop across the valve was obtained for the nominal flowrates expected at each gas generator location (Table 11). At both 200 and 560 R, the pressure drop across the fuel side of the hydrogen gas generator was decreased by a factor of 4 by connecting two four-way valves in parallel. This further required that the response times of the four-way valves be accurately known. During the integrated system testing, a third solenoid four-way valve was placed in parallel

to further decrease the pressure drop on the fuel side of the large gas generator. The resulting pressure drop across the valves was decreased by a factor of 9 from the original value using a single valve.

Six four-way valves were obtained. These valves were tested for opening time response by monitoring the current flowing through the valve coil during operation. A typical current trace is shown in Fig. 73 . Both the electrical delay and the poppet delay for the various valves at ambient temperature conditions are presented below.

FOUR-WAY VALVE RESPONSE TIMES

Valve No.	Electrical Delay, milliseconds	Poppet Delay, milliseconds	Total Delay, milliseconds
1	25	3	28
2	24.5	3	27.5
3	24	3.25	27.25
4	24.3	3	27.3
5	24.	3	27
6	25.5	3.5	29

The closing response times were not available using the current monitoring technique. The electrical coil emits a sufficiently high electromotive force such that the poppet movement is indiscernible. Several four-way valves have been previously tested by Rocketdyne at both ambient and LN_2 temperatures. The energizing times agreed with the results of the current monitoring technique. A consistent de-energizing time of from 5 to 5.5 milliseconds was obtained for the valves. Consequently, it was decided not to attempt any bias of the electrical signal to the four-way valves because of the close similarities of energizing and de-energizing times between valves.

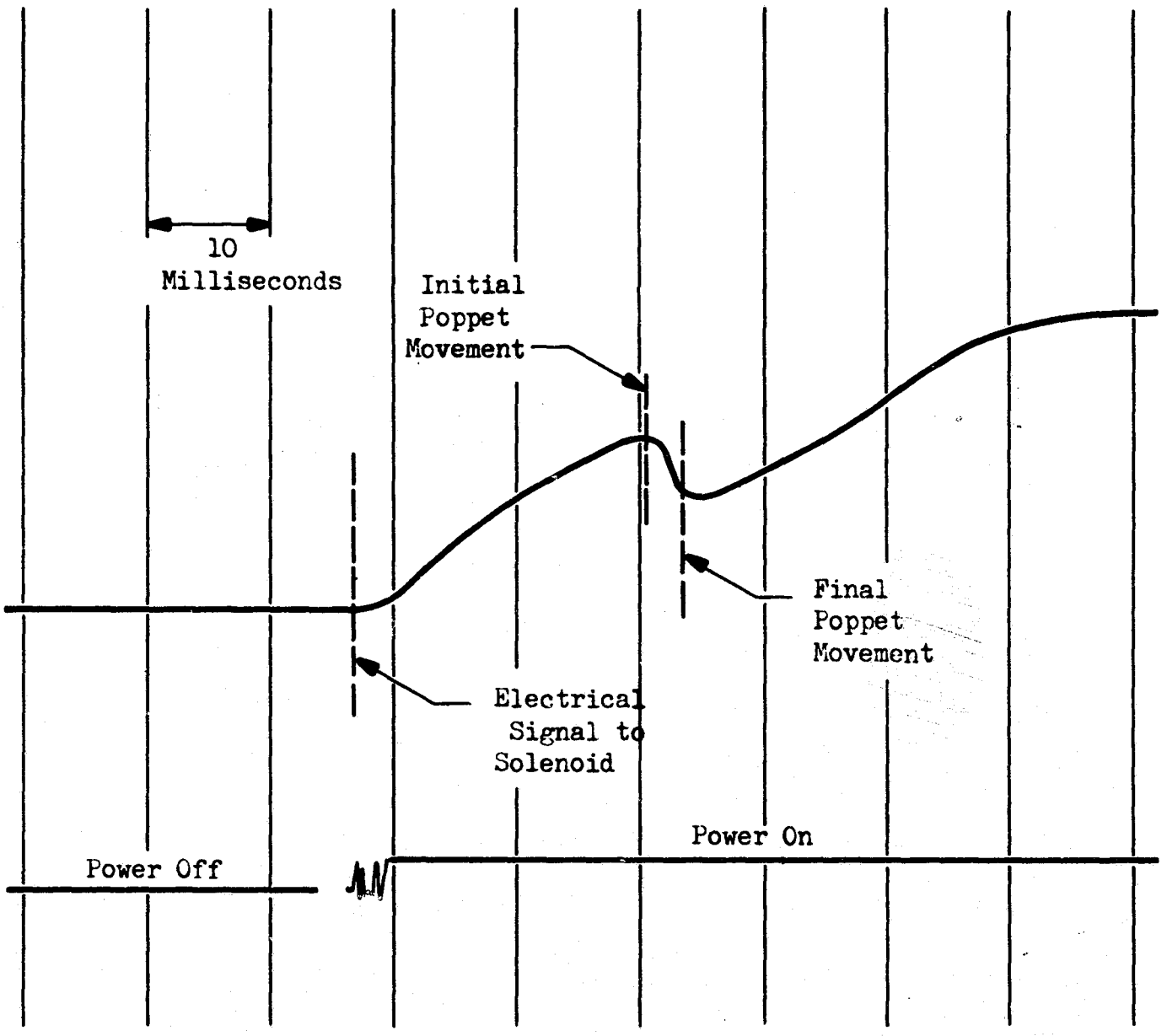

Figure 73. Oscillograph Trace of Current Flowing Through 4-Way Valve Coil During Valve-Opening Operation

Propellant Inlet Valve Operating Characteristics

A rapid-response valve with a low pressure drop was required between both the liquid hydrogen and liquid oxygen dewar vessels and their respective heat exchangers. Each pneumatically controlled valve was operated by the pressure switch during the automatic mode. The equivalent orifice, effective discharge coefficient, and the response times for these valves are as follows:

	Liquid Oxygen Valve	Liquid Hydrogen Valve
Equivalent Orifice Diameter, inches	0.59	0.82
Discharge Coefficient (C_D)	0.57	0.78
Opening Time, milliseconds		
Pneumatic Delay	150	150
Poppet Delay	80	90
Total Valve Delay	230	240
Closing Time, milliseconds		
Pneumatic Delay	40	40
Poppet Delay	20	40
Total Valve Delay	60	80

Although the valves had slightly different response times, the minimum cycling period for both was approximately 300 milliseconds, or a rate of approximately 3 cps.

Follower Valve Characteristics

To determine the effect of a pressure follower valve on the liquid oxygen side instead of an on-off valve, a follower-type valve was adapted from a pressure regulator by changing the head. The equivalent orifice diameter was 0.33 inch and the discharge coefficient (C_D) was 0.8.

A great deal of difficulty was encountered in sealing the follower valve. The original valve was designed to operate at 300 psi with the pressure head used to aid in obtaining a seal. The desired use called for a pressure head of 20 psia; consequently, the seal had to be accomplished in a mechanical manner. A reasonable leakage rate could not be obtained with a variety of seals; the follower valve was therefore eliminated, and two on-off type valves were used to control the pressures in the accumulators.

Gas Generator Experiments

The gas generator experiments were divided into three incremental tasks:

1. Obtain nominal (1500 F and 10 psia chamber pressure) steady-state ignition for an approximate optimum internal configuration determined from the detailed concurrent thrustor studies. To minimize possibilities for undesirable oxidizer-rich startup conditions, the valves were programmed for a fuel lead.
2. Obtain simultaneous opening and closing of the fuel and oxidizer valves. This verified the volume sizing upstream of the catalyst bed.
3. Obtain pulse mode operation to define response time of the gas generators

The apparatus used for these experiments is shown schematically in Fig. 74.

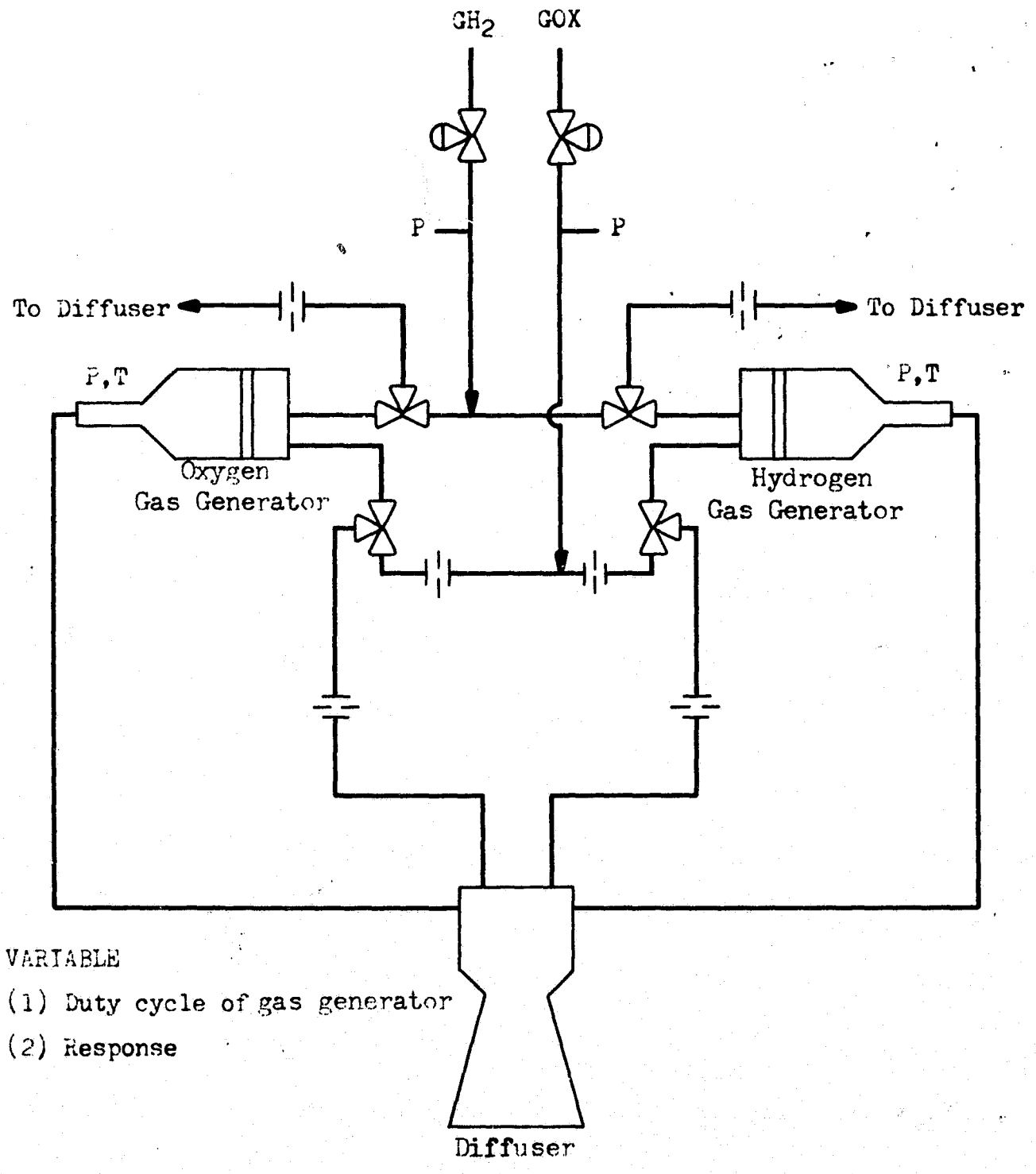

Figure 74. Facility Layout for Gas Generator Checkout Tests

Oxygen-Side Gas Generator Tests. The oxygen gas generator was assembled and connected as shown in Fig. 74 without the heat exchanger coil. Based on the computer analysis, the on-off valve operation was programmed to give a run time of approximately 0.5 second (sufficient for 1500 F ignition). After several short programmed runs which resulted in low ignition temperatures, the valves were operated manually to give a run duration of any desired length. The initial manual run was successful. During the second manual run, erratic ignition occurred and no ignition was obtained for the third run. Inspection of the chamber showed that the tantalum screen retaining the catalyst bed had failed, and the catalyst bed was either blown out of the engine and/or had melted. A new catalyst pack was installed in the engine and the test procedure repeated with results identical to the second run. In addition, the chamber thermocouple had melted, indicating a temperature in excess of 2000 F although the strip recorder had indicated approximately 1500 F. After a third catalytic capsule and new chamber thermocouple were installed, the test procedure was repeated; the target temperature this time was 1000 F, and was obtained by manually adjusting the feed pressures during the run. The run was manually reproduced, indicating no burnout of any kind. Hence, the simultaneous valve opening tests were commenced. The initial test was with a 1000-millisecond hydrogen lead. The hydrogen lead was reduced to 5 milliseconds and no undesirable chamber fluctuations were noted, indicating that the preinjector volumes were in the ratio of the filling rates, a design feature discussed in an earlier section.

Hydrogen-Side Gas Generator Tests. The hydrogen gas generator checkout runs were made by utilizing the procedure developed in the preceding test. First, the feed pressures were manually adjusted to give a 1000 F bed temperature. The simultaneous valve opening test was then performed, and

the procedure was repeated for the nominal design conditions of 1500 F and 10-psia chamber pressure. These tests were concluded by a successful 4-second pulse test.

Additional Heat Exchanger Tests. Careful review of the data obtained in later tests with each gas generator coupled with a heat exchanger coil, revealed that the chamber temperature was approximately 300 F higher than the temperature immediately downstream of the throat. To investigate this phenomenon, it was necessary to reinstall the pressure transducer and thermocouple on the tube inlet and to monitor these variables during a run (Fig. 75 through 80). For the small gas generator it was found that as the chamber temperature was raised to 1700 F, the gas inlet temperature to the tube would lag by 300 to 500 F. A small increase in chamber temperature would cause an instantaneous rise of 300 to 500 F in throat temperature to approximately the chamber temperature.

Sometimes the throat temperature would rise 500 F above the chamber temperature. Careful inspection of the downstream screen on the catalyst pack revealed that the areas near the chamber wall were cooler during operation than the center. When the catalyst pack was held up to the light, spaces near the wall which would allow for gas channeling were seen.

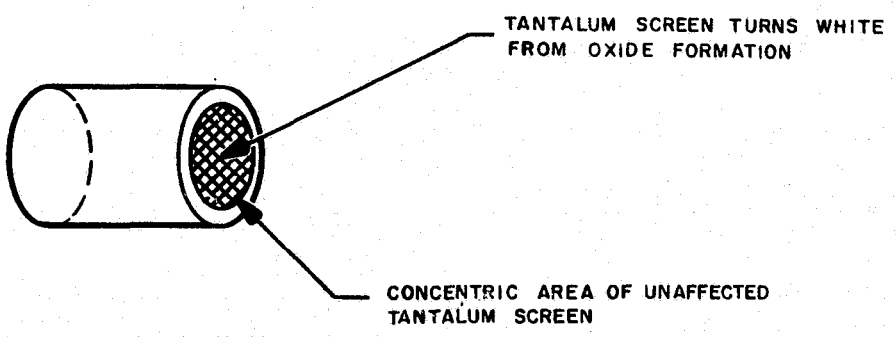

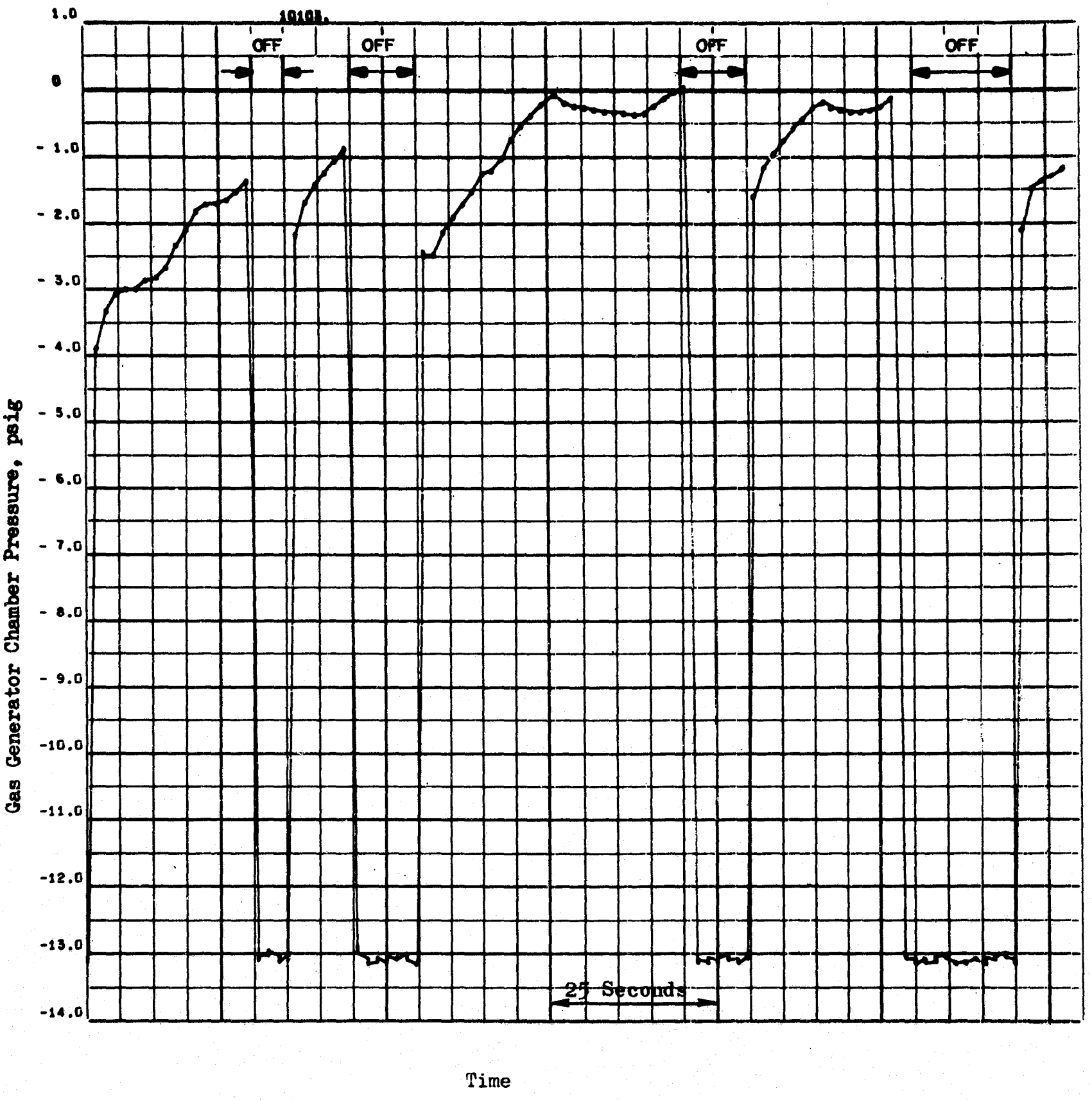

Figure 75. Gas Generator Chamber Pressure With ON-OFF Operation (Gas Generator Experiments)

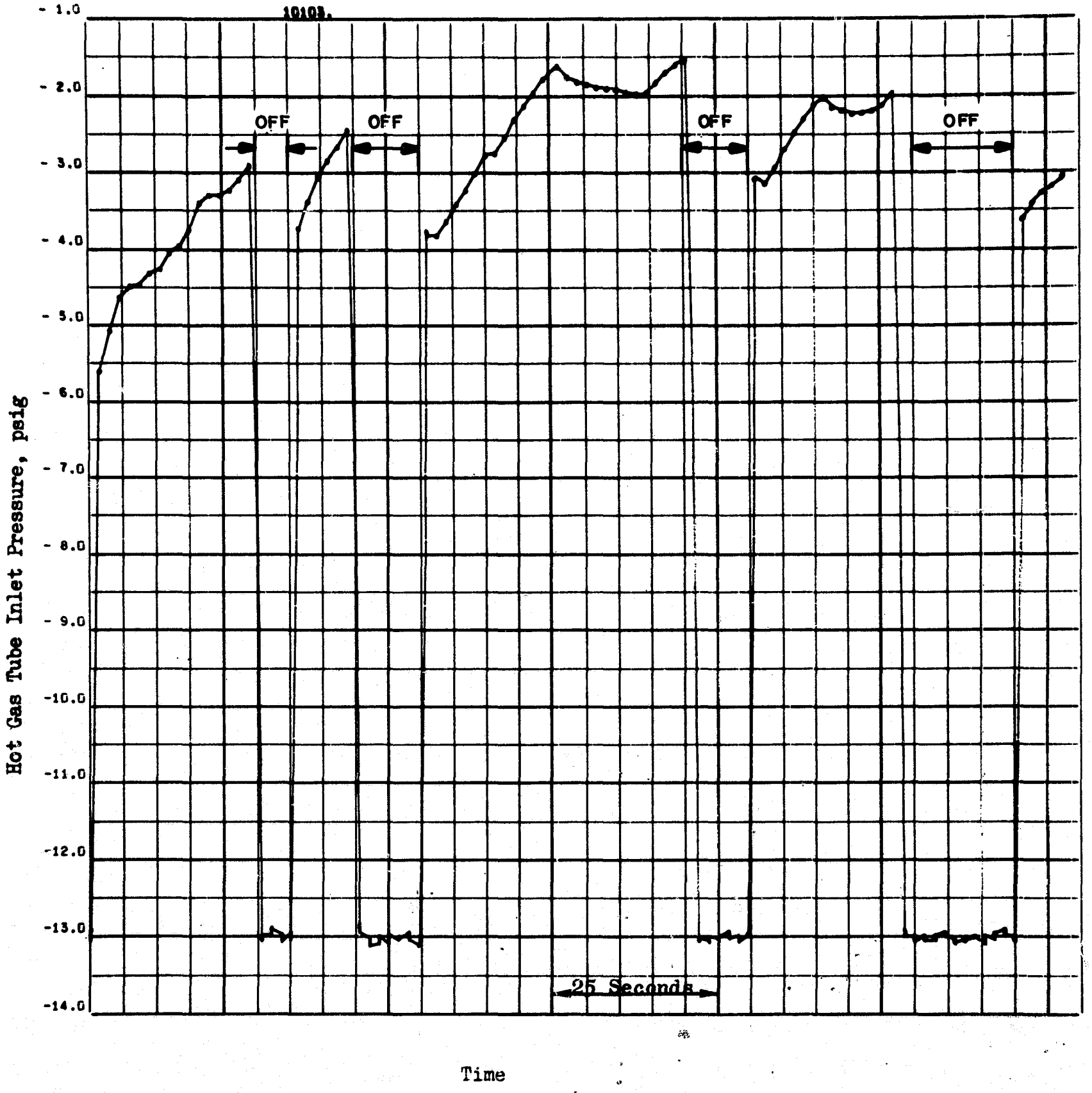

Figure 76. Hot-Gas Tube Inlet Pressure With ON-OFF Gas Generator Operation (Gas Generator Experiments)

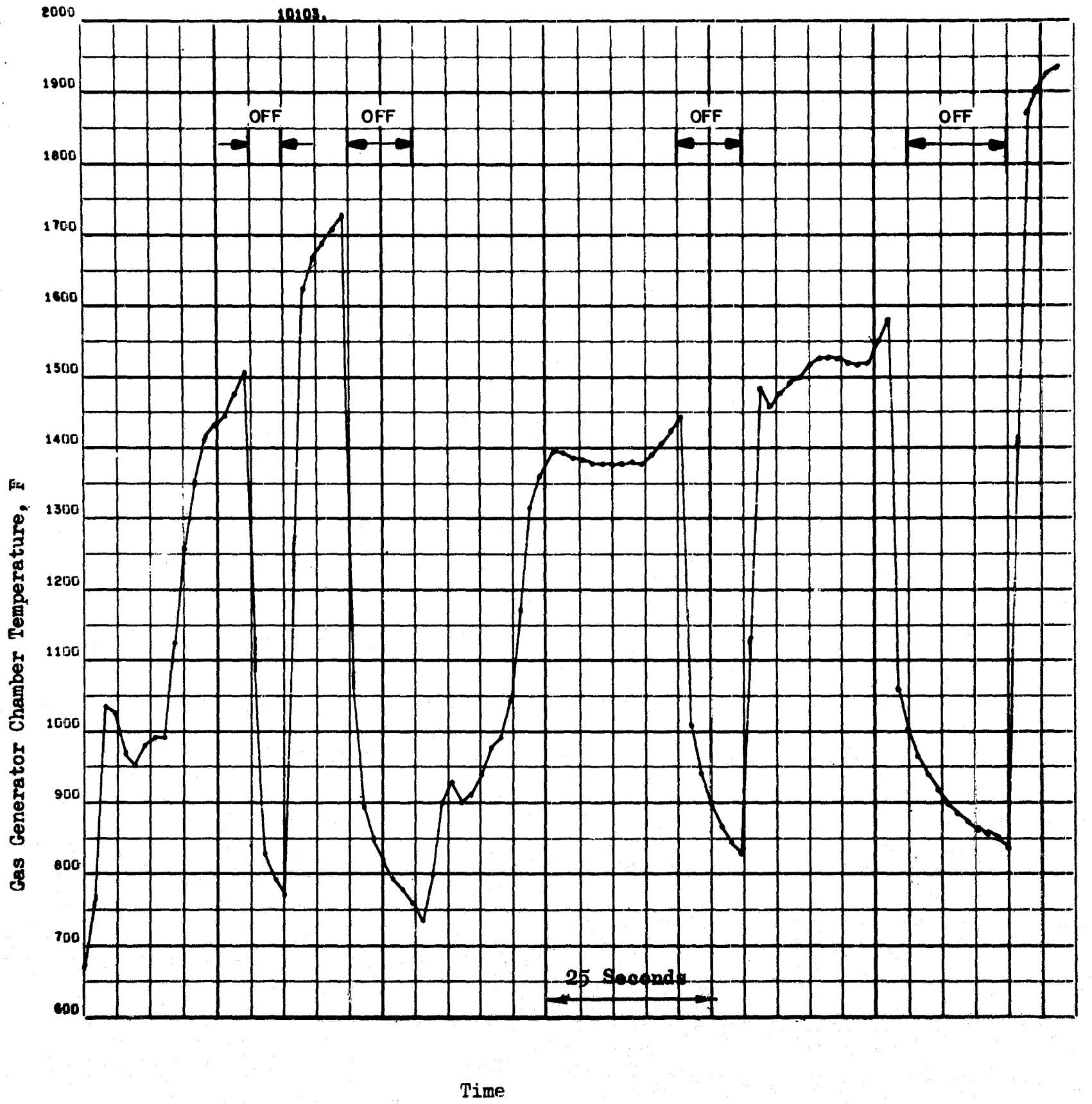

Figure 77. Chamber Temperature for ON-OFF Gas Generator Operation (Gas Generator Experiments)

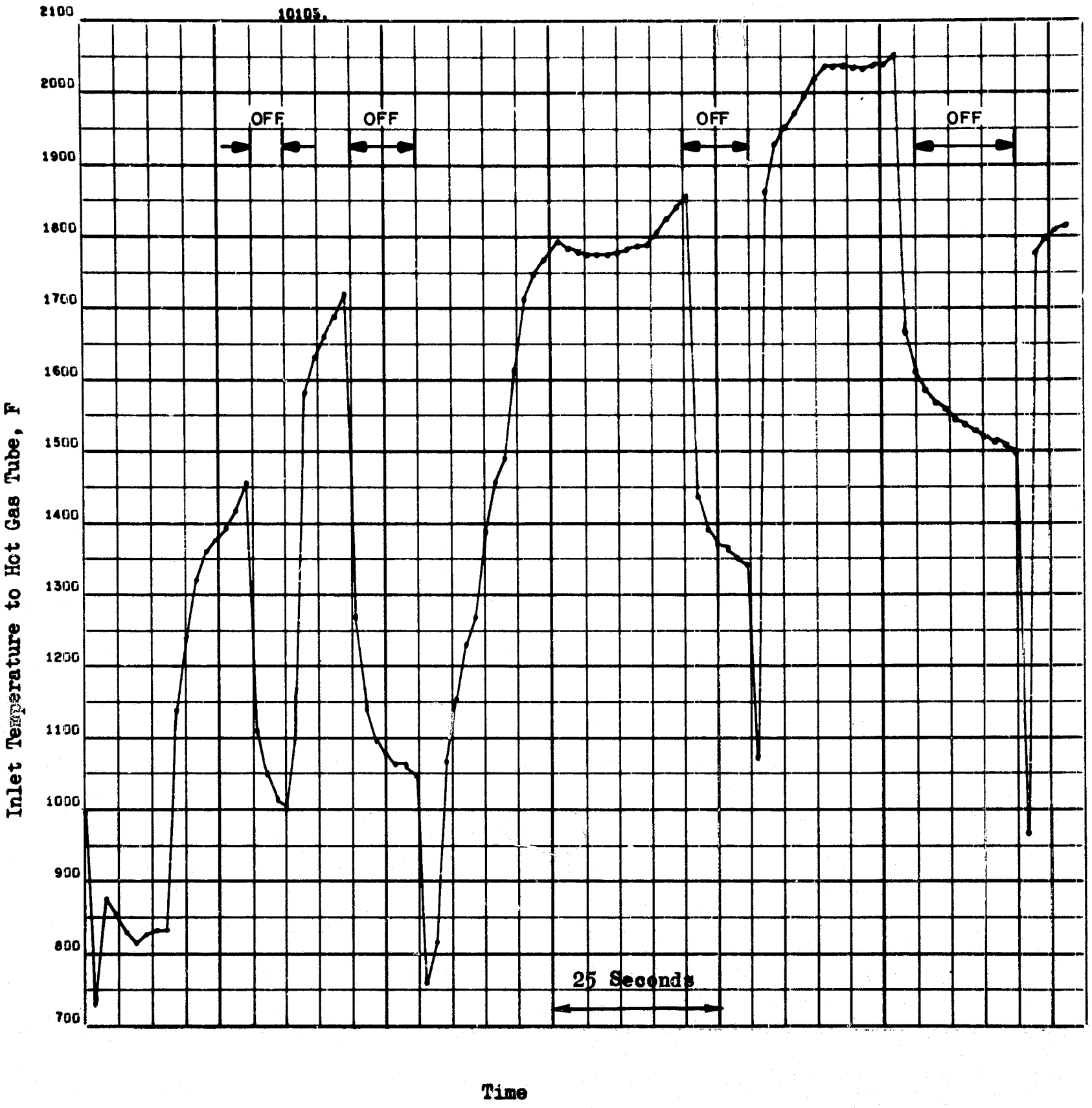

Figure 78. Inlet Temperature to Hot-Gas Coil With ON-OFF Gas Generator Operation (Gas Generator Experiments)

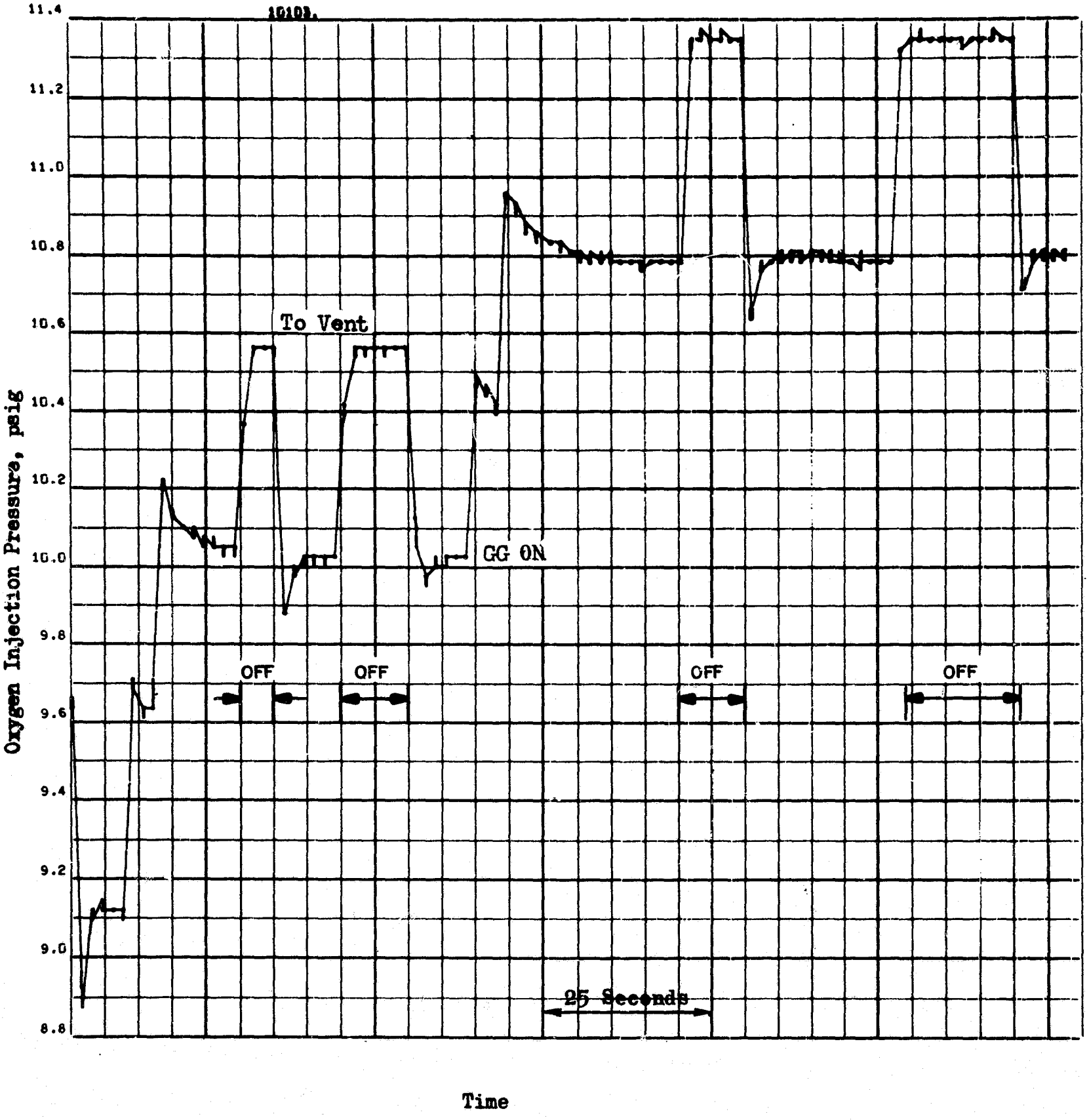

Figure 79. Inlet Temperature to Hot-Gas Coil With ON-OFF Gas Generator Operation (Gas Generator Experiments)

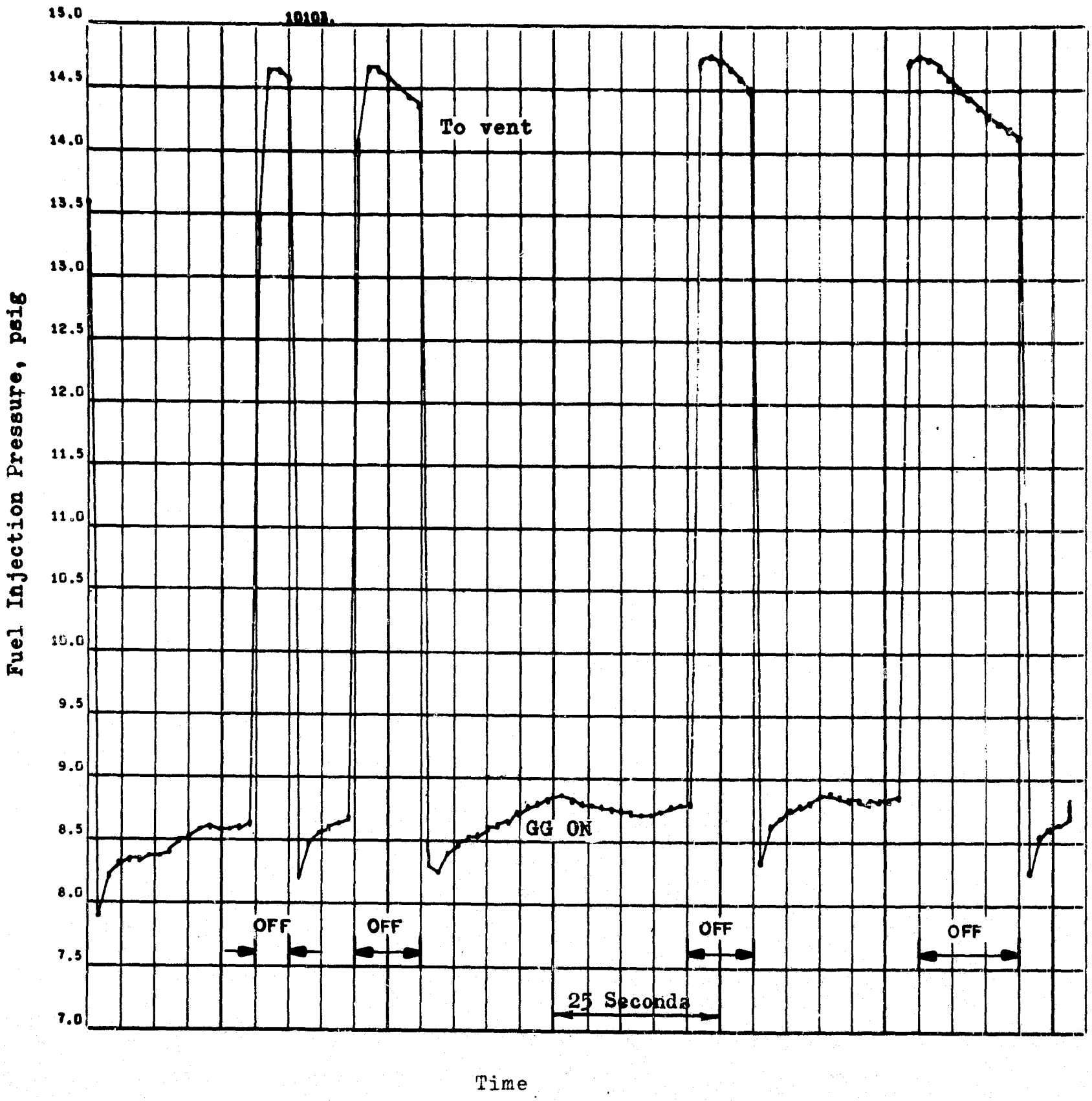

Figure 80. Changes in Fuel Injection Pressure With ON-OFF Gas Generator Operation (Gas Generator Experiments)

It was concluded that gas channels to the outside of the container where the packing density is reduced by the wall effect, and is not ignited until the hot- and cold-gas temperatures are brought to the autoignition temperature. This explanation does not explain why, on occasions, the throat temperature would be 500 F higher than the chamber temperature. The only satisfactory explanation for this phenomenon is either an air leak into the system or mixture ratio variation within the chamber. The latter is suspected because the phenomenon still occurred with chamber pressures greater than atmospheric and because it still occurred after several leaks were found and fixed. The large gas generator performance was qualitatively similar with the exception that the excursions in temperature were somewhat smaller.

A solution to the channeling problem was implemented on the final thrustor studies. This involved installing snap rings near and in the catalyst bed which protruded slightly into the bed. Any gas channeling to the outside would thus be deflected back toward the center of the bed. The deflection ring concept was never tried on the gas generators, but it would be simple to implement.

Conclusions. The objectives of this task were successfully met without major recycles in design and testing. Nominal design conditions could be met; and it was shown that the propellant valves could be opened and closed simultaneously to avoid transient mixture ratio variations. Respnse time was found to be a function of the feed system design. It was concluded, that elimination of the vent lines would produce response times near nominal. It was also concluded that gas channeling to the outside of the bed capsules caused minor erratic ignition. A simple design solution was outlined.

Heat Exchanger Coil Experiments

The primary objective of these experiments was to demonstrate nominal steady-state design conditions with the gas generator and heat exchanger coupled together. A secondary objective was to measure the pressure and temperature response.

Experimental Results. After the gas generators were successfully fired at their nominal conditions of 1500 F and 10 psia, the hot-gas coils were connected to the respective gas generators. The coils were instrumented to obtain the pressure drop and wall temperature gradient during operation. The flow schematic is shown in Fig. 81.

The temperature and pressure shown on this schematic represent steady-state values obtained by the large and small gas generators for representative tests. The temperature immediately downstream of the chamber, TGI, was approximately 350 F lower than the chamber temperature. The drop in temperature between the inlet and outlet of the heat exchanger (TGI to TGO) was caused by heat transfer to the exchanger walls and heat leakage to the surroundings. Because flow at the throat was designed to be sonic, it was possible to estimate the hot-gas flowrate from the area ratio, chamber pressure, and temperature at 0.005 lb/sec. A pressure drop between the chamber and heat exchanger inlet (PCL and PGI) was caused by an abrupt area change.

The combined thermal responses of the gas generator and heat exchanger coil are shown in Fig. 82 and 83. Figure 82 illustrates the chamber temperature and the heat exchanger inlet and outlet gas temperatures, and Fig. 83 shows the outside wall temperature at three of the five equally

The two valves in parallel are replaced by a single valve for the oxidizer side of the conditioning system

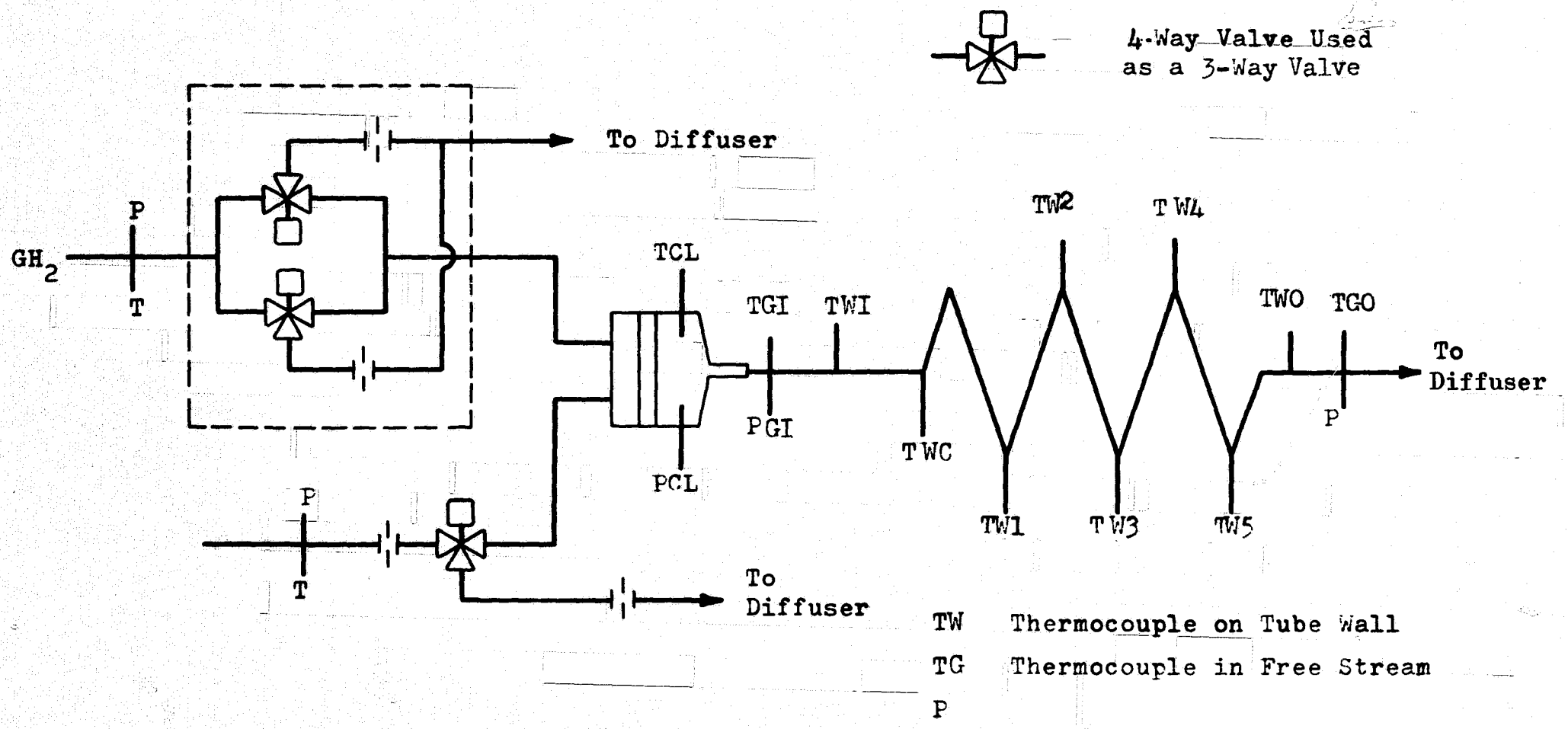

Figure 81. Schematic of Flow System for Heat Exchanger Coil and Gas Generator Experiments on Hydrogen Conditioner Subsystem

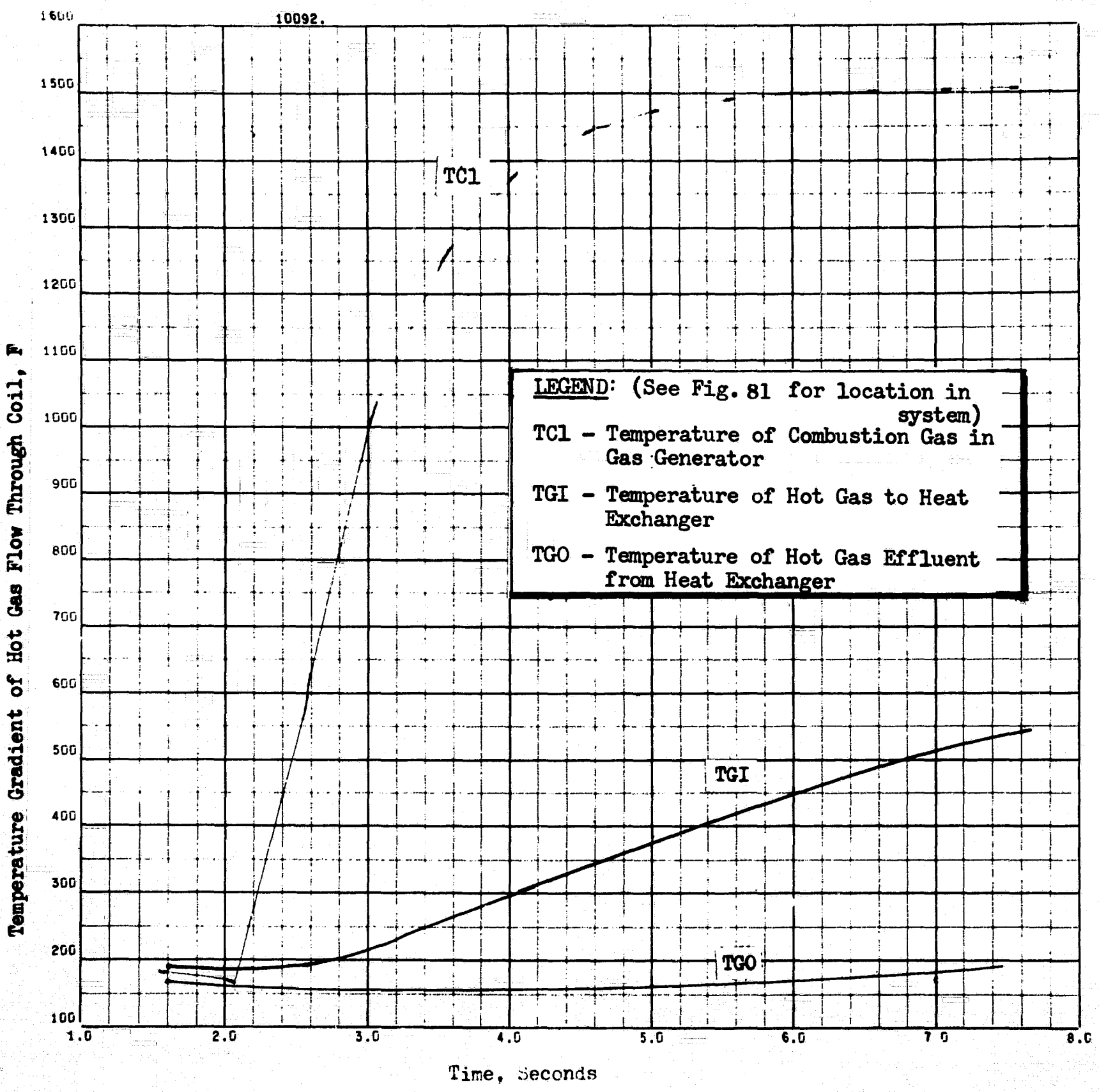

Figure 82. Gas Temperature Characteristics for Hot-Gas Flow Through Heat Exchanger Coil (Heat Exchanger Coil Experiments)

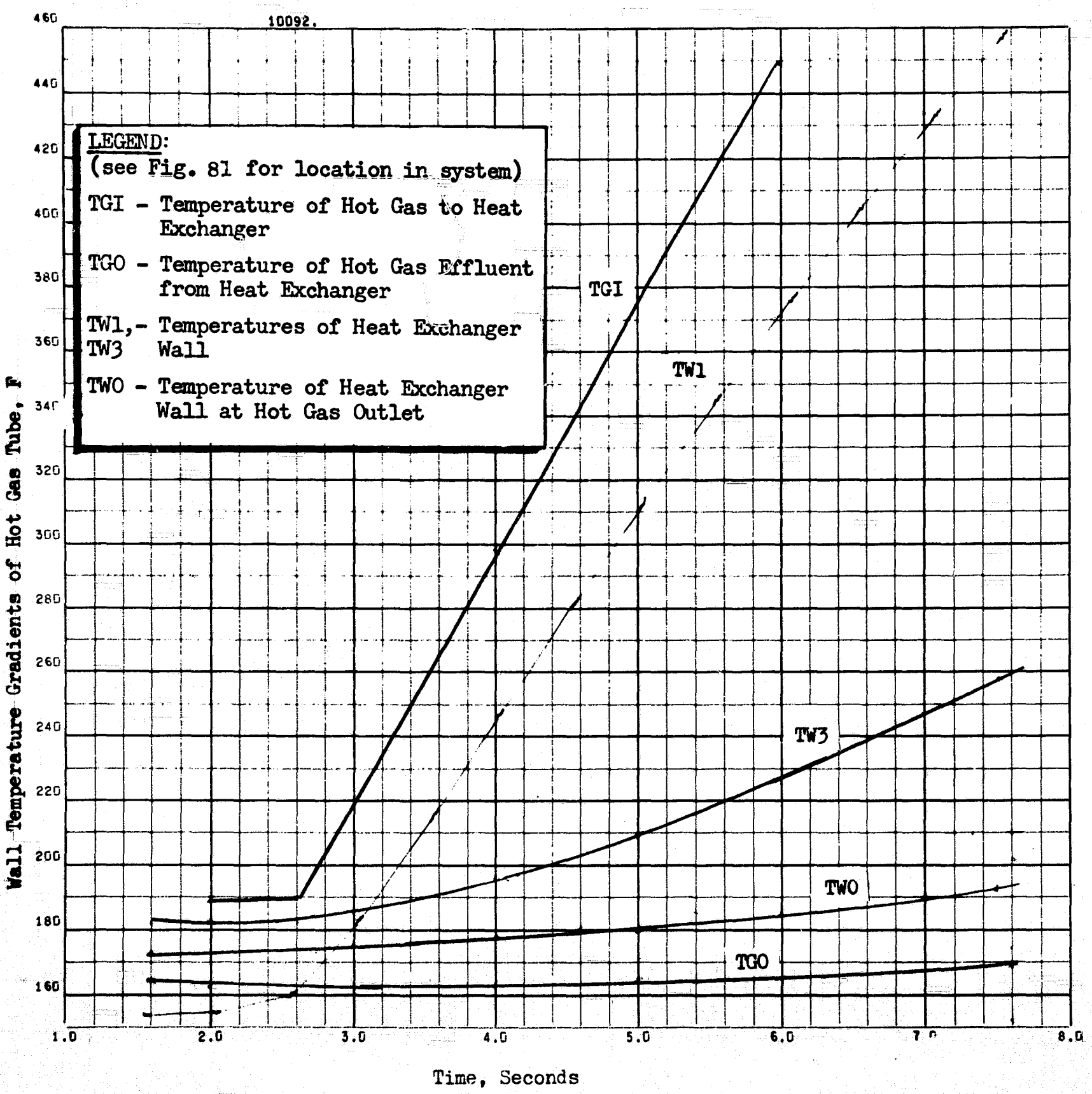

Figure 83. Wall Temperature Characteristics for Hot-Gas Flow Through Heat Exchanger Coil (Heat Exchanger Coil Experiments)

spaced nodes of the heat exchangers. The large difference in time responses between the chamber temperature (TCI) and the temperature of the inlet gas to the heat exchanger (TGI) was caused by the incomplete combustion phenomenon discussed previously and by the heat adsorbed by the mass of the sonic nozzle. It should also be noted that the first part of the heat exchanger follows the inlet temperature (i.e., has a high response), while the outlet temperature and last nodes have a very slow response.

Heat Exchanger Experimental Conclusions. The primary objective of this test (achievement of nominal steady-state designs) was met without any major redesign or testing recycles. A mathematical model for the heat exchanger depicting time-distance response was developed. Inasmuch as many important parameters were estimated, only qualitative correlation of theory with experiment resulted. It was qualitatively concluded that the measured hot-gas heat transfer coefficients were probably two to three times greater than that predicted from conventional correlations.

Summary of Component Tests

The component tests were accomplished in a satisfactory manner with no major delays. The initial gas generator tests showed that the nominal design conditions could be achieved and that pulse-mode operation was feasible. The results showed a tendency for propellant channeling on the periphery. The channeling can be blocked in future designs by employing deflection rings spaced evenly down the bed to force the flow toward the center of the bed.

The results of transient experiments with the gas generators connected to their respective heat exchanger coils indicated the hot-gas heat transfer coefficients to be two to three times larger than originally estimated using conventional correlations. However, the pressure drop results agreed well with those predicted.

The major negative result obtained in the component testing phase was concerned with the follower valve (a modified regulator). The follower valve was to be used for pressure control for one of the propellant systems and an on-off control circuit was to be used for the other. However, the modified valve could not be sealed, eliminating this control concept from further immediate consideration. Two on-off control circuits were employed.

PROPELLANT CONDITIONER SUBSYSTEM
EXPERIMENTAL EVALUATIONS

The second experimental phase of the conditioner effort was the integration of the components into a system with the final goal of achieving a successful demonstration of the feasibility of the RCS operation. However, it is re-emphasized that the system experimentally tested was not designed on the basis of optimization for one or more applications, but rather on its usefulness in developing general design criteria and in exploring problem areas. As the latter were encountered, emphasis was placed on the most expedient solution as opposed to the optimum solution. This approach was taken to allow the achievement of the overall program goals.

The conditioner components were systematically interconnected during the system testing phase. The approach was as follows:

1. Connect the components
2. Add the necessary control circuits
3. Initiate propellant feedback to the gas generators
4. Integrate the conditioner and thrustor for an overall system demonstration

Individual Propellant Subsystem Tests

The first series of system tests was to investigate each propellant side separately and demonstrate the heat exchanger conditioning of the cold fluid to the design point in a stable manner. All system valves were open, which represents the case of the thrustor being used in steady-state mode. If the heat exchanger did not deliver conditioned fluid in the design range, the alternative was to change the heat exchanger area.

A secondary objective was to make pseudocalorimetric measurements so that the overall heat transfer coefficient could be determined.

Experimental Equipment. A photograph of the apparatus in a partially assembled state is presented in Fig. 84. Figure 85 is an instrumentation and teneral schematic. The heat exchanger was divided into three channels by three comb-like spacers positioned 120 degrees apart. One of the three heat exchanger channels was instrumented by installing sevel thermocouples, four in the propellant and three on the tube wall, at adjacent positions. This technique proved impractical because the thermocouple leads partially blocked flow to this channel, causing the channel temperature to be high. A thermocouple was placed at the end of the other two flow paths to determine the amount of channeling in the heat exchanger during the runs. Further, the thermocouples in the liquid may have been influenced by the wall temperature because of the narrow channels, and the wall thermocouples which were spot welded to the tubes were unduly influenced by the liquid.

In the hydrogen heat exchanger experiments, only the inlet and outlet temperatures were measured. Three thermocouples were inserted through fittings in the outlet end plate and positioned near each channel outlet to check for channeling. Water flow tests were conducted prior to assembling the heat exchanger, and the internal parts were custom fitted to give even flow.

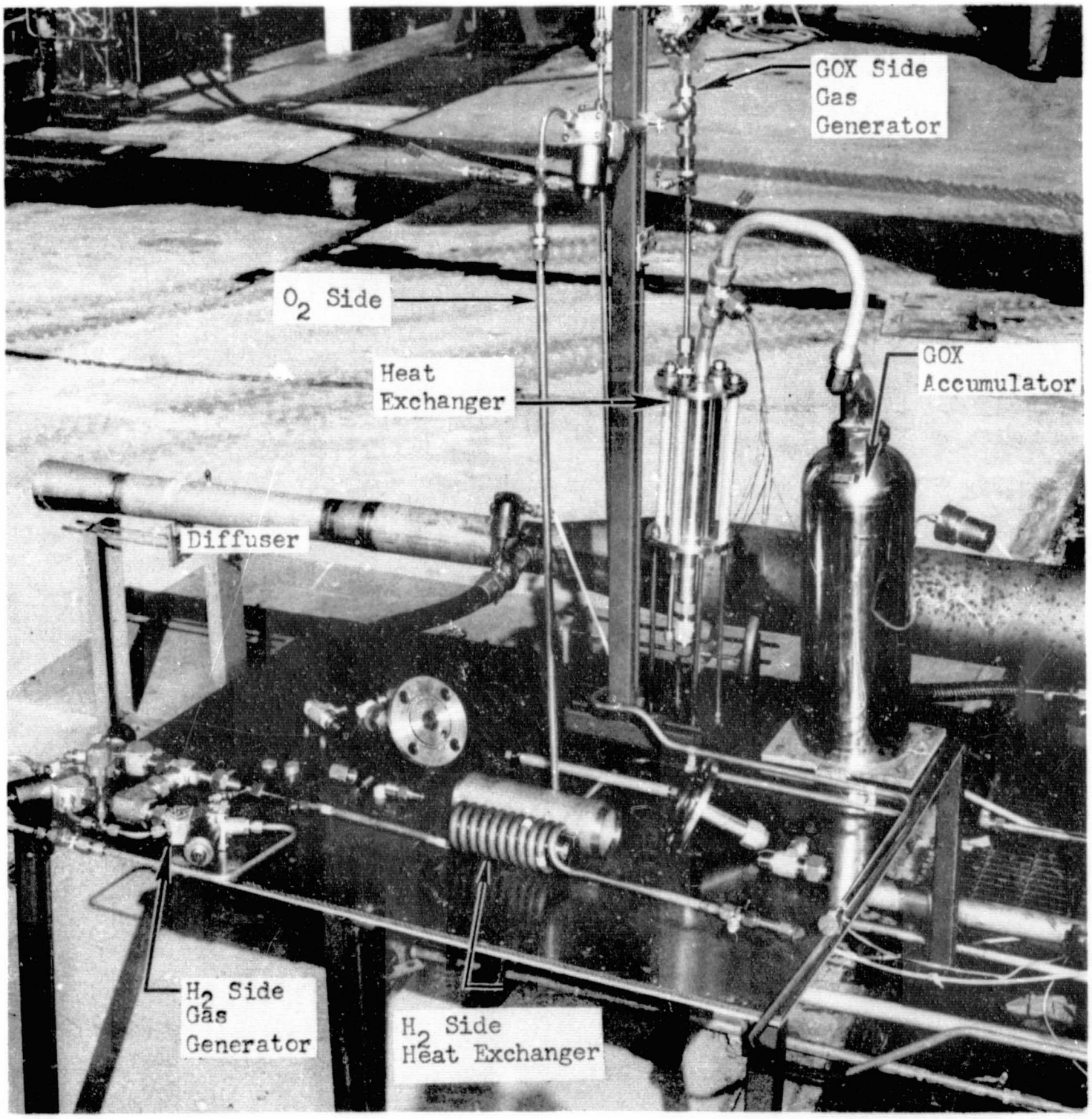

Figure 84. The Conditioning System (Showing the Oxygen Side in an Assembled State, and the Disassembled Hydrogen Side Gas Generator and Heat Exchanger Components)

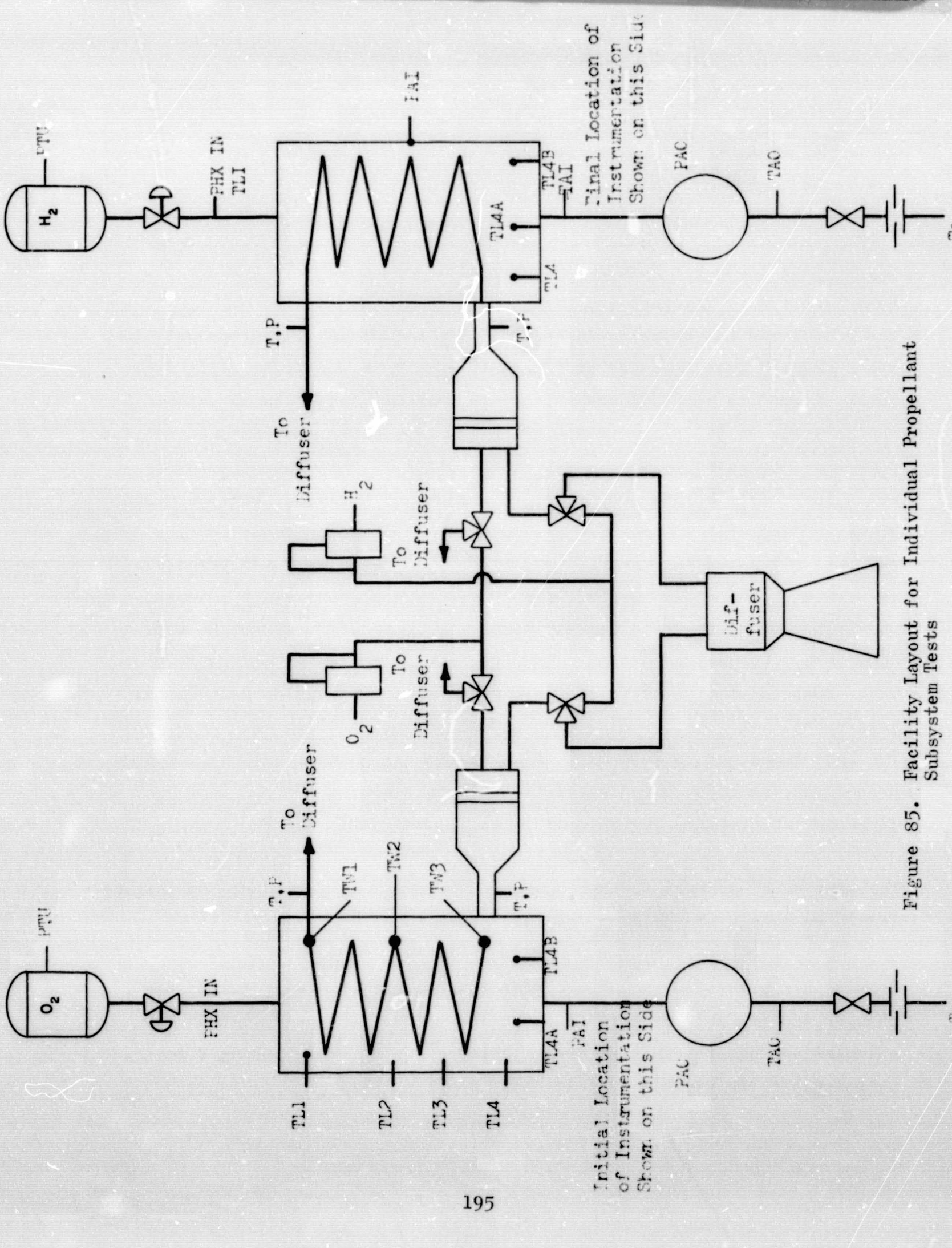

Figure 85. Facility Layout for Individual Propellant Subsystem Tests

Initial tests were conducted using liquid nitrogen as the propellant to be conditioned, to determine the experimental procedure before using liquid oxygen or liquid hydrogen as the cold fluid.

Oxygen Heat Exchanger Results. The results indicated that the overall heat transfer coefficient for liquid oxygen had been underestimated because the cold fluid was being conditioned to 800 R instead of the nominal 200 R. The increased heat transfer coefficients caused an operating difficulty. In an attempt to approach the nominal temperature and pressure values in the accumulator (17 psia and 200 R) the gas generator temperature and flow-rate were decreased to a point where the water in the exhaust products would freeze in the hot tube coil. The freezing would not have occurred if the effective heat transfer area had been optimum to condition the cold propellant to the nominal conditions. To compensate for the high temperature, the effective heat transfer area was decreased by diverting the flow path of the cold fluid through the center post of the heat exchanger by the desired amount. The area was decreased by half such that eight instead of the initial 16 coils were used to transfer heat to the cold propellant. Both countercurrent and cocurrent flows were used in the heat exchanger to determine if any large variance in the conditioned propellant temperature would exist. In both cases, the eight coil heat exchanger conditioned the cold fluid to approximately 480 R.

The heat exchanger was further shortened to near one fourth of the original length to obtain the desired nominal conditions.

Results are presented in Table 13 for the hot-gas side of the heat exchanger and in Table 14 for the propellant side. The objective of the calculations was to close an energy balance on the heat exchanger and to calculate the overall heat transfer coefficients.

TABLE 13

TEST DATA FOR HOT-GAS SIDE OF LOX HEAT EXCHANGER

Test*	Pressure, psia		Temperature, F		MR***	$\dot{w}$, lb_m/sec	$\dot{q}$, Btu/sec
	Inlet**	Outlet	Inlet	Outlet			
1	11.6	3.56	1410	68.5	0.71	0.0018	4.8
2	12.3	4.03	1370	76	0.69	0.0019	5.0
3	9.75	3.33	1425	112	0.71	0.0013	3.4
4	13.4	4.27	1466	183	0.75	0.0013	6.0
5	12.3	3.80	1540	190	0.80	0.0021	5.7

*These data represent tests conducted in the following manner:

1. A countercurrent heat exchanger with the total design hot tube area
2. A countercurrent heat exchanger with one-half the design hot tube area
3. A cocurrent heat exchanger with one-half the design hot tube area
4. A countercurrent run with one-quarter the heat exchanger area
5. A cocurrent run with one-quarter the heat exchanger area

**Chamber pressure

***Estimated (discussed in the text)

TABLE 14

TEST DATA FOR PROPELLANT SIDE OF LOX HEAT EXCHANGER

Test*	Temperature, F Inlet	Outlet	$\dot{w}$,** lb_m/sec	$\dot{q}$, Btu/sec	Pressure in Accumulator, psia	Area, ft^2	T_{lm}, F	U, $Btu/hr\text{-}ft^2$
1	-297	430	0.00207	5.2	16.8	1.07	830	20
2	-297	12.0	0.024	3.8	16.3	0.54	780	32
3	-297	5.0	0.024	3.6	16.2	0.54	980	25
4	-297	-295	0.18	16.	23.9	0.27	980	81
5	-297	-240	0.043	4.5	17.4	0.27	1020	75 to 58

*These data represent tests conducted in the following manner:

1. A countercurrent heat exchanger with the total design hot tube area
2. A countercurrent heat exchanger with one-half the design hot tube area
3. A cocurrent heat exchanger with one-half the design hot tube area
4. A countercurrent run with one-quarter the hot tube area
5. A cocurrent run with one-quarter the hot tube area

**Estimated (discussed in the text)

The heat balances are subject to several uncertainties. For the hot-gas heat load (1) the mixture ratio was obtained from calculated theoretical combustion temperature vs mixture ratio curves, (2) the flowrate was estimated from gas generator chamber pressure and temperature assuming sonic flow at the gas generator throat, and (3) the average hot-gas heat capacity was obtained from Rocketdyne's theoretical preformance programs. Because of incomplete combustion in the gas generator, the hot-gas inlet temperature was subject to some uncertainty (reported earlier). An analysis was conducted on the enthalpy received from the hot gas when it was possible for water to condense in the outlet stream. It was concluded that water would begin to condense near 100 F and that an approximate 16 percent increase in heat load could be realized by utilizing the heat of condensation. Thus the heat loads reported in Table 13 are also subject to substantial increases when the outlet temperature approaches 100 F.

To obtain the heat load on the propellant side, it was necessary to assume saturated liquid at the heat exchanger inlet and a coefficient for the uncalibrated orifice. Nevertheless, comparison of the heat received by the liquid oxygen with the estimated heat given up by the hot gas shows a good closure considering the assumptions that have been made. Because of ambient heat leak to the vaporizing liquid oxygen, it was suspected that the liquid heat load would always be biased above that of the hot gas.

From a knowledge of the heat load, area, and average driving temperature, it was possible to estimate the overall heat transfer coefficient (Table 14). This coefficient is based on the circumferential area of the spiral tube, although the actual effective liquid area was not known because of the heat exchanger construction and liquid flow pattern. It was interesting to note how the overall heat transfer coefficient changes as the split in heat load changes with vaporizing liquid or superheating vapor. Because of this change, it was not possible to make one run and simply calculate a new heat transfer area that would give the desired propellant temperature. The actual heat transfer coefficients range from

two to four times those theoretically predicted. It was reported in the previous experiment and correlation work that it was qualitatively apparent that the hot-gas heat transfer coefficient could be several times higher than that predicted from conventional correlations. Because the method of instrumentating the heat exchanger channel for adjacent gas, wall, and propellant temperatures proved impractical, it was impossible to determine the position of the tube wall profile in relation to the gas and propellant profiles. A tube wall temperature near the hot-gas temperature would have indicated a high hot-gas coefficient and would have confirmed the previous experiment.

Liquid Hydrogen Heat Exchanger Results. The liquid hydrogen conditioner system was operated four times, and the reduced data are shown in Tables 15 and 16. During the first run it was desired to condition the fuel to the new nominal condition, Case V or Case VI of Table 15. Under the indicated steady-state conditions, it was possible to increase the fuel flow to nominal and thus lower the accumulator temperature because the hot-gas outlet temperature from the heat exchanger coil was near the freezing point of water. This run was subsequently repeated with increased flowrates, both fuel and hot gas, but the accumulator outlet temperature remained high (near 100 F). Thus, it was concluded that it was necessary to shorten the hot tube coil for satisfactory steady-state operation of the gas generator.

An alternative was to increase the size of the gas generator and operate it in the pulse mode phase. This involved increasing both the hot-gas flowrate and chamber temperature to a maximum (double nominal) and operating the gas generator in the pulse mode (30 to 40 percent on) to maintain a conditioned fuel temperature in the range of 0 to -50 F. Thus, the fuel flowrate and temperature were brought to nominal conditions using the existing heat exchanger, which was found to have excessive area for steady-state gas generator operation. Unfortunately, high feed pressures to the

TABLE 15

TEST DATA FOR HOT-GAS SIDE OF THE LH_2 HEAT EXCHANGER

Test	Pressure, psia		Temperature, F		MR	w, lb/sec	U, Btu/sec
	Inlet	Outlet	Inlet	Outlet			
I	10.8	3.4	1520	48	0.85	0.0049	14 → 16.9
II	13.6	5.4	1540	197	0.85	0.0067	18.0
III	17.7	6.4	1680	199	0.85	0.0078	21.0
IV*	20.8**	6.8	1600	90 (average)		—	28 (30- to 40-percent on)

*Pulse mode gas generator operation with a steady liquid hydrogen flow.

**42 psia ambient feed gases

These data represent a countercurrent test with the total design hot tube area.

TABLE 16

TEST DATA FOR THE PROPELLANT SIDE OF THE LH_2 HEAT EXCHANGER

Test	Temperature, F		w, lb/sec	$\dot{q}$, Btu/sec	Pressure in Accumulator, psia	Area, ft^2	T_{lm}, R	U, Btu/ $hr\text{-}ft^2\text{-}R$
	Inlet	Outlet						
I	-437	142	0.0075	16	15.35	0.954	1057	75
II	-437	306	0.0066	18	14.85	0.954	895	76
III	-437	235	0.0078	19	18.0	0.954	920	86
IV*	-437	-20			17.0			

*Pulse mode gas generator operation with a steady liquid hydrogen flow.

These data represent a countercurrent test with the total design hot tube area.

TABLE 17

DESIGN CONDITIONS STEADY-STATE OPERATION OF CONDITIONER

Conditions	Case No.	Propellant at Conditioner Inlet or Propellant Tanks				Propellant at Gas Generators			Percent of Total Flow to Gas Generator	Propellant at Thrustor		Combined Temperature, F
		Oxygen State	$\dot{w}_o$, lb/sec	Hydrogen State	$\dot{w}_f$, lb/sec	MR, o/f	$\dot{w}_o$, lb/sec	$\dot{w}_f$, lb/sec		$\dot{w}_o$, lb/sec	$\dot{w}_f$, lb/sec	
200 R Conditioned Propellants and 20-pound Thrust	I	O_2 Liquid	0.03852	Liquid H_2 with 5-percent He	0.01642	1.32	0.002822	0.002121	9.0	0.0357	0.0143	3570
	II	O_2 Liquid	0.0388	H_2 Liquid	0.0174	1.00	0.00309	0.00309	11.0	0.0357	0.0143	3570
	III	O_2 Vapor	0.03722	H_2 Vapor	0.01582	1.00	0.00152	0.00152	5.73	0.0357	0.0143	3570
500 R Conditioned Propellants and 20-pound Thrust	IV	O_2 Liquid	0.04518	H_2 Liquid	0.02457	0.85	0.00948	0.01117	29.2	0.0357	0.0143	3750
500 R Conditioned Propellants and 10-pound Thrust	V	O_2 Liquid	0.01918	H_2 Liquid	0.01119	0.85	0.00406	0.0049	29.2	0.01572	0.00629	3750
400 R Conditioned Propellants and 10-pound Thrust	VI	O_2 Liquid	0.01901	H_2 Liquid	0.00992	0.88	0.00313	0.00357	23.1	0.01588	0.00635	3690

gas generator of the order of 30 to 50 psig were necessary for this mode of operation. This mode of operation did not appear to be compatible with the low accumulator pressures which eventually drive the gas generators. Consequently, it was necessary to shorten the heat exchanger.

Heat Exchanger Nominal Design Point Changes. Because thrustor ignition at temperatures below 360 R and approximately 10 psia with 1/16 inch catalyst pellets was unsatisfactory, the nominal design point for the conditioned propellant temperature was raised. Heat and material balances are presented for temperatures of 500 and 400 R and 10- and 20-pound thrustors in Table 17. The most striking changes in the nominal design were the heat load on the hydrogen heat exchanger, which increased by a factor of 4, and the percent of total propellant flow diverted to the conditioner, which increased by a factor of 3. To utilize the existing gas generators, thrust was reduced to nominally 10 pounds. Thus, the conditioning system was operated in the range from 400 to 500 R for a 10-pound thrustor.

Using the experimentally determined heat transfer coefficient of 70 Btu/hr-ft^2-R and the flowrates for a 10-pound thrustor (Table 12), it was estimated that a seven-coil heat exchanger would condition liquid hydrogen to the range of 400 to 500 F. The construction and installation of this coil and heat exchanger was completed for the succeeding test series. Comparison of the original nominal liquid oxygen conditions (Table 11, Case II), with the revised conditions (Case V) shows approximately the same gas generator flowrate and heat exchanger loading. It was necessary to size a heat exchanger to conform with the experimental heat transfer coefficient of approximately 25 Btu/hr-ft^2-R (Table 14). This resulted in the fabrication of a six-coil heat exchanger for the oxygen side of the conditioner.

Conclusions. Both the liquid oxygen and liquid hydrogen overall heat transfer coefficients were found to be several times higher than those initially predicted. Thus, it was necessary to reduce the heat exchanger area to meet the original nominal conditions.

Water freezing near the hot-gas outlet of the heat exchanger was found to be a primary failure mode. Two approaches to minimizing this failure mode were investigated: (1) reduce the heat exchanger area, and (2) increase the total heat output of the gas generator and operate it in the pulse mode fashion. The latter proved to be the better solution, but time did not permit building a new gas generator for the remainder of the present testing, so the heat exchanger area was reduced.

Evaluation of Accumulator Characteristics

At the start of the experimental program little was known about boiling instability, subsequent problems of pressure and temperature perturbations, and the ability of the accumulator to attenuate these perturbations. Experimental data of the accumulator mixing characteristics were gathered in conjunction with the concurrent system testing (Test VI). At the same time a mathematical model describing the operation of the accumulator was developed and programmed in a computer program. The data gathered from the experiments and the sizings were fed to the model to define an optimum geometry which minimizes the temperature and pressure fluctuations.

The size of the accumulator selected for experimental evaluation depended primarily on the weight flowrate and the response of the control circuit. Because the response of the propellant valves was rather slow, it was necessary to select relatively large accumulators (700 cu in. for oxygen and 4000 cu in. for hydrogen). Because a good portion of the system weight and volume was represented by the accumulator, an important part of this experiment was to minimize the accumulator size.

Experimental Results for Oxygen Accumulator. The approach was to initially instrument the oxygen system as shown in Fig. 85 and to rapidly optimize location and measurements as shown on the liquid hydrogen system. Figures 86 through 90 show the time-pressure traces during a liquid oxygen steady-state, concurrent run with one-half the original heat exchanger area. The pressure transducers nomenclature and locations were:

PTU	ullage pressure on liquid oxygen dewar
PHXIN	pressure at bottom of heat exchanger
PAI	located on the heat exchanger shell near the middle of the spirally wound coils
PAO	outlet pressure from the accumulator
TAO	outlet temperature from the accumulator

The critical behavior of these pressure and temperature traces were analyzed and the results are summarized below:

Parameter	Measured Ranges	Oscillation Frequency, cps
PTU	3.348 ±0.03 psig	0.07
PHXIN	3.10 ±0.2 to 0.02 psig	0.46
	3.0 ±0.3 to 0.4 psig	0.07
PAI	2.40 ±0.65 psig	0.46
	2.30 ±0.40 psig	0.08
PAO	2.40 ±0.58 psig	0.46
	2.40 ±0.35 psig	0.08
TAO	-6 ±2 F	0.385

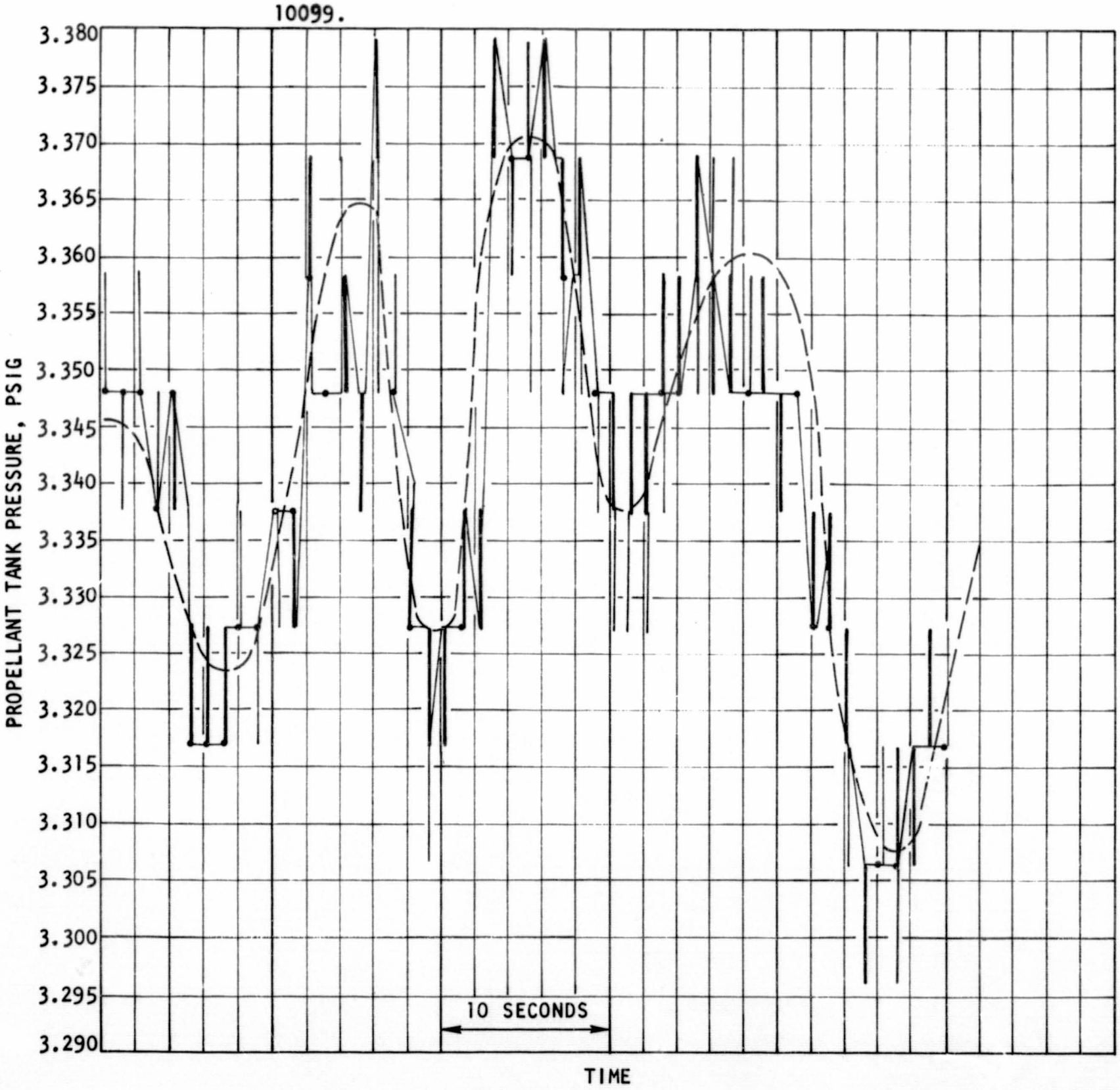

Figure 86. Propellant Tank Pressure (Evaluation of Accumulator Characteristics for the Oxygen Conditioner Subsystem)

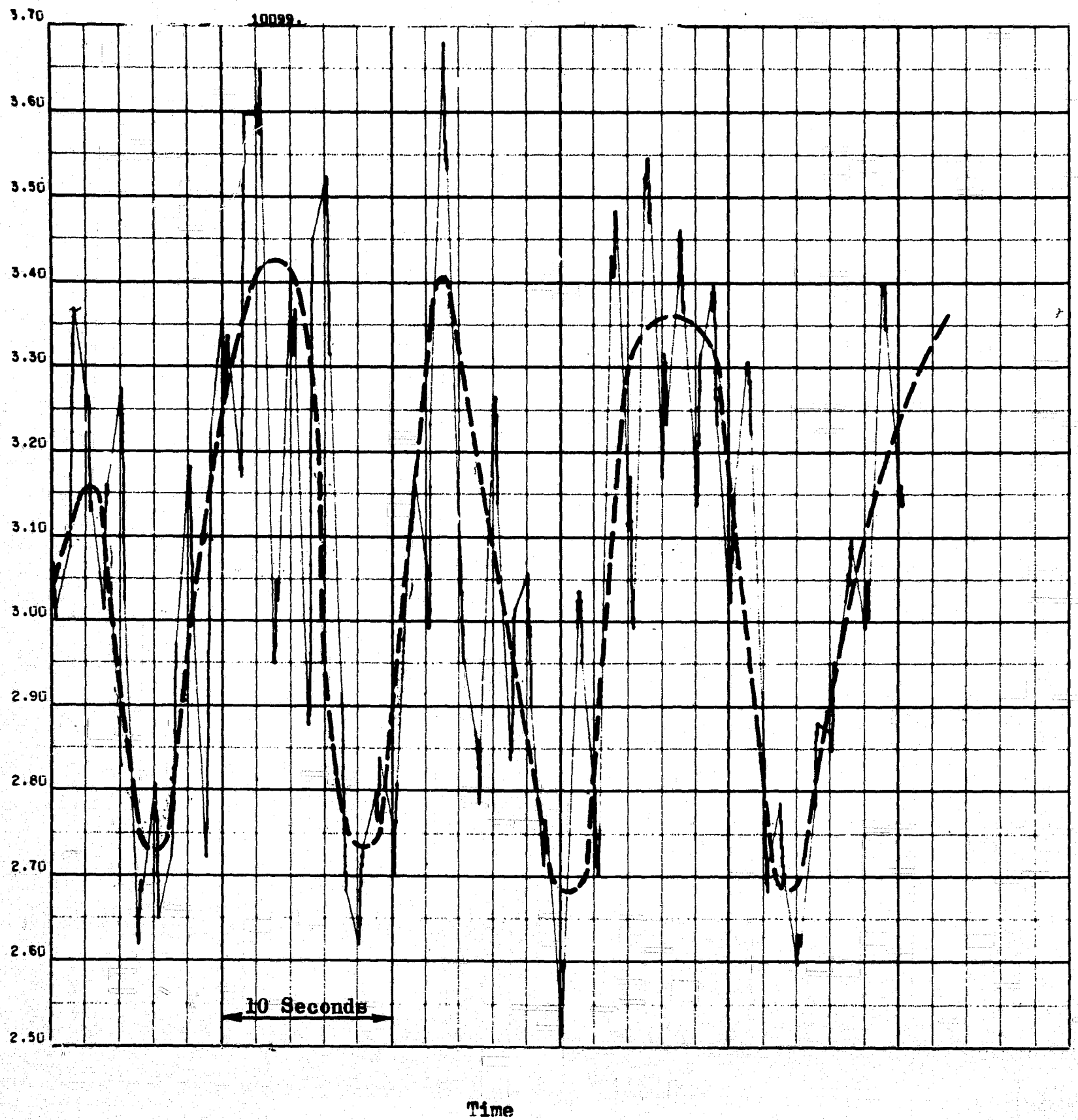

Figure 87. Feed Pressure to the Heat Exchanger (Evaluation of Accumulator Characteristics for the Oxygen Conditioner Subsystem)

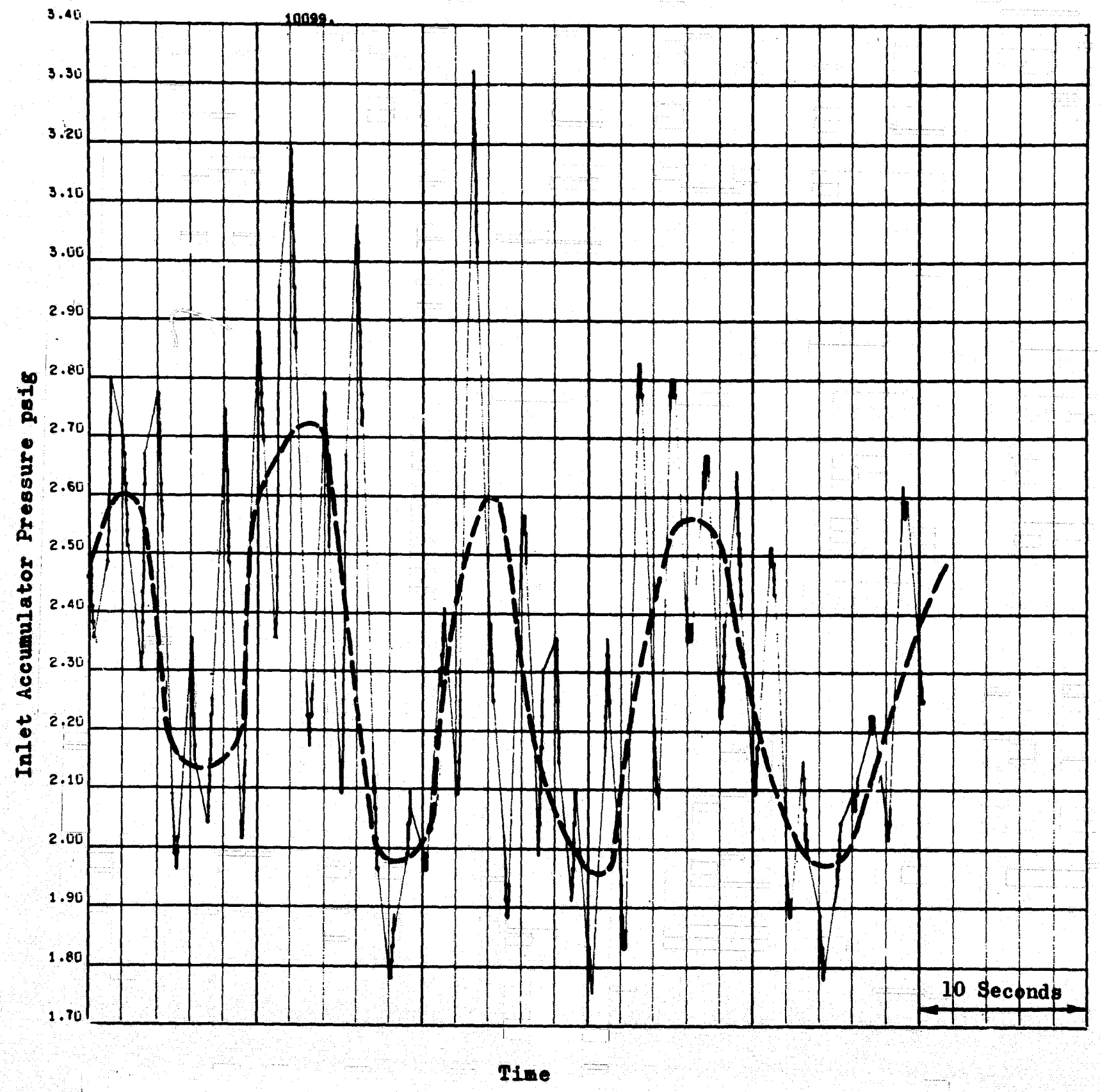

Figure 88. Pressure at the Inlet of the Accumulator (Evaluation of Accumulator Characteristics for the Oxygen Conditioner Subsystem)

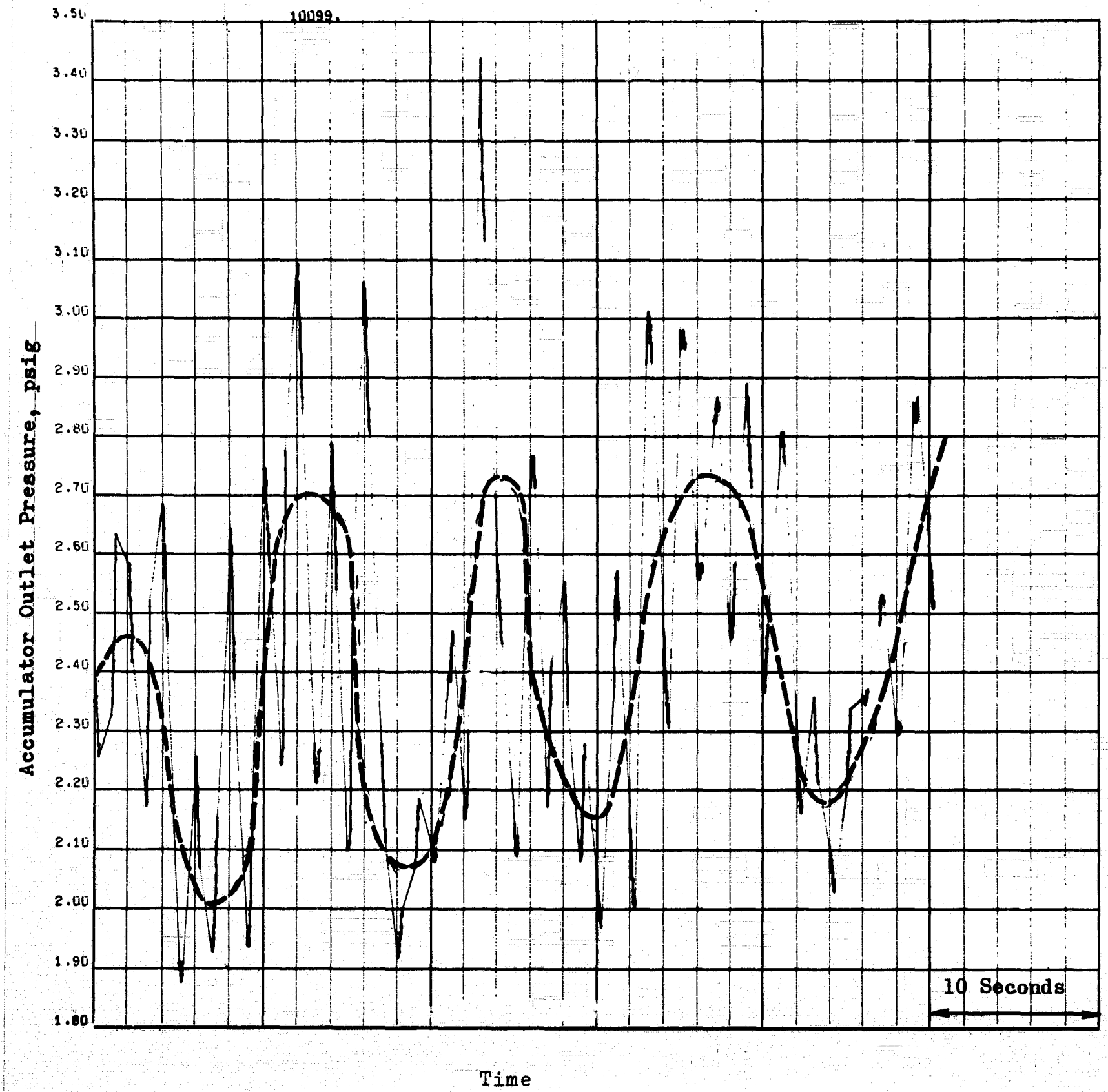

Figure 89. Pressure at the Outlet of the Accumulator (Evaluation of Accumulator Characteristics for the Oxygen Conditioner Subsystem)

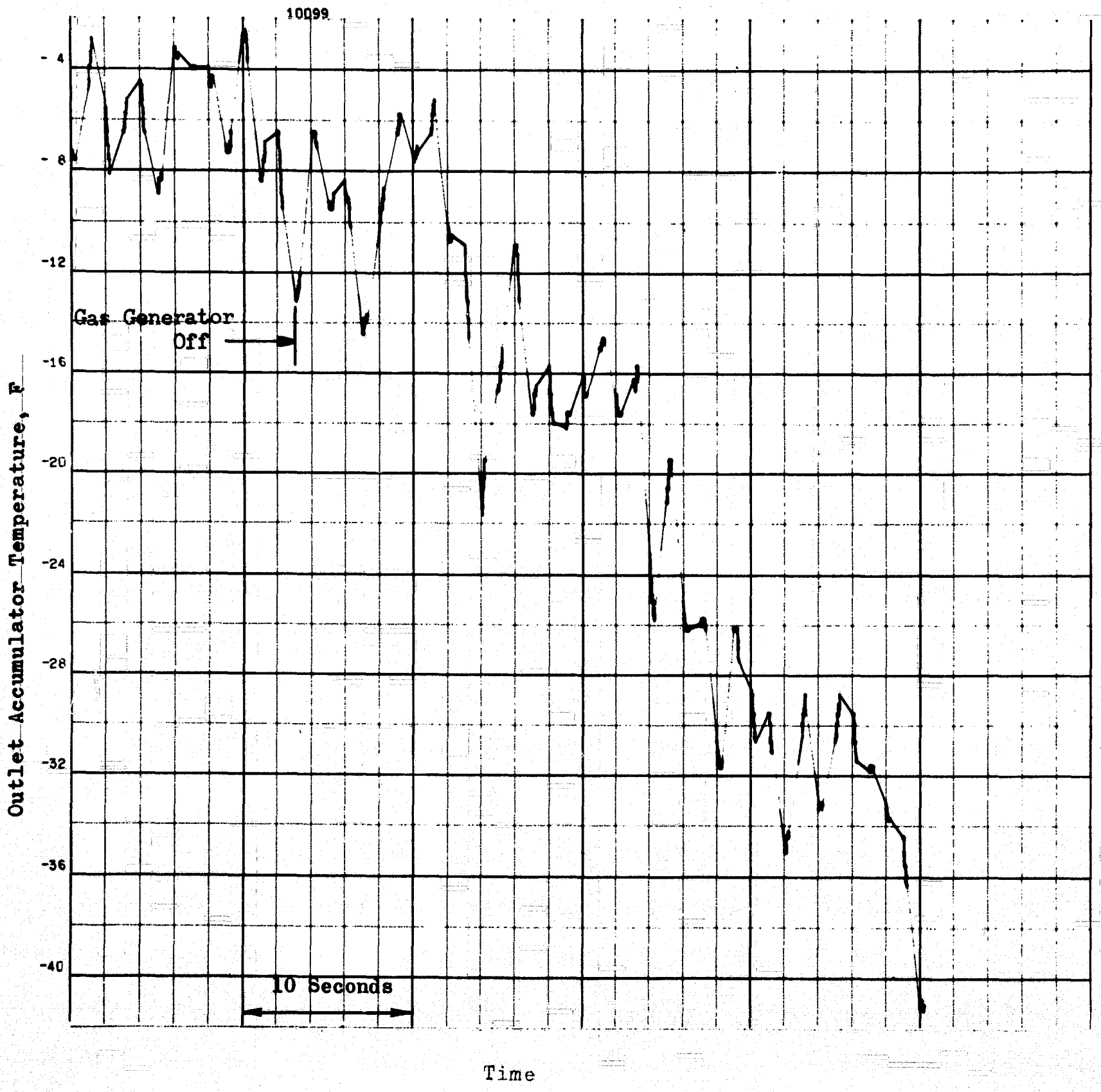

Figure 90. Temperature of the Gas at the Outlet of the Accumulator (With the Decay Caused by a Termination of Gas Generator Operation-Accumulator Characteristics for the Oxygen Conditioner Subsystem)

Two oscillation frequencies are apparent. Also, the slow frequency oscillation appears in the tankage ullage pressure. Comparison of the ullage pressure (Fig. 86) with the pressure at the inlet of the heat exchanger (Fig. 87) shows the pressure at the heat exchanger inlet frequency spikes to values greater than the ullage pressure. Therefore, it was concluded that these spikes caused a backflow into the liquid oxygen ullage, creating the previously discussed slow oscillations. The flow from the heat exchanger into the accumulator remained positive because of the higher pressure in the heat exchanger as can be seen from Fig. 88 and 89.

Comparison of the cycle amplitudes for inlet pressures with the accumulator outlet pressure (PAI and PHXIN with PA0) shows that the accumulator attenuates the pressure oscillation by approximately 0.05 psig or 10 to 15 percent.

Figures 91 and 92 give the inlet (PAI) and outlet (PA0) pressure traces for the liquid oxygen countercurrent heat exchanger with one-fourth of the original exchanger area. Comparison of these figures with the previous ones shows a lack of consistency as variables such as flow direction and heat exchanger area are changed. In this case the high frequency oscillation is at 2.3 cps, and the accumulator almost completely attenuates this fluctuation, leaving only the low frequency oscillation.

Experimental Results for Hydrogen Accumulator. Boiling instability for the hydrogen conditioning system was very similar to that encountered on the oxygen conditioning system; a low frequency of approximately 0.3 cps with an amplitude variation of near ±0.8 psi was predominant. A faster instability of approximately 2 cps with perturbations of approximately 0.4 psi was again partially damped by the 4000-in.^{3} accumulator. The inlet temperature perturbation of ±20 F was damped to ±7 F at the outlet.

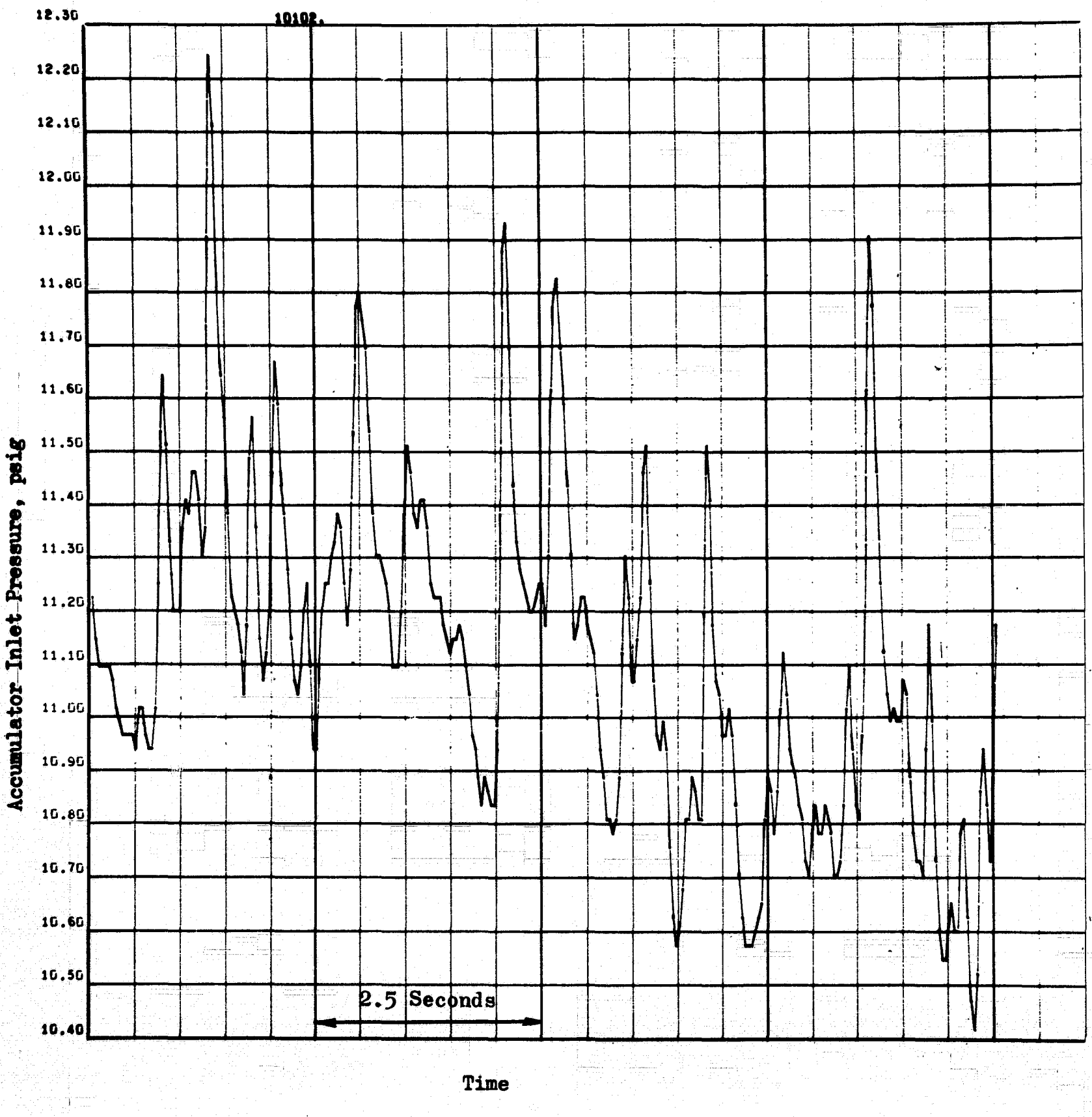

Figure 91. Pressure at the Inlet of the Accumulator, Evaluation of Accumulator Characteristics for the Oxygen Conditioner Subsystem (Heat Exchanger Area Reduced to 1/4 of Original)

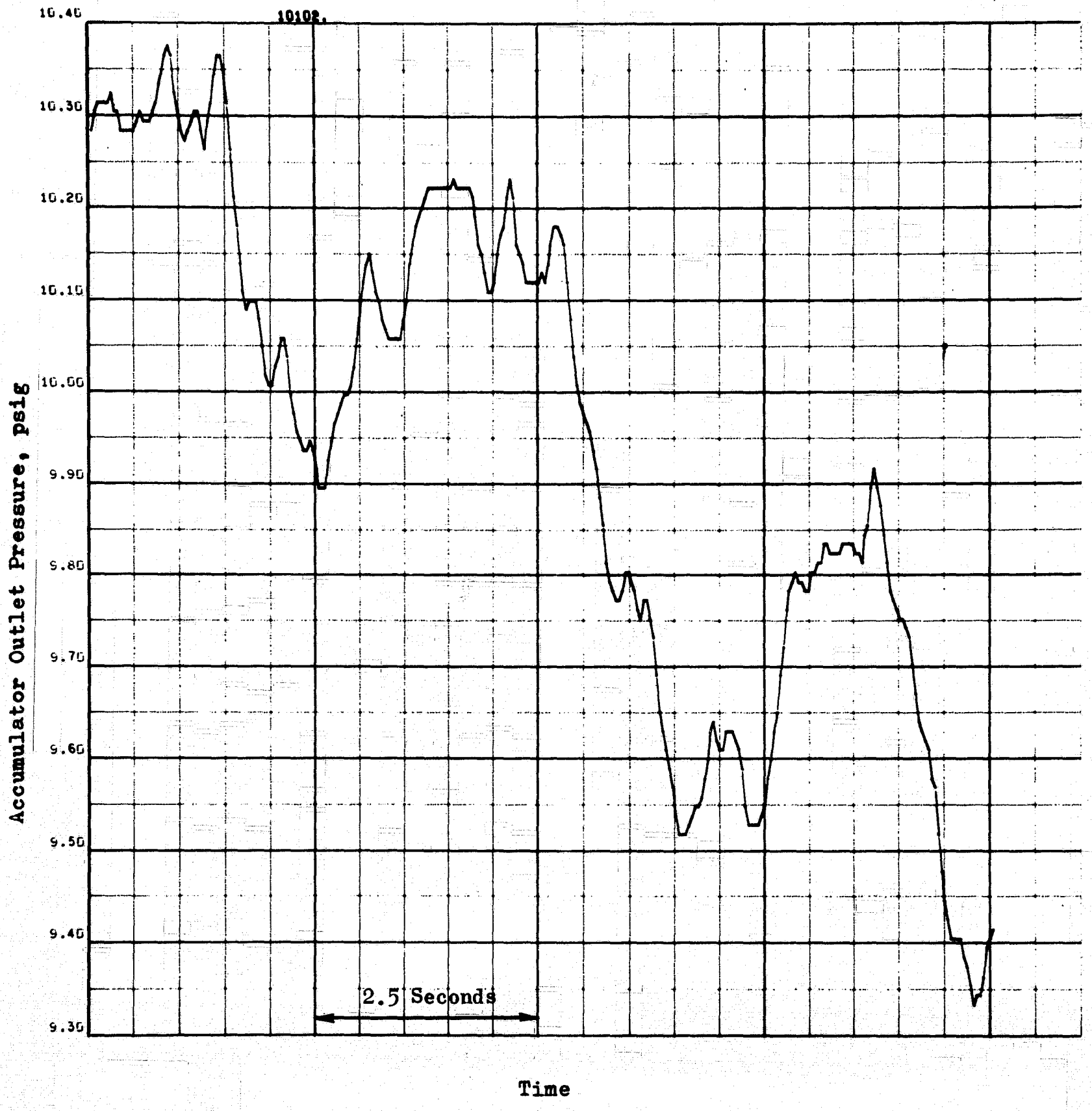

Figure 92. Pressure at the Outlet of the Accumulator, Evaluation of Accumulator Characteristics for the Oxygen Conditioner Subsystem (Heat Exchanger Area Reduced to 1/4 of Original)

The primary cause of the major low frequency instability seems to be caused by two-phase flow or perhaps a vapor slug entering the bottom of the heat exchanger.

The accumulators used for the experiments, 700 in.^{3} for the oxygen side and 4000 in.^{3} for the hydrogen side, were sufficiently large to attenuate the high-frequency (2.3 cps) pressure and temperature perturbations produced by the flow through the heat exchanger. Lower frequency oscillations (0.5 cps) caused by an interaction between the liquid oxygen supply dewar and the heat exchanger were not attenuated. An analysis of the behavior showed that the system could be successfully modeled, and that the oxygen accumulator volume would have to be increased by a factor of about five to attenuate the low frequencies oscillations. This increase was not made; the control system was to be used, instead, to eliminate these perturbations.

Both Propellant Systems (Oxygen and Hydrogen) Run Concurrently

The overall objective of this task was to achieve automatic and concurrent operation of both propellant conditioner systems. This was to be achieved in two major steps; (1) connection of the gas generators to the accumulators to achieve propellant feedback, and (2) installation and use of the control loops (pressure and temperature) to achieve automatic control (Fig. 93).

Experimental Effort. Each system was operated individually in the steady-state mode before initiating the closed-flow test. During these experiments the gas generator fuel and oxidizer valves were opened separately, and the propellant feed pressure to these valves was adjusted separately during the run to give the desired chamber pressure and temperature. The

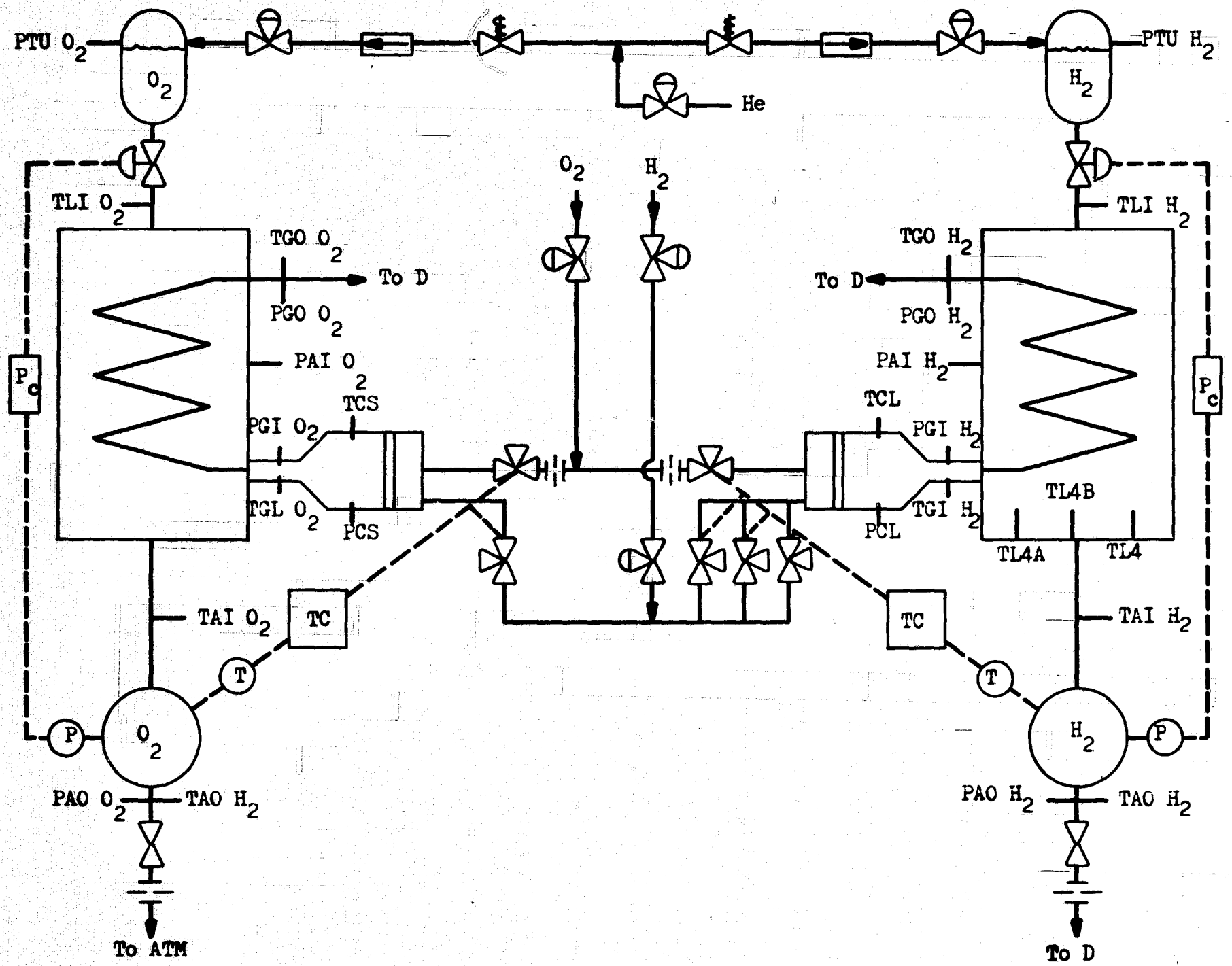

Figure 93. Facility and System Schematic for Tests With Both Propellant Conditioner Subsystems Run Concurrently and the Control Systems Activated

feed pressures were somewhat higher than nominal to offset the increased pressure drops caused by ambient conditioning requirements. Because of uneven pressure drops, propellant inlet pressures sometimes differed by several psi. Thus, before simultaneous operation of the gas generators could be initiated, it was necessary to (1) open oxidizer and fuel valves simultaneously with the same electrical signal, (2) feed both gas generators with equal (5 psig) pressure propellants, and (3) reduce pressure drop through the hydrogen side.

Feeding both gas generators with identical pressures necessitated installing balancing orifices on the oxidizer inlets, which was a trial-and-error procedure. The pressure drop on the large gas generator was reduced by installing a third valve to the fuel side and doubling the injector face area. The small gas generator injector face area was also doubled. However, the pressure drops between valve inlets and the chamber for both gas generators still varied from 6 to 8 psig. This was high in view of the limited driving pressure available.

After the technique of simultaneous gas generator operation was mastered, effort was directed to manual concurrent operation of both systems. Pressure control in the system was achieved by controlling the ullage pressures with a helium supply controlled by two regulators in series. Temperature control was achieved manually by calling for on-off operation. A major problem became apparent during this mode of operation. To prevent water from freezing in the hot-gas coil, the propellant flowrate had to be reduced, which lowered the nominal thrustor rating from 20 to 10 pounds. During pulse mode operation of the hydrogen side, the heat exchanger tube cools during the off cycle; at the beginning of the start cycle, the outlet hot-gas temperature spikes below 32 F. Thus, it was apparent that the gas generators should be overdesigned such that they may be capable of supplying

approximately 50 percent more than the maximum heat load. One method of minimizing the water freezing hazard was investigated on the hydrogen side, where the problem was most acute. This constituted operating the heat exchanger in a cocurrent flow configuration, since the tube wall temperatures are higher for cocurrent flow.

Another problem which became apparent when simulating thrustor pulsing was the increase in system pressure when both the thrustor and liquid inlet valves were closed. The increase in pressure was attributed to vaporization of the trapped liquid in the line between the inlet valve and the heat exchanger. The relief valves located on the accumulator proved to be inadequate because of their low capacity, leakage, and inconsistent cracking pressure. The solution to this problem involved removing the relief valves, minimizing the volume of trapped liquid, and wiring the control circuit so that the inlet valves would open when the thrustor valve closed. Thus, the system pressure stabilized at the ullage pressure in the off mode. This proved to be satisfactory as long as the ullage pressure was relatively constant.

At this time the first set of pressure and temperature controls was received. The oxygen system response was first checked and optimized with the controls (Fig. 94), then the controls were transferred to the hydrogen side for a response check. Initially, pressure control checkout proved to be difficult because of the shift in setpoint from run to run. Eventually, a technique of adjusting the setpoint in the 4- to 5-psig range prior to each run was developed.

It was considerably easier to adjust the temperature controller in the range of 0 to -50 F, and it was noted that this setpoint did not vary with time. Cathode ray tube (CRT) plots of these experiments are not presented in the text because they would be redundant to those presented for the final experiment.

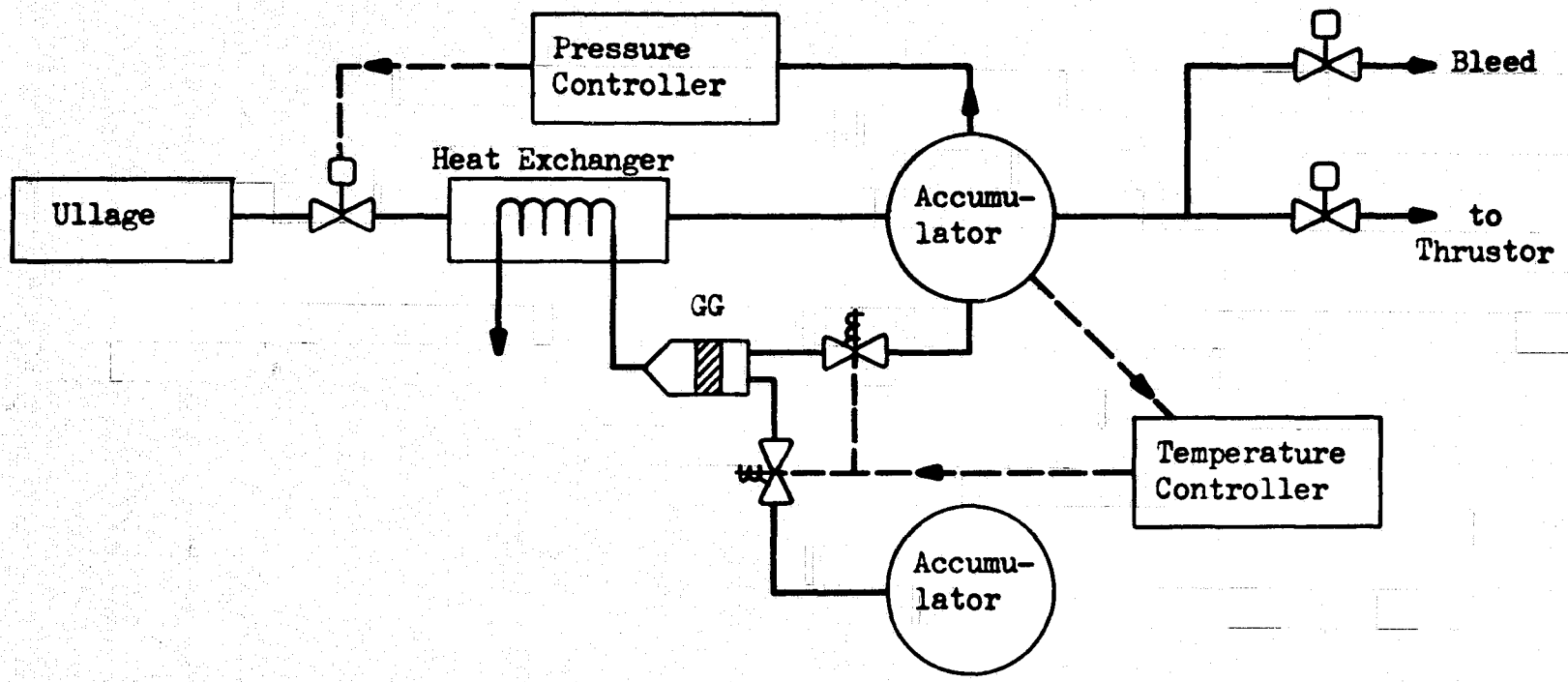

Temperature Controller. The gas generator valves open when the accumulator temperature is below a certain level and close when the temperature exceeds a given value.

Pressure Controller. Operates the ullage tank valve within given limits to control accumulator pressure.

Operation	Bleed Valve	Thrustor Valve	Pressure Controller
	Open	Open	In operation
	Open	Closed	In operation
	Closed	Open	In operation
	Closed	Closed	Not operating and ullage valve held open

Figure 94. The Control System Operation for One Side of the Conditioner

Conclusions and Summary. The major objective of achieving automatic and concurrent operation of both propellant systems was successfully achieved. The most difficult step in this task was the connection of the gas generators with the accumulators, which involved a substantial orificing effort to ensure proper flow control to the gas generators. Freezing of ice in the hydrogen heat exchanger was circumvented by changing the exchanger operation from countercurrent to cocurrent. A better solution for future operation would be to oversize the gas generator and operate in a pulse mode.

A desired increase in the outlet conditioner temperature could not be achieved at the original design flowrates because of a limited hydrogen heat exchanger capacity. Therefore, the flowrates were adjusted to fit the capacity of this limiting component.

Pressure oscillations during steady operation were measured throughout the system. The low frequency oscillation (at approximately 0.08 cycles per second) was probably caused by vaporization of liquid in the line connecting the heat exchanger to the tankage. This oscillation could be attenuated by the on-off control system. A higher frequency oscillation at approximately 0.4 cycles per second was also measured downstream of the heat exchanger. The accumulator acted to attenuate this oscillation as predicted by system modeling analysis.

When the upstream on-off valves were closed, the propellant trapped in the heat exchanger would expand and cause the accumulator pressure to increase. The pressure relief valves did not function properly, so the control circuit was modified to open the upstream on-off valves in the absence of thrustor demand. This allowed the system to come to tank pressure.

COMPUTER MODELING

Predicted Gas Generator Performance

The thrustor computer model was used to predict the transient behavior of the gas generator prior to the actual experiment. Because the gas generators were previously designed for a nominal 200 R feed, it was specifically desired to determine the effect on nominal design by feeding with ambient propellants. The selected internal parameters were based on the thrustor experimental studies, which indicated that 1/2 inch of catalyst bed with a 1/4-inch-long mixing section of 1/16-inch stainless-steel bearings would approximate optimum performance. An example of the transient response is given in Fig.95 , 96, and 97 for the nominal inlet pressure of 17 psia. The following was concluded from several computer runs such as this:

1. The overall mixture ratio would be reduced to about 0.8 to account for the inlet temperature of 460 instead of 200 R.

2. The use of ambient propellants caused an uneven increase in pressure drop. To maintain the nominal 10-psia chamber pressure, the fuel and oxidizer inlet pressures to the large gas generator had to be increased to 24 and 19 psia, respectively. To prevent H_2 flow into the oxidizer line, an orifice was placed in the oxidizer line so that balanced fuel and oxidizer pressures could be used. The analysis for the small gas generator showed that the inlet pressures should be near 18 psia with a similar balancing orifice in the 0_2 feed.

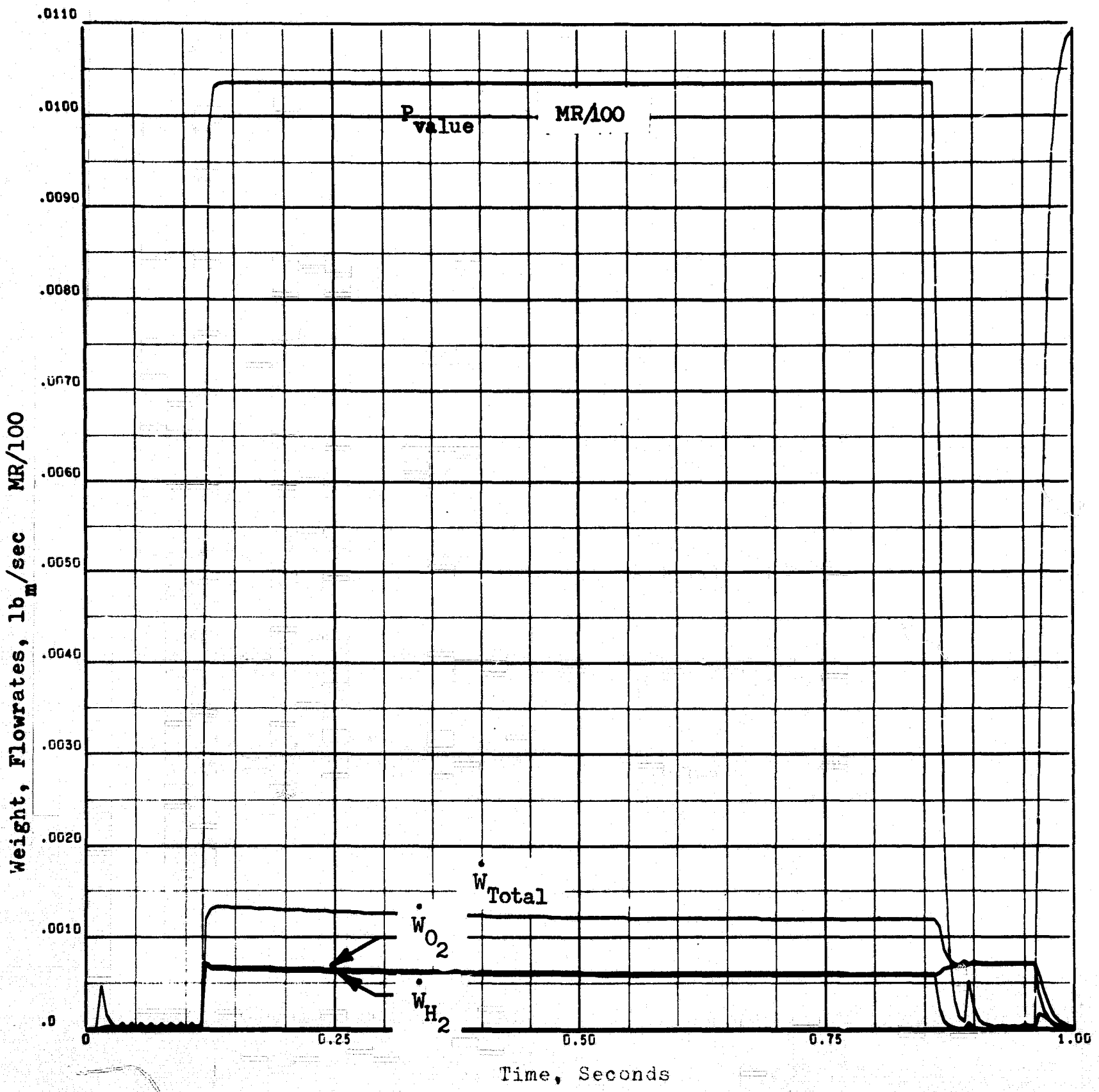

Figure 95. Thrustor Computer Model Results for Pressure Response of the Oxygen Gas Generator Using Ambient Propellants

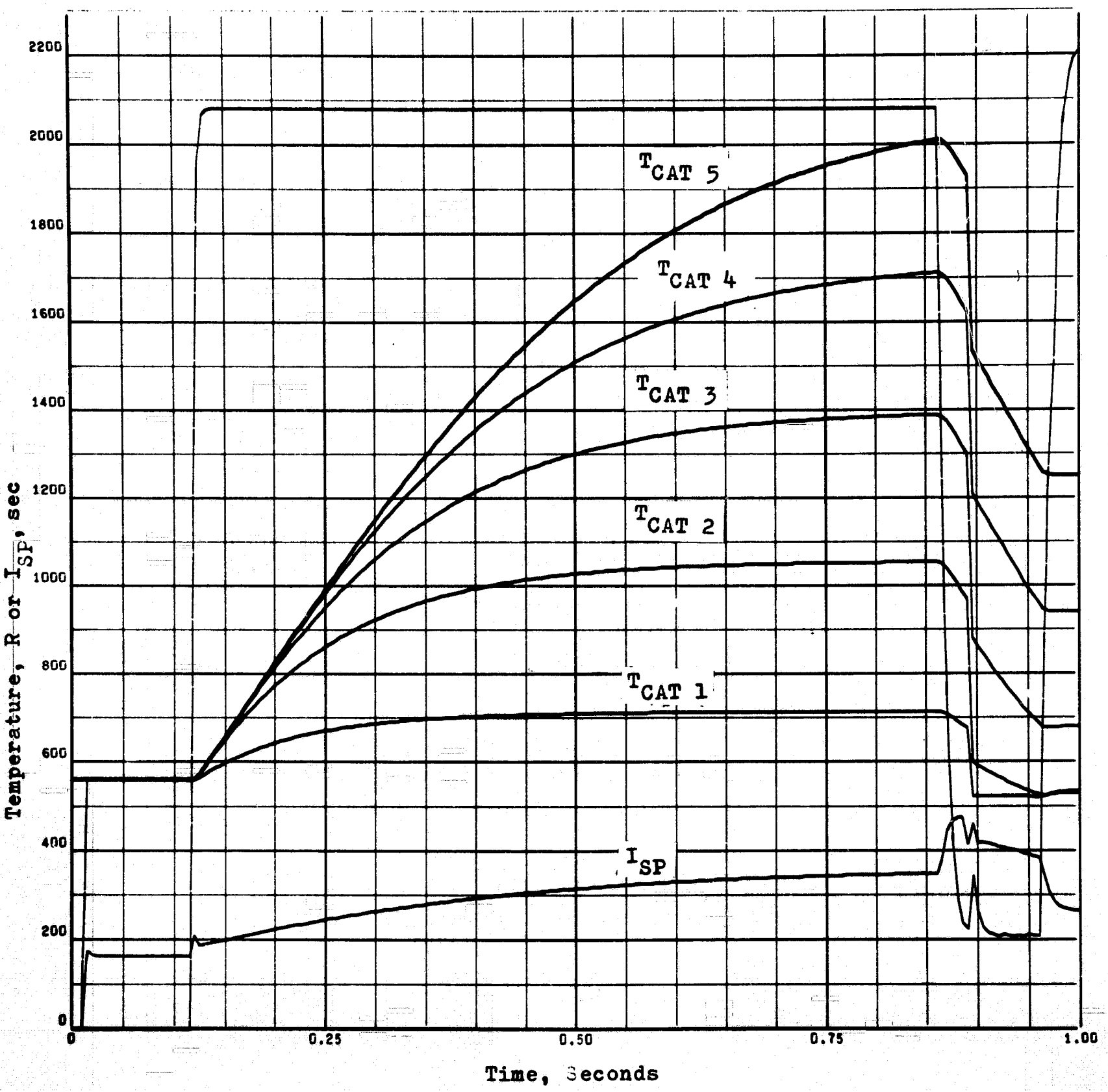

Figure 96. Thrustor Computer Model Results for Temperature Response of the Oxygen Gas Generator Using Ambient Propellants

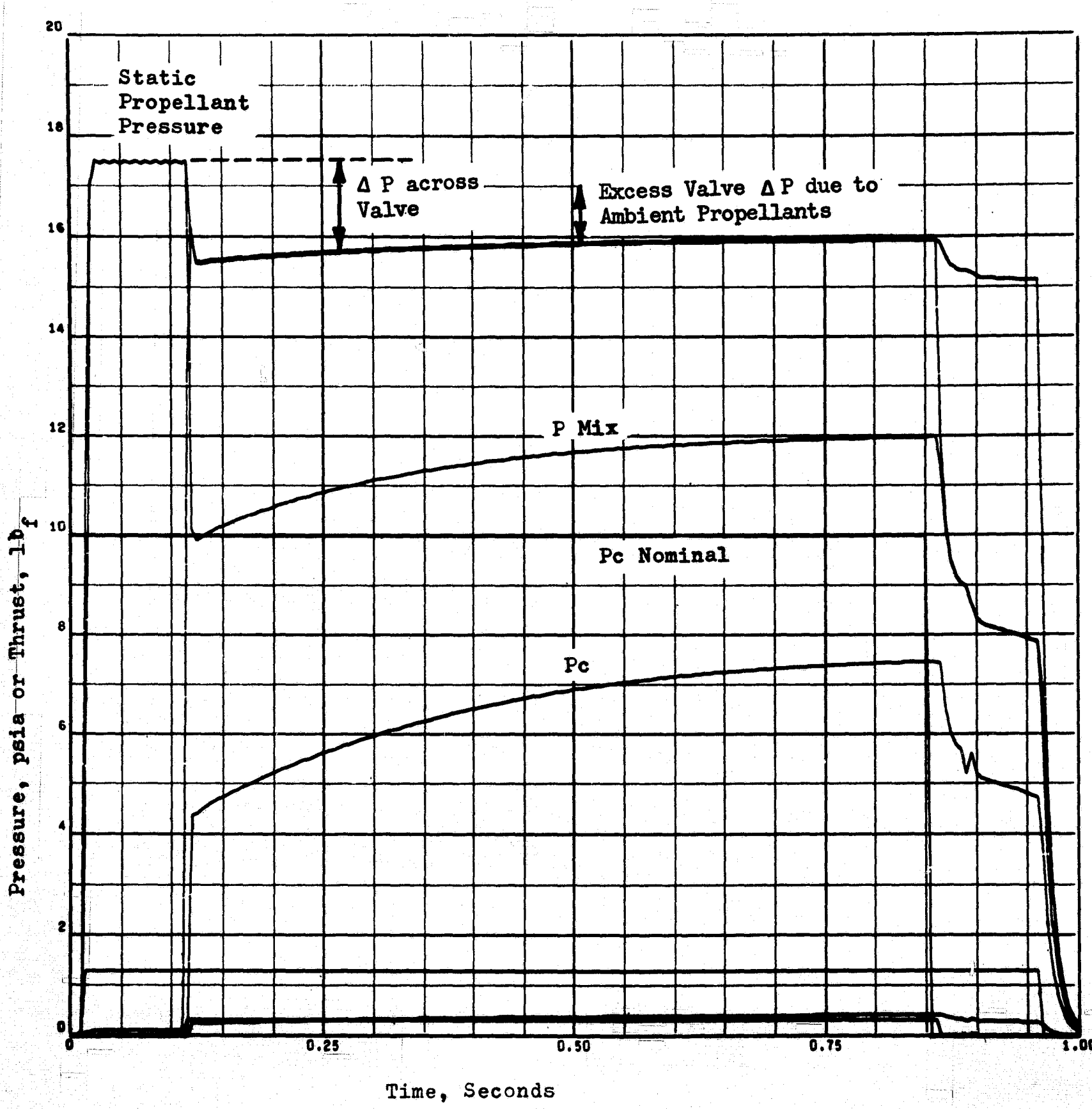

Figure 97. Thrustor Computer Model Results for Flowrate Response of the Oxygen Gas Generator Using Ambient Propellants

Heat Exchanger Modeling

In an effort to determine the hot-gas heat transfer coefficient, the single-node model in the system program was expanded to a five-node model so that calculated wall and gas responses for various heat transfer coefficients could be compared to the experimental characteristics. The nodal schematic depicted below shows the basis for the mathematical model.

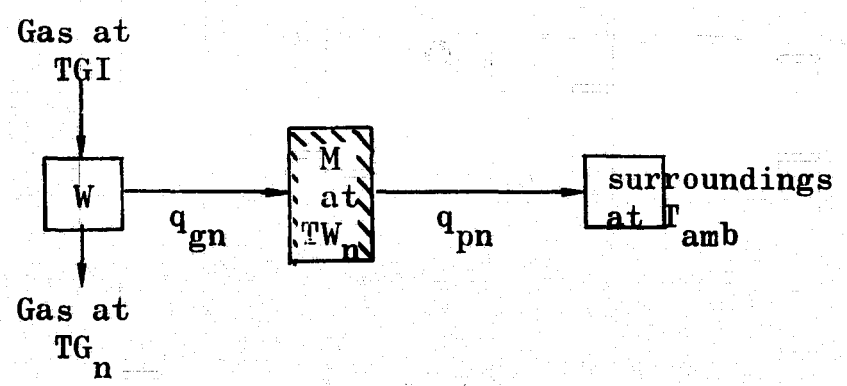

$$q_{gn} = h_{gn} A (TG_n - TW_n) \quad (20)$$

$$q_{pn} = h_{amb} A (TW_n - T_{amb}) \quad (21)$$

where

$$q_{gl} = h_g A (TG_1 - TW_1) \quad (22)$$

$$q_{pl} = h_{amb} A (TW_1 - T_{amb}) \quad (23)$$

A heat balance on the wall gives

$$MC_p \frac{\partial TW_n}{\partial \theta} = q_{gl} - q_{pl} \quad (24)$$

and a heat balance on the hot gas node gives

$$WC_p \frac{TG_n}{\partial \theta} = \dot{w}_i C_p TGI - \dot{w}_o C_p TG_n - q_{pn} \quad (25)$$

where

$$W = \frac{MW}{R}\,\frac{PV}{T_{gn}} \tag{26}$$

Ignoring the change in temperature of the hot gas $\gamma TG_n/\partial\theta$, remaining in the node, and solving for TG_n gives

$$TG_n = \frac{\dot{w}_i\, C_p\, TGI + h_{gn}\, A\, TW_n}{\dot{w}_o\, C_p + h_{gn}\, A} \tag{27}$$

The solution for the nodal wall and gas temperatures was obtained by simultaneous solution of Eq. 20 through 26 using the Midas technique (Ref. 12). However, the computer time required was excessive until Eq. 25 was replaced by Eq. 27. Figure 98 gives the calculated results for the following input paramters:

Heat Transfer Area in the Node, A	0.20 sq ft
Mass of Wall in the Node, M	0.312 pounds
Heat Capacity of Wall Mass, C_p	0.135 Btu/lb-F
Heat Capacity of Hot Gas, C_p	2.23 Btu/lb-F
Heat Transfer Coefficient to Ambient, h	6.75 Btu/ft^2-hr-F*
Flowrate of Hot Gas, $\dot{w}$	0.005 lb/sec
Gas Inlet Temperature, TGI	f (θ) as shown in Fig.

The hot-gas heat transfer coefficient was varied from 70 to 600 Btu/hr-ft^2-R. The higher heat transfer coefficients gave a much faster TWI response and a slow TGO response confirming the experimental data. A low heat transfer

*Calculated from the steady-state data in Fig. 98.

coefficient causes the heat distribution to change only slightly. Thus, the disagreement between experiment and theory was attributed to the uncertainty in estimating the hot-gas flowrate. The hot-gas flowrate or heat capacity was obviously underestimated.

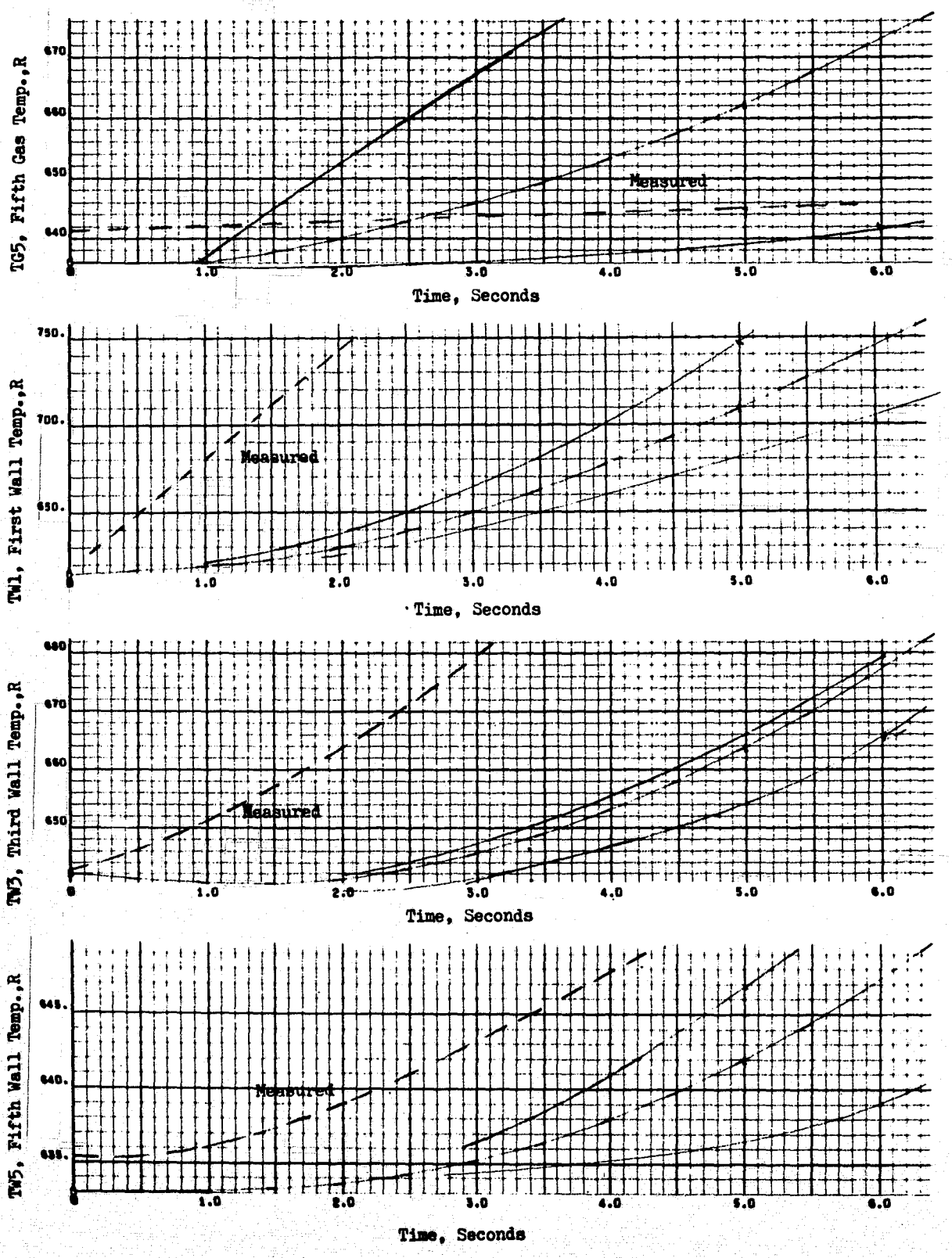

Figure 98. Computer Model Results Using the Midas Technique (Ref. 12) and Experimental Results (Heat Exchanger Wall Temperature and Gas Outlet Temperature Responses, Thermocouple Locations as Defined in Fig. 85)

Accumulator Modeling

The model was built on preliminary conclusions reached by analyzing the experimental data as follows:

1. The driving force for the pressure and temperature perturbations was the heat exchanger
2. The temperature and pressure perturbations were in phase, i.e., when the pressure was a maximum, the temperature was also a maximum.
3. Flow from the heat exchanger to the accumulator was continuous while the flow from the LOX dewar oscillated both positive and negative.

Based upon these tentative conclusions, the following schematic was constructed:

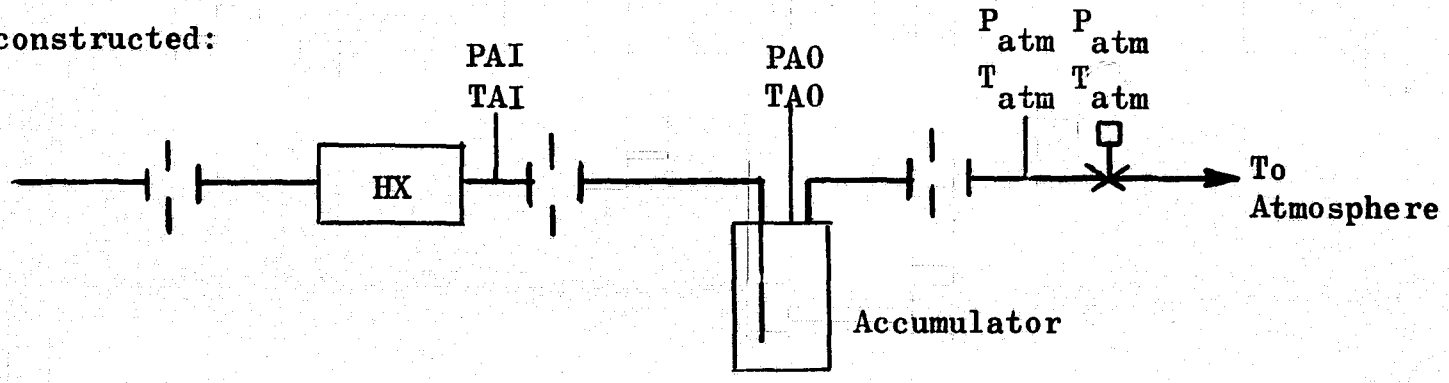

The temperature and pressure at the outlet of the heat exchanger were assumed to be the independent variables:

$$PAI = K_1 + K_2 \sin K_3\theta \qquad (28)$$

or

$$PAI = K_b + (K_7 + K_8 \sin K_9\theta) \sin K_{10}\theta \tag{29}$$

and

$$TAI = K_4 + K_5 \sin K_3\theta \tag{30}$$

where K_n is a constant.

The flowrate into the accumulator from the heat exchanger was considered as a perturbation from nominal across the orifice:

$$\dot{w}_{in}^{\ 2} = \dot{w}_{nom}^{\ 2} \frac{PAI\ TAI_{nom}}{PAI_{nom}\ TAI} \left(\frac{PAI - PA0}{\Delta PI_{nom}}\right) \tag{31}$$

where

$$\Delta PI_{nom} = PAI_{nom} - PA0_{nom} \tag{32}$$

The flow from the accumulator was described by a similar equation:

$$\dot{w}_{out} = \dot{w}_{nom} \frac{PA0}{PA0_{nom}} \left(\frac{TA0_{nom}}{TA0}\right) \left(\frac{PA0 - P_{atm}}{\Delta P0_{nom}}\right) \tag{33}$$

where

$$\Delta P\ ACC_{nom} = PA0_{nom} - P_{atm} \tag{34}$$

The next step is to write the differential equations describing instantaneous heat and material balances and instantaneous pressure from the ideal gas law.

Material balance:

$$\frac{\partial W}{\partial \theta} = \dot{w}_i - \dot{w}_o \tag{35}$$

Heat balance:

$$C_p \frac{\partial (W\ TA0)}{\partial \theta} = \dot{w}_i\ TAI\ C_p - \dot{w}_o\ TA0\ C_p \tag{36}$$

Rearranging gives:

$$\frac{\partial TA0}{\partial \theta} = \left[\dot{w}_i\ TAI - TA0\ \left(\dot{w}_o + \frac{\partial W}{\partial \theta}\right)\right] \frac{1}{W} \tag{37}$$

Ideal gas law:

$$\frac{\partial PA0}{\partial \theta} = \frac{R}{V\ MW} \frac{\partial (W\ TA0)}{\partial \theta} = \frac{R}{V\ MW} \left[\dot{w}_i\ TAI - \dot{w}_o\ TA0\right] \tag{38}$$

or

$$\frac{\partial PA0}{\partial \theta} = \frac{R}{V\ MW} \left[TA0 \frac{\partial W}{\partial \theta} + \frac{W \partial\ TA0}{\partial \theta}\right] \tag{39}$$

or

$$\frac{\partial (PA0)}{\partial \theta} = \frac{R\ (TA0)}{V\ MW} \frac{\partial W}{\partial \theta} + \frac{PA0}{TA0} \frac{\partial (TA0)}{\partial \theta} \tag{40}$$

These equations were simultaneously integrated using the Midas technique, and a typical output is given in Fig. 99 through 102. The input data conform fairly closely to the actual experimental data previously presented. The accumulator volume was set at 700 in.^{3}, closely approximating the oxygen accumulator. The input pressure perturbation of ± 0.5 psi was attenuated to only 0.42 psi, while the temperature perturbation of ± 10 F was attenuated to approximately ± 5 F. Perhaps the most important dependent variable is the flowrate out of the accumulator, which cycles at 0.5 cps, because it controls the mixture ratio.

Each parameter in this accumulator model was changed, while holding all others constant, to determine the effect of that parameter. First, the frequency of the boiling instability was increased to 2.5 cps, approximating that of the previously mentioned countercurrent experimental run. The pressure perturbation of ± 0.5 psi was attenuated to ± 0.13 psia, while the temperature perturbation of ± 10 F was damped to ± 3 F. It was concluded that the accumulator can adequately damp high frequency perturbations and will not attenuate those at low frequencies.

The second parameter to be varied was the accumulator volume. The frequency was changed back to the slower frequency of 0.466 cps. The results summarized below:

$\Delta P_{HX} = \pm 0.5$ psi

$\Delta T_{HX} = \pm 10$ F

Volume, in.^{3}	ΔP ACC, psi	ΔT ACC, F
100	± 0.50	± 9
700	± 0.42	± 5
7000	± 0.07	± 0.3

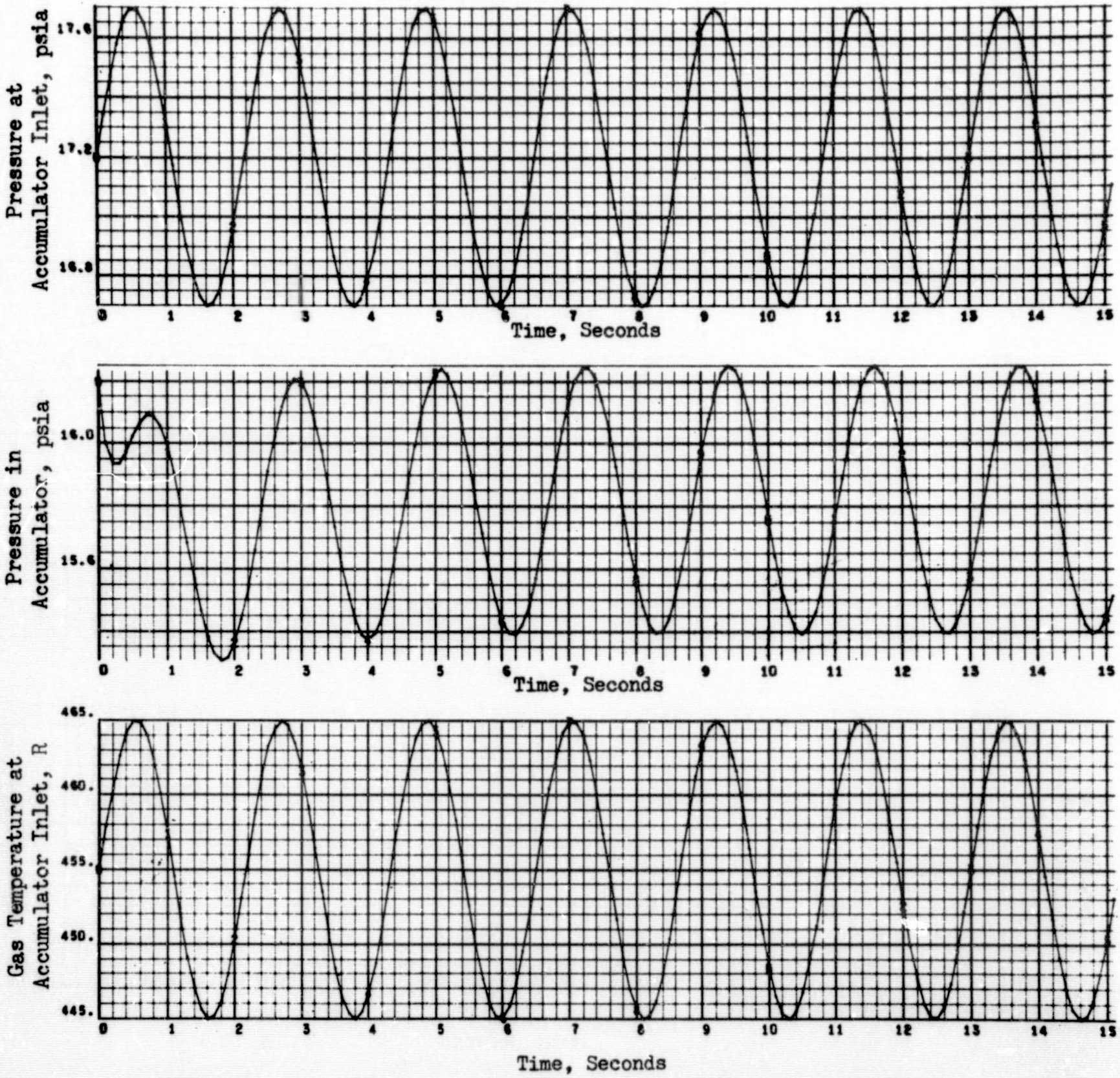

Figure 99. Accumulator Computer Model Results Using the Midas Technique (Ref. 12), Inlet Gas Temperature and Pressure Characteristics and Accumulator Pressure Response

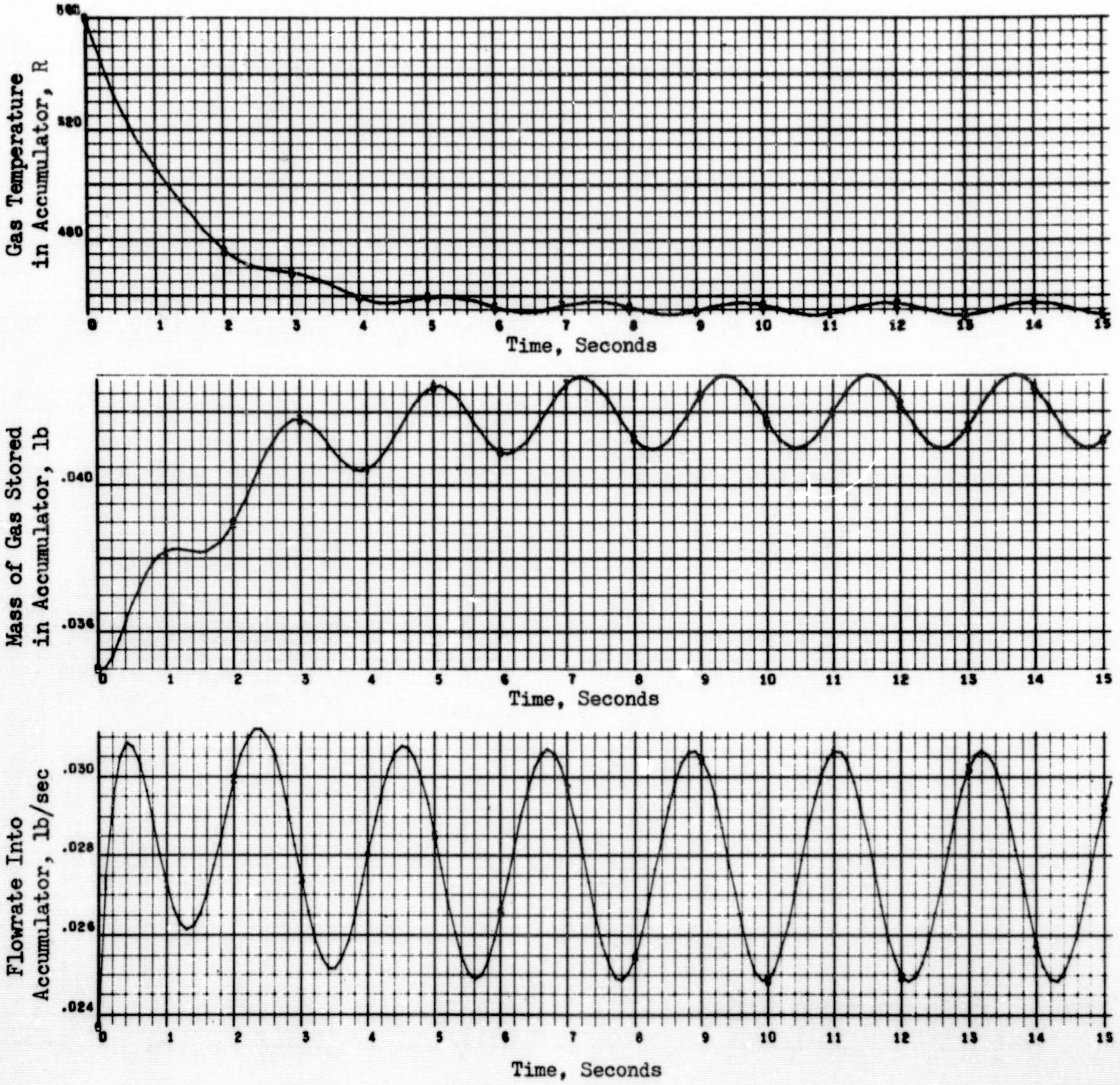

Figure 100. Accumulator Computer Model Results Using the Midas Technique (Ref. 12), Flowrate Into Accumulator, Gas Temperature in the Accumulator, and Mass of Gas Stored in Accumulator

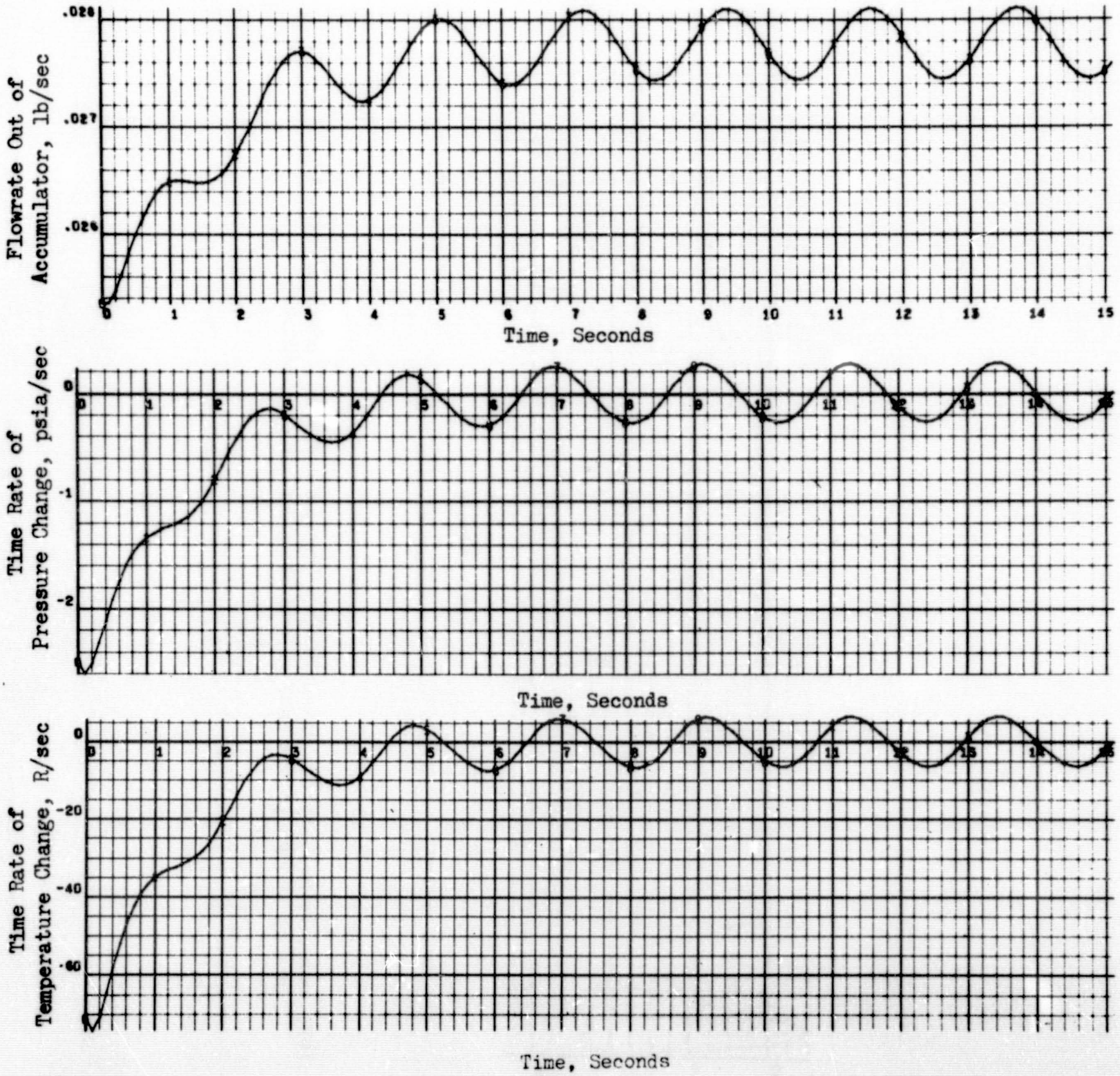

Figure 101. Accumulator Computer Model Results Using the Midas Technique (Ref. 12), Rate of Change in Accumulator Pressure and Temperature, and Flowrate Out of the Accumulator

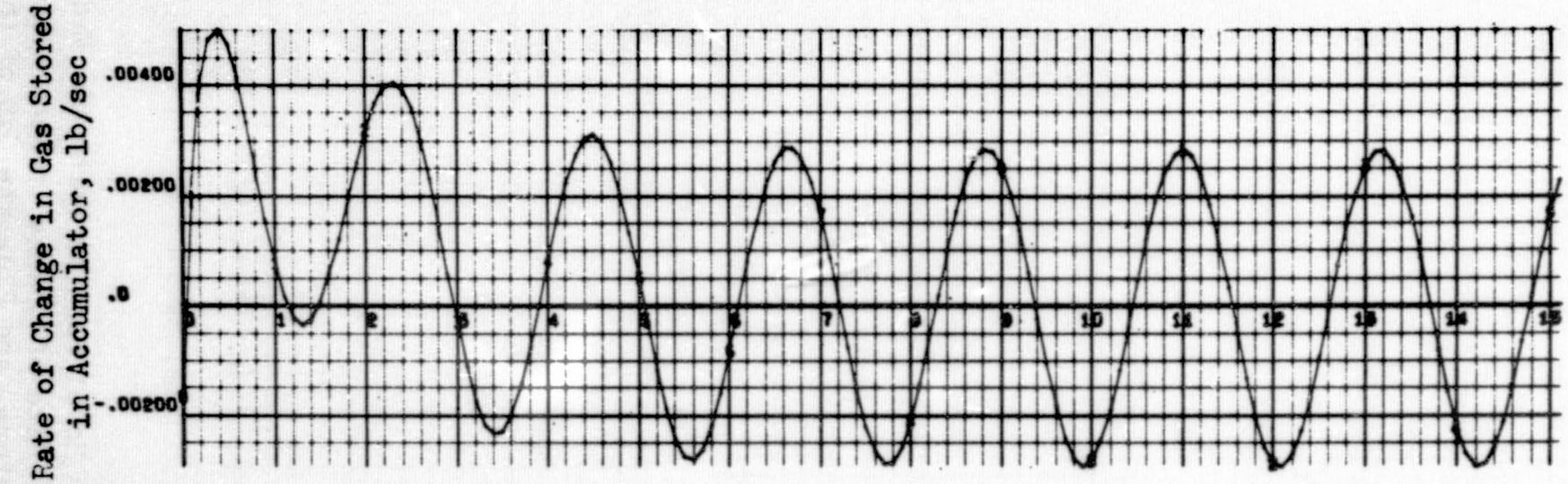

Figure 102. Accumulator Computor Model Results Using the Midas Technique (Ref. 12)
Rate of Change in the Mass of Gas Stored in the Accumulator

These results rather conclusively show that it is impractical to attempt to damp the low boiling frequencies. It was also realized at this time that the frequency response of the control circuit was much faster than the low boiling frequencies and therefore, would act to attenuate these low frequencies.

The accumulator mathematical model was adapted to the liquid hydrogen data. No significant conclusions deviating from those found for the liquid oxygen side were noted.

A simplified mathematical representation of the relationship between accumulator volume and the amplitude of the temperature and pressure oscillations can be obtained in the following manner, assuming (1) ideal gas, (2) PV = n RT, and (3) sonic flow at both the inlet and exit of the accumulator.

The accumulator can be shown as

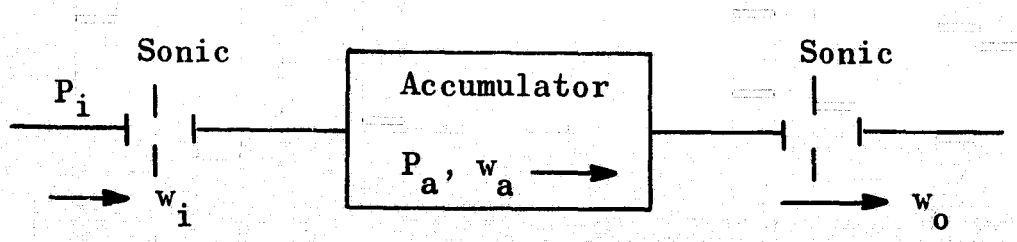

where

$$\dot{w}_o = K_1 \frac{P_a}{\sqrt{T_a}}$$

$$\dot{w}_i = K_2 \frac{P_2}{\sqrt{T_i}}$$

for a perfect gas

$$\frac{P_a V_a}{R T_a} = \int \frac{dw_a}{dt} \, dt$$

From a conservation of mass

$$\frac{dw_a}{dt} = \dot{w}_i - \dot{w}_o$$

The solution of this system of equations assuming constant temperature can be expressed in a Bode plot such that

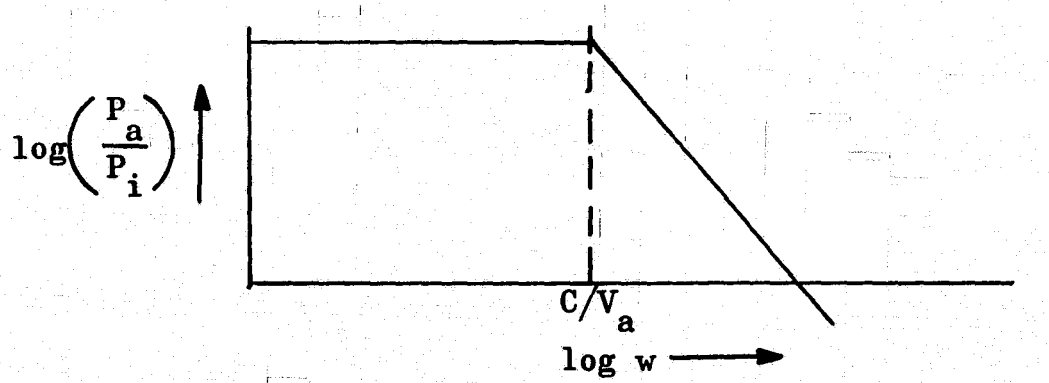

Thus, as the accumulator volume is increased, the attenuation of the pressure oscillations leaving the accumulator will be increased for a given frequency. The accumulators used in the experiments were of sufficient size to attenuate the high-frequency pressure oscillations, but had no

effect on low-frequency oscillations. In addition to attenuating the outlet pressure, the phase lag between the input and outlet pressure oscillations is increased such that the lag is 45 degrees at the break point (C/V_a). Consequently, the phase lag at a given frequency can be decreased by increasing the accumulator volume.

RCS DEMONSTRATION

The principal goal of this series of experiments, as well as the project, was to demonstrate the feasibility of an integrated thrustor-conditioner system. This represented the next experimental objective after making the conditioner a completely independent system. The conditioner system had been previously run with the conditioned propellants being bled to the diffuser. The components and flow restriction orifices in the conditioning system were not changed from the previous tests; consequently, the thrustor was operated on the available conditioned fluid. The thrustor used for the feasibility demonstration was the multielement workhorse engine described in the Thrustor Design section.

PROCEDURE AND APPARATUS

EXPERIMENTAL SYSTEM

The final operational integrated thrustor-conditioner apparatus and instrumentation schematic is presented in Fig.103. This system evolved from the separate thrustor and conditioner subsystem tests.

Equipment details for the heat exchangers, accumulators, valves, gas generators, and the workhorse thrustor were given in previous sections. The thrustor flow orifices were sized on the basis of the maximum amount of liquid hydrogen that could be conditioned in the previous tests consistent with a 1500 F catalyst bed temperature and 3500 F chamber temperature. Only the oxygen feed to the gas generators was orificed so that the maximum amount of hot gas could be produced in order to condition the maximum amount of propellants.

Table 18 further defines the instrumentation nomenclature. Three pressure and three temperature measurements were made in each propellant system to define its operating characteristics completely, e.g., heat exchanger inlet and outlet conditions and accumulator outlet or thrustor and gas generator inlet conditions. These data define the dynamic characteristics of propellant vaporization (boiling stability), accumulator temperature, and pressure damping, as well as the control circuit performance. Gas generator-coil dynamics are defined by two temperature measurements, one or two pressure measurements, and a valve signal measurement. From these data, it is possible to calculate the hot-gas flow and the heat exchanger heat load. Thrustor instrumentation was sufficient to allow for the determination of thermal and pneumatic responses.

The deadbands for the temperature and pressure controllers are presented in Table 19. These setpoints were used during the integrated workhorse thrustor-conditoner experiment.

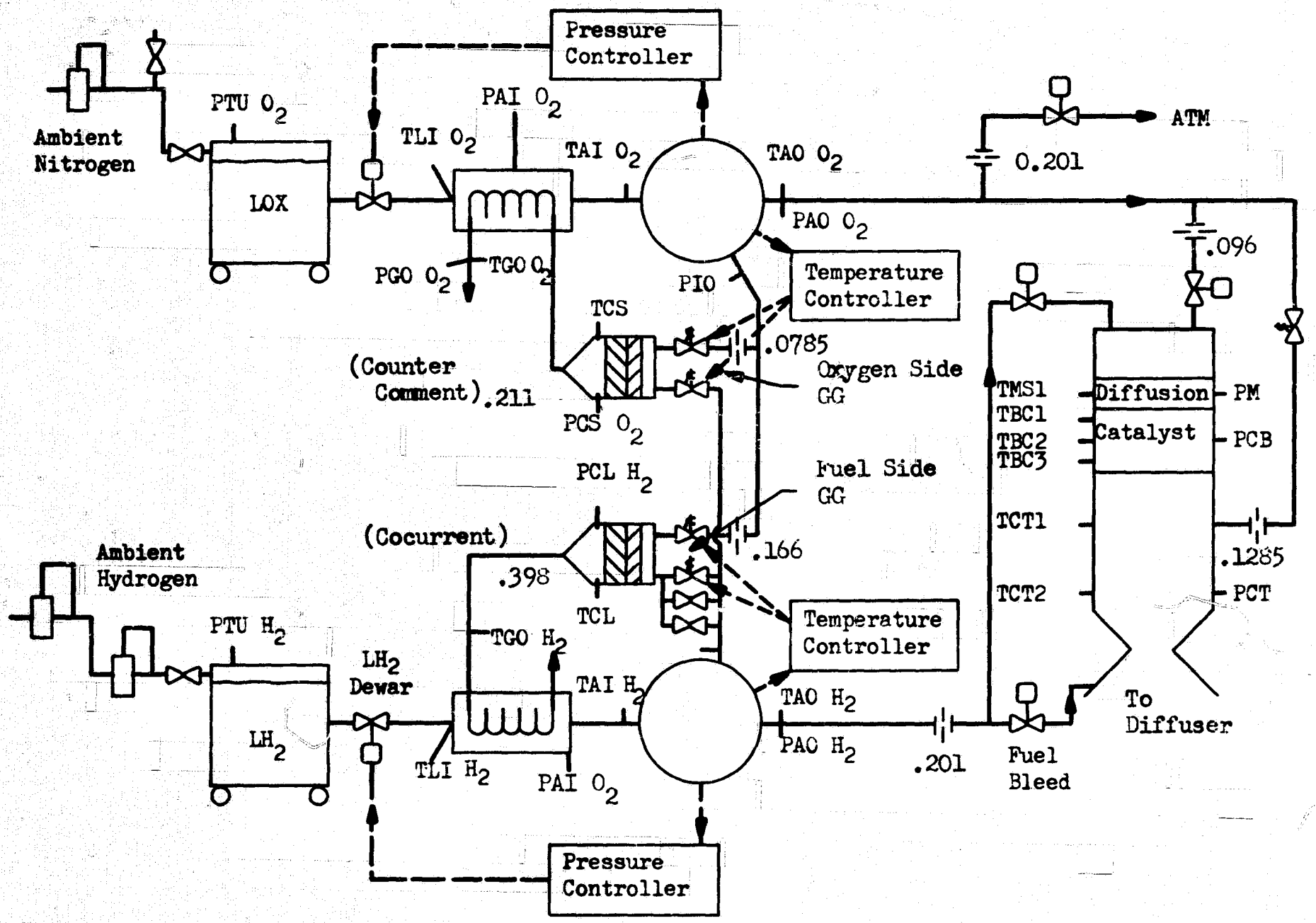

Figure 103. Schematic of Facility and Apparatus for the Integrated Thrustor-Conditioner RCS Demonstration

TABLE 18

IDENTIFICATION FOR THE INTEGRATED THRUSTOR-CONDITIONER SYSTEM EXPERIMENT

296	Oxygen side valve operation	
297	Hydrogen side valve operation	
TL1H2	Temperature of LH_2 at heat exchanger input	Fuel Side
TAIH2	Temperature of accumulator input	
TADH2	Temperature of accumulator output	
TCL	Temperature in large gas generator chamber	
TGOH2	Temperature of hot-gas outlet from coil	
TLI02	Temperature of LOX at heat exchanger input	Oxidizer Side
TAI02	Temperature of accumulator input	
TA002	Temperature of accumulator output	
TCS	Temperature in small gas generator chamber	
TG002	Temperature of hot-gas outlet from coil	
TMS1	Temperature of mixing section in thrustor	Thrustor
TBC1	Temperature of catalyst bed in thrustor	
TBC2	Temperature of catalyst bed in thrustor	
TBC3	Temperature of catalyst bed in thrustor	
TCT1	Chamber temperature in thrustor	
TCT2	Chamber temperature in thrustor	
PTU02	Ullage pressure	Oxidizer Side
PAI02	Accumulator input pressure	
PA002	Accumulator outlet pressure	
PI0	Injection pressure (redundant)	
PCS02	Chamber pressure of small gas generator	
PG002	Outlet hot-gas pressure	
PTUH2	Ullage pressure	Fuel Side
PAIH2	Accumulator input pressure	
PAOH2	Accumulator outlet pressure	
PIF	Injection pressure (redundant)	
PCLH2	Chamber pressure of large gas generator	
PM	Pressure of mixing section	Thrustor
PCB	Catalyst bed pressure	
PCT	Chamber pressure	

TABLE 19

DEADBANDS AND SETPOINTS FOR TEMPERATURE AND PRESSURE CONTROLLERS DURING THE INTEGRATED WORKHORSE THRUSTOR-CONDITIONER EXPERIMENT

Propellant	Pressure Controller			
	On		Off	
	inches of water	psig	inches of water	psig
Oxygen	137	4.95	144	5.20
Hydrogen	133	4.80	139	5.01

Temperature Controller

Propellant	On, F	Off, F
Oxygen	-27	-15
Hydrogen	-24	-22

EXPERIMENTAL PROCEDURE

Prior to system startup, the setpoint of the pressure and the temperature controller switches was checked. After the valves were checked out and the tank pressures adjusted to near the pressure controller setpoints, the run began by starting the diffuser and evacuating the hydrogen side. Each conditioning system was started separately. With the bleed valve open, the liquid oxygen or liquid hydrogen valve was manually opened and the system pressure noted and checked against the tank pressure. Then the automatic pressure controller was energized and checked for cycling. Occasionally, tank pressure was adjusted slightly to increase system pressure so that it would go into the pressure control mode. After the first system was operating satisfactorily, the other system was started and checked out in a similar manner. Then the gas generators were manually cycled on and off to check the combustion temperature. A high combustion temperature indicated that the pressure switches would have to be readjusted, while no ignition indicated that a catalyst bed probably had burned out. Generally, the gas generator checkout was satisfactory, and the automatic temperature control circuit was energized.

Thrustor operation began when both temperature controllers were cycling. First, the hydrogen was switched from the bleed to the thrustor for the cooldown transient. The thrustor oxygen valve was then opened and the bleed was closed in this sequence to prevent the control circuit from allowing the pressure control circuit to momentarily lock the liquid oxygen valve open and bring the oxygen system to the tank pressure. When the catalyst bed temperature outlet reached 1300 F, the downstream injector valve was opened and the system was allowed to reach steady state. Shutdown was

achieved by reversing the valve operations. Six time sections of the experiment were recorded on the Beckman data acquisition unit:

1. Conditioner system operation with flow out the bleeds
2. Startup transient of the thrustor
3. Downstream injector intermittently cycled
4. Long-duration downstream injector pulse
5. Simultaneous operation of both gas generators and the thrustor with downstream injector cycled
6. Repeat of No. 5 with small gas generator off

The total length of the recorded portion of the run was 260 seconds, the maximum tape length for the Beckman data acquisition unit. During this time, propellant was flowing through the thrustor catalyst bed, the downstream injector, the large gas generator, and the small gas generator for 3 minutes 47 seconds, 50 seconds, four minutes 29 seconds and 41 seconds, respectively. The total run length was approximately 10 minutes as a result of the fact that the Beckman system was started and stopped 4 times. Because 32 individual parameters were measured during each experiment, it was not possible to present all data. The fifth time section was selected for presentation because it shows simultaneous steady-state operation of all components.

SYSTEM RESULTS AND DISCUSSION

RESULTS

The data for all systems operating (both gas generators and thrustor with downstream injection) are presented as cathode ray tube output (CRT) in Fig. 104 through 135. The CRT's can be identified by the key presented in Table 20, and the placement of the instrumentation is given in Fig. 103. The data are presented in order, starting with propellant tank and proceeding to the gas generators for the oxygen side and hydrogen side. Because of the large number of CRT's, each CRT is not discussed individually.

The first CRT's for both the oxygen and hydrogen side (Fig. 104 and 116) show the sequence of events taken from valve signals. From the liquid oxygen valve operation (the left-hand side of Fig. 104), it can be seen that, initially, the oxygen thrustor main valve and the oxygen gas generator are open while the oxygen bleed is closed. These valves remain fixed in this position for the CRT duration. At approximately 8.7 seconds, the DSI valve was manually opened and closed at 11.6 seconds. The liquid oxygen tank main valve, indicated by an increase of 2000 counts, was cycling at 1 and 2 cps when the DSI valve was open. The hydrogen side valves were operating in a similar manner.

On the oxygen side liquid was being delivered to the heat exchanger (Fig. 105) as indicated by the thermocouples placed at the heat exchanger inlet (TL102). The corresponding measurement for hydrogen (TL1H2) indicated that saturated hydrogen was entering the heat exchanger except for an occasional surge of superheated vapor.

TABLE 20

CRT-COUNT DEFINITION FOR VALVE OPERATION FOR THE INTEGRATED THRUSTOR-CONDITIONER EQUIPMENT

PID 296, Oxygen Side

Valve Sequence	Counts
LOX Tank Main Open	2000
Oxygen Thrust Main Open	1000
Oxygen-Side Gas Generator Open	400
Oxygen Bleed Closed	200
Downstream Injector Open	100

PID 296, Hydrogen Side

Sequence	Counts
LH_2 Dewar Open	2000
Fuel Thrustor Open	1000
Fuel-Side Gas Generator Open	400
Fuel Bleed Open	200

NOTE: LOX bleed is normally open; LH_2 bleed is normally closed

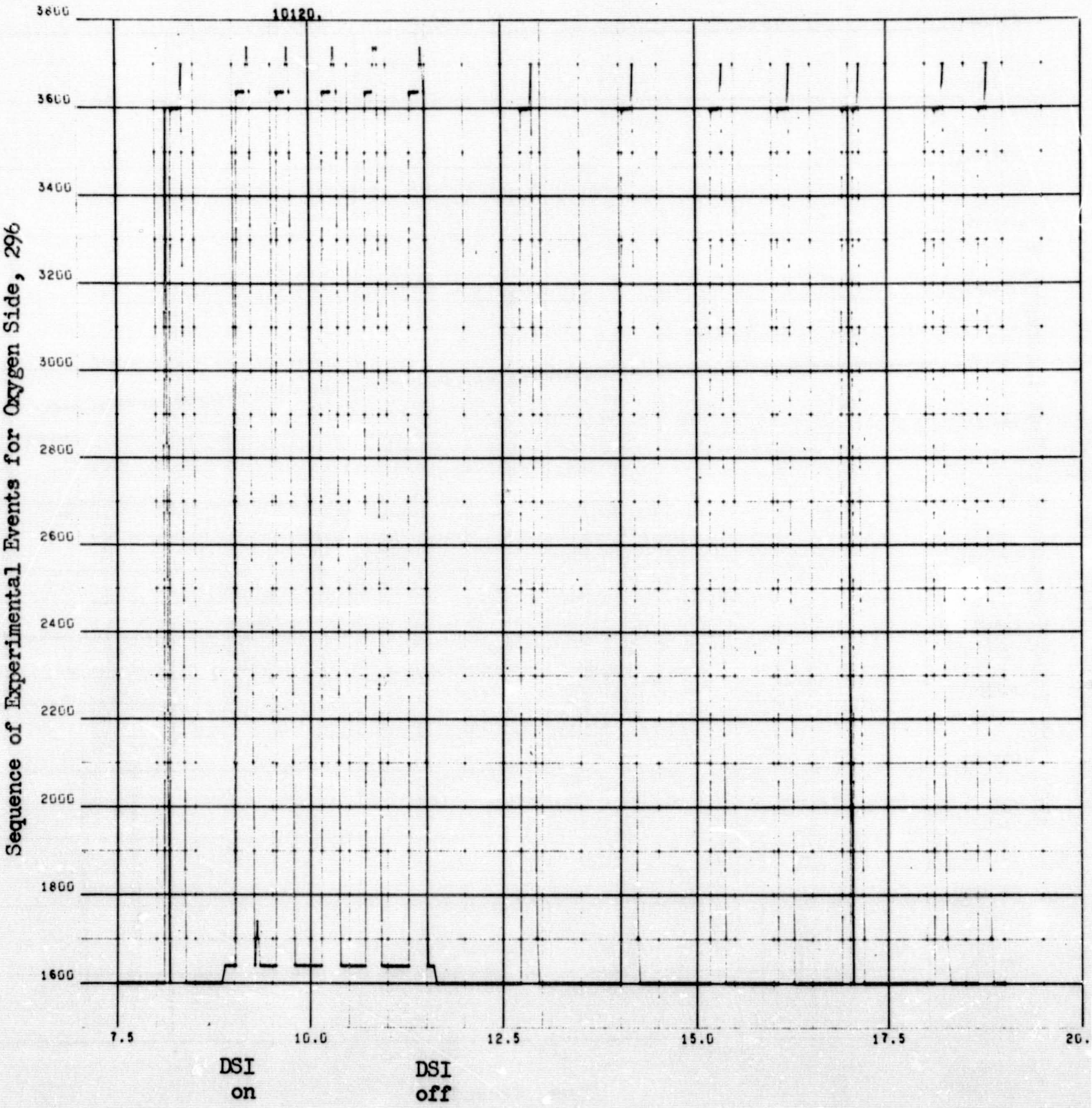

Figure 104. Sequence of Experimental Events, Oxygen Side of the Thrustor, Conditioner System

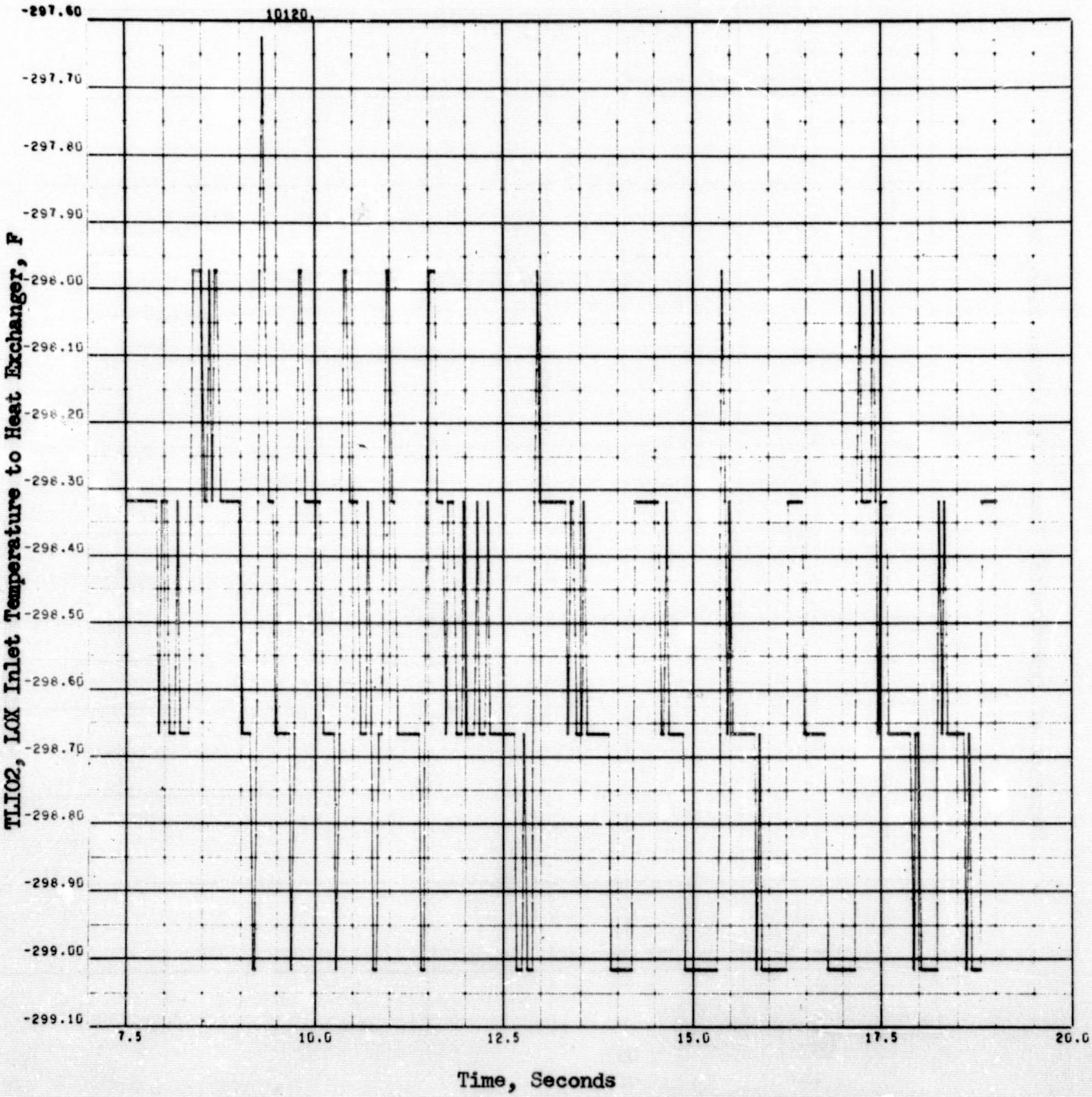

Figure 105. LOX Inlet Temperature to the Heat Exchanger,(Oxygen Side of the Thrustor, Conditioner System)

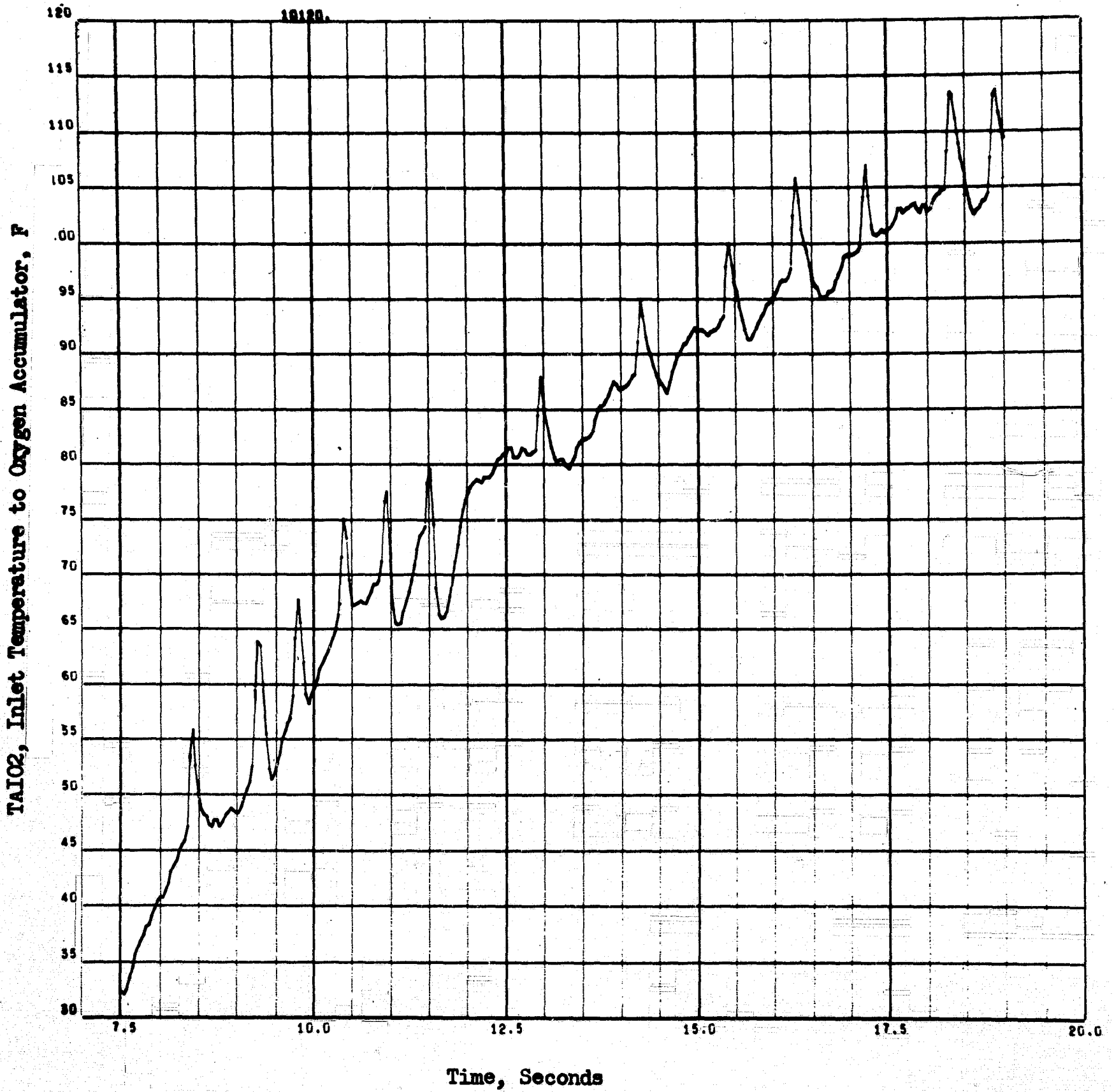

Figure 106. Inlet Temperature to the Oxygen Accumulator, (Oxygen Side of the Thrustor, Conditioner System)

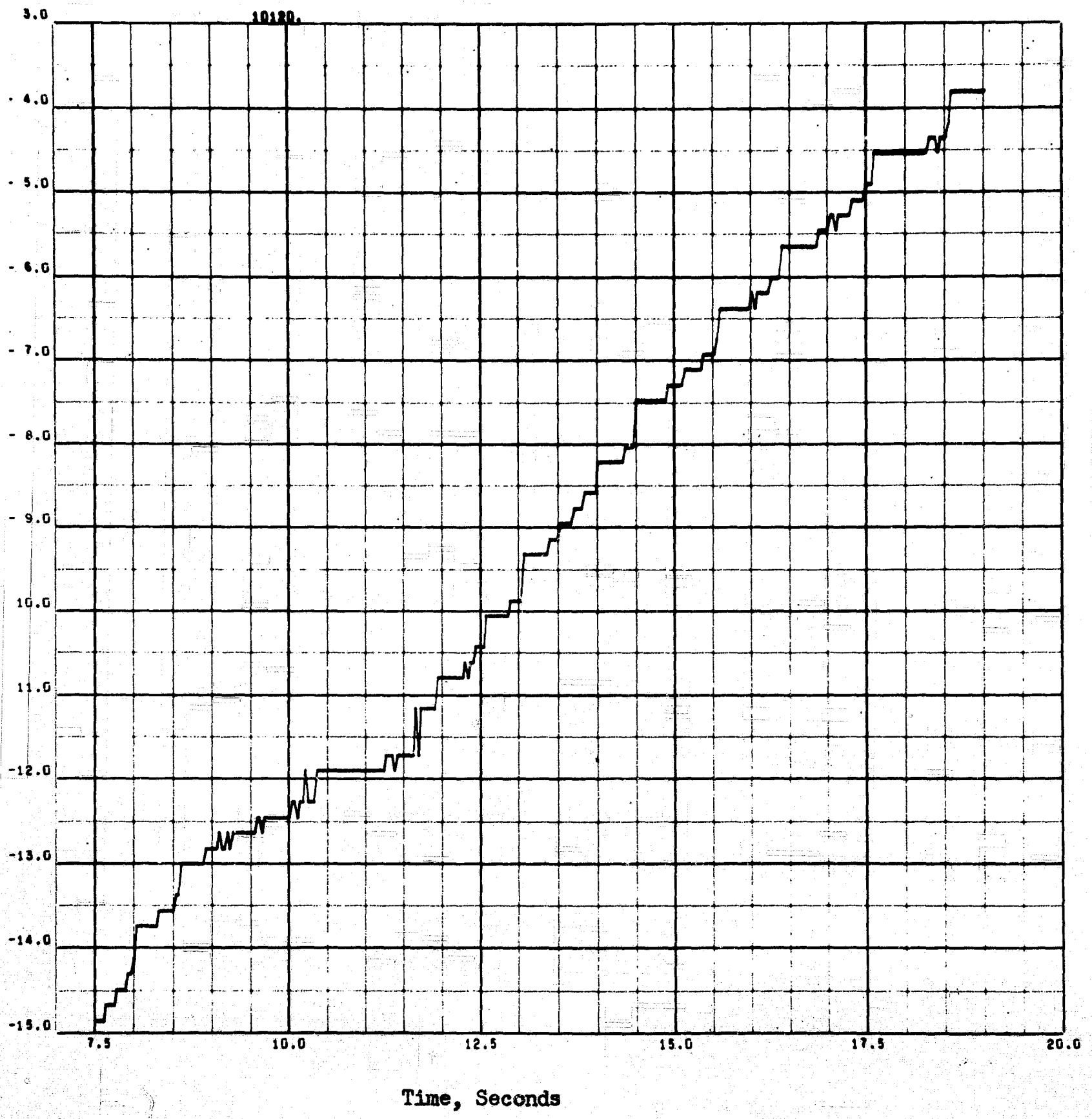

Figure 107. Outlet Temperature From the Oxygen Accumulator, (Oxygen Side of Thrustor, Conditioner System)

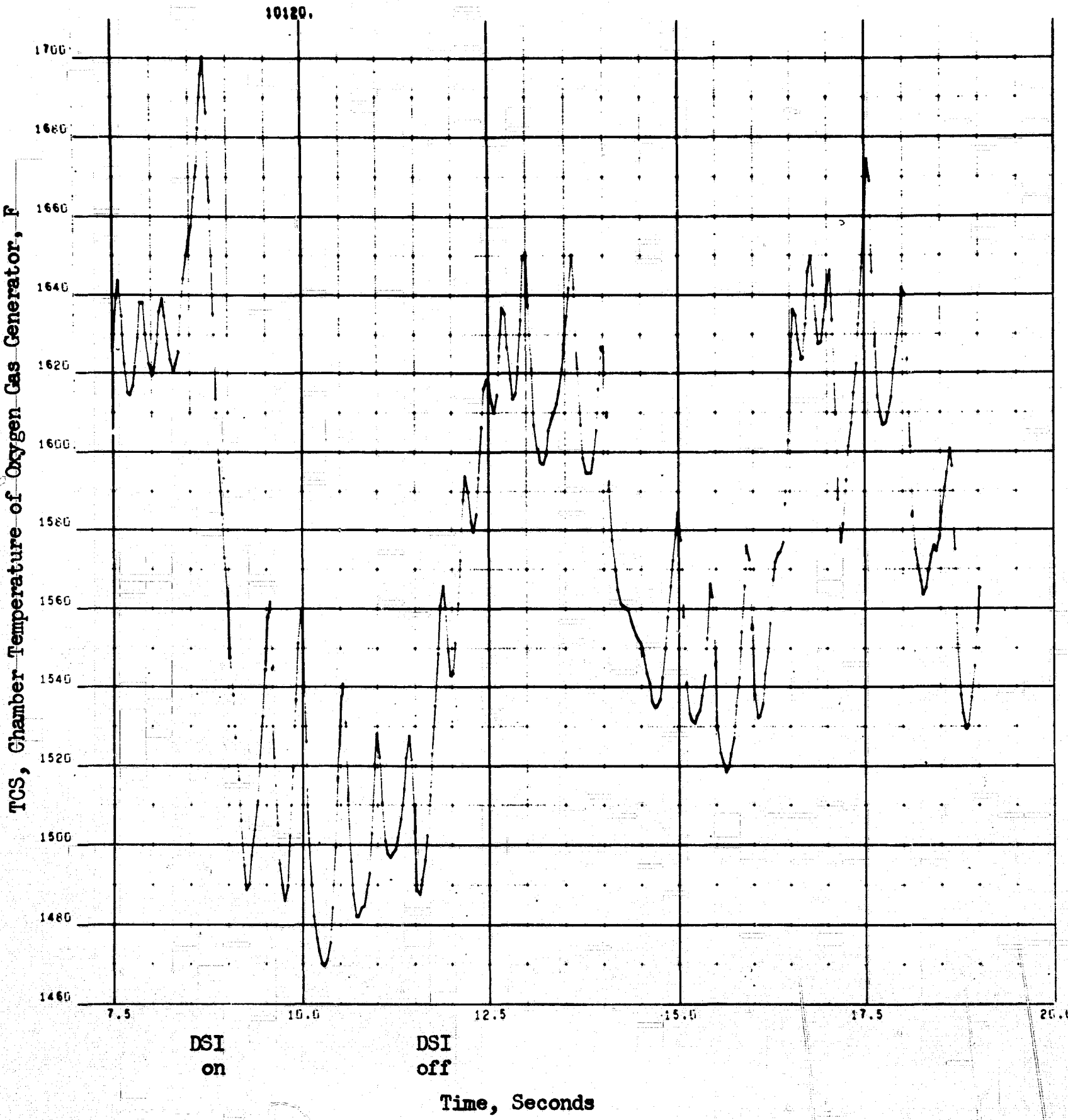

Figure 108. Chamber Temperature for the Small Gas Generator, (Oxygen Side of the Thrustor, Conditioner System)

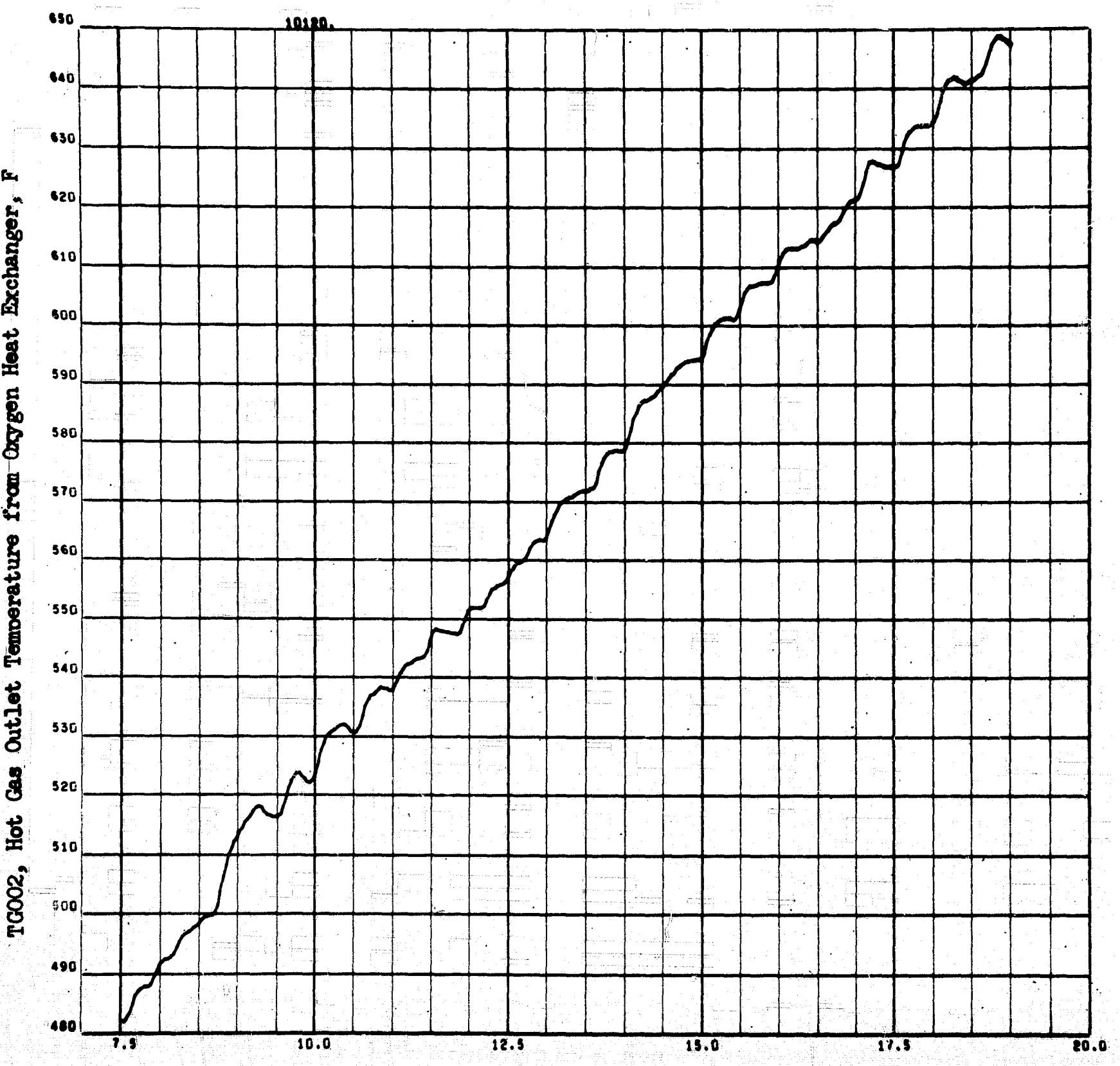

Figure 109. Hot-Gas Outlet Temperature From Oxygen Heat Exchanger, (Oxygen Side of the Thrustor, Conditioner System)

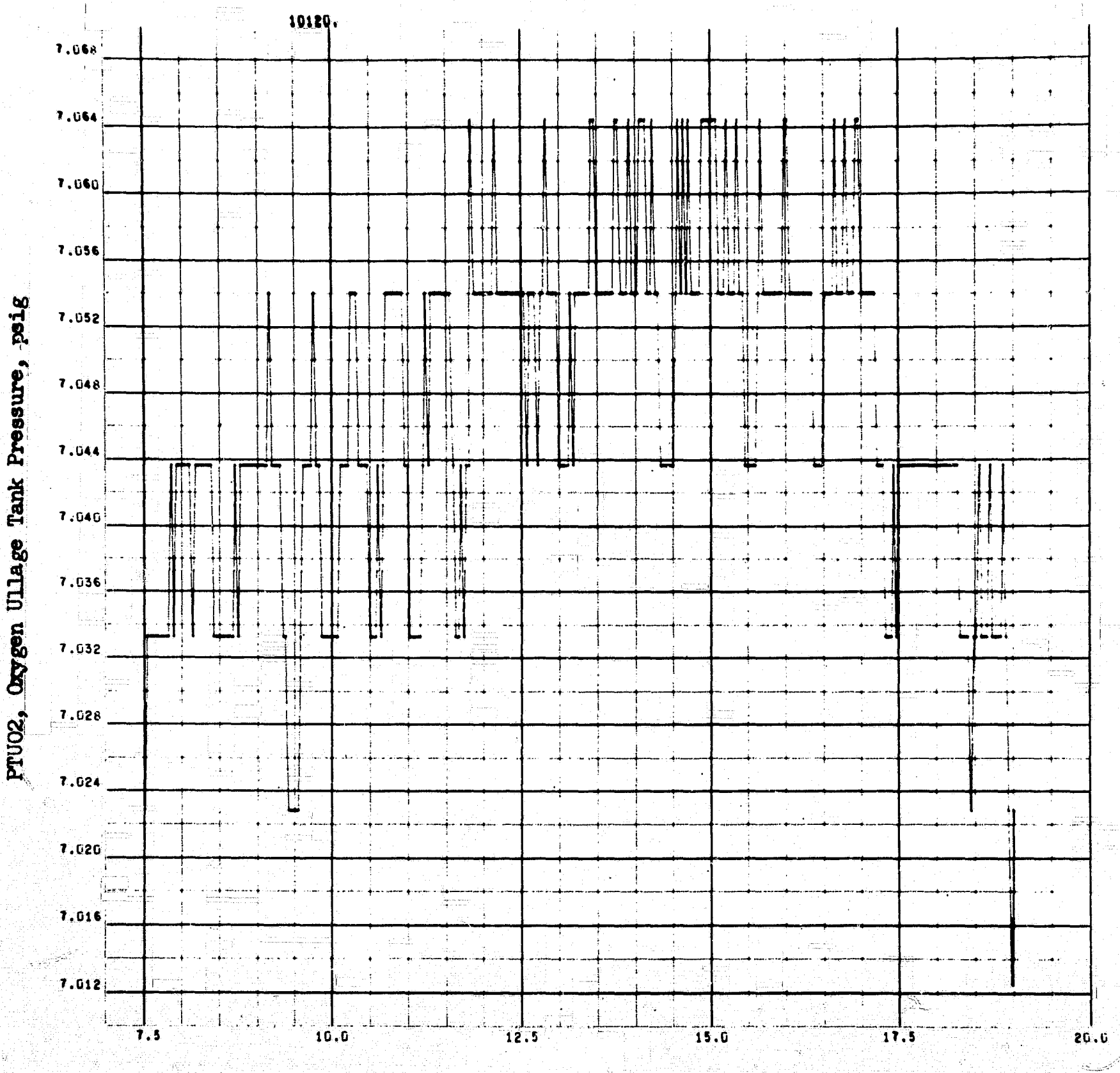

Figure 110. Oxygen Ullage Tank Pressure, (Oxygen Side of the Thrustor, Conditioner System)

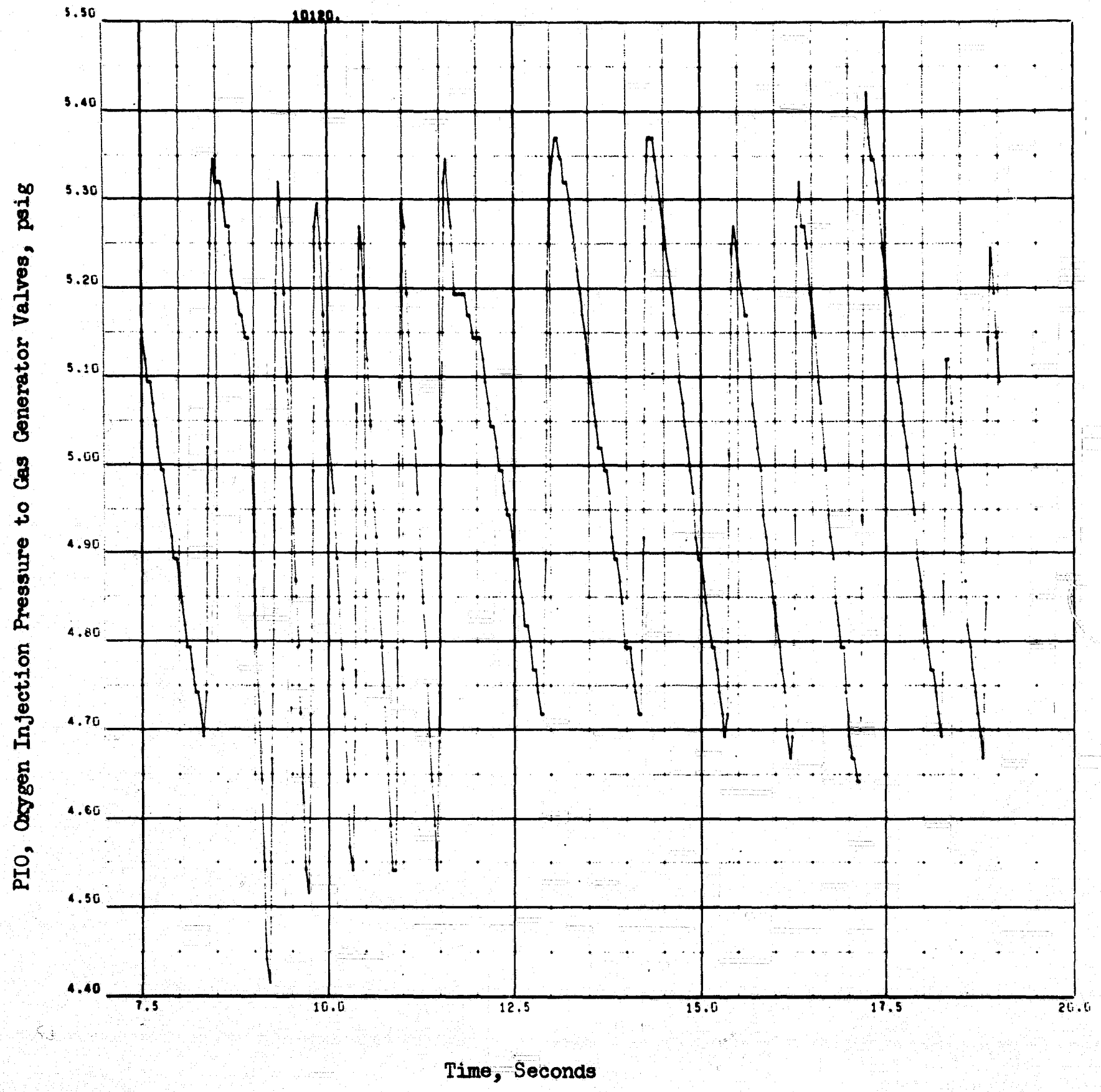

Figure 111. Oxygen Injection Pressure to Gas Generator Valves, (Oxygen Side of the Thrustor, Conditioner System)

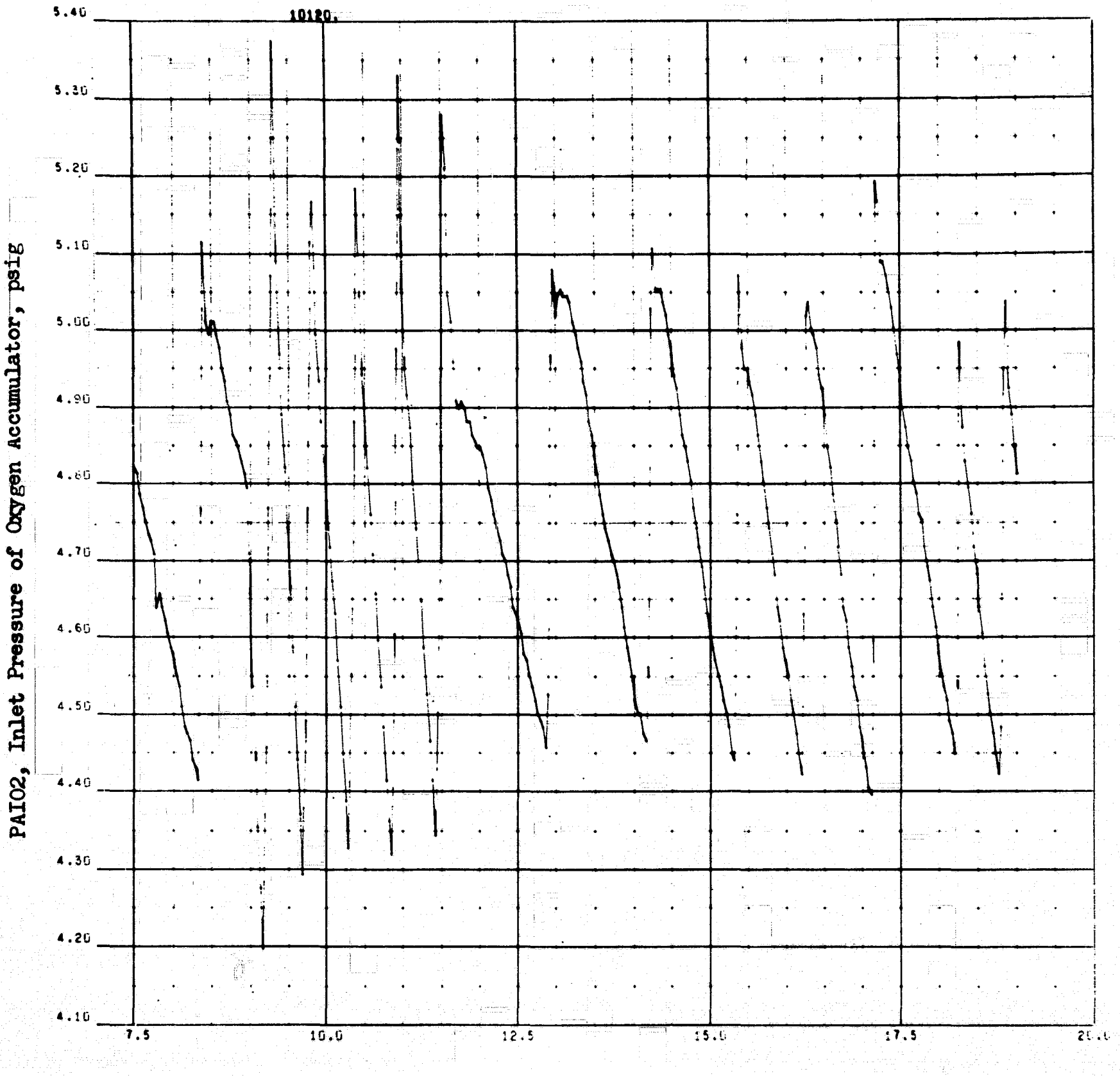

Figure 112. Inlet Pressure of Oxygen Accumulator,(Oxygen Side of the Thrustor, Conditioner System)

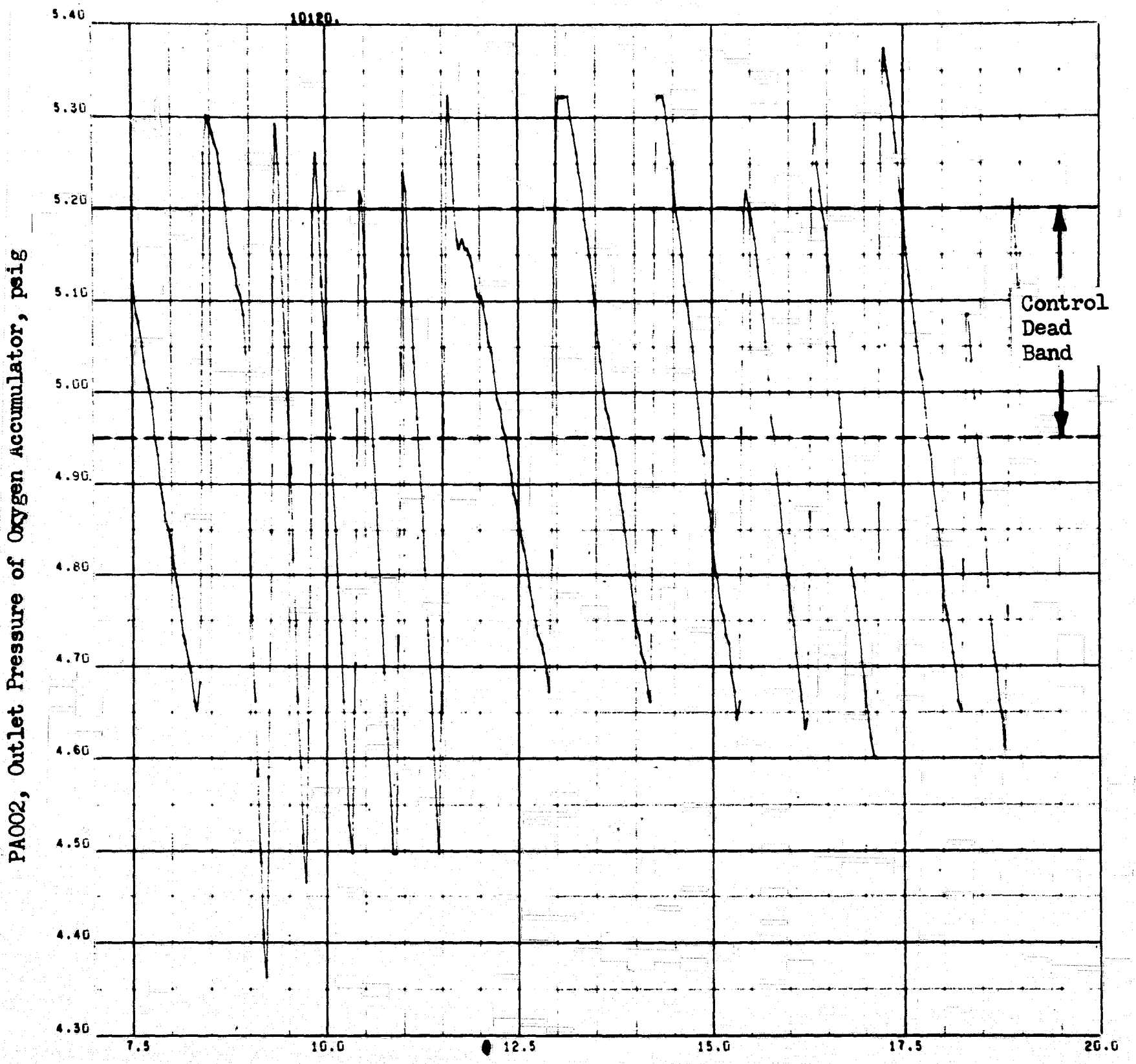

Figure 113. Outlet Pressure of Oxygen Accumulator, (Oxygen Side of the Thrustor, Conditioner System)

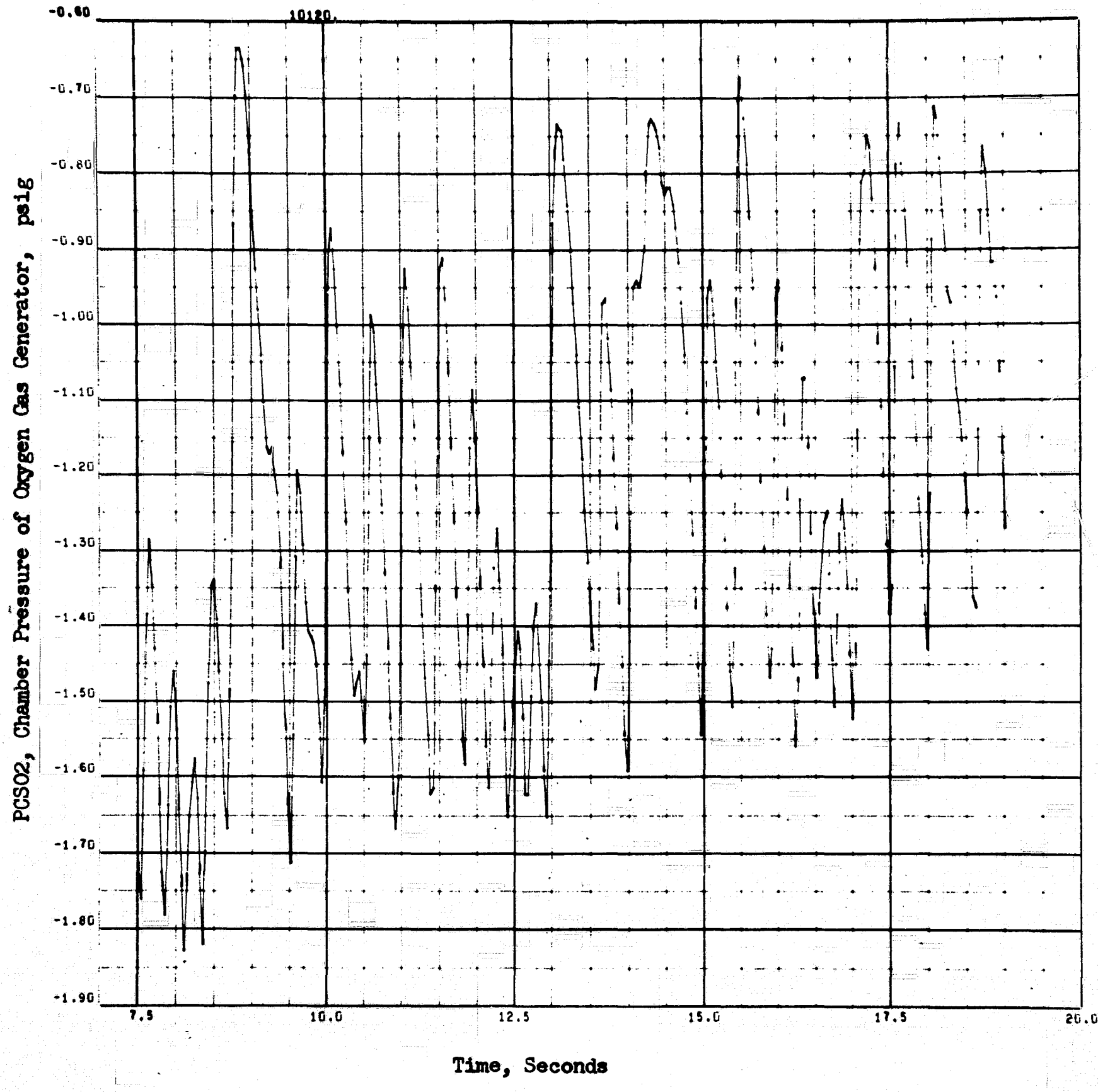

Figure 114. Chamber Pressure of the Small Gas Generator, (Oxygen Side of the Thrustor, Conditioner System)

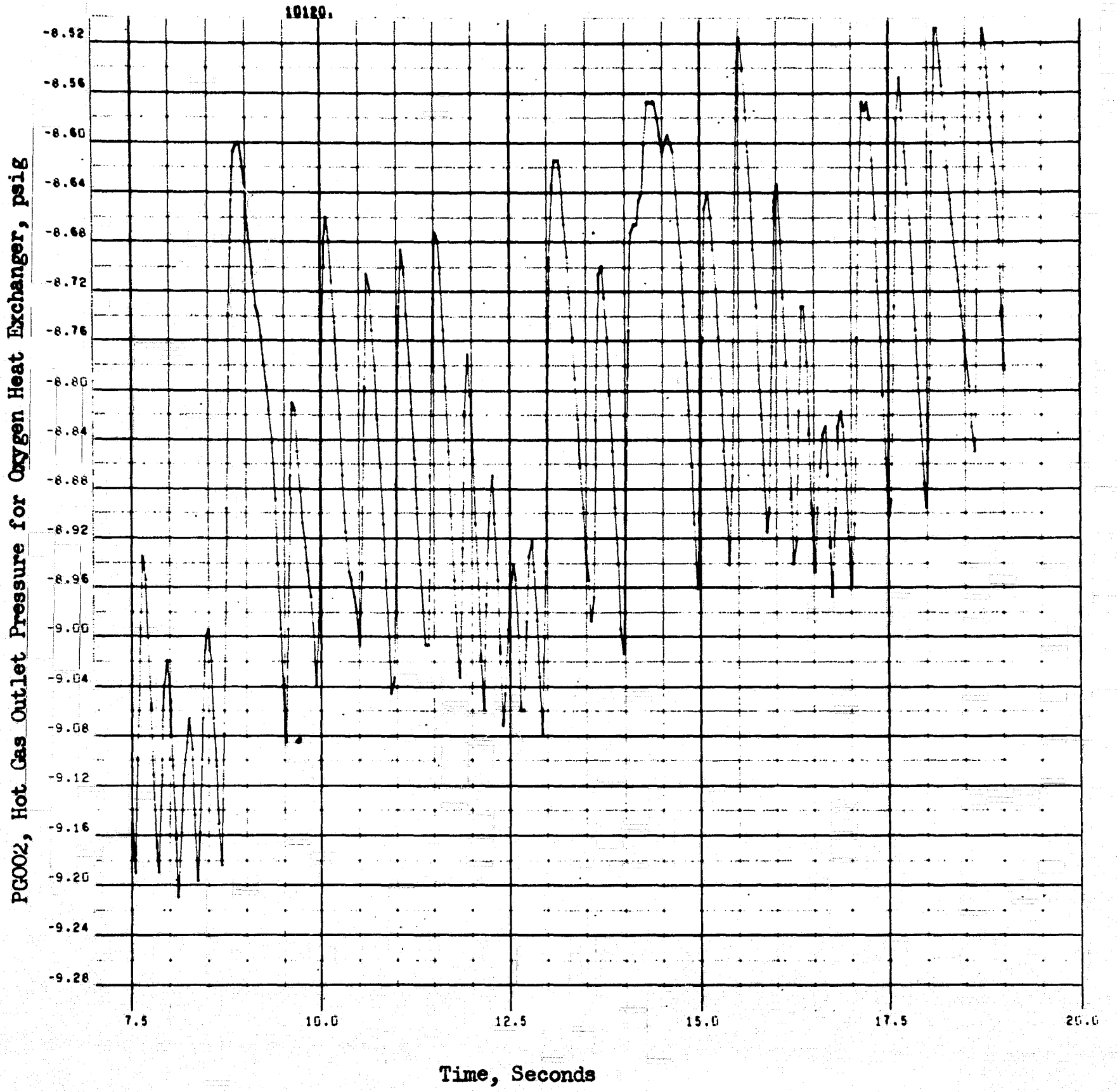

Figure 115. Hot-Gas Outlet Pressure for Oxygen Heat Exchanger, (Oxygen Side of the Thrustor, Conditioner System)

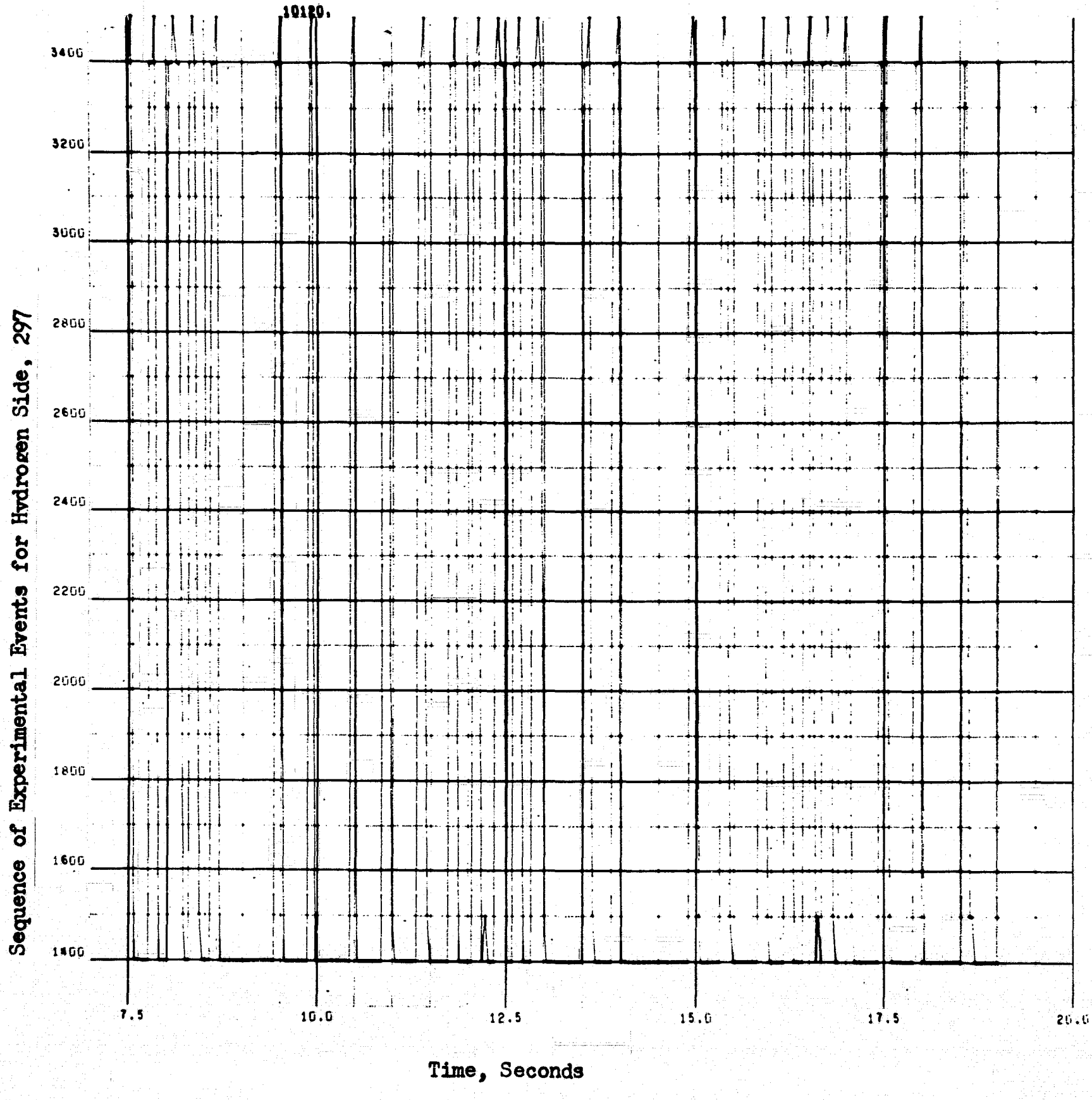

Figure 116. Sequence of Experimental Events, Hydrogen Side of the Thrustor, Conditioner System

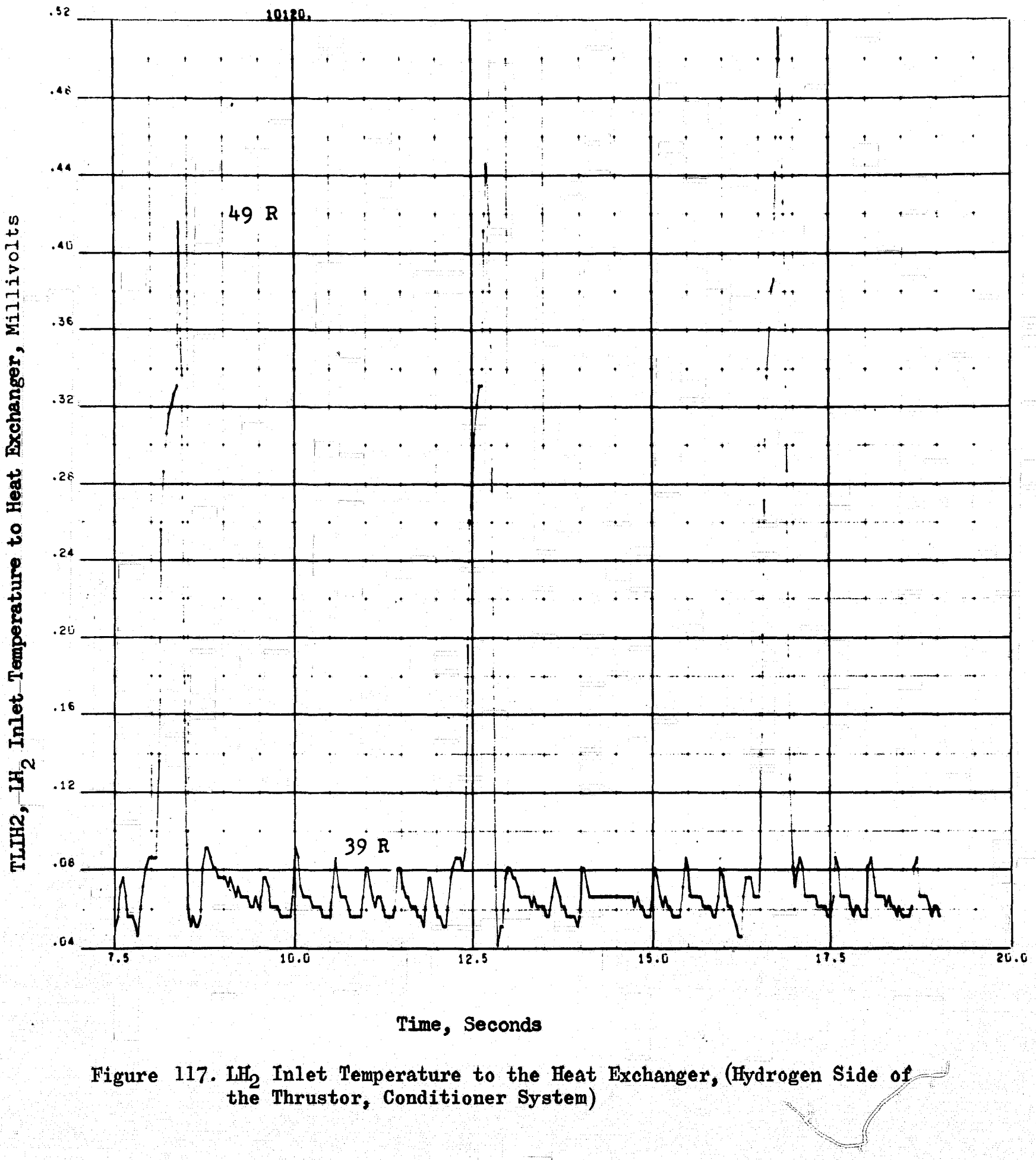

Figure 117. LH_2 Inlet Temperature to the Heat Exchanger, (Hydrogen Side of the Thrustor, Conditioner System)

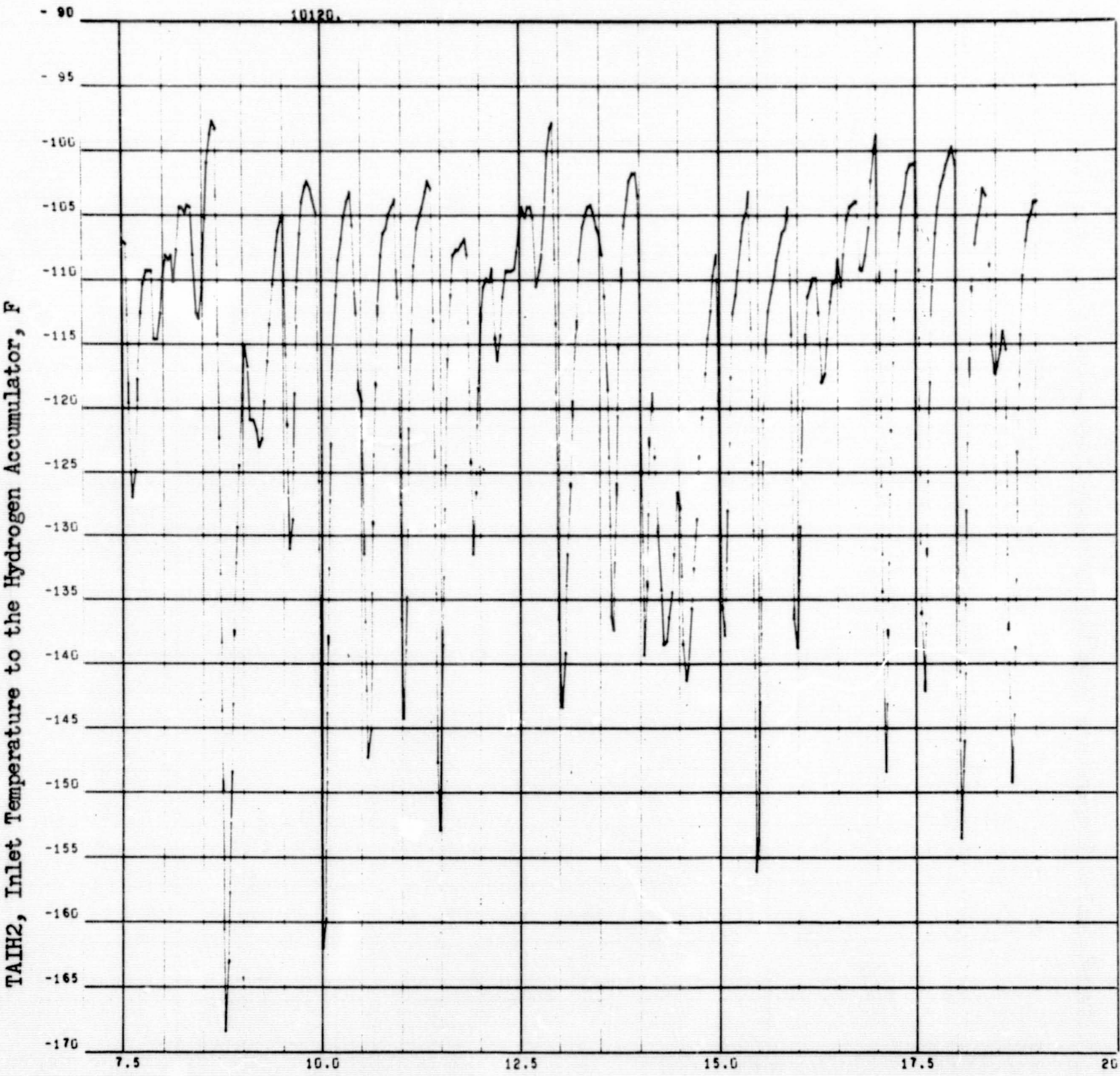

Figure 118. Inlet Temperature to the Hydrogen Accumulator, (Hydrogen Side of the Thrustor, Conditioner System)

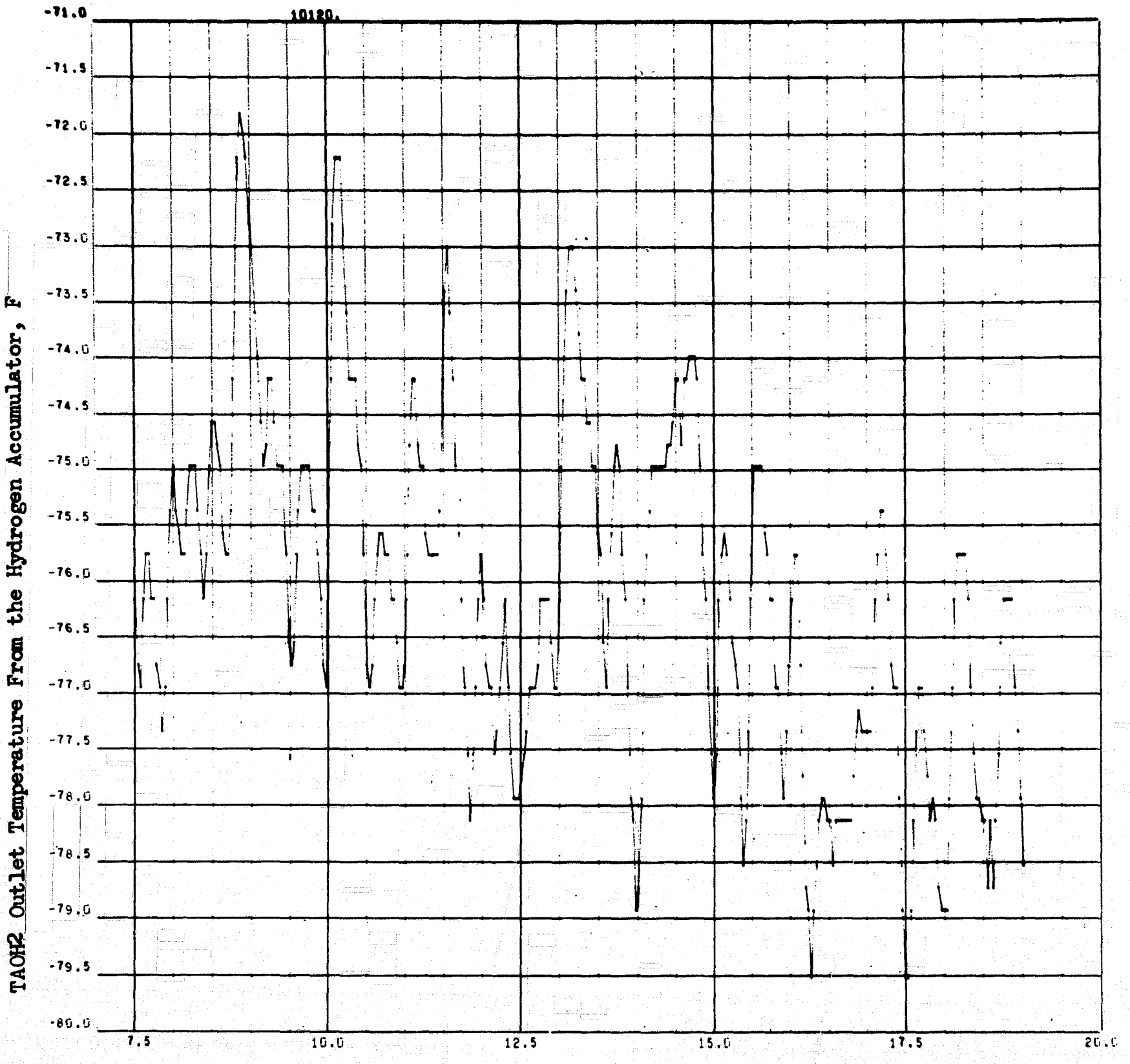

Figure 119. Outlet Temperature From the Hydrogen Accumulator,(Hydrogen Side of the Thrustor, Conditioner System)

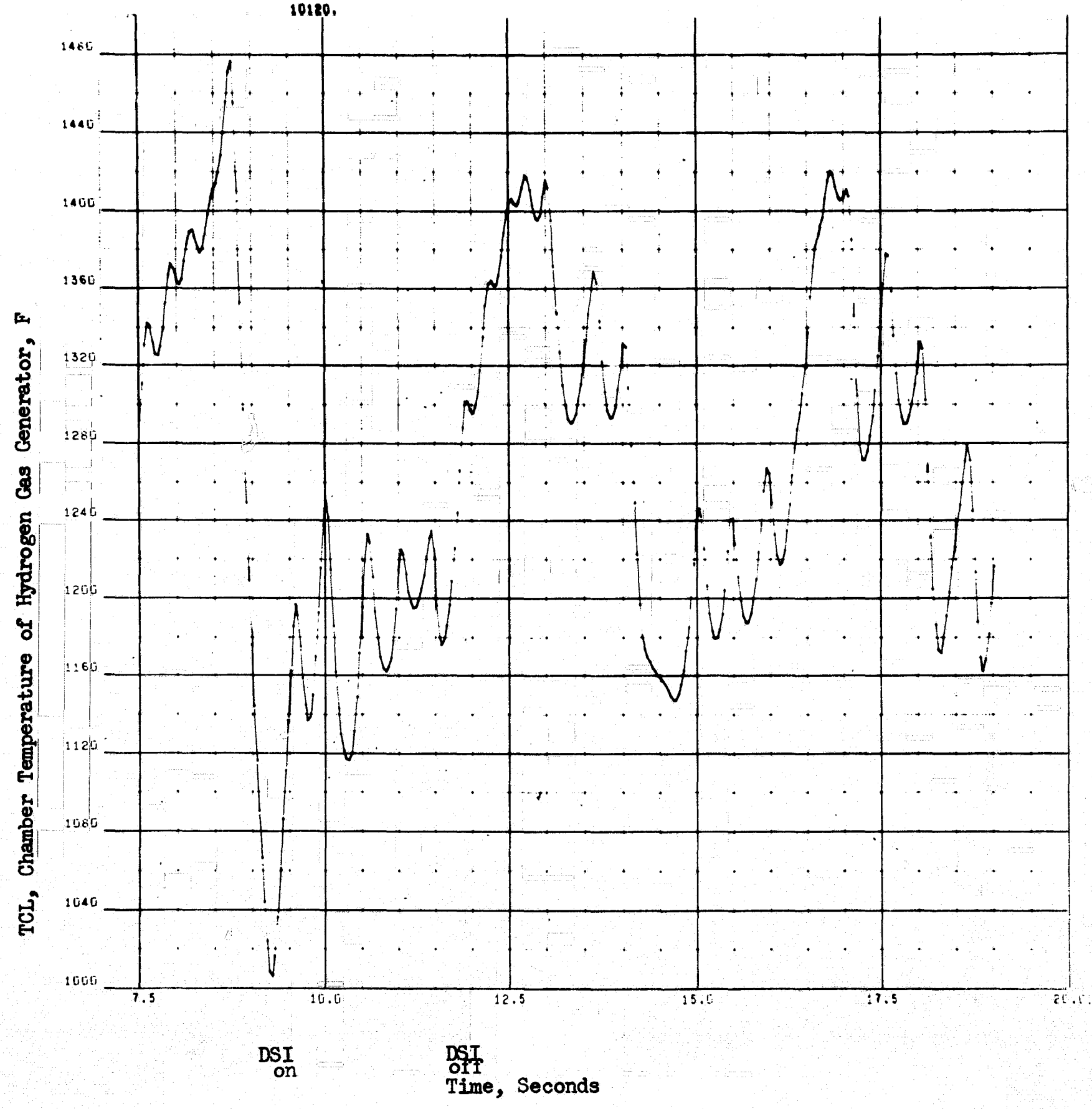

Figure 120. Combustion Temperature of the Gas Generator,(Hydrogen Side of the Thrustor, Conditioner System)

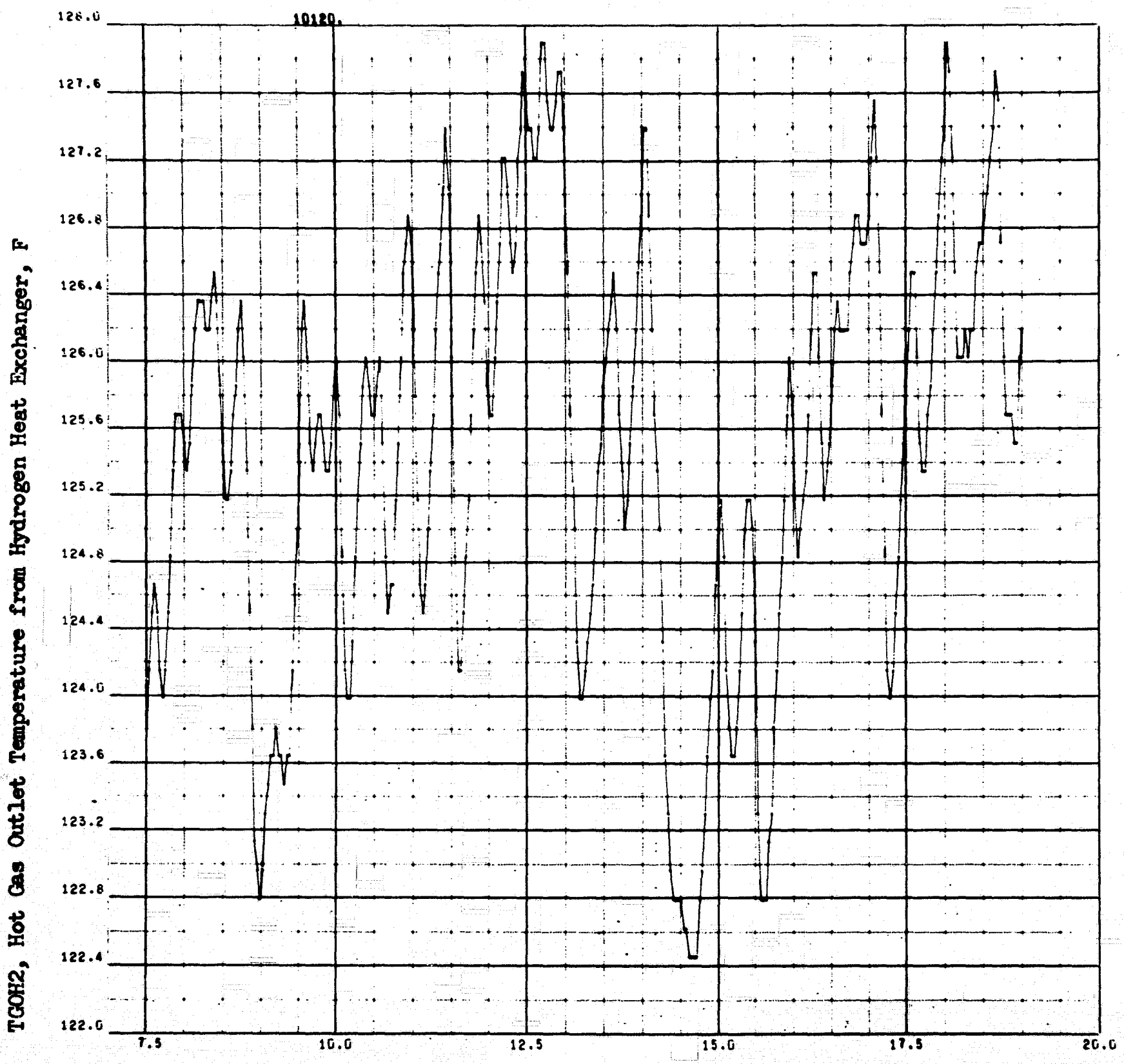

Figure 121. Hot-Gas Outlet Temperature From the Hydrogen Heat Exchanger, (Hydrogen Side of the Thrustor, Conditioner System)

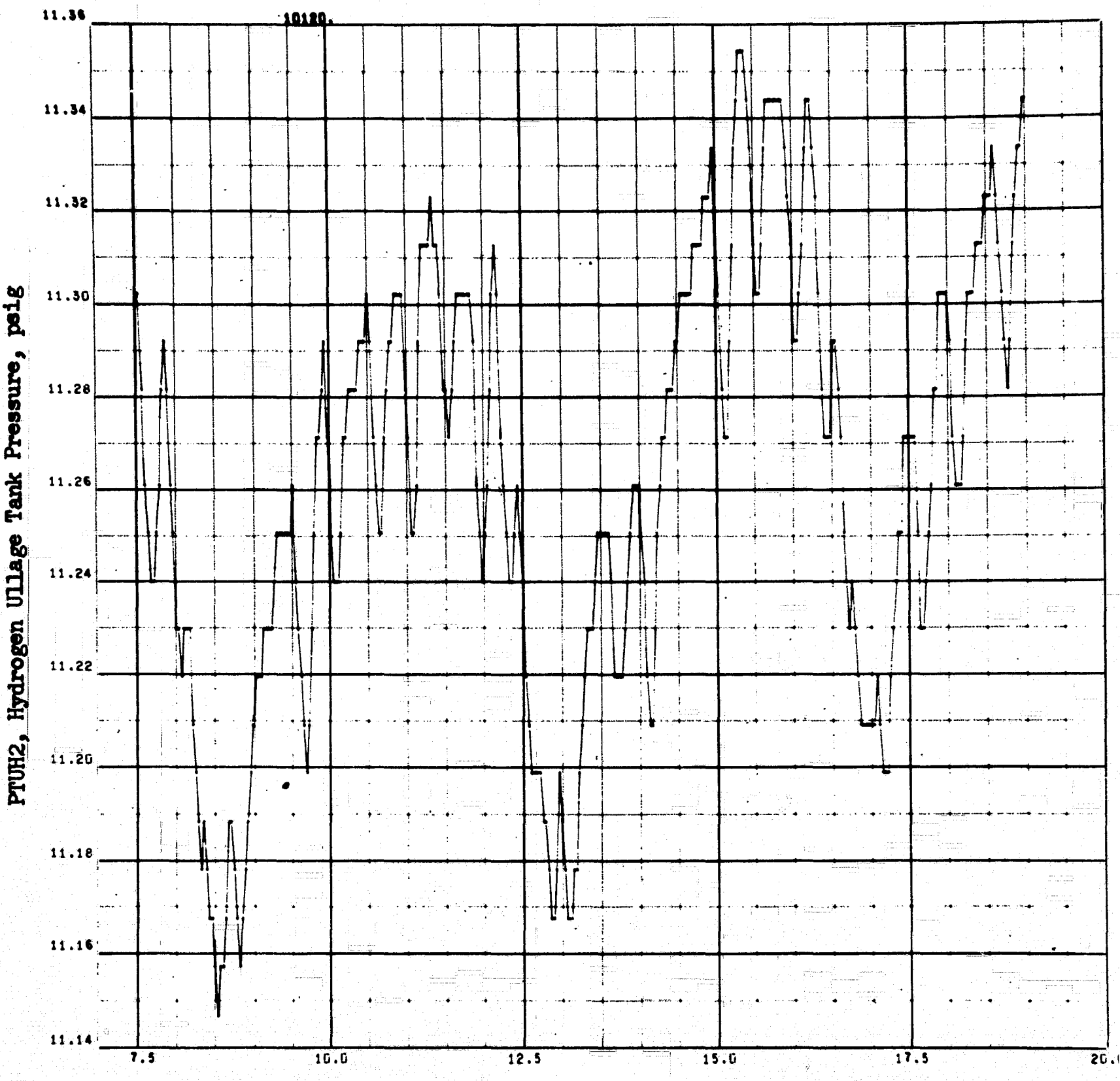

Figure 122. Hydrogen Ullage Tank Pressure, Hydrogen Side

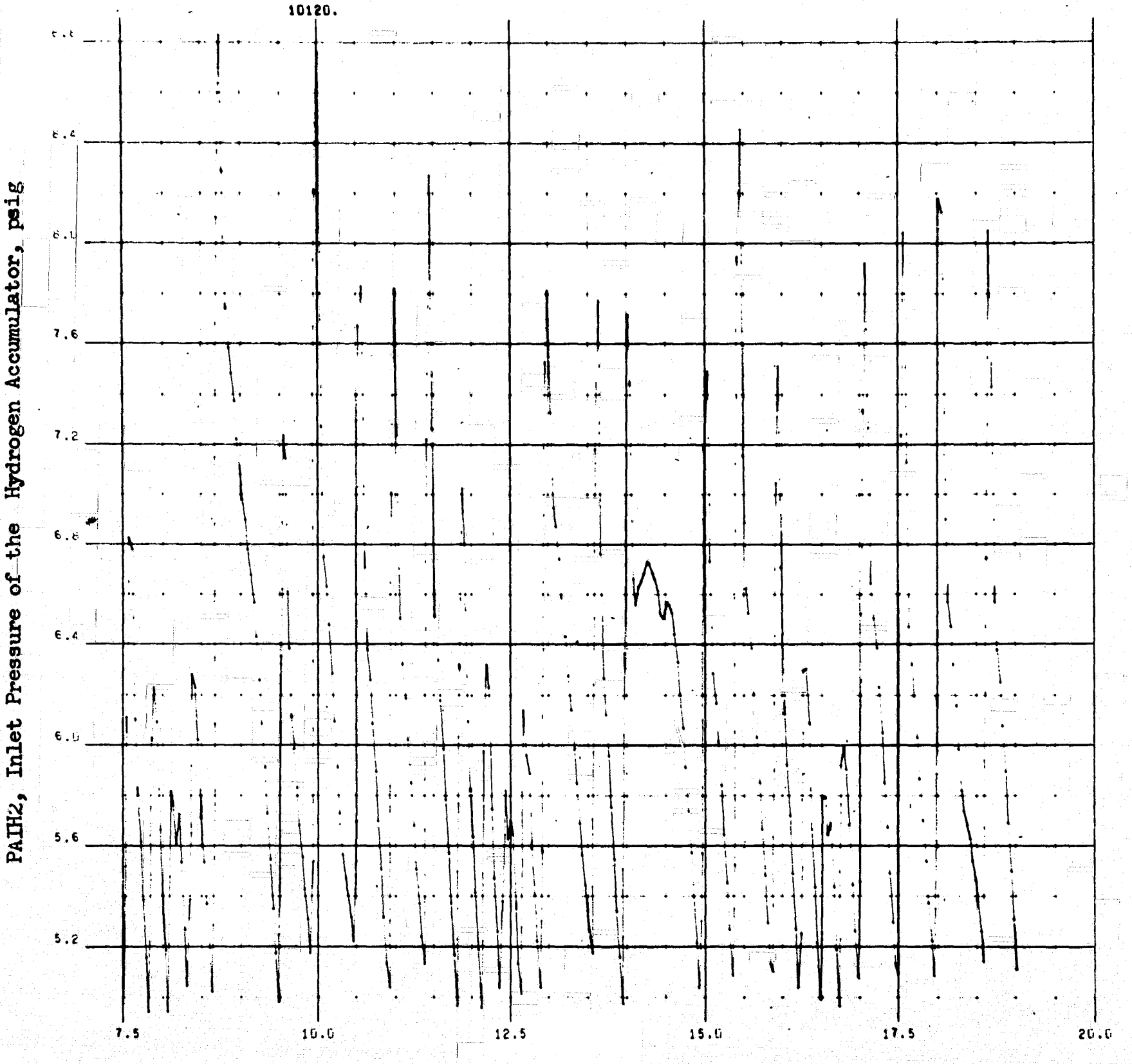

Figure 123. Inlet Pressure of the Hydrogen Accumulator,(Hydrogen Side of Thrustor, Conditioner System)

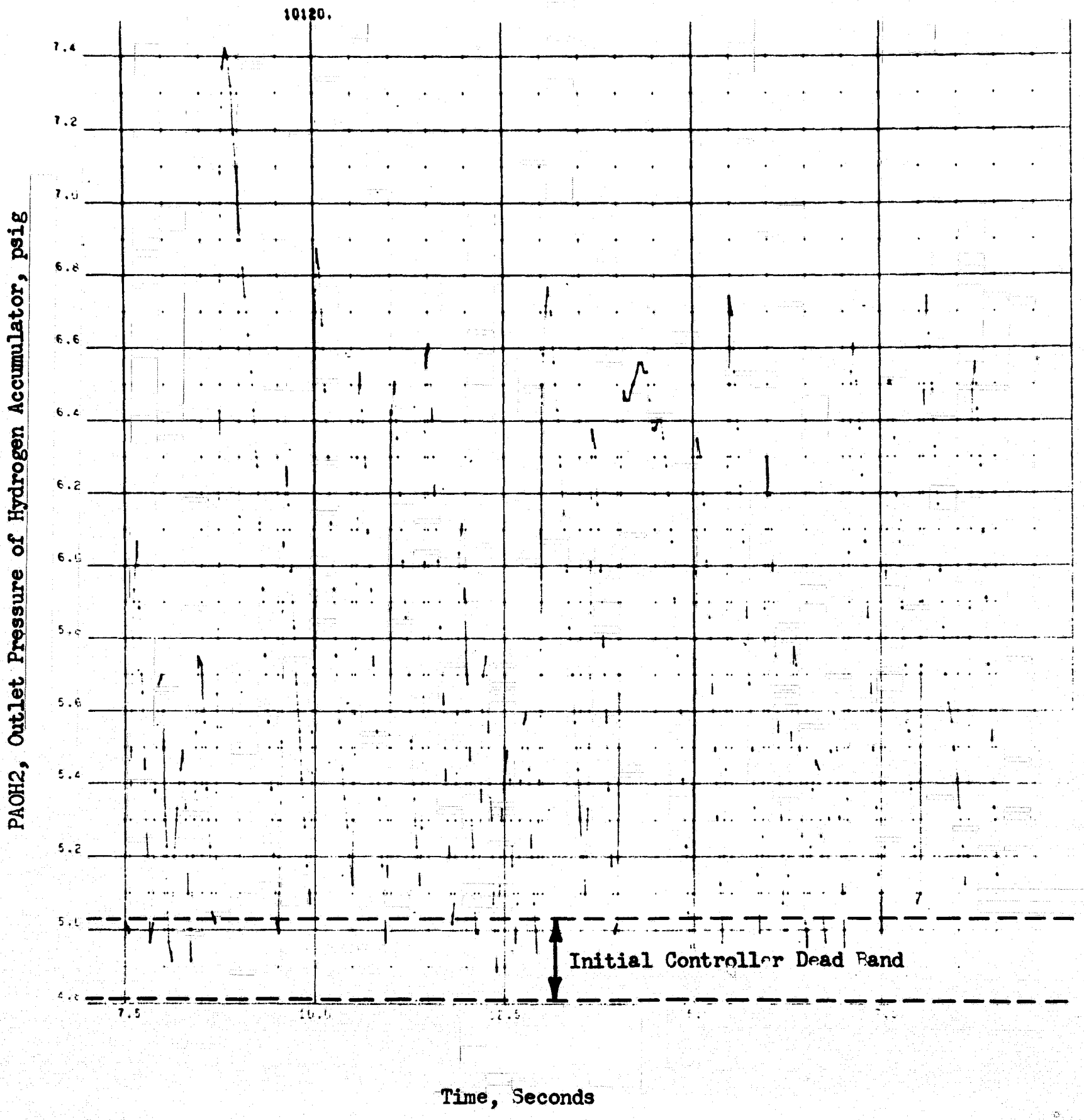

Figure 124. Outlet Pressure of Hydrogen Accumulator, (Hydrogen Side of the Thrustor, Conditioner System)

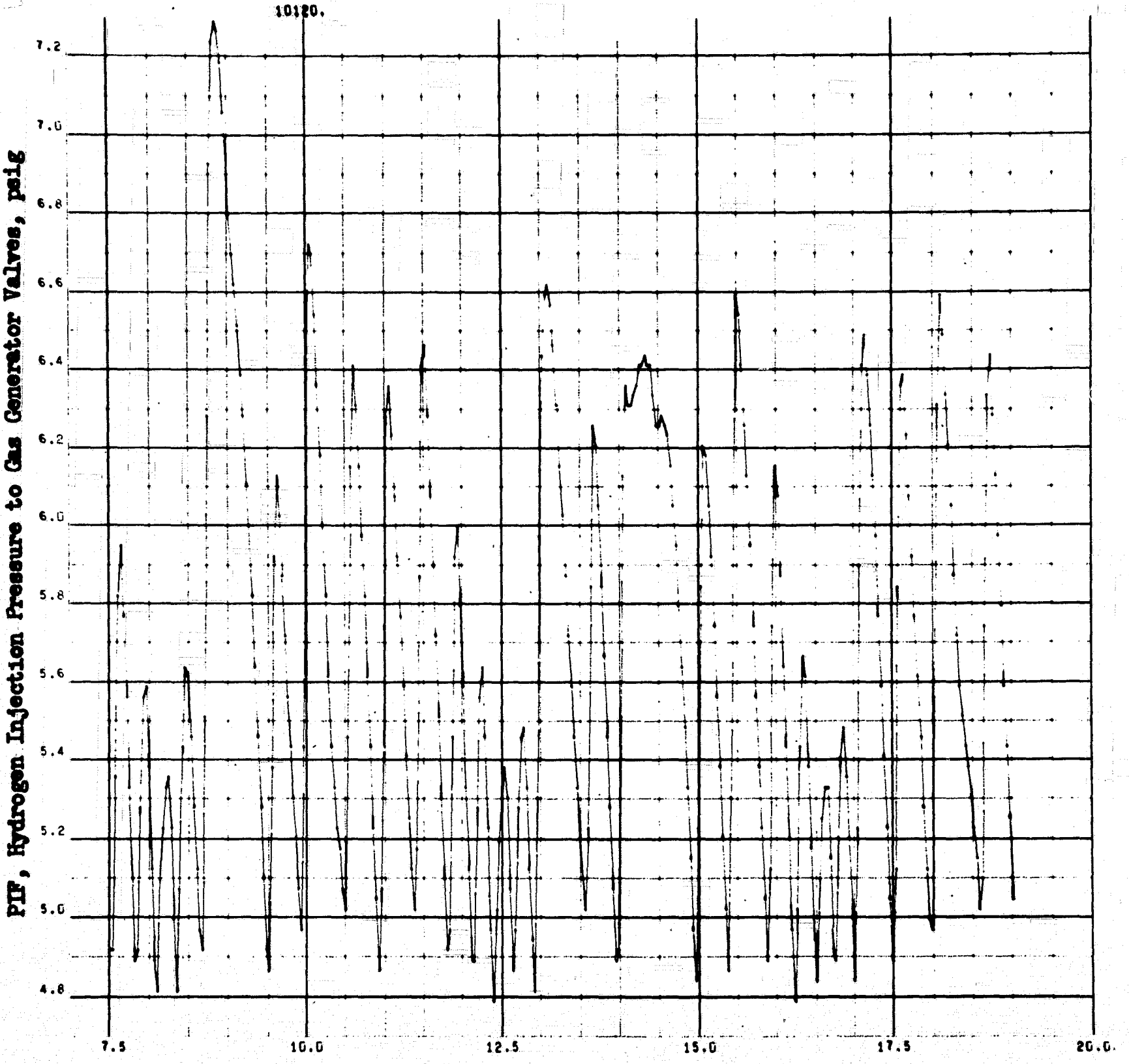

Figure 125. Hydrogen Injection Pressure to the Gas Generator Valves, (Hydrogen Side of the Thrustor, Conditioner System)

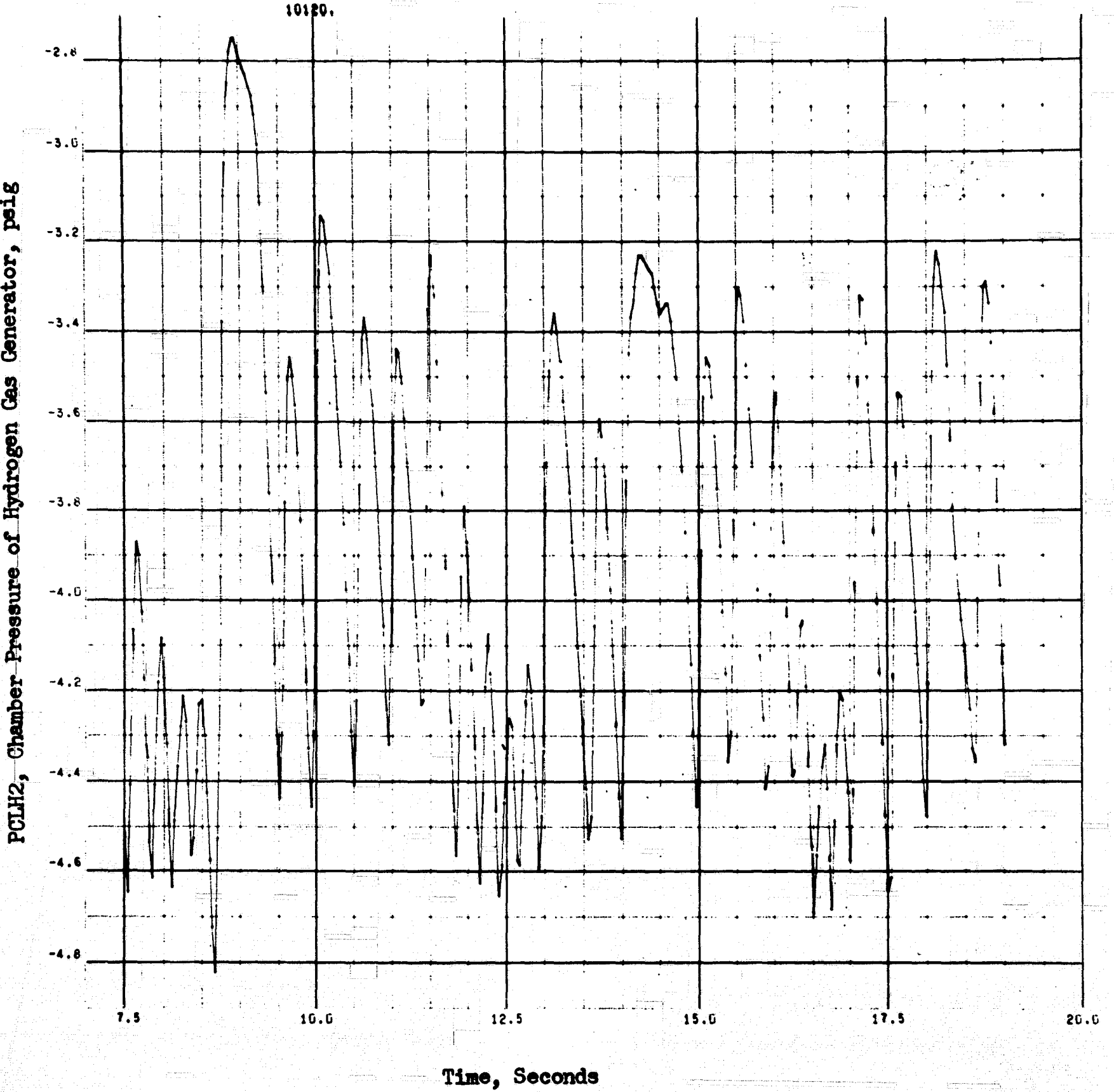

Figure 126. Chamber Pressure of the Large Gas Generator, (Hydrogen Side of the Thrustor, Conditioner System)

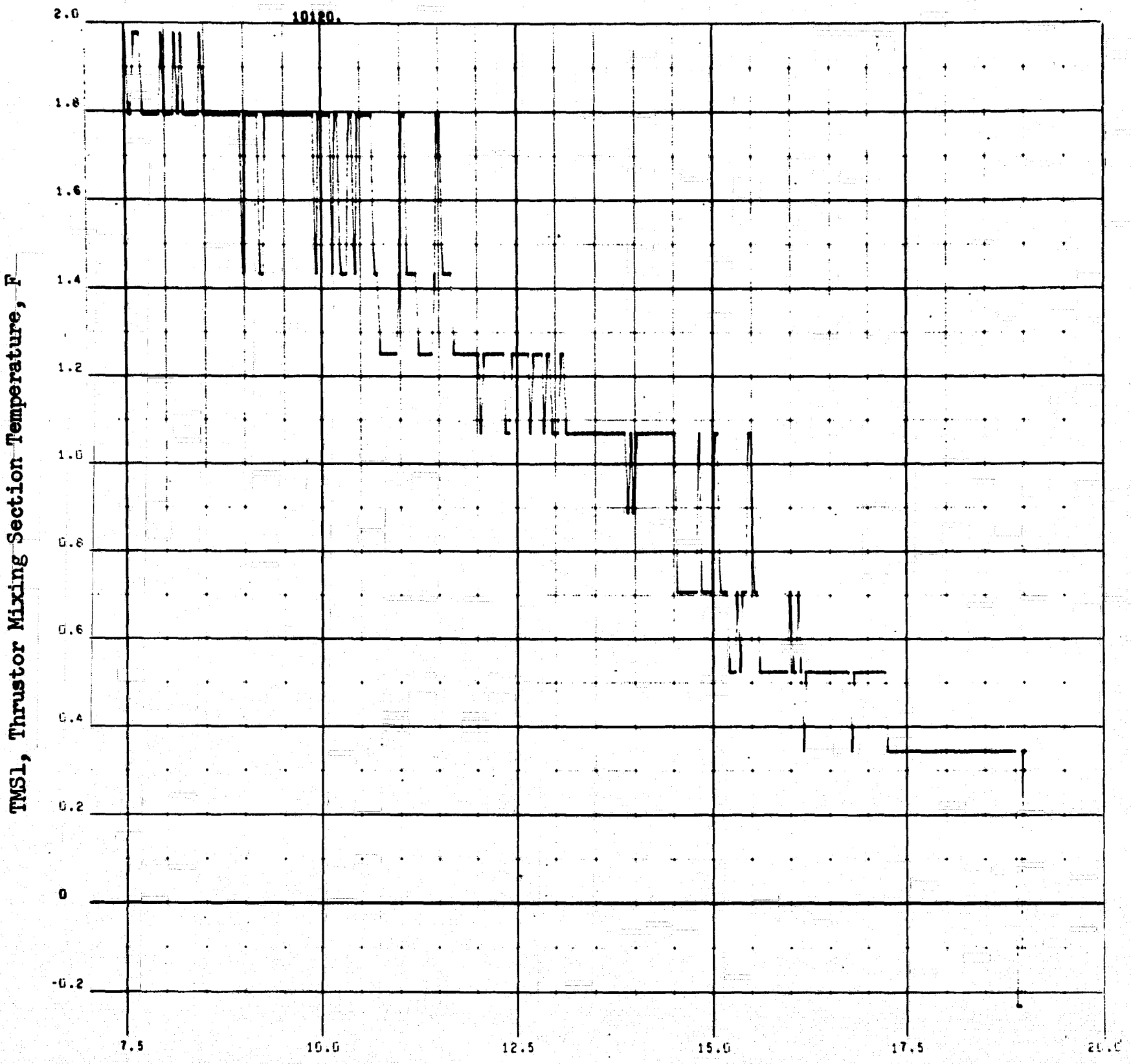

Figure 127. Thrustor Mixing Section Temperature, Thrustor Part of the Thrustor, Conditioner System

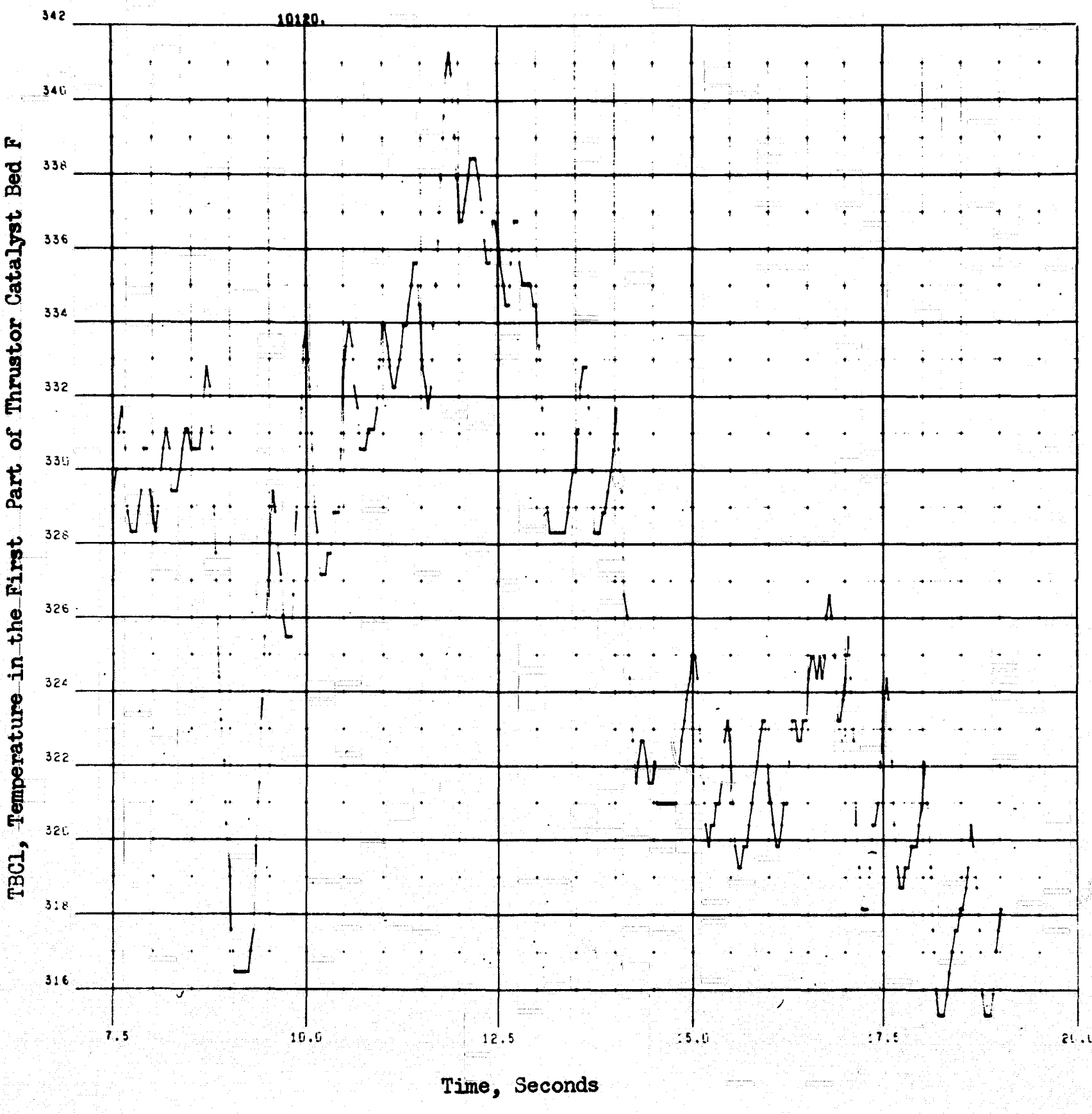

Figure 128. Temperature in the First Part of the Catalyst Bed,(Thrustor Part of the Thrustor, Conditioner System)

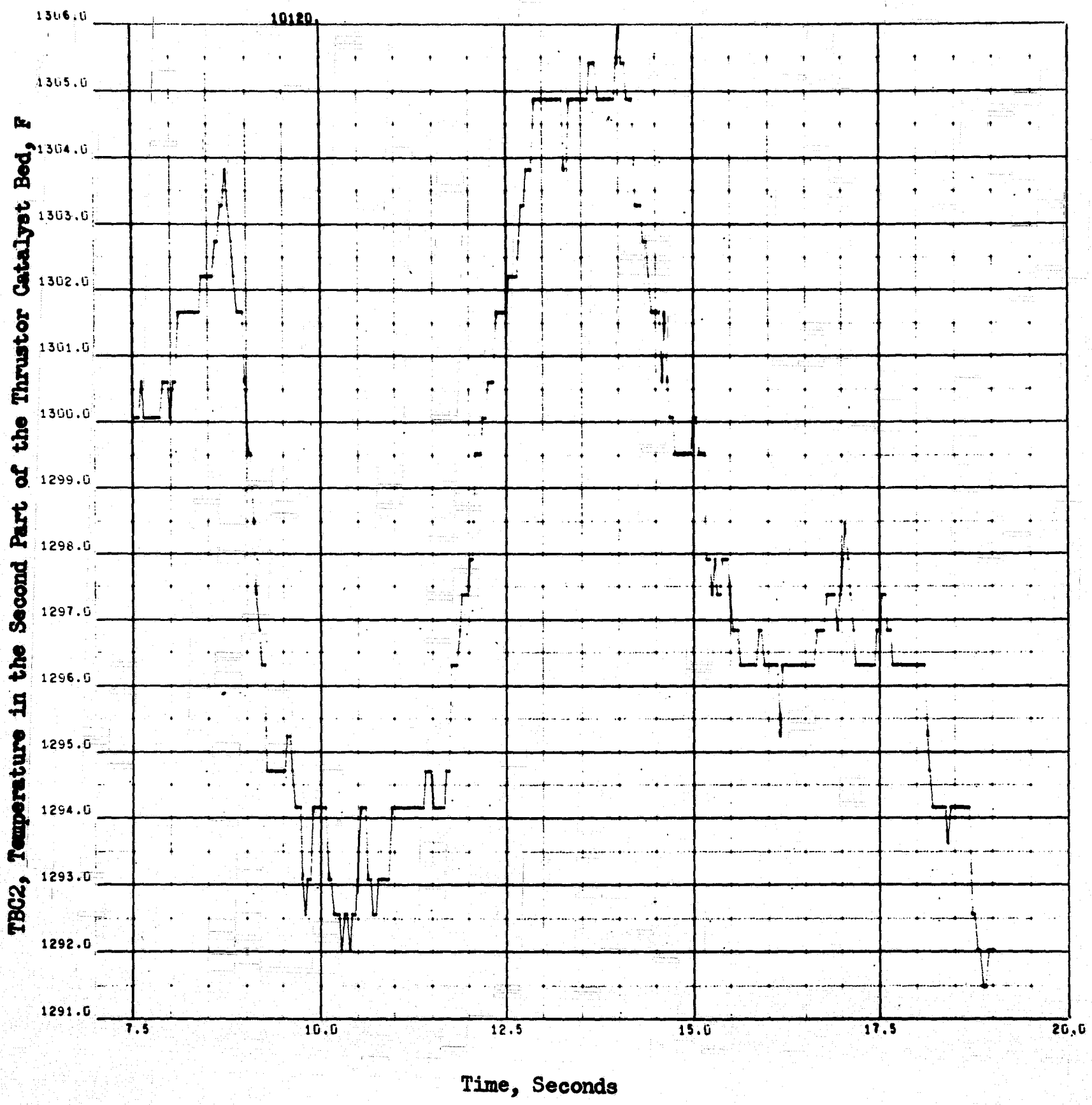

Figure 129. Temperature in the Second Part of the Catalyst Bed, (Thrustor Part of the Thrustor, Conditioner System)

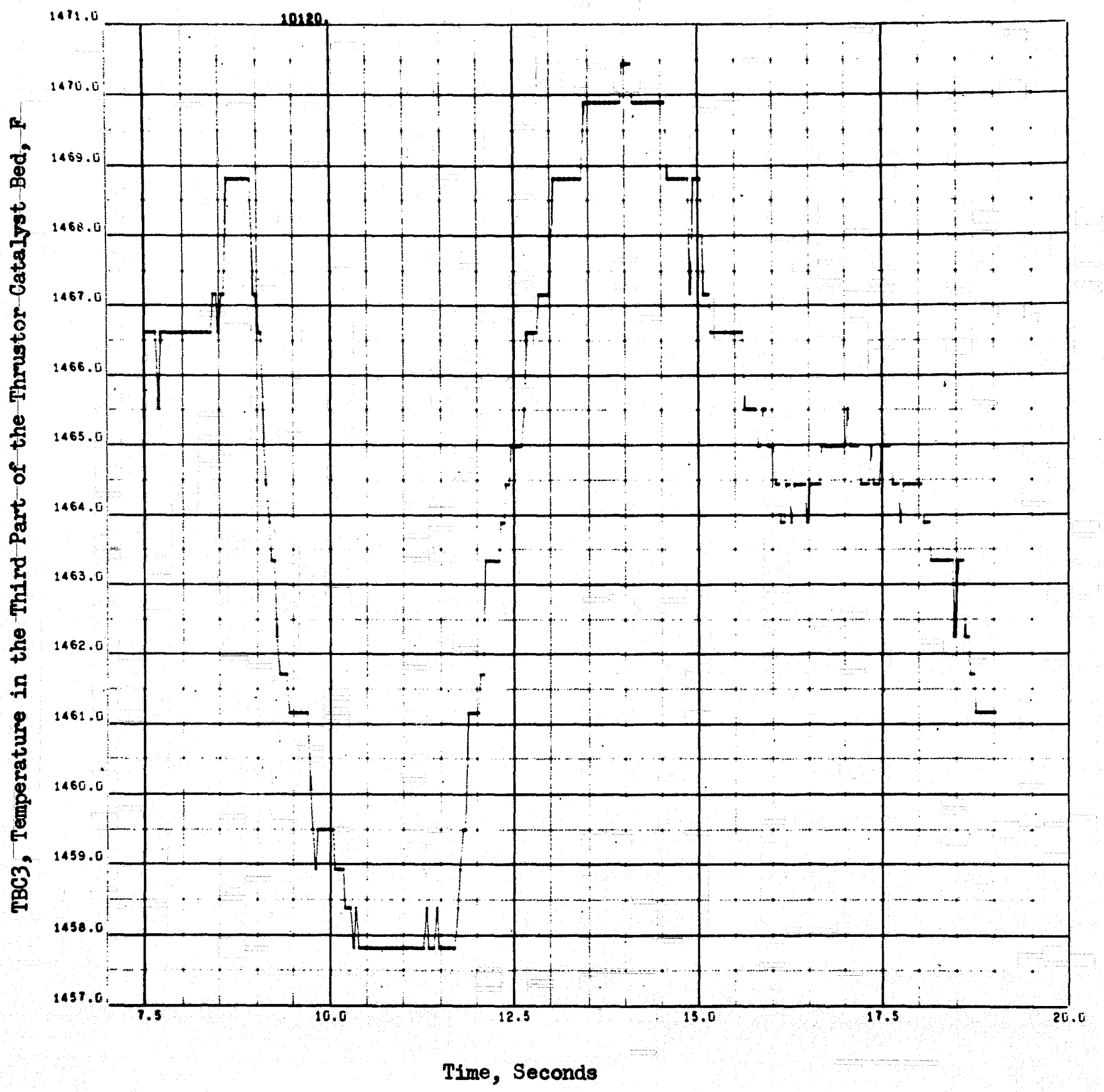

Figure 130. Temperature in the Third Part of the Catalyst Bed, (Thrustor Part of the Thrustor, Conditioner System)

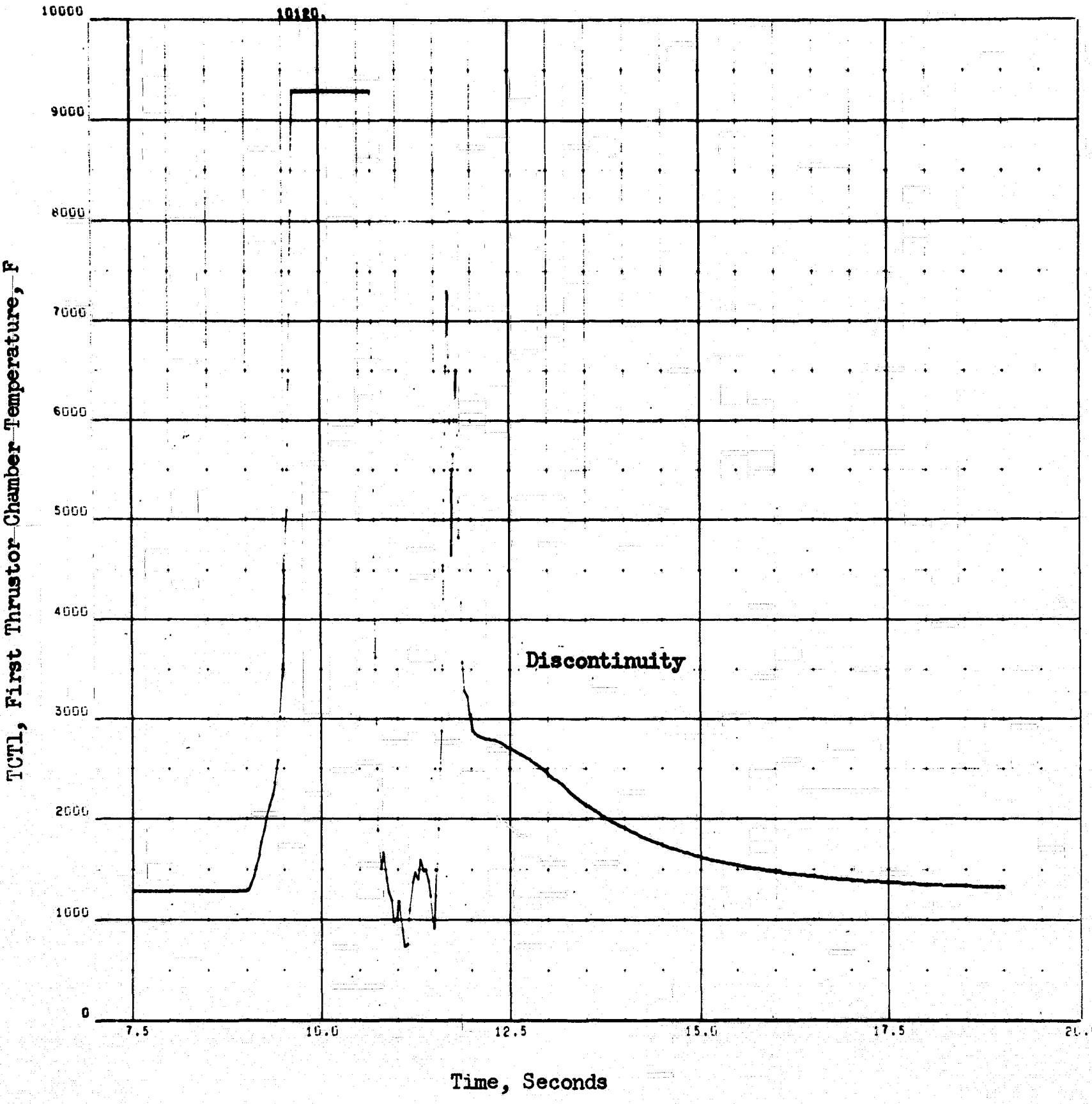

Figure 131. First Chamber Temperature, (Thrustor Part of the Thrustor, Conditioner System)

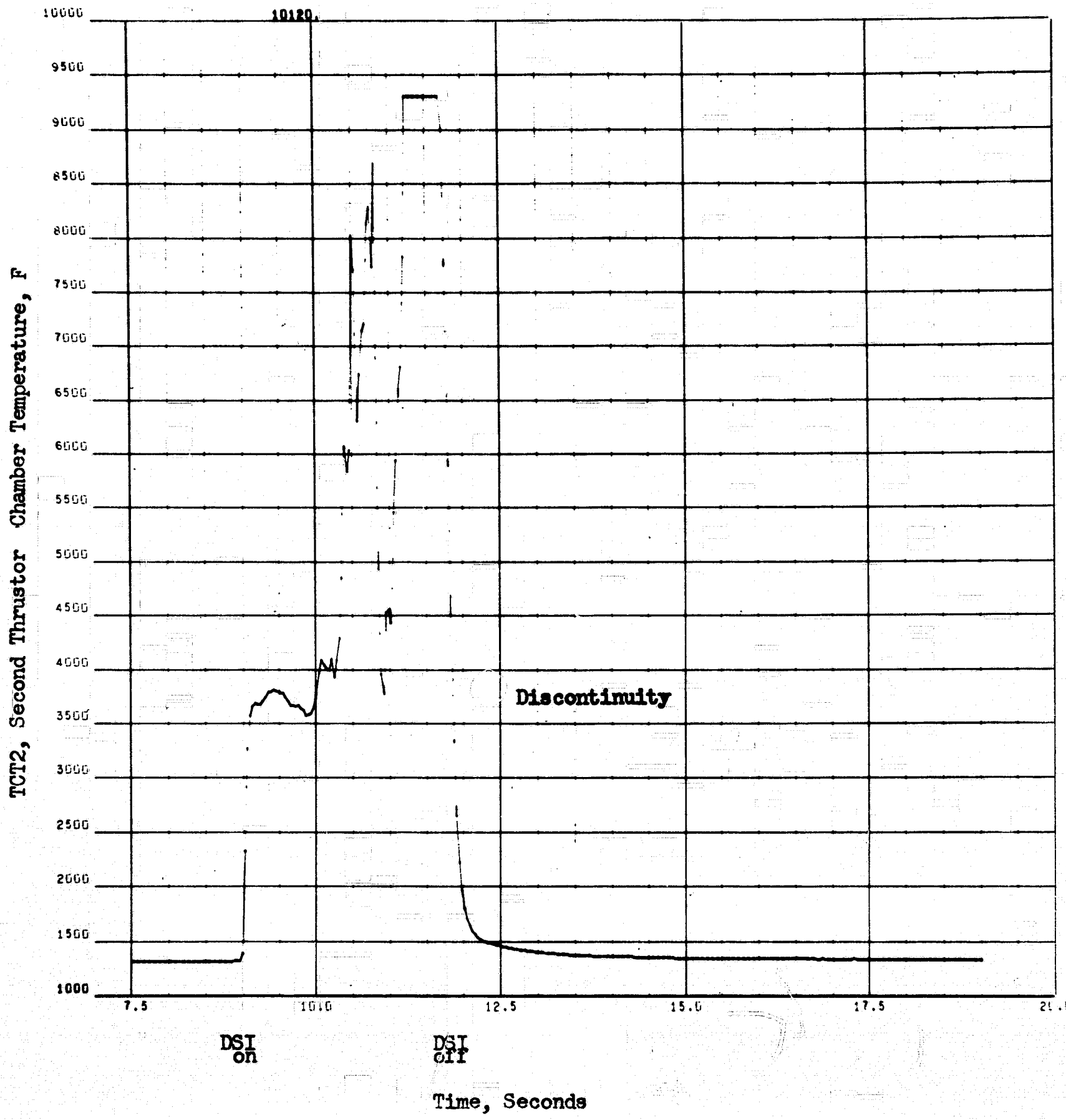

Figure 132. Second Chamber Temperature, (Thrustor Part of the Thrustor, Conditioner System)

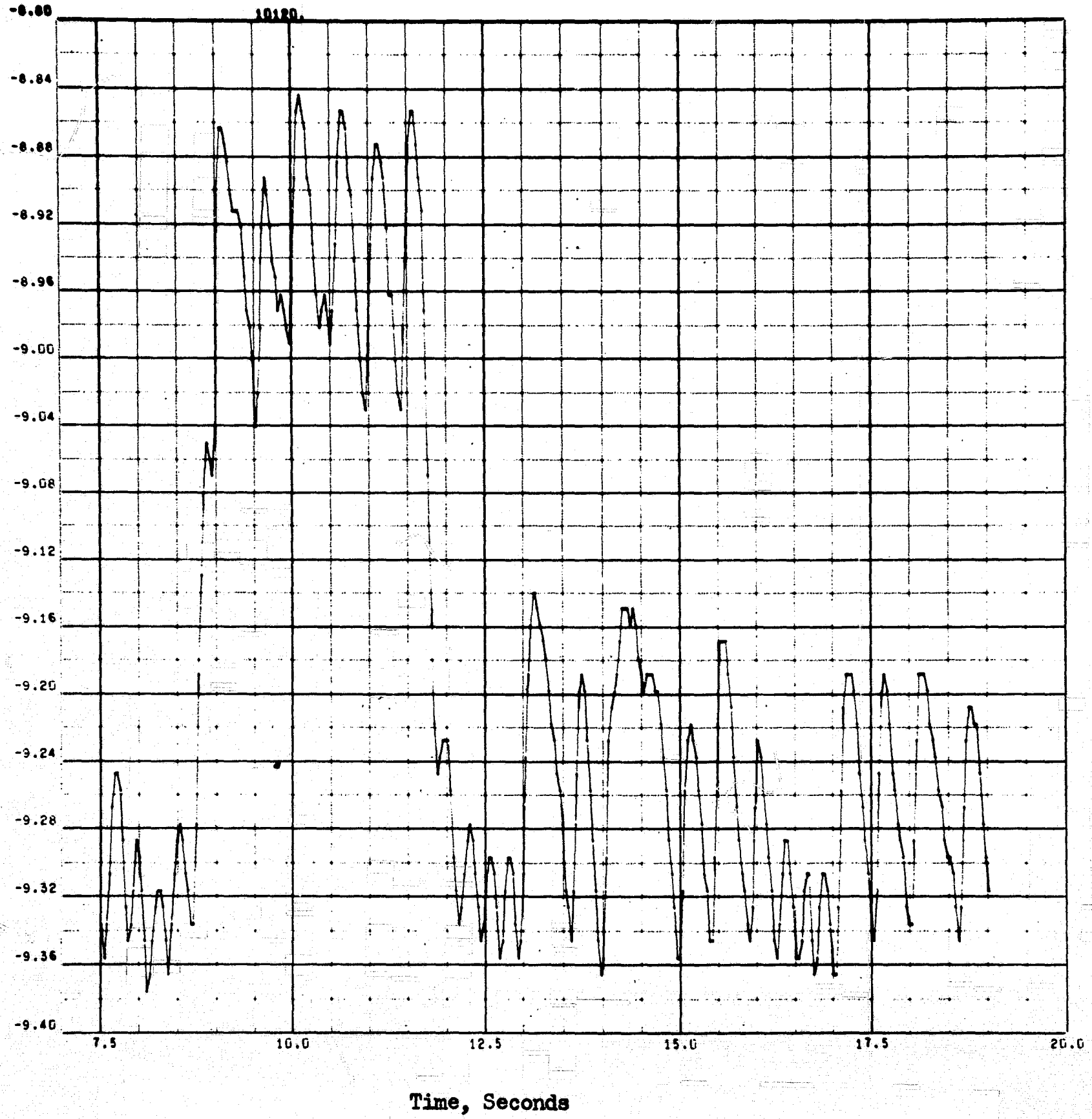

Figure 133. Mixing Pressure, (Thrustor Part of the Thrustor, Conditioner System)

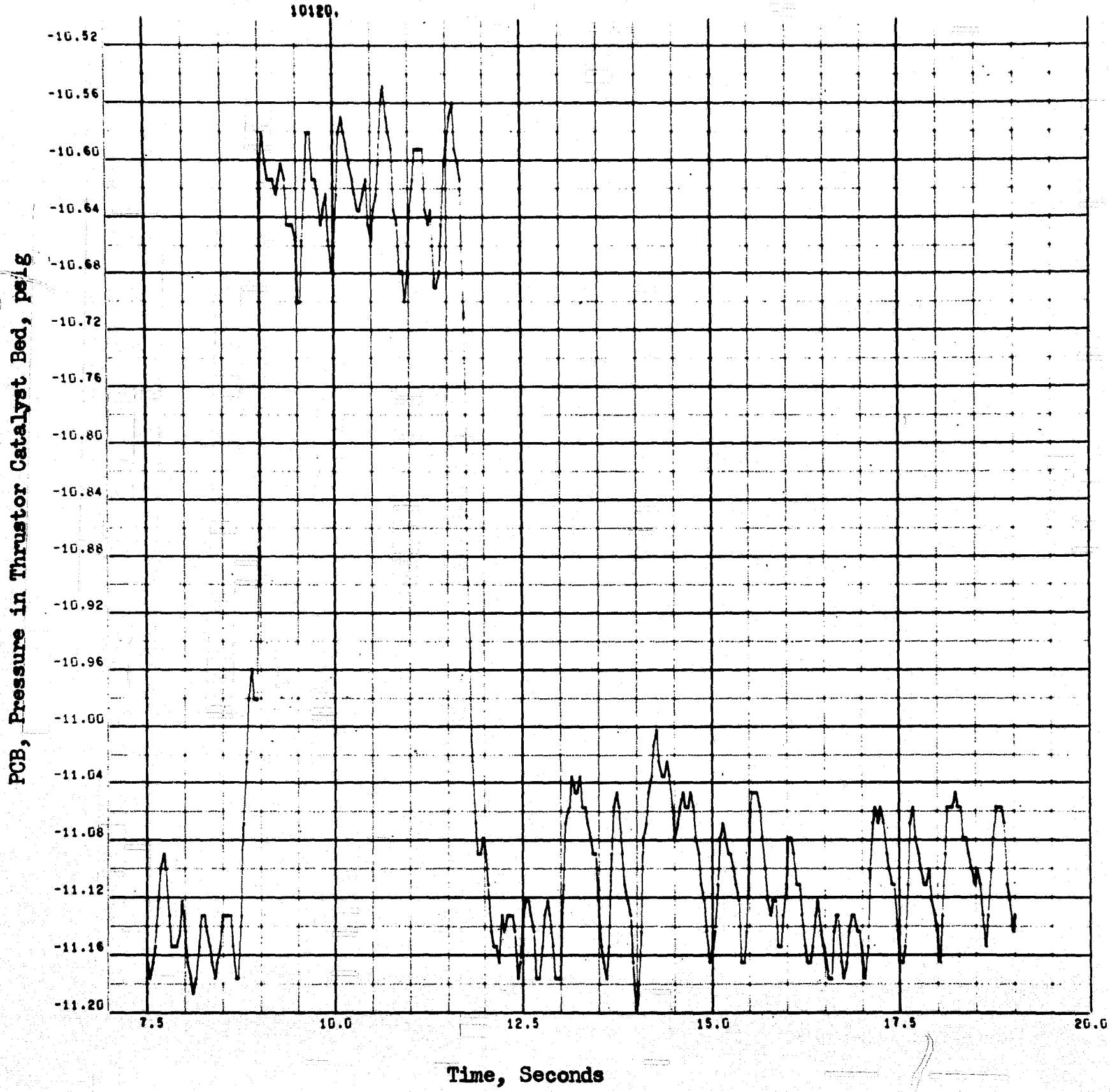

Figure 134. Catalyst Bed Pressure, (Thrustor Part of the Thrustor, Conditioner System)

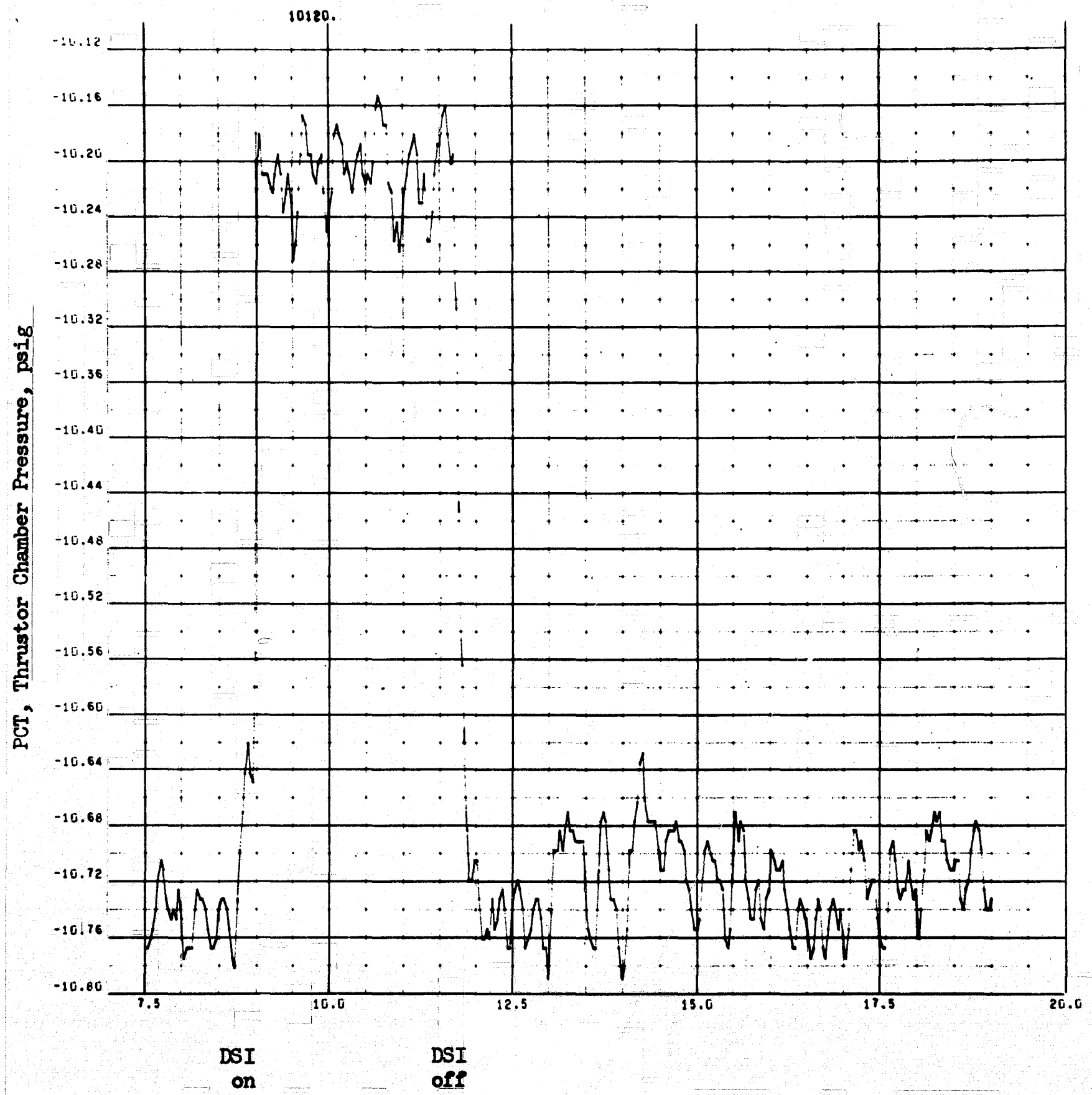

Figure 135. Chamber Pressure, (Thrustor Part of the Thrustor, Conditioner System)

Heat exchanger outlet temperatures (or accumulator inlet temperatures) are shown in Fig. 106 and 118. The oscillation in the hydrogen temperature is associated with the cycling of the liquid hydrogen tank valve.

Accumulator outlet temperatures are presented in Fig. 107 and 119 and show how the inlet temperature fluctuations are attenuated. The hydrogen accumulator outlet temperature is slightly lower than the nominal control point (Table 19) because of the undersized gas generator and the desire for the maximum hydrogen flowrate. The oxygen temperature increase indicates that the small gas generator is capable of supplying the required energy.

The gas generator combustion temperatures (or the heat exchanger hot-tube inlet temperatures) are given in Fig. 108 and 120. The small gas generator is operating slightly above nominal, while the reverse is true for the large gas generator. The low hydrogen feed temperature to the gas generator is partially responsible for the low propellant outlet temperature. The fluctuations in combustion temperature of the large gas generator were more than 100 F and can be correlated with the oscillations in accumulator pressure and injector pressure drops.

Hot-gas outlet temperatures are smoothly increasing (Fig. 109 and 121). The hydrogen gas generator temperature ($TGOH_2$) is nearly nominal, while that for the oxygen gas generator ($TGOO_2$) is far above nominal. When the oxygen heat exchanger coil was shortened, it was impractical to reduce the tube diameter because this would have involved major design changes. Thus, when the tube was shortened, the pressure drop decreased, and the outlet temperature increased.

Propellant ullage tank pressures are given in Fig. 110 and 122. Originally, the ullage pressures were set at 6 to 7 psig. However, heat leak to the hydrogen transfer tube causes some backflow into the hydrogen tank and a pressure buildup to 11 psig, 4 psi above nominal.

The traces in Fig. 112 and 123 show the pressures of the vaporizing propellants inside the heat exchanger. The pressures at these points were monitored to determine if boiling instability existed. But, as noted previously, the control circuit overrides low frequency boiling instability.

Accumulator outlet pressures (or thrustor and gas generator inlet pressures) are given in Fig. 113 through 124. The dashed lines indicate the points at which the pressure switches signal the valve to open or close. The injection pressures (PIF and PIO) are redundant measurements of the accumulator outlet pressures ($PAOH_2$ and $PAOO_2$, respectively).

Gas generator chamber pressures are shown in Fig. 114 and 126. The chamber pressure for the gas generator was slightly low because of the slightly low combustion temperature and the fact that the hydrogen inlet valves limited the hydrogen flow. The oscillations in the chamber pressures follow the hydrogen inlet pressure oscillations.

The hot-gas outlet pressure from the oxygen heat exchanger is shown in Fig. 115. The nominal design pressure is -11.8 psig (2 psia), 3 psi lower than the operating pressure. When the hot-gas coil was shortened, the coil diameter should have been reduced, but this would have necessitated major heat exchanger modifications. The hydrogen coil outlet pressure was not monitored.

Figures 127 through 132 present the temperature profile through the thrustor. A better example of a stable temperature in the downstream chamber during this run was presented in the Thrustor Response section. In this particular case, the thermocouple tip continuity was failing. Otherwise, the temperature profile was nominal.

Figures 133 through 135 give the pressure profile through the thrustor. Since the flowrate was throttled to approximately 1/5 nominal, the pressures are near 2 psia rather than the nominal 10 psia.

DISCUSSION OF RESULTS

Table 20 presents a mass and energy balance on the conditioner system while both gas generators were operating and the downstream injector valve in the thrustor was both open and closed. The flowrate values compare quite favorably to the predicted flowrates presented in Table 17 in the Conditioner Subsystem Design section. The flows were obtained for the gas generators by assuming sonic flow at the throats, complete combustion, and no heat loss in the chamber.

The thrustor flows were calculated for two cases, sonic flow at the throat and at the orifices upstream of the main thrustor valves (Fig.103). Evidently, sonic flow conditions did not exist at the thrustor throat, as evidenced by results presented in Table 21. The fuel flowrate appears to be low by a factor of two (0.0059 vs 0.0029 lb/sec) based on the sonic orifices upstream of the thrustor valves. In addition, the chamber pressure did not substantially increase when the downstream injector was opened, which further verifies the absence of sonic flow. Although the diffuser cell pressure was not monitored during the run, past experience with this facility indicated (based upon volumetric flow rates) that the cell pressure was about 2 psia.

TABLE 21

MASS AND ENERGY BALANCE OF INTEGRATED
THRUSTOR-CONDITIONER SYSTEM FOR THE FINAL EXPERIMENT

Thrustor	W_{H_2} *	W_{O_2} *	MR	Flow Percent, Fuel	Flow Percent, Oxidizer	W_{H_2} **	W_{O_2}
Without Downstream Injector	0.0033	0.0027	0.81	54	52	0.0059	0.0043
With Downstream Injector	0.0033	0.0075	2.2	55	74	0.0029	0.0074
Large Gas Generator and Downstream Injector	0.0020	0.0019	0.96	33	36		
Large Gas Generator and Without Downstream Injector					19.0		
Small Gas Generator With Downstream Injector	0.00078	0.00066	0.85	13	12		
Small Gas Generator Without Downstream Injector	0.00073	0.00067	0.092	12	7		

Energy Balance	Heat Flux, Btu/sec
Fuel Side Without Downstream Injector = 0.0061	8.6
Fuel Side With Downstream Injector = 0.0061	8.6
Oxidizer Side Without Downstream Injector = 0.0053	5.8
Oxidizer Side With Downstream Injector = 0.010	11.2

*Assuming sonic flow at orifices upstream of the valves for thrustor (Fig. 103)
**Assuming sonic flow at throat of thrustor

The effective operation of the control switches can be demonstrated by analyzing an accumulator outlet pressure. For the pruposes of this discussion, refer to the oxygen accumulator pressure ($PAOO_2$). The control deadbands are shown as dotted lines on the CRT (Fig. 113). During thrustor operation with the downstream injection of oxygen, the pressure is oscillating at 1 cps; when the downstream injector is opened, the pressure oscillates at 2 cps because of the increased demand placed on the system accumulator. The oxygen tank valve closes approximately twice as fast as the opening time. Consequently, the amplitude of the pressure oscillations exceeded the upper value of the control deadband less than at the lower value. When the downstream injector valve was open, the added propellant demand increased the amplitude of the oscillation.

SYSTEM CORRELATION WITH COMPUTER MODELING

The system computer model with the new input parameters presented in Table 22 was not run. However, some qualitative comparisons of experimental responses with the original system analysis can be made. Figure 136 depicts how the liquid oxygen accumulator pressure and main valve cycle under a constant thrustor demand. Qualitative comparison of these predicted results with the experimental results (Fig. 104 and 113) shows good agreement.

TABLE 22

IMPORTANT INPUT PARAMETERS FOR THE CONDITIONER COMPUTER MODEL

Parameter	LH_2	LOX
Accumulator Temperature ±Deadband, F	-23	-21 ±6
Accumulator Pressure ±Deadband, in. Hg	136 ±3	140.5 ±3.5
Accumulator Heat Leak	*	*
Main Propellant Delay Opening, milliseconds	240	230
Main Propellant Delay Closing, milliseconds	80	60
Gas Generator Valve Delay Opening	*	*
Gas Generator Valve Delay Closing	*	*
Liquid Line Volume	*	*
Gas Generator Injector Volume, $in.^3$ (mix void + preinjector)	6.6	7.02
Hot-Side Volume	*	*
Accumulator Volume, $in.^3$	4000	700
Other Conditioner Properties		
Amplitude	*	*
Frequency	*	*
Thrustor Flow	0.0033	0.0075 (with downstream injector)
Thrustor With Gas Generator	0.0061	0.010
Ullage Pressure		
Amplitude, psig	25.0	20.8
Frequency, cps	0	0
Thermal Resistance		
Liquid Vaporized Liquid Hot Gas	75 (overall)	25 (overall)
Hot-Gas Coil		
Mass, pounds	0.481	0.455
Area, $in.^2$	87.5	61.5

*Not recorded

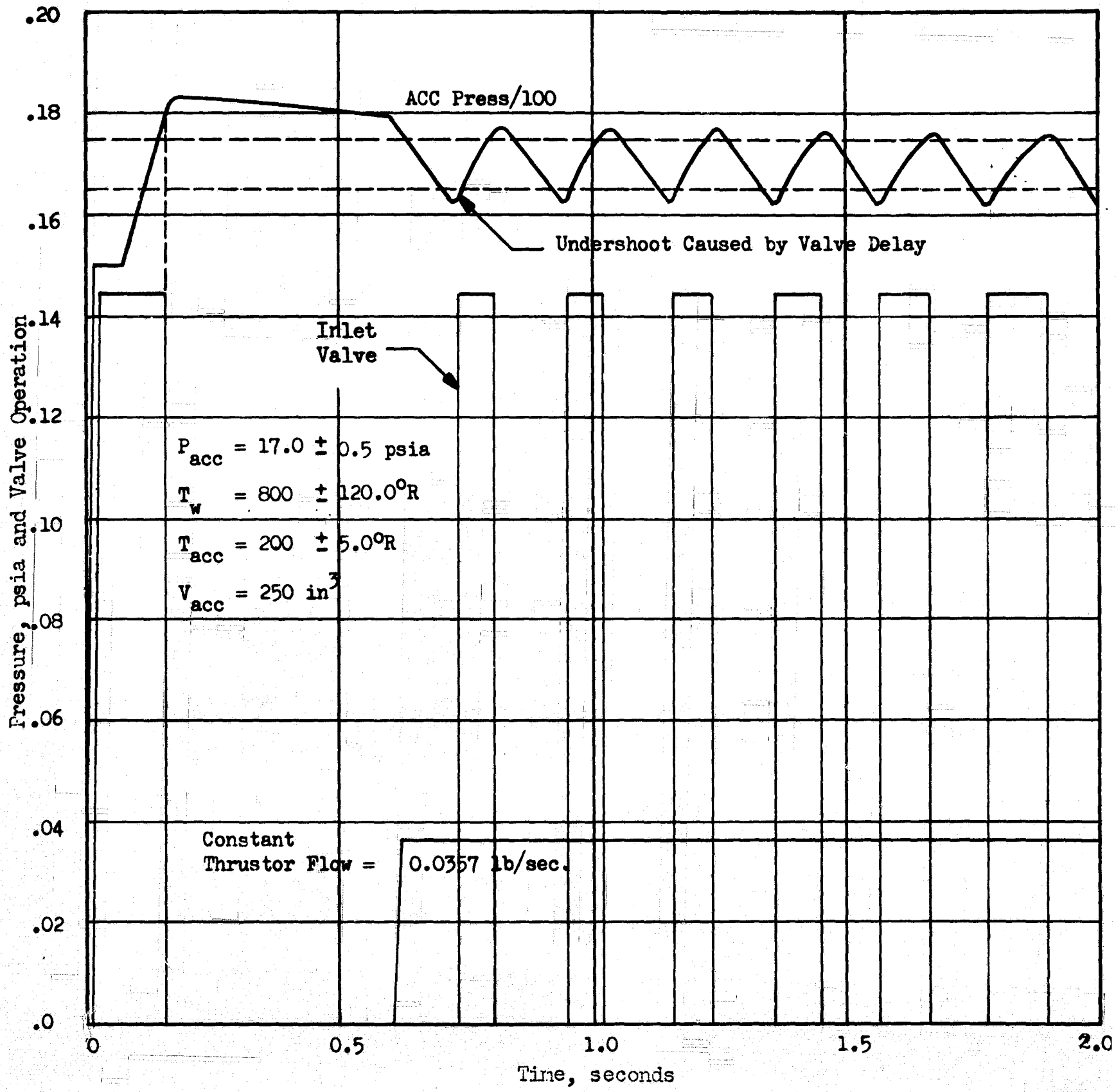

Figure 136. Computer Model Results Showing Accumulator Pressure Cycling and Propellant Inlet Valve Operation(for a Constant Thrustor Flowrate Condition)

Both the system model and the experimental results show accumulator pressure spikes outside the desired deadband. This spiking can be predicted by Eq. 41:

$$\frac{dp}{dt} = \dot{w}_T \frac{R\ T}{V(MW)} \qquad (41)$$

The pressure spiking on the oxygen side, can be estimated to be 0.85 psi and on the hydrogen side to be o.13 psi. An actual pressure undershoot of from 0.6 to 0.45 psia was observed on the oxygen side. Because of an upward shift in the preset control pressure of the hydrogen pressure switch during the run, it was impossible to note the exact amount of spiking on either side of the controller deadband. But one can note pressure cycling far in excess of that (0.13 psi) predicted by the valve delay except during several short periods when spiking approaches nominal. During these short periods the hydrogen inlet temperature ($TLIH_2$) spikes up to 49 R (Fig. 117), indicating that slightly superheated vapor is flowing into the heat exchanger. During the remainder of the time it is speculated that any residual liquid hydrogen in the line between the inlet valve and the top of the heat exchanger would drain into the heat exchanger and, after the valve was closed, be vaporized and cause the pressure spikes.

These pressure spiking results can be scaled up to a 20-pound thrustor, showing that the oxygen accumulator pressure would spike down almost 2.8 psi while that for the hydrogen side would be 0.30 psi with the present accumulators and inlet valve delays. It was concluded that the speed with which the inlet valve operates controls the required accumulator volume.

Catalyst bed temperature perturbations caused by the accumulator pressure cycling can be noted by observing TCS, TCL, TBC1, TBC2, TBC3, and TCT2. Both gas generators are cycling near ±100 F, while the thrustor oscillations (±7 F) are practically insignificant because of the large pressure drop through the orifices at the inlet to the thrustor.

It can be seen, by comparing the chamber temperatures (TCS and TCL) with the hydrogen accumulator pressure ($PAOH_2$), that the temperature fluctuations are 180 degrees out of phase with the pressure fluctuations. When the hydrogen accumulator pressure is at a maximum, the mixture ratio and, consequently, the combustion temperature is at a minimum. Also, when the downstream injector valve was opened, the average oxygen accumulator ($PAOO_2$) pressure dropped slightly, causing a small decrease in combustion temperatures.

It was previously hypothesized that the oscillation in chamber pressure (PCS) correlated directly with the oscillations in the hydrogen accumulator pressure ($PAOH_2$). Obviously, the oscillations in the oxygen accumulator ($PAOO_2$) are overridden. This phenomenon is caused by the fact that the volumetric flowrate of hydrogen is much larger than that of oxygen (by a factor of 16 through the catalyst bed).

SUMMARY

The integrated thrustor-conditioner system was successfully operated with liquid oxygen and liquid hydrogen being delivered to the respective heat exchangers. A cyclic demand was placed on the conditioner by intermittently pulsing the downstream injector on and off once the catalyst bed obtained steady-state conditions. The integrated system was hydrogen-limited because the conditioning system was originally sized to deliver propellants to the thrustor at 260 R, and a design change was accomplished during the experimental program to condition the propellants to 410 R. As a result, the hydrogen gas generator was undersized for the required flowrates and remained on throughout thrustor operation, while the oxygen side gas generator pulsed infrequently. Good correlation was obtained between the expected values and experimental results for the mass and energy balances.

REFERENCES

1. NASA-CR-72176, Final Report, Evaluation and Demonstration of the Use of Cryogenic Propellants (O_2-H_2) for Reaction Control Systems, Volume I, Conceptual Design and Analytical Evaluation, Rocketdyne, a Division of North American Aviation, Inc., 6633 Canoga Avenue, Canoga Park, California, June 1967.

2. JPL Memo No. 30-5, Criteria for Optiumu Mixture Ratio Distribution Using Several Types of Impinging-Stream Injector Elements, G. W. Elverum and T. F. Morley, Jet Propulsion Laboratory, Pasadena, California, February 1965.

3. NASA CR-54657, Investigation of Catalytic Ignition of Oxygen/Hydrogen Systems, R. W. Roberts, H. L. Burge, and M. Ladacki, Rocketdyne, a Division of North American Aviation, Inc., Canoga Park, California, December 1965.

4. Schneider, P. S. Temperature Response Charts, Wiley, New York, 1963.

5. NASA CR-54086, Investigation of Catalytic Ignition of Oxygen/Hydrogen Systems, R. W. Roberts, Rocketdyne, a Division of North American Aviation, Inc., Canoga Park, California, September 1964.

6. NASA CR-72118, Development of Hydrogen/Oxygen Catalysts, T. J. Jennings, W. E. Armstrong, and H. H. Voge, Shell Development Company, Emeryville, California, July 1966.

7. AFRPL-TR-65-107, Performance Characteristics of Compound A/Hydrazine Propellant Combination, Volume I, Contract AF04(611)-9573, Rocketdyne a Division of North American Aviation, Inc., Canoga Park, California, May 1965, CONFIDENTIAL.

8. JPL Report No. 32-387, Calculation of Turbulent Boundary-Layer Growth and Heat Transfer in Axi-Symmetric Nozzles, D. G. Elliot, D. R. Bartz, and S. Silver, Jet Propulsion Laboratory, Pasadena, California, February 1963.

9. Zabetakis, M. G., Forth Symposium on Combustion, Williams and Wilkins, Baltimore, 1953.

10. Lewis, B., Von Elbe, G, Combustion Flames and Explosions of Gases, Second Edition, Academic Press, New York, 1961.

11. Brown, G. G. Unit Operations, John Wiley & Sons, New York, N.Y., 1950.

12. Harnett, R. T., F. J. Sanson, and L. M. Warshawsky, "Midas--an Analog Approach to Digital Computation," Simulation, (September 1964).

13. Fan, L. T., "Effects of Viscous Dissipation on Heat Transfer Parameters for Flow Between Parallel Plates," AD-632, 42, 66-13 FLD. 20/13.

APPENDIX A

DETAILS OF THE SURVEY FROM CONTROL COMPONENTS

Approximately 20 outside vendors as well as internal Rocketdyne groups were contacted during a survey of available control components such as valves and regulators. The chief requirements for these components were: (1) low-pressure operation with a small pressure drop, (2) rapid response (50 milliseconds or better), and (3) compatibility with a liquid hydrogen and/or a liquid oxygen environment.

CONTROL COMPONENTS

Large Fast-Acting Valves

Siebelair Co., Los Angeles, California, previously manufactured a large, 0.875-inch orifice, fast-acting (50 milliseconds open and 17 milliseconds closed), lightweight (5.3 pounds), electrically operated valve. This valve would have been particularly amenable for the on-off controller and the thrustor valve. It would have been necessary to adopt the internal seals for cryogenic operation. The approximate cost was $800.

Regulators and Bipropellant Valves

Fox Valve Development Co. Inc., Hanover, N. J., a pioneer in the development of bipropellant valves for small pulsing rockets, advised Rocketdyne that they had previously built a cryogenic heat exchanger-accumulator

regulator that could be adopted to the proposed system in approximately 12 weeks for a cost of about $4000. They also suggested a pneumatically linked bipropellant valve for the thrustor. This company has published several articles showing the desirability of using venturis and flow nozzles for transient mixture ratio control and the possibility of using the throat of the venturi as the valve seat. In this manner, it is possible to reduce markedly the size of the valve, thus cutting power requirements, improving response, and minimizing valve weight and volume. The approximate minimum size fo valve seats is shown below.

SONIC VENTURI SIZES FOR A 200 R CONDITIONER
AND A 20-POUND THRUSTOR

Component	Approximate Throat Diameter, inches H_2	O_2	
Small Gas Generator	0.0765	0.039	
Large Gas Generator	0.1295	0.0656	
Thrustor	0.323	0.202	0.260
Downstream Injector		0.165	

In-House Inquiries

Rocketdyne's Liquid Rocket Division has had extensive experience designing and buidling cryogenic valves and regulators. Most of the experience is with high-pressure application where large pressure drops are tolerable. It was reported that low-pressure cryogenic applications are unusual and, therefore, little off-the-shelf hardware exists for these applications.

Regulators and Followers

Both the Fischer and Maxitrol companies fabricate low-pressure, high-volume regulators for home natural gas regulation. However, Maxitrol was reluctant to recommend their use because of possible compaitibility problems and lack of response to the accumulator oscillations.

Bellows-Type Accumulator

A brief survey was made to find a company that could supply a high-response bellows for equalizing propellant pressure. These discussions culminated with a bid of approximately $200 per item with a nonrecurring charge of $850 and with a lead time of approximately 3 months.

Conclusions

As a result of these discussions, it became apparent that the experimental study would be limited by hardware parameters. It was also apparent that before an optimum flightweight design can be completed, an extensive controls hardware design and development program was necessary. Specific propulsion applications should be defined prior to such action.

APPENDIX B

CALIBRATION PRECISION MONITORING

Overall calibration procedures include a highly sophisticated numerical analysis data control system for continuous monitoring of the individual measuring system precision numbers. The control system, Random Walk for Measurements Analysis of Static Systems, has as its basis , input calibrations which may be taken at any time. The program utilizes all input data with the most recent input receiving top priority. A typical output is shown in Table B-1. The first line of output for each system gives the test stand, recording system identification, recorder type, pickup serial number, range, ID for data cards, and physical parameter being measured by the system. The next set of numbers is the most recent raw calibration data. On the left are the readings for the calibration input steps. On the right are the precalibrate throw zero (Z1), the calibrate throw (R-CAL) reading (CT), the postthrow zero (Z2), the precalibration zero (Z3), and the postcalibration zero (Z4). The first two zeros are averaged and subtracted from the throw to get a reduced throw. For each calibration step, a linear interpolation is performed between the final two zeros (Z3 and Z4), and the interpolated zero is subtracted from the reading to obtain a reduced reading. Each reduced reading is then divided by the reduced throw to obtain a scaled output. All scaled output values from all calibrations in the system history are then listed by the appropriate input values (e.g., pressures). Each calibration is given a line, with the most recent first and the oldest last. The calibration dates are given at the right of each line.

The next three items of information are the estimates of the measurement variance in the input-to-scaled output ratio (σ_m^2) the random walk variance

TABLE B-1

TYPICAL NUMERICAL ANALYSIS OUTPUT OF CURRENT NASA O_2/H_2 CATALYTIC PROGRAM

UNCLE 004 BKM. 700 004006 PC1

LATEST OUTPUT					Z1	CT	Z2	Z3	Z4	TIME
772	1023	1275	1523	1773	20	2021	23	23	23	1- 4-65

INPUT

300	400	500	600	700

SCALED OUTPUT					TIME
0.3746	0.5001	0.6262	0.7502	0.8752	1- 4-65
0.3761	0.5025	0.6269	0.7522	0.8776	12- 8-64
0.3757	0.5013	0.6270	0.7522	0.8778	12- 8-64
0.3763	0.5022	0.6270	0.7513	0.8767	11-19-64
0.3771	0.5027	0.6272	0.7523	0.8794	11-19-64
0.3765	0.5025	0.6270	0.7525	0.8780	11-19-64
0.3763	0.5012	0.6257	0.7506	0.8776	11-19-64

MEASUREMENT VARIANCE IN INPUT-TO-SCALED OUTPUT RATIO	=	0.27919E-00	
RANDOM WALK VARIANCE IN INPUT-TO-SCALED OUTPUT RATIO	=	0.13799E-00	
RATIO OF SHORT-TERM VARIANCE TO RANDOM WALK VARIANCE	=	0.20233E 01	(DAYS)
COEFFICIENT OF SHORT-TERM VARIATION	=	0.066	(PERCENT)
COEFFICIENT OF RANDOM WALK VARIATION	=	0.0465	(PERCENT/DAY**.5)
REQUIREMENT FOR COEFFICIENT OF VARIATION OF REDUCED DATA	=	1.500	(PERCENT)

SYSTEM NOW PASSES TEST FOR LINEARITY (TYPE I ERROR=.05).

DATA REDUCTION FORMULA IS

(INPUT) = (7.9949E 02)*(SCALED OUTPUT)

ABOVE OUTPUT-INPUT MODEL IS SATISFACTORY (TYPE I ERROR=.05).

SYSTEM SHOULD BE CALIBRATED ON OR BEFORE 2- 3-65

COEFFICIENT OF VARIATION OF REDUCED DATA ON 2- 3-65 = 0.26 PERCENT
COEFFICIENT OF VARIATION OF REDUCED DATA ON 1- 6-65 = 0.10 PERCENT

DATA REDUCTION MATRIX

(	4.84201E-02	0.)
(		)
(	0.	0.)

in the input-to-scaled output ratio (σ^2), and the ratio of the former variance to the latter variance (k). The first two numbers are intended principally for computing the data reduction imprecision. The next line of output gives the coefficient of short-term variation (σ_m), expressed as a percentage of the average-input-to-scaled-output ratio. This quantity is generally the largest component of data reduction imprecision. If it is greater than the previously read in system imprecision requirement, or only slightly less, the system is unsatisfactory. The coefficient of random walk (long-term) variation (σ), expressed as a percentage of mean input-to-scaled-output ratio, is meaningful only after calibrations are obtained with time. The final item in this block of output is the system data reduction imprecision requirement expressed as a percentage.

Based on various equations in Ref. B-1 and B-2 and on the estimated value of k, revised scaled output values are calculated to correspond to the state of the system at the time of the most recent calibration. These values are then fit by least squares with either a linear or a cubic function. The null hypothesis is that the function is linear, and the specified error (the probability that a truly linear function is mistakenly concluded to be nonlinear) is printed out. (A small error specification reduces the chance of this type of error, but also makes it more difficult to spot the truly nonlinear cases.) If the linearity hypothesis is rejected, a cubic fit is performed. The formula for converting scaled outputs to estimated inputs is then printed. If the input-output relationship is cubic, a table is given for the convenience of the data reductionist in addition to the explicit cubic formula. Rocketdyne experience indicates most systems can be satisfactorily fit by the linearity hypothesis.

Another test is now made as to whether the input-output model is consistent with the estimate of σ_m (the root-mean-square estimate for the curve fit and σ_m should be roughly the same). An unsatisfactory answer indicates a significant intercept or outright error in the input data for the program as long as $k \neq 0$. When $k = 0$, no clear interpretation can be given of this test.

The next line indicates the ability of the system to meet the previously established requirement. The calibration data may indicate that the system can never meet the requirement, that it will fail it within the next 2 days, or that it will meet it up to a certain date. The corresponding program outputs are: (1) system can never meet required precision and should be replaced, (2) system does not now meet required precision and additional calibration(s) should be performed immediately, and (3) system should be calibrated on or before a given date. In the latter case, the estimated data reduction imprecision is given for test data taken 2 days after the most recent calibration, and for a reading on the specified recalibration day.

The next output, denoted by R, is a 2 x 2 matrix useful in estimating data reduction imprecision at any other time of interest and for any scaled output. If s is a scaled output taken h days after the most recent calibration, and if P denotes the estimate of the standard deviation of a reduced datum point, then:

$$P = \left[V + s^2 \left(h \sigma^2 + \sigma_m^2 \right) \right]^{1/2} \qquad \text{(B-1)}$$

where

$$V = (s, s^3) R \left(\frac{s}{s^3} \right) \qquad \text{(B-2)}$$

Finally, if a cubic function has been chosen to fit the calibrations for data reduction, an alternative best approximate linear formula is given when required. With the present digital system, only linear formulas can be used; however, this will soon be modified to allow for cubic conversion formulae. At the end of the printouts for each test stand, a summary sheet is printed.

REFERENCES

B-1. Rothman, D., Random Walk Program for Measurements Analysis of Static Systems, RM-1119-351, Rocketdyne, a Division of North American Aviation, Inc., Canoga Park, California, 25 January 1965.

B-2. Rothman, D., A Random Walk Model for Non-Uniform, One-Parameter, Static, Linear Measurement Systems, RR-59-47, Rocketdyne, a Division of North American Aviation, Inc., Canoga Park, California, 15 December 1959.

Unclassified

Security Classification

DOCUMENT CONTROL DATA - R & D

(Security classification of title, body of abstract and indexing annotation must be entered when the overall report is classified)

1. ORIGINATING ACTIVITY *(Corporate author)*
Rocketdyne, a Division of North American Rockwell Corporation, 6633 Canoga Avenue, Canoga Park, California 91304

2a. REPORT SECURITY CLASSIFICATION
Unclassified

2b. GROUP

3. REPORT TITLE
Fifth Prel. Final, Evaluation and Demonstration of the Use of Cryogenic Propellants (O_2/H_2) for Reaction Control Systems

4. DESCRIPTIVE NOTES *(Type of report and inclusive dates)*

5. AUTHOR(S) *(First name, middle initial, last name)*
N. Rodenwald, G. Falkenstein, P. Herr, and E. Prono

6. REPORT DATE	7a. TOTAL NO. OF PAGES	7b. NO. OF REFS
31 October 1968	318	13

8a. CONTRACT OR GRANT NO.	9a. ORIGINATOR'S REPORT NUMBER(S)
NAS3-7941	
b. PROJECT NO.	R-6838-2
c.	9b. OTHER REPORT NO(S) *(Any other numbers that may be assigned this report)*
d.	NASA CR-72244

10. DISTRIBUTION STATEMENT

11. SUPPLEMENTARY NOTES	12. SPONSORING MILITARY ACTIVITY
	NASA

13. ABSTRACT

The feasibility of a catalytically ignited spacecraft reaction control system using cryogenic (hydrogen-oxygen) propellants was experimentally demonstrated. The system studied utilized propellant conditioners to prepare the incoming propellants to a temperature and pressure acceptable to the thrustor. A portion of the propellants at a mixture ratio of 1.0 was passed through a catalyst bed. Additional oxygen was injected into the hot fuel rich gas. Experimental results for the thrustor and conditioner subsystems and a system demonstration are presented. Design criteria for the ultimate development of an operational system are also presented.

DD FORM 1 NOV 65 1473

Unclassified

Security Classification